Coastal and Hydraulics Laboratory

US Army Corps
of Engineers®
Engineer Research and
Development Center

Sabine-Neches Waterway, Sabine Pass Jetty System: Past and Future Performance

William C. Seabergh, Ernest R. Smith, and Julie D. Rosati

April 2010

Sabine-Neches Waterway, Sabine Pass Jetty System: Past and Future Performance

William C. Seabergh, Ernest R. Smith, and Julie D. Rosati

Coastal and Hydraulics Laboratory
U.S. Army Engineer Research and Development Center
3909 Halls Ferry Road
Vicksburg, MS 39180-6199

Final report

Abstract: This study evaluated the present and future functionality of the Sabine Pass jetties considering planned deepening of the Sabine-Neches Waterway Navigation Channel from 42 to 48 ft mean low water (MLW) and possible rehabilitation of the jetty system. The Sabine Pass jetties were constructed to their full length (East jetty, 25,270 ft; West jetty, 21,860 ft) between 1880 and 1930 and, during the 130 years since construction began, have incurred loss of elevation and damage because of regional subsidence, scour at the base of the structures, storms, disintegration of the original fascine (willow) mats used as foundation for the structures, and consolidation of the underlying substrate. This study evaluated the 2003 condition of the jetties and anticipated functionality in 50 years given change in relative sea level at the site, future consolidation of the underlying substrate, and possible storm damage. Three integrated tasks evaluated 1) the stability of the jetties to storm waves, 2) the decrease in structure elevation through time relative to the mean water level caused by consolidation of the underlying substrate and relative sea level rise, and 3) waves, currents, and potential sediment transport pathways in the vicinity of the jetties and navigation channel. Each task assessed the 2003 "existing" condition, a hypothetical jetty condition in 50 years without rehabilitation, and two repair scenarios that were assumed to occur in 2010 and were assessed after 50 years. The repair scenarios were rehabilitation of the entire length of both jetties vs. rehabilitation of the seaward 4,000 ft. Both alternatives would be constructed to elevations of +9.2 ft MLW (East) and +9.3 ft MLW (West). Shear stresses from numerical calculations of waves, currents, and water levels were applied to indicate the potential for cohesive sediment transport and channel shoaling magnitudes.

Recommendations from these analyses were that the jetties should be rehabilitated to +9.2 ft/+9.3 ft MLW to ensure safe navigation and reduce channel shoaling, and that stone size should be increased to approximately 17-18 tons for stability during storms and higher water levels. Repair of the seaward 4,000 ft of both jetties provided similar navigation benefits (reduction in waves and currents, no change in total shoaling) as restoration of the full length of both jetties. Physical model studies are recommended to optimize stone size for rehabilitation. Numerical modeling is recommended to assess the potential for scour of the seabed in the vicinity of the jetties, and to determine magnitudes of channel shoaling for cohesive sediment. Numerical shoreline modeling with anticipated water levels over the project lifetime is recommended to assess the likelihood for structure flanking and minimize adjacent beach erosion.

Contents

Figures and Tables

Figures

Tables

Preface

Unit Conversion Factors

Multiply	By	To Obtain
cubic yards	0.7645549	cubic meters
degrees (angle)	0.01745329	radians
feet	0.3048	meters
knots	0.5144444	meters per second
miles (nautical)	1,852	meters
miles (U.S. statute)	1,609.347	meters
miles per hour	0.44704	meters per second
pounds (force)	4.448222	newtons
pounds (force) per foot	14.59390	newtons per meter
pounds (force) per square foot	47.88026	pascals
square feet	0.09290304	square meters
square miles	2.589998 E+06	square meters
tons (force)	8,896.443	newtons
tons (force) per square foot	95.76052	kilopascals
yards	0.9144	meters

1   Introduction

Project overview

Sabine-Neches Waterway (SNWW) is a 64-mile-long, deep-draft federal navigation channel that serves the ports of Beaumont, Port Arthur, and Orange, Texas and is located in Jefferson and Orange Counties, Texas, and Cameron Parish, Louisiana, on the Louisiana-Texas border (Figure 1). Nationally, the SNWW ranks 5th in tonnage with an average of more than 135 million tons of goods from 2002-2007 (U.S. Army Corps of Engineers (USACE), 2009b). The SNWW includes six sections of channels maintained at the following dimensions: Sabine Bank, Sabine Pass Outer Bar, and Sabine Pass Jetty channels at 42 ft depth relative to mean low water (MLW) and 800 ft width offshore, narrowing to 500 ft width between the jetties; Sabine-Neches Canal and Neches River Channel at a depth of 40 ft MLW by 400 ft width; and the Sabine-Neches Canal to Sabine River at 30 ft MLW depth and 200 ft width. Increased economic development and growth of the ports have led to a need for deeper and wider navigation channels to accommodate larger vessels and increased navigation traffic. Proposed channel improvements include offshore reaches in the Gulf of Mexico deepened from 42 to 50 ft MLW, lengthened by 13.1 miles, at a width of 700 ft; and inshore channels (Sabine Pass Jetty Channel to Port of Beaumont) deepened from 40 to 48 ft MLW and widened to 700 ft.

Two previous studies have investigated the effects of the channel deepening. Maynord (2003) investigated ship wakes and potential erosion of channel banks within confined portions of the SNWW. Brown et al. (2009) conducted a numerical model study to evaluate changes in circulation and salinity with the deepened and widened channel. The present study supplements these previous reports with a focus on the Sabine Pass channel and jetties, and whether the present condition of the jetty system is sufficient to ensure safe navigation with the channel improvements.

Figure 1. Sabine-Neches Waterway.

Purpose of study

The U.S. Army Engineer District, Galveston (SWG) requested the U.S. Army Engineer Research and Development Center's (ERDC) Coastal and Hydraulics Laboratory (CHL) to assess the need for future rehabilitation of jetties at the SNWW. These jetties were constructed during the 1880-1930 period and have been rehabilitated multiple times in the 130 years since initial construction. The jetties have been damaged during storms; lost elevation due to consolidation of the underlying seabed, regional subsidence, and sea level rise; and possibly have degraded due to post-construction settlement and scour at the base of the structure. SWG asked CHL to help assess whether the jetties, in their present condition, are sufficient for safe navigation now and for 50 years into the future with

a proposed channel deepening to 48-ft MLW. A long-range plan is needed to manage the jetties at the SNWW to best support the Federal navigation project.

Specific questions that the SWG asked CHL to address were:

1. Should the jetties be maintained, rehabilitated for the entire length, or only partially rehabilitated for sections that have been damaged (or for sections that have not been maintained in the past)?
2. For various jetty repair scenarios, what are the short-term and long-term patterns and magnitudes of waves, currents, and sediment transport at the entrance channel, and how do these processes affect structural stability, channel shoaling, and navigability?
3. Will subsidence of the existing jetties continue, and how will it be altered with any rehabilitation of the structures?
4. How will a possible increase in storm severity and change in relative sea level impact the navigation channel and structures?

To address these questions, the study had three collaborative tasks that assessed (1) the stability of the jetty to storm waves; (2) the decrease in jetty elevation through time due to consolidation of the underlying substrate, and the likely increase in relative sea level at the site; and (3) waves, currents, and potential sediment transport in the vicinity of the jetties and navigation channel. Each task assessed the existing condition, a hypothetical jetty condition in 50-years without rehabilitation, and various repair scenarios that would be constructed in 2010 and assessed in 50-years (year 2060) with the increase in relative sea level over this period.

Overview of report

This report is organized in 9 chapters and two appendices. Chapter 1 presents a brief background of the site and goals of the study. A review of the study site and history of the project are presented in Chapter 2, and Chapter 3 discusses coastal processes and storm conditions in the project area. Chapter 4 evaluates changes to the jetty system to understand past and forecast future subsidence of the structures. Chapter 5 presents an analysis of structural stability and potential damage to the present-day jetty system through application of synthetic hurricanes and typical yearly storms over a 50-year period. Based on the stability analysis, several rehabilitation designs were refined in conjunction with SWG, as presented in Chapter 6. Chapter 7 presents numerical modeling of hydrodynamics

and calculated sediment transport shear stresses for the existing condition and rehabilitated jetties for various storm sequences. The calculated shear stresses are applied to infer cohesive sediment suspension and deposition, and qualitatively compare shoaling patterns and magnitudes for the restoration alternatives. Chapter 8 summarizes all results, and Chapter 9 provides recommendations for jetty rehabilitation and future studies. Appendix A documents numerical model flow and shear stress calculations for each alternative and storm, and Appendix B shows difference plots comparing hydrodynamic results between alternatives.

2   Background

Introduction

This chapter reviews historical information about the local and regional setting, as well as engineering activities for the project. The construction and rehabilitation history of the jetty system and historical dredging rates for the Sabine Pass and Outer Bar channels provide a baseline with which to evaluate operation of the jetty system in the past, a future condition with channel deepening but without structure rehabilitation, and a future condition with various rehabilitation alternatives.

Geologic setting and coastal processes

The present-day SNWW occupies a portion of the ancient Sabine River valley that ranged from 4 to 8 miles in width when sea level was at a low stand during the last glacial maximum (Nelson and Bray 1970). In the vicinity of modern-day Sabine Pass, the base of the buried channel was estimated to be more than 120 ft below present sea level (Kane 1959) (on the order of 90 ft below the modern seabed), which has been filled with sediment as sea level rose. Sediment cores taken by Nelson and Bray (1970) in the vicinity of Sabine Pass indicated that clay and mud extend 50 to 60 ft below the modern sea bed and overlay a base of quartz sand and silt that extends to the depth of the cores (at least another 20 ft thickness). Beneath the sand-silt layer is the Pleistocene-Holocene surface, called the Beaumont Clay formation.

The significance of the ancient channel and present-day SNWW system is that the clay, silt, and mud deposited above the Beaumont Clay subsurface form a thick deposit, possibly 50 to 90 ft thick, that is susceptible to consolidation as it is loaded with additional sediment or structures. Consolidation occurs as fluid or gas that is trapped in the voids between sediment grains is expelled and the grains shift and deform due to loading. Thicker layers of sediment, greater weight loading the layer, and longer time periods incur larger magnitudes of consolidation. Thus, the weight of the jetties has caused compression, or consolidation, of the underlying sediment, which has reduced the relative elevation of the structures.

The beaches adjacent to the jetty system are composed of a thin layer of sand overlying cohesive silt, clay, and mud, and are backed by marsh and ridge complexes. Beaches east of Sabine Pass were formed as the ancient Calcasieu River headland eroded and sediment was transported to the west, depositing in Chenier ridges seaward of Sabine Lake. Based on data from 1883 to 1994, the modern shoreline between Calcasieu and Sabine Passes has been stable in the east, erosional near Holly Beach, and accretive in the west (McBride and Byrnes 1997). The coast immediately west of Sabine Pass has beach ridges that indicate a local reversal in net sediment transport towards the east (McBride et al. 2007) (Figure 2).

The Louisiana and Texas coastal areas experience regional subsidence, downward displacement of the landmass, caused by a combination of regional tectonics, compaction of strata, and groundwater off-take (Dokka 2006). Regional subsidence rates for the Sabine Pass area were estimated by Shinkle and Dokka (2004), and indicate a range of 0.35-0.55 in/year (9-14 mm/year) for Sabine Pass (Figure 3).

Net longshore sand transport rates along the western Louisiana and northern Texas coast are generally to the southwest, although there is a local reversal in the vicinity of Sea Rim State Park, located 10 miles west of Sabine Pass (Figure 2). In a longshore transport modeling study, King (2007) estimated average annual net longshore transport rates at Sea Rim State Park ranging from 200,000 to 220,000 cu yd/year directed to the northeast (towards Sabine). Morang (2006) formulated a sediment budget for the upper Texas Coast and estimated the growth rate of the fillet west
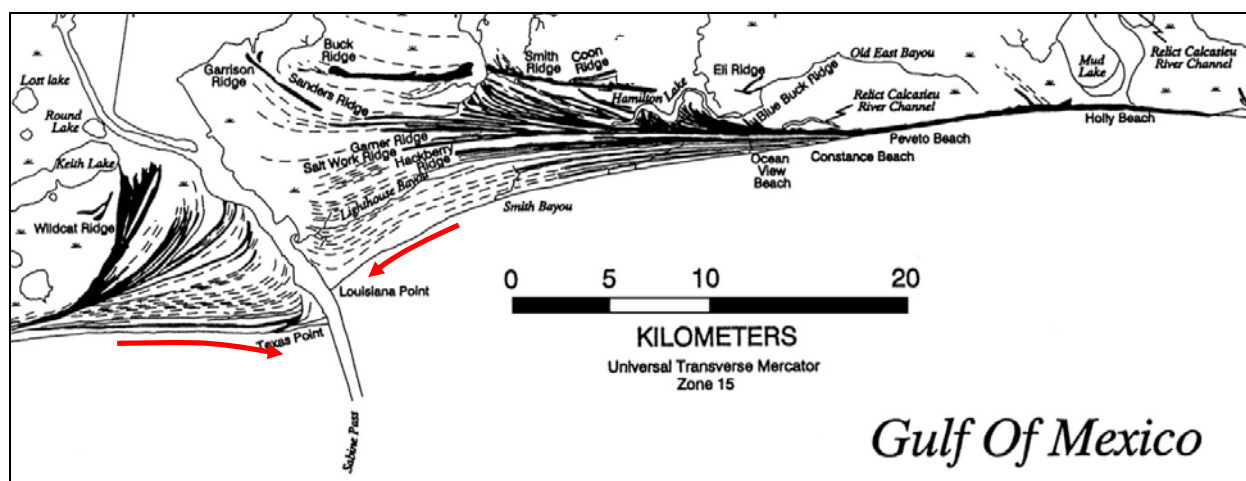
Figure 2. Geomorphology of Chenier ridges and accretive beaches both east and west of Sabine Pass, with inferred long-term net transport pathways (adapted from McBride et al. 2007).
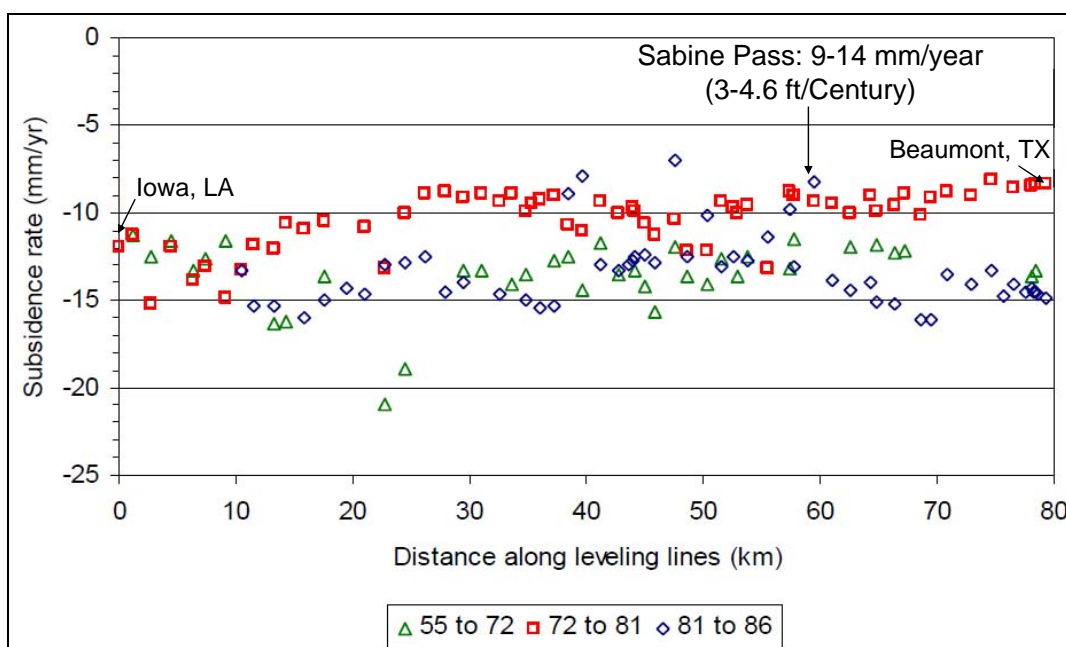
Figure 3. Regional subsidence rates for Sabine Pass (adapted from Shinkle and Dokka 2004).

of Sabine Pass as 10,500 cu yd/year. Morang found no evidence of recent fillet growth east of the Pass. Other estimates of transport rates at Sea Rim State Park include Mason (1981), with a rate of 35,300 cu yd/year to the northeast, and the U.S. Army Engineers District (USAED) Galveston (1983), with a rate of 70,600 cu yd/year to the southwest, both calculated based on littoral environment observations. Typical and storm conditions are discussed in detail in Chapter 3.

Navigation and port development

Nationally, the SNWW ranks 5th in tonnage with an average of more than 135 million tons of goods from 2002-2007 (U.S. Army Corps of Engineers, Navigation Data Center, 2009). SNWW provides access to Port Arthur TX, Port of Orange, TX, and the Port of Beaumont, TX. Proposed plans will reduce transportation costs for crude petroleum imports, chemical products, grain exports, steel and iron ore, and liquefied natural gas. SNWW is the Nation's number one crude oil arrival port. The Port of Beaumont is a Strategic Port of Embarkation and handles more military cargo than any other U.S. port. Other details concerning shipping may be found in the Galveston District's Feasibility Report (USAED Galveston, 2007).

Historically, the SNWW channel has been deepened to meet shipping needs. Authorized channel depths have progressively deepened from 25 ft MLW in 1912, 30 ft MLW in 1922, 34 ft MLW in 1936, 36 ft MLW in 1946, and 40 ft MLW in 1962. The SNWW will be deepened to 48 ft MLW and widened to improve navigational efficiency and safety while maintaining and restoring coastal and estuarine resources.

Project history

Channel

The Sabine Neches Waterway from the Gulf of Mexico to Beaumont was federally authorized in 1912. The authorization included deepening the channel approximately 15 ft to 26 ft MLW. The channel was subsequently widened and deepened to accommodate larger vessels and increased traffic. A summary of channel improvements is given in Table 1 (USAED Galveston, 1999).

Presently (2009), the navigation channel extends 18.1 miles into the Gulf of Mexico and has an authorized depth of 40 ft MLW. The Gulf portion of the Sabine Pass channel is divided into three reaches: the Jetty Entrance Channel, Outer Bar Channel, and Sabine Bank Channel (Figure 4).

Table 1. History of Sabine Pass Chanel.

Date	Channel Work Authorization
1912	26-ft MLW depth channel through Sabine Pass, Port Arthur Canal and Port Arthur turning basin; and a 26-ft MLW turning basin at Port Arthur
1922	Deepen channels to 30 ft MLW from Gulf to Beaumont, with increased widths
1927	Widen Sabine Pass and Jetty Channel.
1935	Deepen to 32 ft MLW from Gulf to Beaumont turning basin
1935	Deepen channels to 34 ft with increased widths from Gulf to Beaumont turning basin.
1938	Increased widths of channels from Gulf to Beaumont turning basin
1946	Deepen Sabine Pass Outer Bar Channel to 37 ft MLW, Sabine Pass jetty channel to 36 ft MLW at inner end, deepen Sabine Pass Channel to 36 ft MLW
1954	Rectification of certain reaches of existing Sabine Pass Channel, Sabine-Neches Canal, and Neches River and Sabine River Channel; widen Entrance channel to Port Arthur turning basins to 350 ft
1962	Improve Outer Bar Channel to 42 ft and enlarge Entrance Channel to Port Arthur turning basins.
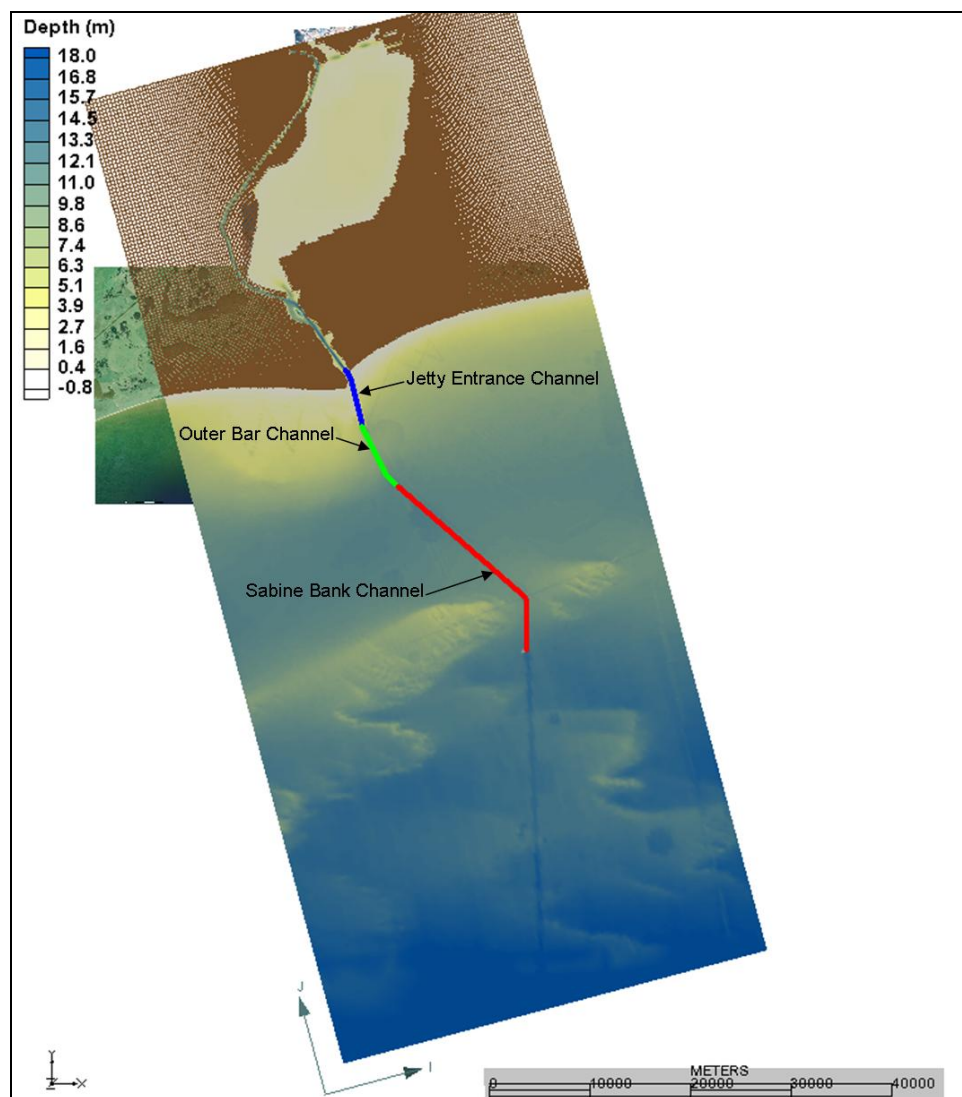
Figure 4. Sabine Pass channel reaches in study area.

Jetties

Jetty construction at SNWW was initiated in the 1880s using the method typical of that time period, consisting of multiple layers of fascine (willow) mats and stone ballast. The jetties were extended several times and eventually reached lengths of 25,270 ft (1920, East jetty) and 21,860 ft (1924–1928, West jetty). In discussion of the 1883-1900 construction history, Sargent and Bottin (1989) reported "subsidence of the jetties was significant, caused by a combination of scour and consolidation of the underlying soil and consolidation and deterioration of the fascine mats. Portions of the jetties (usually at their outer ends) were damaged or destroyed during passing storms, resulting in repair or reconstruction of these sections." Figures 5 and 6 show the construction history for each jetty.
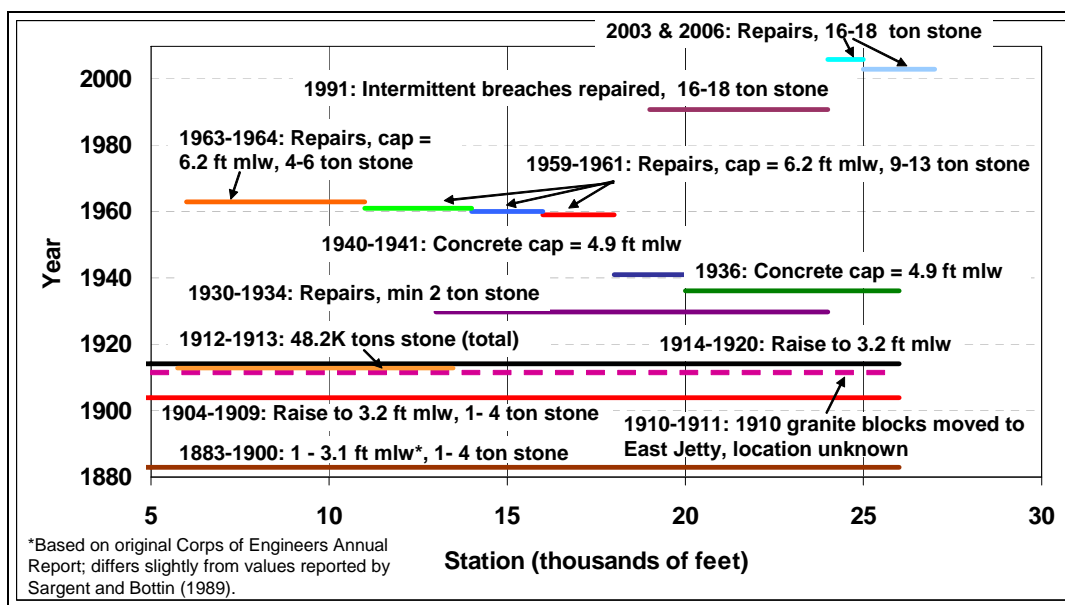
Figure 5. History of East jetty construction at SNWW.
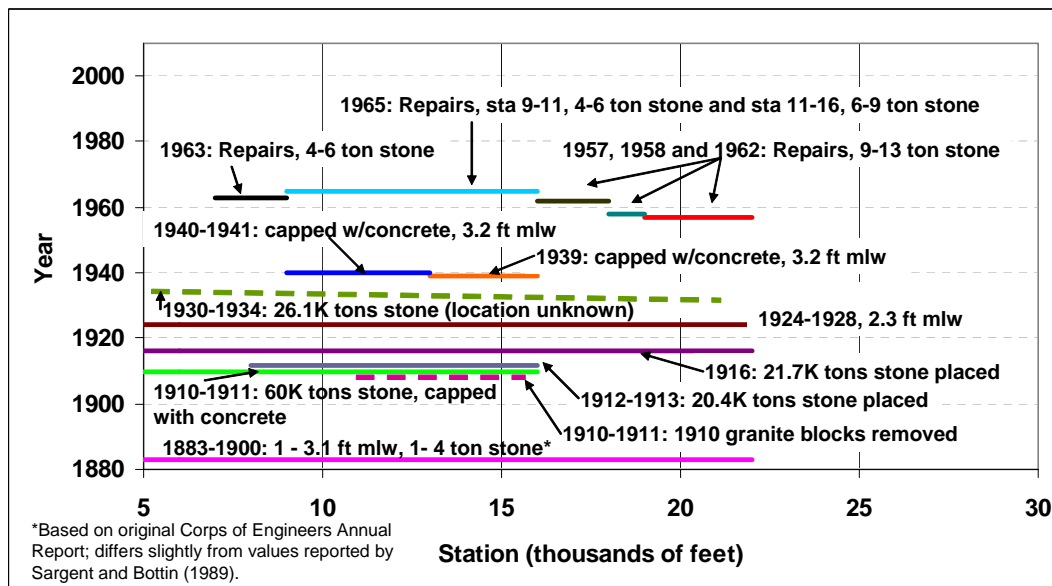
Figure 6. History of West jetty construction at SNWW.

A survey in 2003 indicated that the jetties presently have a variable crest elevation with two small boat access channels located approximately at 14,500 ft (East) and 16,000 ft (West) as measured from the shore (Figures 7 and 8). Figures 7 and 8 also show the greatest as-constructed jetty crest elevation for each site. The rehabilitation history for the East and West jetties is documented in Tables 2 and 3. Datums discussed in Tables 2 and 3 are reviewed in Chapter 3. (Note that the rehabilitation history does not provide complete details about every modification.
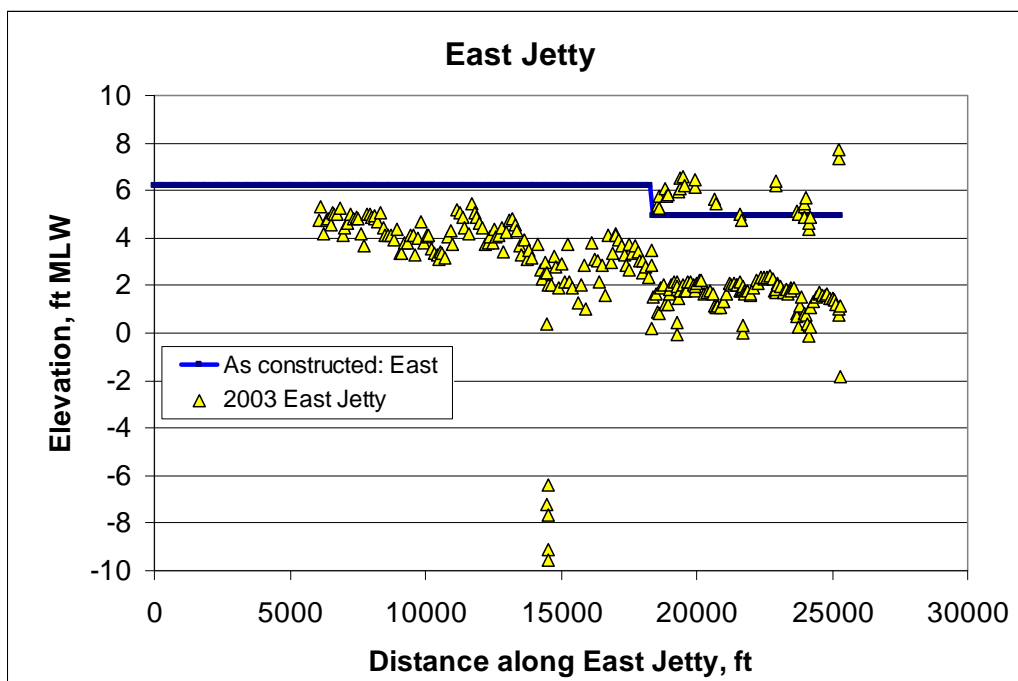
Figure 7. East jetty crest elevations in 2003.
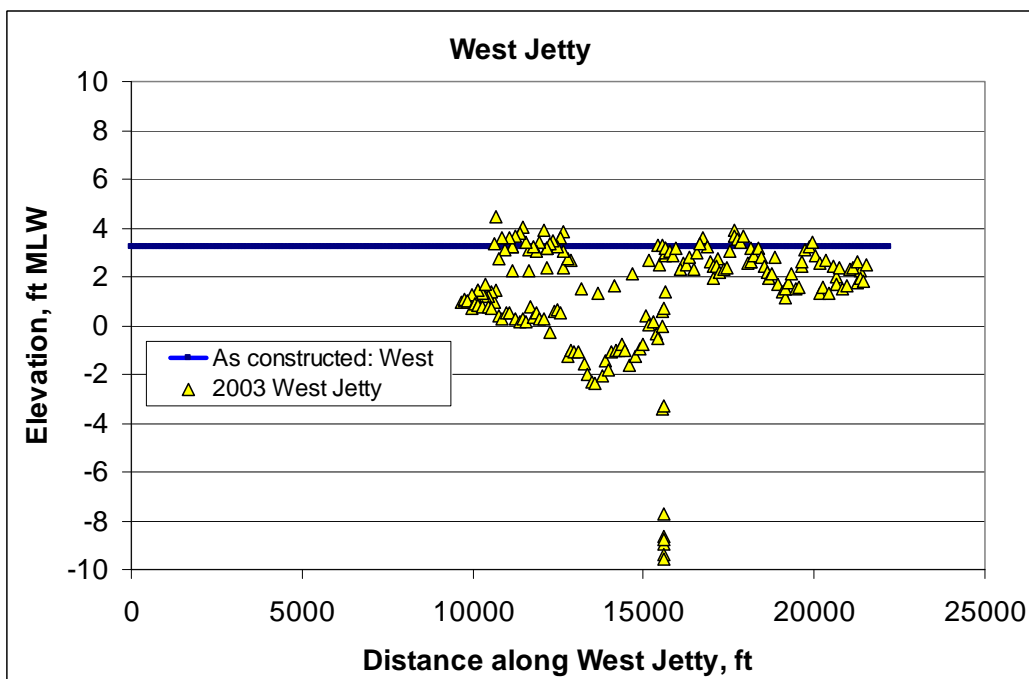
Figure 8. West jetty crest elevations in 2003.

Table 2. History of East jetty.

Date	Construction and Rehabilitation History [1]
1883-1900	Total length 25,000 ft. Elevation + 2 ft MHW (~2.54 ft MSL) for shoreward 21,820 ft. 1- to 4-ton stone used on cover layer
1904-1909	Repaired and raised up to +4 ft MLT (~2.7 ft MSL)
1910-1911	Granite blocks transferred from West jetty to East jetty. Placement location and elevation unknown.
1912-1913	Stone (48,200 tons) is placed from Sta.53+00 to Sta.138+50.
1914-1918	East jetty extended and raised to +5 ft MLG (~3.7 ft MSL) from Sta.0+00 to Sta.243+00.
1920	East jetty completed to project length of 25,270 ft (end Sta.253+10) and elevation +5 ft MLG (~3.7 ft MSL).
1930-1934	Repairs between Sta.129+15 and Sta.240+95. 67,700 tons of stone placed, with min weight of two tons.
1936	East jetty cap of concrete placed from Sta.196+44 to Sta.253+10 (end Station) at elevation of 5.7 ft MLT (+4.4 ft MSL) and crown width of 10 ft.
1940-1941	Concrete cap placed from Sta.183+57 to Sta.196+44 at elevation of +5.7 ft MLT (+4.4 ft MSL). Concrete cap has 10-ft width.
1959	Repairs made from Sta.164+50 to Sta.183+57. Elevation increased to +7 ft MLT (+5.7 ft MSL), crown width of 9 ft and side slopes of 1V:1.5H.
1960	Repairs made from Sta.141+50 to Sta.164+50. Elevation increased to +7 ft MLT (+5.7 ft MSL), crown width of 9 ft and side slopes of 1V:1.5H.
1961	Repairs made from Sta.110+00 to Sta.141+50. Elevation increased to +7 ft MLT (+5.7 ft MSL), crown width of 9 ft and side slopes of 1V:1.5H.
1963-1964	Additional core stone and cover stone (4-6 tons) are placed along existing core stone from Sta.60+00 to Sta.110+00. Elevation increased to +7 ft MLT (+5.7 ft MSL), crown width of 9 ft and side slopes of 1V:1.5H.
1991	Breaches on both sides of concrete cap from Sta.185+58 to Sta.241 +31 repaired using jetty stone (consisting of blanket stone(1/2"-200 lbs), core stone (200-4000 lbs), and cover stone (16-18 tons). Locations repaired were: Sta.185+58 to Sta186+27, Sta.188+44 to 189+51, Sta192+99 to Sta.193+96, Sta.194+81 to Sta.195+55, Sta.199+00 to Sta.199+66, Sta.206+51 to Sta.207+10, Sta.228+85 to Sta. 229+51, Sta.236+76 to Sta.237+90, Sta.239+59 to Sta.240+11 and Sta.240+76 to Sta.241+31.
2003	Filler core stone (200-1,000 lbs) and cover stone (16-18 tons) placed on both sides of jetty from Sta.249+60 to 253+10 (end of jetty). Toe protection (200-4,000 lbs) placed along east side of jetty.
2006	Repairs from Sta.239+60 to Sta.249+60 with core stone (200–1,100 lbs and 200–3,500 lbs) and cover stone 16-18 tons.

[1] Datums are discussed in Chapter 3. MHW = Mean High Water, MSL= Mean Sea Level, MLT = Mean Low Tide; MLG = Mean Low Gulf.

Table 3. History of West jetty.

Date	Construction and Rehabilitation History [1]
1883-1900	Total length 22,000 ft. Elevation + 2 ft MHW (~2.54 ft MSL) for shoreward 15,560 ft. 1- to 4-ton stone used on cover layer
1910-1911	Capped with concrete from landward end (at Sta.0+00) to Sta.157+80 and granite blocks (2-4 ton) transferred from West jetty to East jetty due to subsidence of West jetty to lighten weight. A total of 11,580 cu yd of concrete placed on jetty.
1912-1913	20,400 tons of stone are placed from Sta.80+00 to Sta.157+50.
1916	Repairs made with 21,700 tons of stone. 15,900 ft of jetty at +4 ft MLG (+2.7 ft MSL) and 2,200 ft of seaward end was at -4 ft MLG (-5.3 ft MSL).
1924-1928	Jetty raised and extended to its project length of 21,860 ft (end Sta.219+05) and elevation of +4 ft MLG (+2.7 ft MSL). 178,700 tons of stone placed.
1930-1934	Repairs made by adding 26,100 tons of stone on each side of concrete cap. Locations of repairs are unknown.
1939	Jetty capped with concrete, placed on existing cap to elevation of +4 ft MLT (+2.7 ft MSL) with 10-ft width. This was due to settlement between Sta.131+72 and Sta.157+80.
1940-1941	Due to further settlement between Sta.90+75 and Sta.131+72, concrete cap constructed over existing cap placed in 1911. Elevation is +4 ft MLT (2.7 ft MSL), with 10-ft width.
1957	Jetty repaired using 60,200 tons of stone from Sta.196+00 to 219+05 (end station). Cover stone weighed 9-13 tons each.
1958	Riprap and 9-13 ton cover stone placed from Sta.179+50 to Sta.196+00.
1962	Cover stone placed from Sta.157+80 to Sta.179+50.
1963	Additional core stone (25-200 lbs) and cover stone (4-6 tons) placed along existing concrete cap of jetty from Sta.68+00 to Sta.90+75. Core stone placed along concrete cap. Cover stone placed atop the core stone. to 1 ft MLT (-0.3 ft MSL)
1965	Placement of core stone (25-200 lbs) and cover stone from Sta.90+75 to Sta 157+80. 4-6 ton stone placed on both sides of jetty from Sta 90+75 to 110+50. 6-9 ton cover stone placed on both sides of jetty from Sta.110+50 to Sta 157+80. Core stone placed to elevation of 1 ft MLT (-0.3 ft MSL) and covered with cover stone.

[1] Datums are discussed in Chapter 3. MHW = Mean High Water, MSL= Mean Sea Level, MLT = Mean Low Tide; MLG = Mean Low Gulf.

For some rehabilitations, data are not available to describe where the stone was placed or do not indicate the elevation to which the structures were repaired. Thus, Figures 7 and 8 show some 2003 jetty crest elevations above the as-constructed elevation, implying that some repair must have occurred at these locations but is not noted in the rehabilitation history.)

To summarize, the SNWW jetties have a history of more than 100 years of construction and rehabilitation. A survey in 2003 indicates that most of the jetty is at an elevation below the highest as-constructed elevation. Reasons for the degradation of the structure are believed to be storm damage, disintegration of the original fascine mats, settlement and consolidation, and scour at the base of the structure resulting in slumping of stone (Sargent and Bottin 1989). In addition, regional subsidence has reduced the elevation of the jetties relative to mean water level.

Evaluation of present shoaling conditions

Sediment samples collected by Parchure et al. (2005) in the Sabine-Neches channel indicate the material dredged is mostly cohesive: 11 percent sand and 89 percent silt and clay in the jetty entrance channel reach, 4 percent sand and 95 percent silt and clay in the outer bar reach, and 24 percent and 76 percent silt and clay in the Sabine bank reach. Quantitative modeling of cohesive sediment transport requires site-specific information about the sediment characteristics, including percentage of fine-grained particles (especially clay), clay shape and type, salinity, sediment concentration, particle size distribution and organic material. Shoaling in the Sabine navigation channel was examined qualitatively in the present study. Dredging records between 1996 and 2005 and before- and after-dredge surveys between 2000 and 2007 were examined in this study to evaluate present shoaling.

Figures 9 and 10 show the volume dredged per foot over each station's reach for the jetty entrance channel, outer bar and Sabine bank reaches, respectively. The plots show that the most frequent dredging occurs in the outer bar reach with volumes generally higher than the other reaches. The jetty entrance channel was dredged only twice over the period.

The difference in depth between an after-dredge survey and the subsequent before-dredge survey was normalized to an annual rate (m/yr) to compare the shoaling rate between years and location. Figure 11 shows the annual shoaling rate between surveys in the jetty entrance channel between May and October 2000. Most locations in the channel required less than 0.5 m/yr of material dredged.
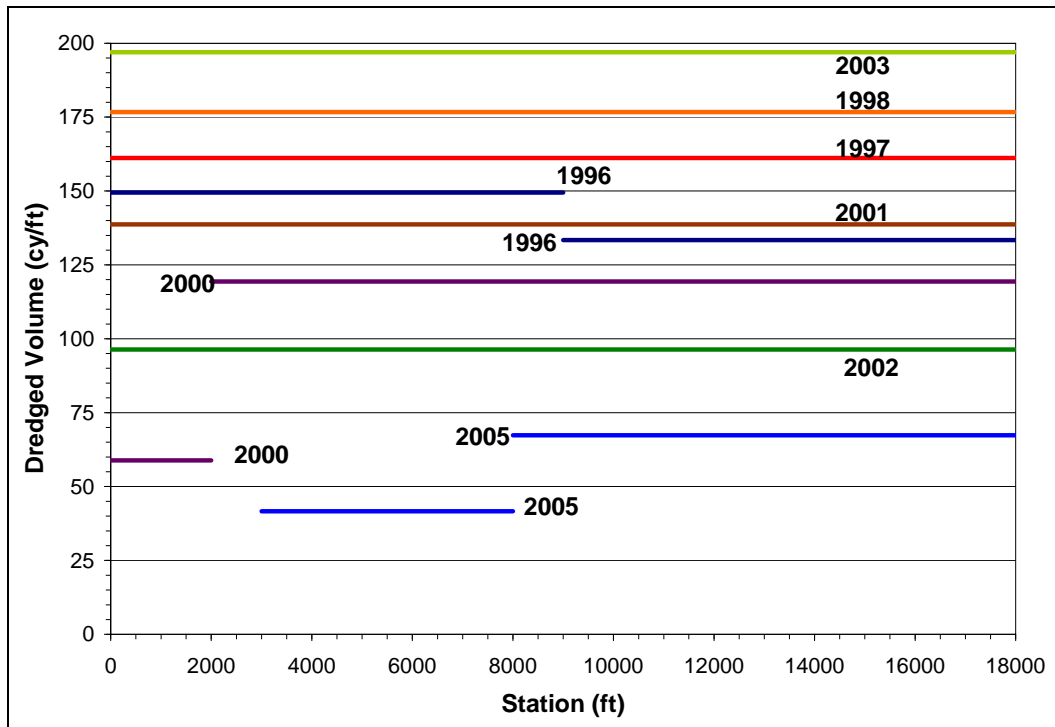
Figure 9. Dredged volume in outer bar channel.
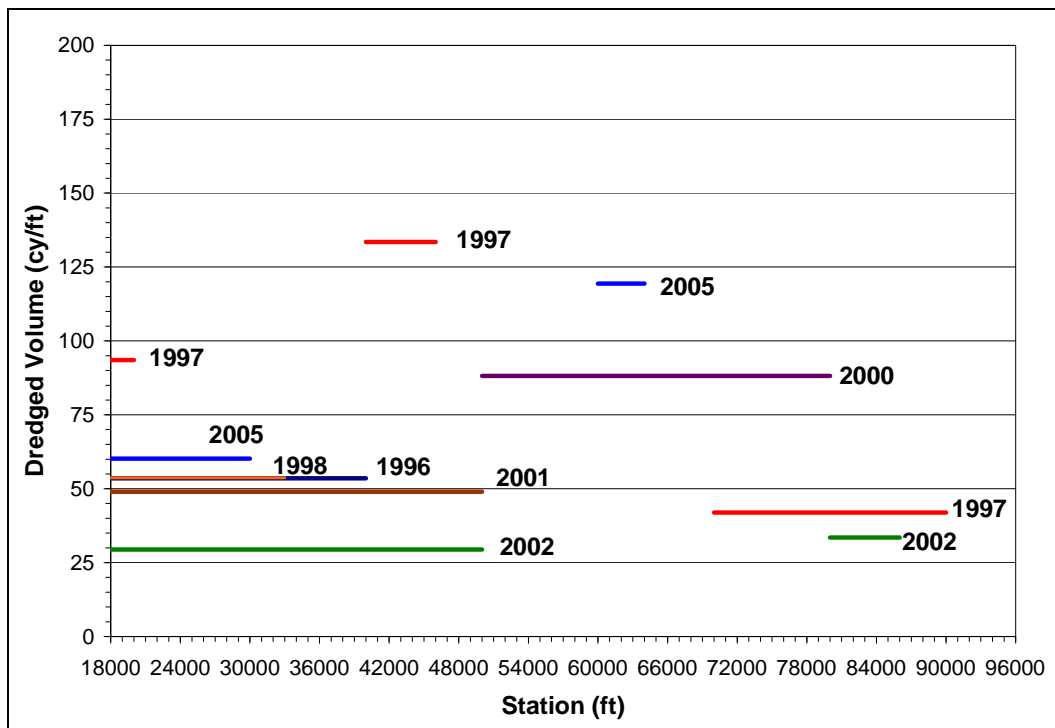
Figure 10. Dredged volume in Sabine bank channel.
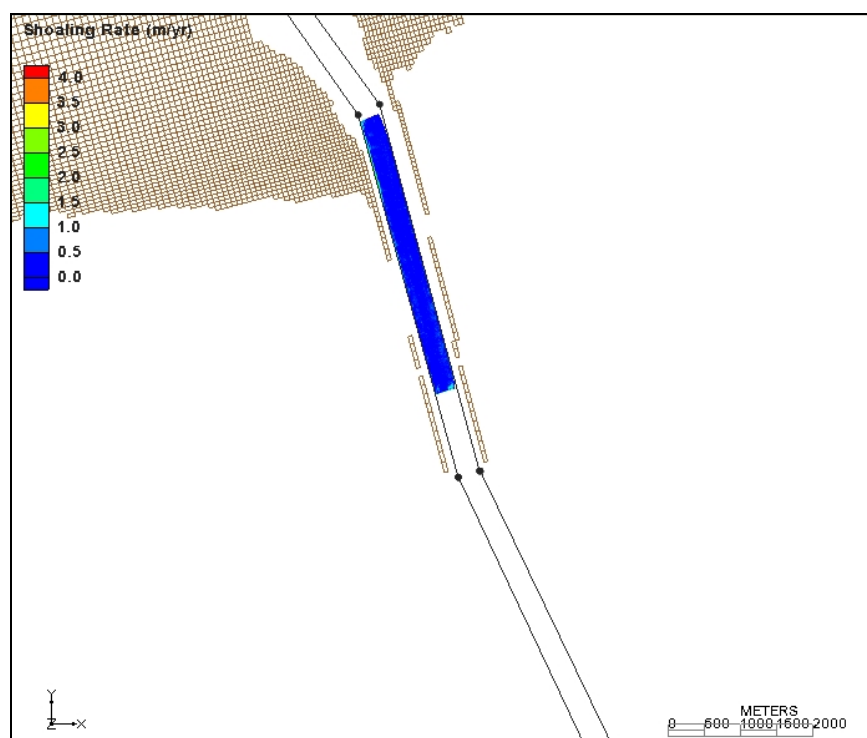
Figure 11. Shoaling rate in jetty channel, May–Oct 2000.

Depth differences in the outer bar are shown in Figures 12 through 16. The channel shoaling rate between May 2000 and May 2001 is shown in Figure 12. Several locations show shoaling rates greater than 2 m/yr and some locations exceed 3 m/yr. The shoaling rate between June 2001 and July 2002 is shown in Figure 13 and indicates many areas required dredging of more than 2 m/yr. Figure 14 shows that the shoaling rate was greater than 2 m/yr at most locations in the reach between the August 2002 and August 2003 surveys. A small portion of the outer bar was compared between the September 2003 and December 2004 surveys (Figure 15). The figure shows lower shoaling rates than the previous years; however, rates greater than 2 m/yr are evident. Figure 16 shows shoaling rates between 1 to 1.5 m/yr between January 2005 and December 2007.

At present the outer bar reach has required regular dredging, whereas the jetty entrance channel has not. Part of the evaluation of the proposed plans is to determine whether the resultant currents will decrease poten-tial channel shoaling in the outer bar reach, which would lead to less dredging required. Likewise, the plans will be evaluated for an increase in potential channel infilling in the jetty entrance channel and outer bar reaches, which may increase future dredging costs.
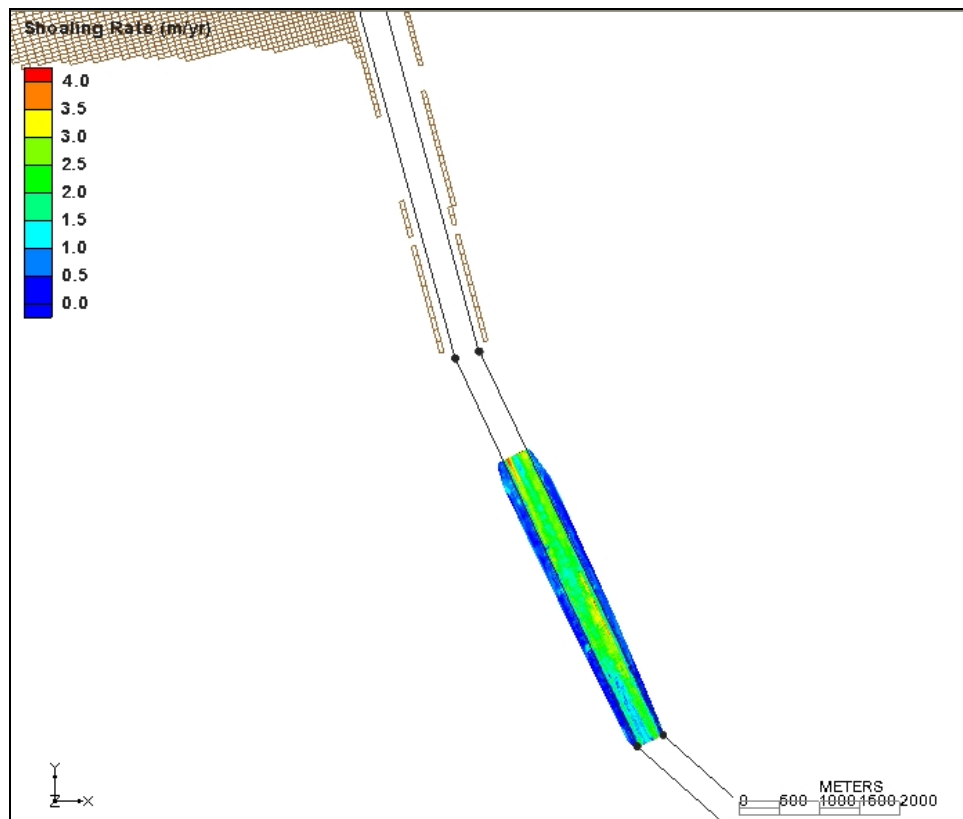
Figure 12. Shoaling rate in outer bar channel, May 2000-May 2001.
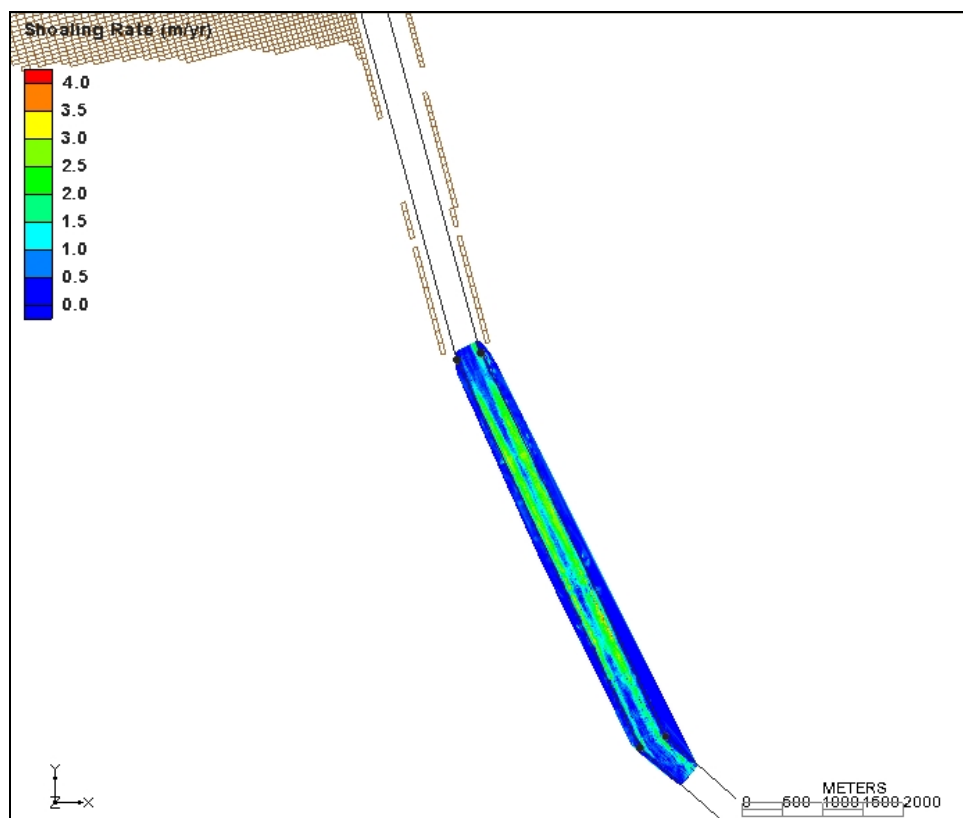
Figure 13. Shoaling rate in outer bar channel, June 2001–July 2002.
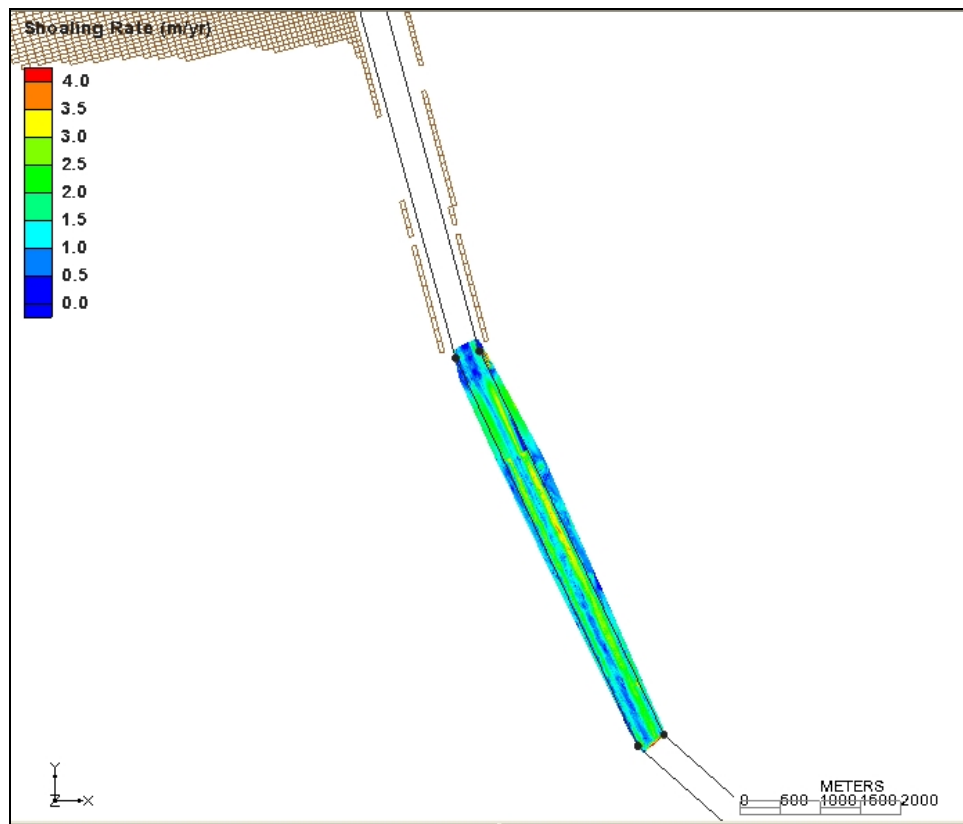
Figure 14. Shoaling rate in outer bar channel, Aug 2002–Aug 2003.
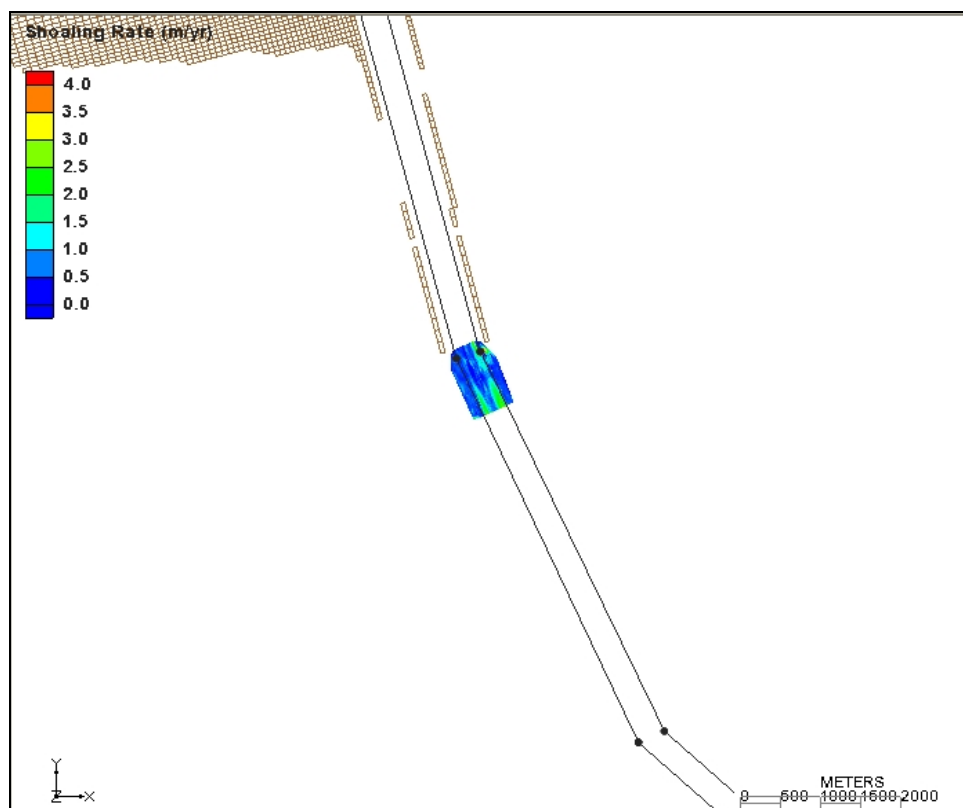
Figure 15. Shoaling rate in outer bar channel, Sep 2003–Dec 2004.
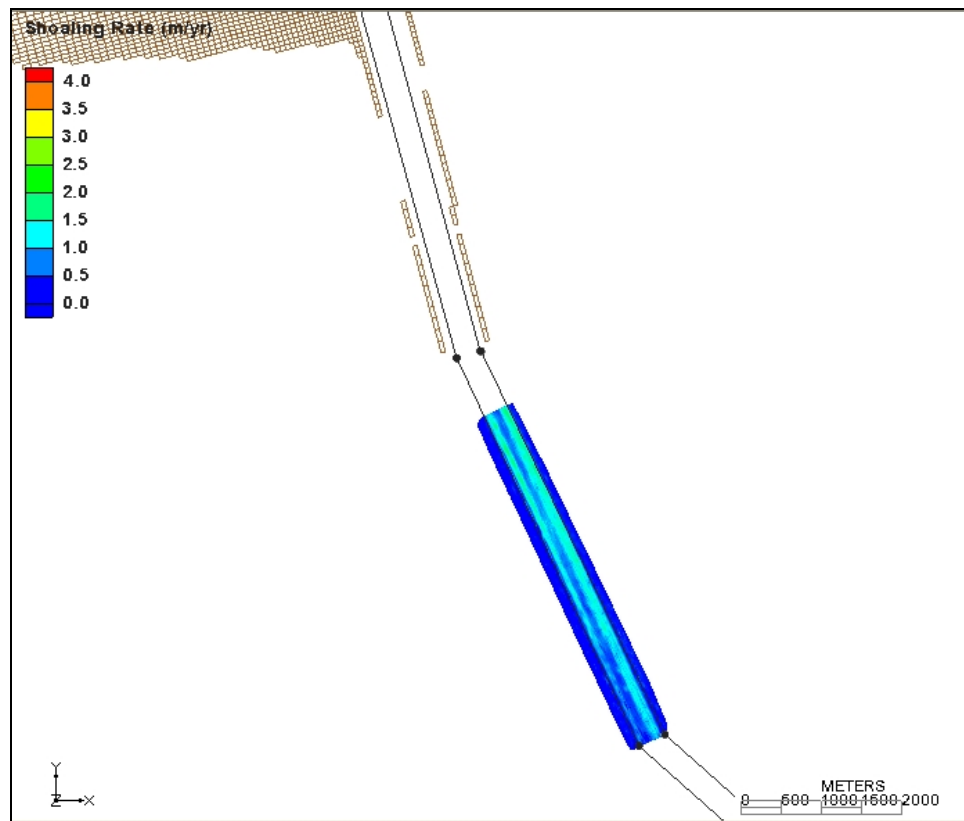
Figure 16. Shoaling rate in outer bar channel, Jan 2005–Dec 2007.

3 Waves and Water Levels

Overview

This chapter presents information to characterize typical waves and tides, datums for water level, salinity characteristics of the Sabine-Neches region, and hurricane climate and storm tracks. This chapter also includes information on hurricane data extracted from the Louisiana Coastal Protection and Restoration study, and concludes with a discussion of sea level rise in the area.

Water levels

Tides and tidal datums

All elevations used in the study were adjusted to the MLW datum. Tidal benchmark information from National Oceanographic and Atmospheric Administration (NOAA) (2005) was applied in converting datums (see Figure 17).

Sabine Pass

Tide Gage

Primary Bench Mark
0570 A 1985

MHHW=Mean Higher High Water
MHW= Mean High Water
MSL=Mean Sea Level
MTL=Mean Tide Level
NAVD88=North American Vertical Datum 1988
MLW = Mean Low Water
MLLW=Mean Lower Low Water
MLT=Mean Low Tide

MHHW=+1.20 ft
MHW=+1.09 ft
MSL=+0.56 ft
MTL=+0.55 ft
NAVD88=+0.013 ft
MLW=0 ft
MLLW= -0.41 ft=MLG
MLT= -0.77 ft

Epoch Used
1983-2001   09/19/2007 00:00 - 09/19/2007 00:12

0.000 STND

Figure 17. Relationship between tidal datums at Sabine Pass, referenced to MLW (adapted from NOAA 2005).

Tides in the Gulf of Mexico near Sabine Pass have maximum monthly ranges occurring at summer and winter solstices (June and December) and minimum ranges at solar equinoxes (September and March). However, seasonal tidal range is not in phase with water level that responds to wind and steric effects. Onshore winds and warm, less dense water produce maximum levels in September and minimum levels in February, when water is coldest (Mason 1981).

Tides near Sabine Pass entrance are mixed, with a strong diurnal component. The diurnal range (between mean higher high water and mean lower low water) is 1.61 ft, and the mean range (between mean high water and mean low water) is 1.09 ft. These tides were measured at the Sabine Pass North, TX, tide station (NOAA 2008a) located inside the jetties near the west shoreline. The tide range within Sabine Lake is less than in the pass, about 50-60 percent less, and responds to other meteorological effects of wind and rainfall (Mason 1981).

Freshwater inflow and salinity

The Sabine and Neches Rivers provide freshwater flow into the bay at an average rate of 14,650 cubic feet per second, and during storms flows may exceed 200,000 cubic feet per second (Mason 1981). Salinity in the system can vary from 34 parts per thousand (ppt) in the open Gulf to 0 ppt in the upper reaches of the river channels emptying into Sabine Lake, which itself is a brackish water estuary varying from 15 ppt at its southern connection with Sabine Pass to 0 ppt, at times, at its northern end, where freshwater enters (USAED Galveston, 2007).

Waves

Typical waves and winds

The Sabine Pass near shore waves and winds were examined using the Wave Information Studies (WIS) database (USACE 2009c). Station 92 of the WIS database was selected to be representative for the wave climate near Sabine Pass. Wave and wind roses at this station are shown in Figure 18 based on twenty years (1980–1999) of hindcasting. Predominant winds and waves are from the southeast. The mean significant wave height at Station 92 is 3.0 ft with a standard deviation of 1.6 ft. Mean wave period is 5.0 sec with a standard deviation of 1.6 sec. The maximum monthly average wave height of 3.6 ft occurs in March and April, and the minimum
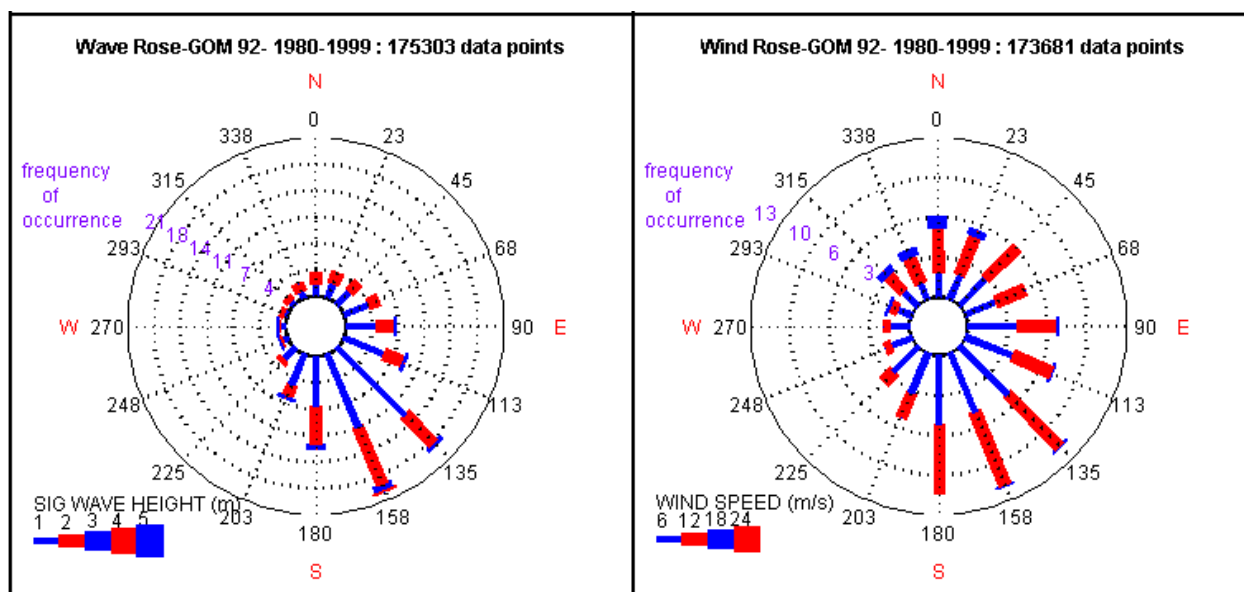
Figure 18. Wave and wind roses at WIS Station 92 (measurements are in meters for waves and m/s for wind speed, and compass points are direction from).

monthly average is 2.3 ft in August. NOAA National Data Buoy Center's (NDBC) buoy 42035, in the Gulf off Galveston, in deeper water than the WIS gauge 92, indicates a similar mean wave height of 3.2 ft. King (2007) also verifies the excellent agreement between the WIS hindcast results and buoy measurements.

Storm waves

The WIS database was also used to perform an extremal significant wave height analysis with the Coastal Engineering Data Analysis System (CEDAS) group of programs (USACE 1992). Station 92, in 36 ft depth of water, was selected for wave height information. Input data consisted of the monthly maximum significant wave height for the twenty-year record of the hindcast wave information. From this analysis, the best-fit distribution (correlation coefficient = 0.9973) was a Fisher-Tippett Type 1 distribution. Figure 19 shows the wave distribution, and Table 4 shows return periods for 95 percent confidence interval (lower bound-upper bound) wave heights. This wave information was used in the Monte-Carlo structure stability analysis discussed in Chapter 5.
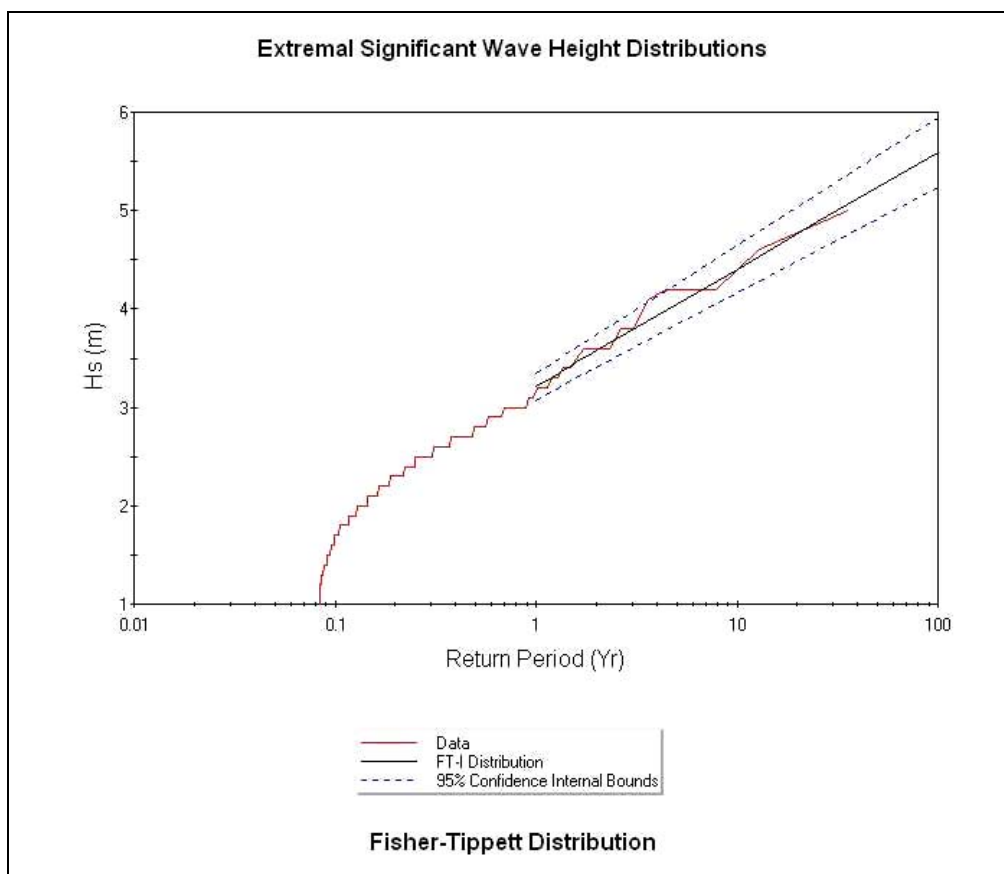
Figure 19. Extremal significant wave height distribution at WIS gage 92.

Table 4. Return period (yr) from extremal analysis for WIS Gauge 92.

Return period (yrs)	Lower-bound wave height, ft	Upper-bound wave height, ft
5	12.6	14.0
10	13.7	15.3
25	15.1	16.9
50	16.1	18.2
100	17.2	19.5

The Fisher-Tippett Type 1 distribution is described mathematically as:

$$F(H_s) = e(-e^{(-(Hs-B)/A)}) \tag{1}$$

with H_s the significant wave height in feet, and from this analysis, $A = 1.682$ ft, and $B = 6.414$ ft. With a random number equal to $F(H_s)$ and solving for H_s, the following expression was used to represent random storm waves based on the developed distribution:

$$H_s = 1.682[-\ln(-\ln RN)] + 6.414 \qquad (2)$$

with RN = random number. A correlation analysis of wave period for these storm waves (with R^2 = 0.65) resulted in the relationship:

$$T = 1.7655 * (H_s)^{0.7319} \qquad (3)$$

with T = significant wave period, in seconds. These relationships were used in the Monte Carlo simulation for structure stability.

Tropical storms

Storm tracks

The Gulf Coast region has been an active zone for tropical storms approaching from the east, usually developing off the West African coast. Figure 20 shows hurricane tracks crossing the region at and near Sabine Pass which have occurred for a little over the last 120 years. With the devastation in recent years, especially by Hurricane Katrina in the New Orleans area, special studies have evolved to help produce greater understanding of the intensity and frequency of hurricanes approaching the Louisiana coast. One such study was begun after Hurricane Katrina and is known as Louisiana Coastal Protection and Restoration, or LACPR (USACE New Orleans District, 2009). This study covered the entire coast of Louisiana and produced a synthetic set of hurricanes representative of intensity and frequency of hurricanes approaching the Louisiana coast.

Surge elevations and waves

LACPR used the ADvanced CIRCulation (ADCIRC) hydrodynamic model (Leuttich et al. 1992) to estimate storm surge. ADCIRC is a finite-element hydrodynamic circulation numerical model for the simulation of water level and current over an unstructured gridded domain that can simulate tide-, wind-, and wave-driven circulation in coastal waters as well as hurricane storm surge and flooding. Imposing the wind and atmospheric pressure fields, the ADCIRC model can replicate tide-induced and storm-surge water levels and currents. In two dimensions, the model is formulated with the depth-averaged shallow-water equations for conservation of mass and momentum.
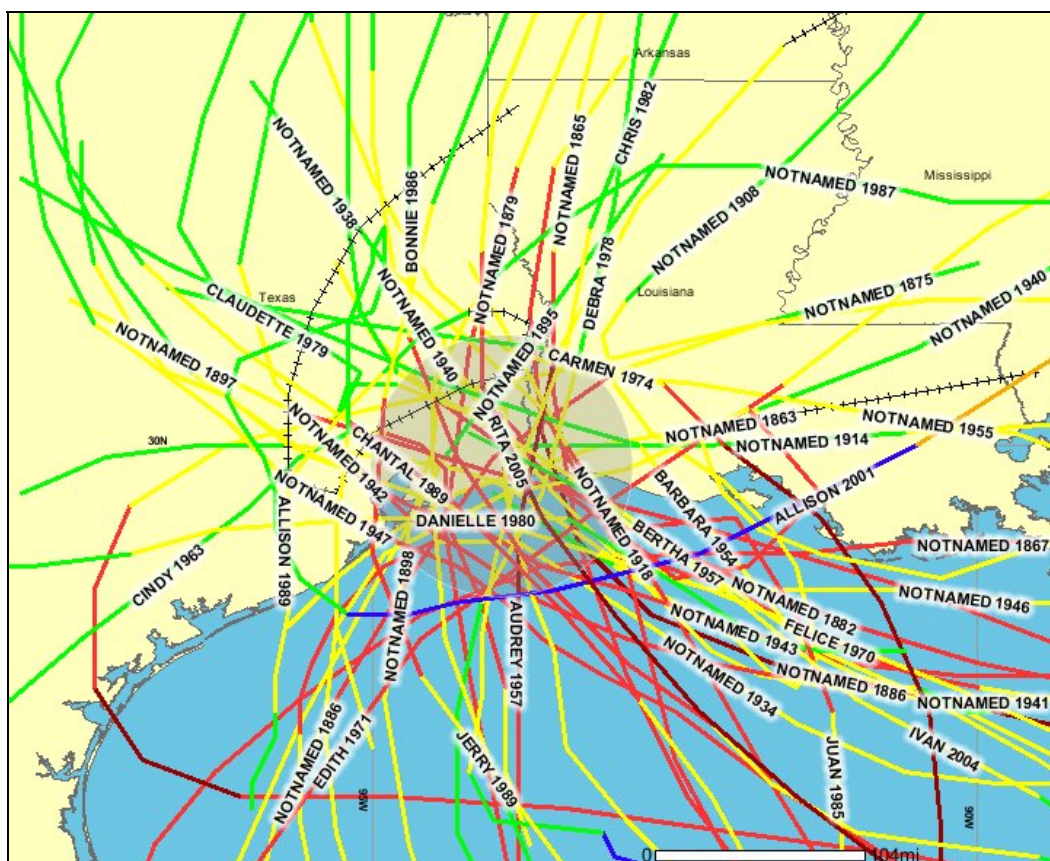
Figure 20. Hurricane tracks crossing the Texas and Louisiana coast for over the last 120 years near Sabine Pass (NOAA 2009).

The generation of the wave field and directional wave spectra for the various hurricane storm tracks is based on the implementation of a third generation discrete spectral wave model called WAM (Komen et al. 1994). A nested grid approach was applied for the offshore wave simulations. This effectively reduces the computational demand and maximizes the use of higher resolution wind estimates in the coastal area. The purpose of the offshore wave simulations is to supply input for the near shore wave modeling effort supported by STWAVE (Smith et al. 2001).

Information derived for Sabine-Neches

The LACPR included a numerical modeling effort that used a parametric study of hurricane surge and associated wave heights. A part of the numerical simulations focused on the west coast of Louisiana, where a suite of hurricane scenarios were developed to provide storm surge water elevation, return period, and storm wave height and period, associated with each hurricane simulated. Figure 21 shows all the tracks that were simulated. Of these tracks, the 152 westernmost storms comprised the data set which was used for this study.
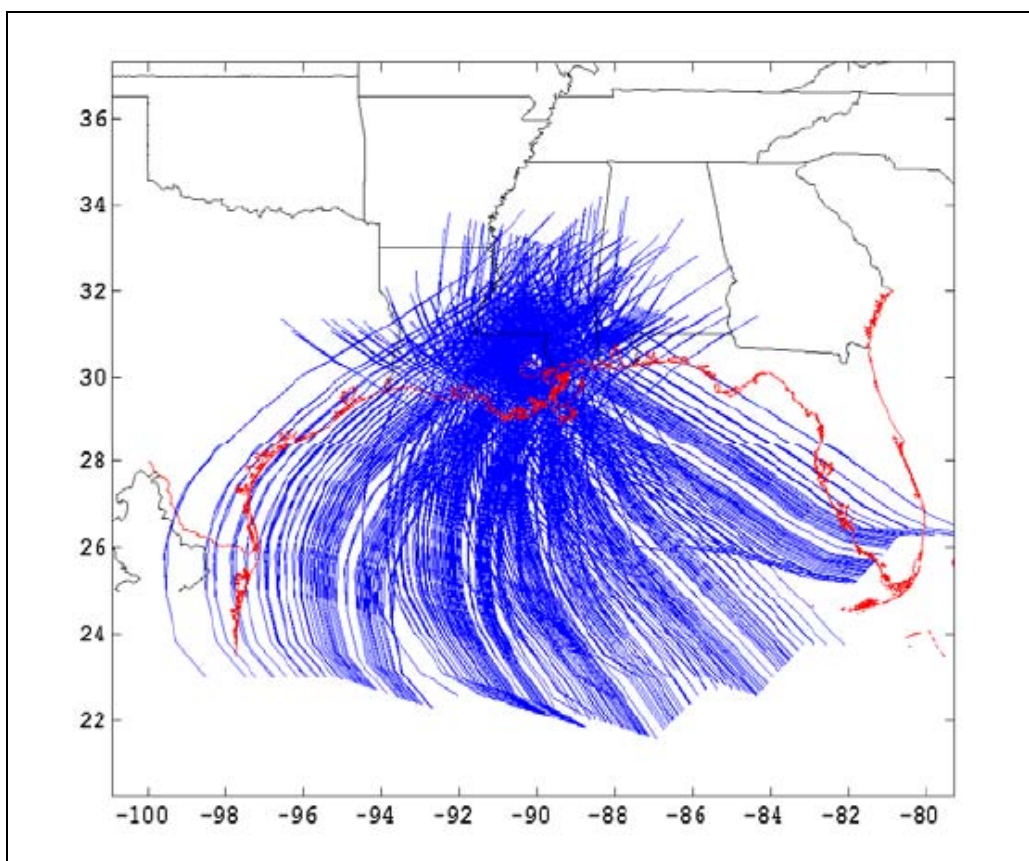
Figure 21. LACPR hurricane paths studied to determine surge and wave height along
the Louisiana coast.

Figure 22 is derived from results of the maximum wave heights, as pre-
dicted by STWAVE simulations (Smith 2007), with wave heights up to
18 feet near the coast but are reduced inland by bottom friction. Figure 23
shows maximum surge level. It is important to note that these heights are
not stochastic representations of a certain return period but are maximum
values for the 152 storms set at each grid point, or data collection location.

To use this data for the Monte Carlo structure stability analysis, return
periods for surge height (Figure 24) were determined for two grid points
near Sabine Pass where surge data had been saved. The two locations are
on the shoreline near the Sabine Pass and are representative of the open
coast. Surges at locations further shoreward are typically reduced due to
friction in the wetland areas and submerged land areas. Wave height and
surge level data were pulled from the full set of data at the locations shown
in Figure 25. Node location 5, at the tips of the jetties, provided the best
location to extract wave information with respect to the jetties stability
analysis. The use of these data for jetty structure analysis is discussed in
Chapter 5.
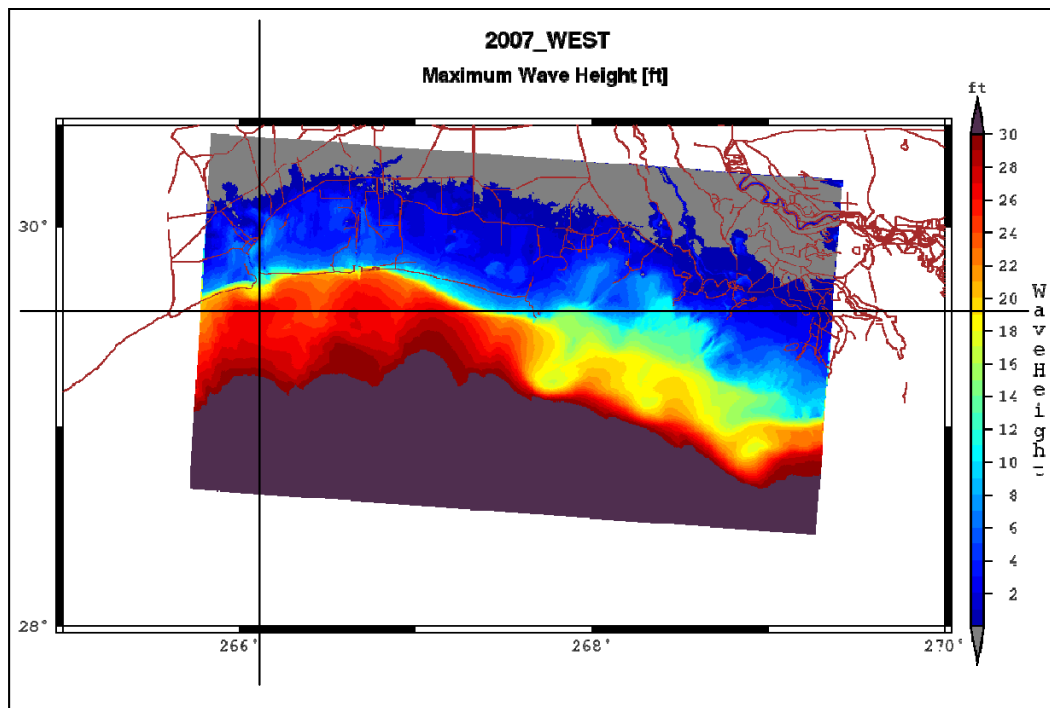
Figure 22. Maximum wave height results for 152 west LACPR simulations.
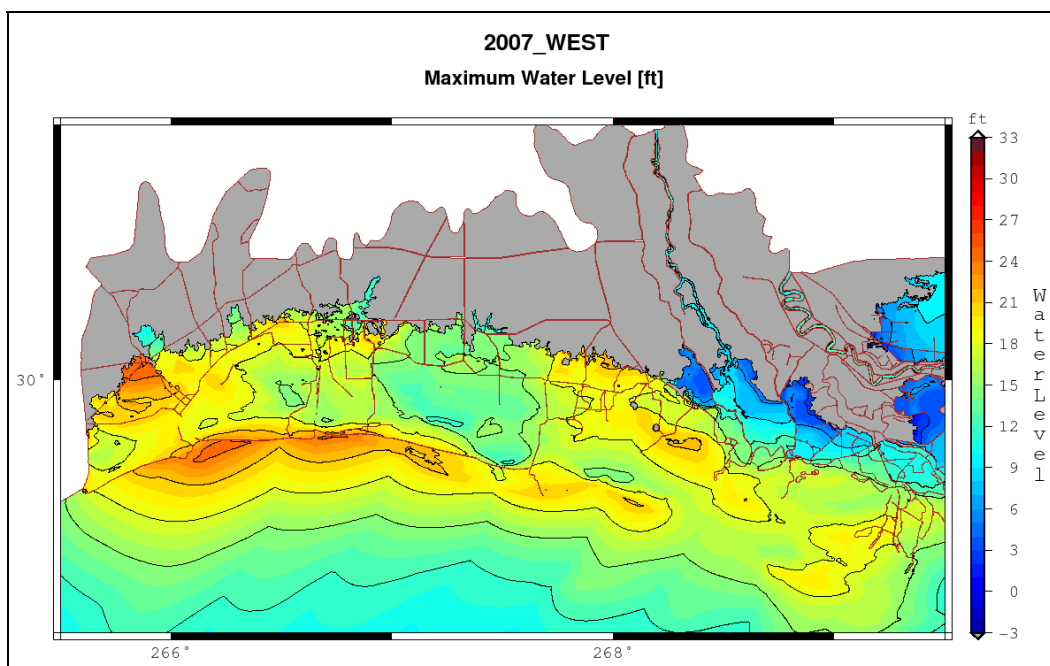
Figure 23. Maximum surge levels recorded for the 152 west LACPR storms.
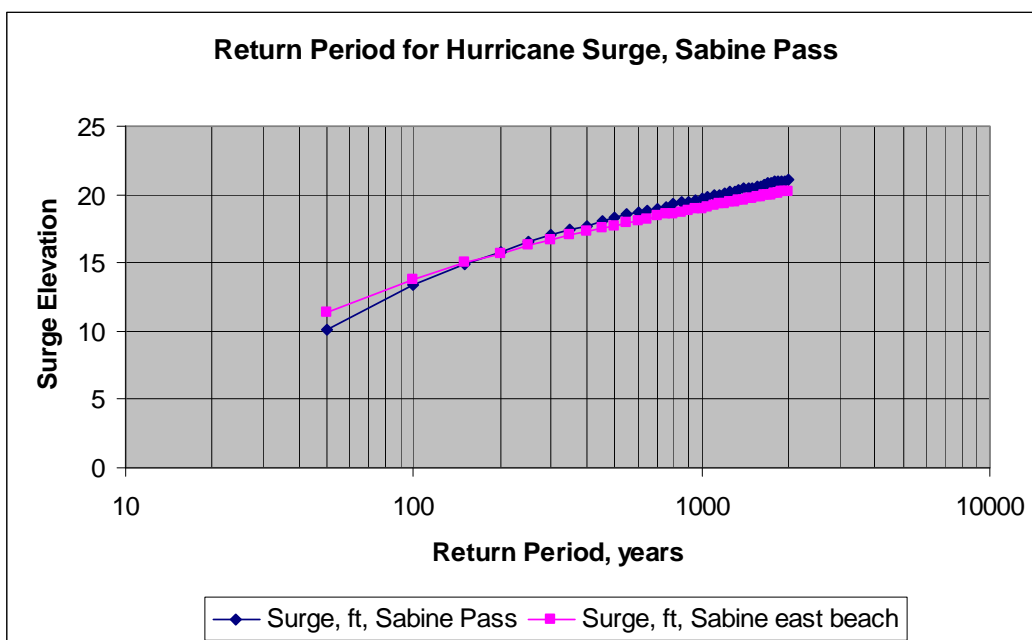
Figure 24. Return period for hurricane surge, in ft.
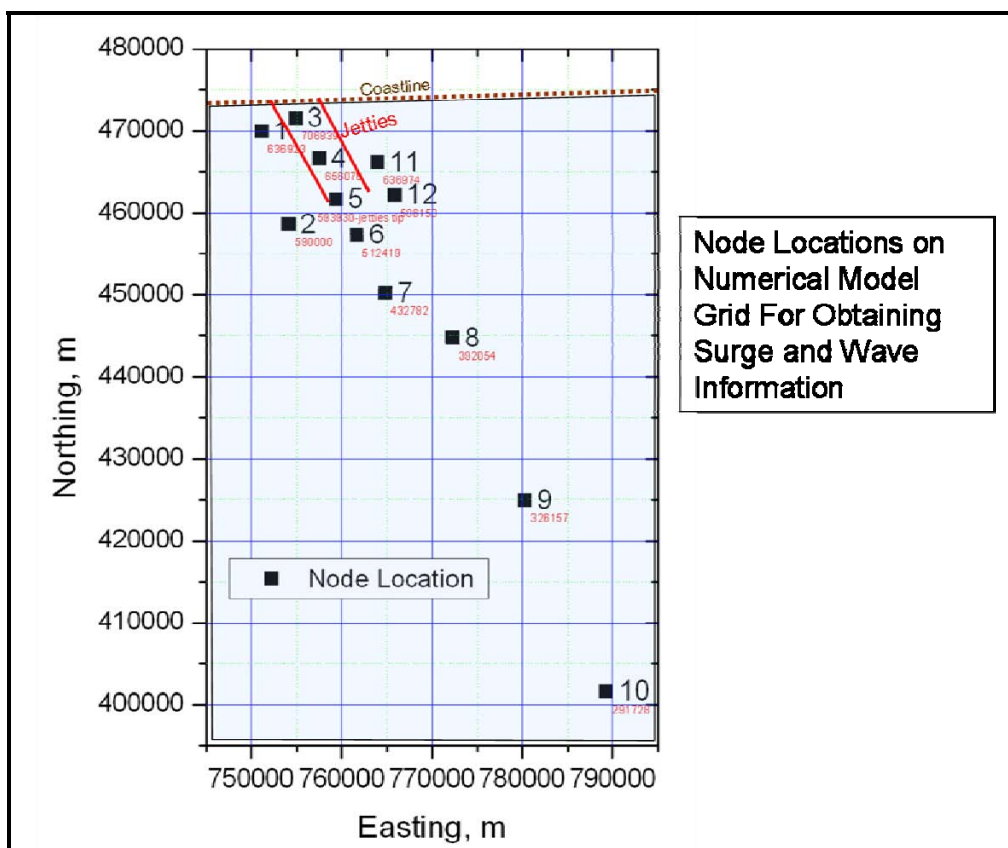
Figure 25. Node locations for extracting wave and surge data from LACPR files.

An example of the information derived from a hurricane simulation is shown below in Figure 26. In that figure, top left is a contour map of maximum surge elevation, top right shows surge elevation at selected node points, bottom left shows wave period at selected node locations, and bottom right shows wave height at selected node locations. Not shown is a wave direction plot.
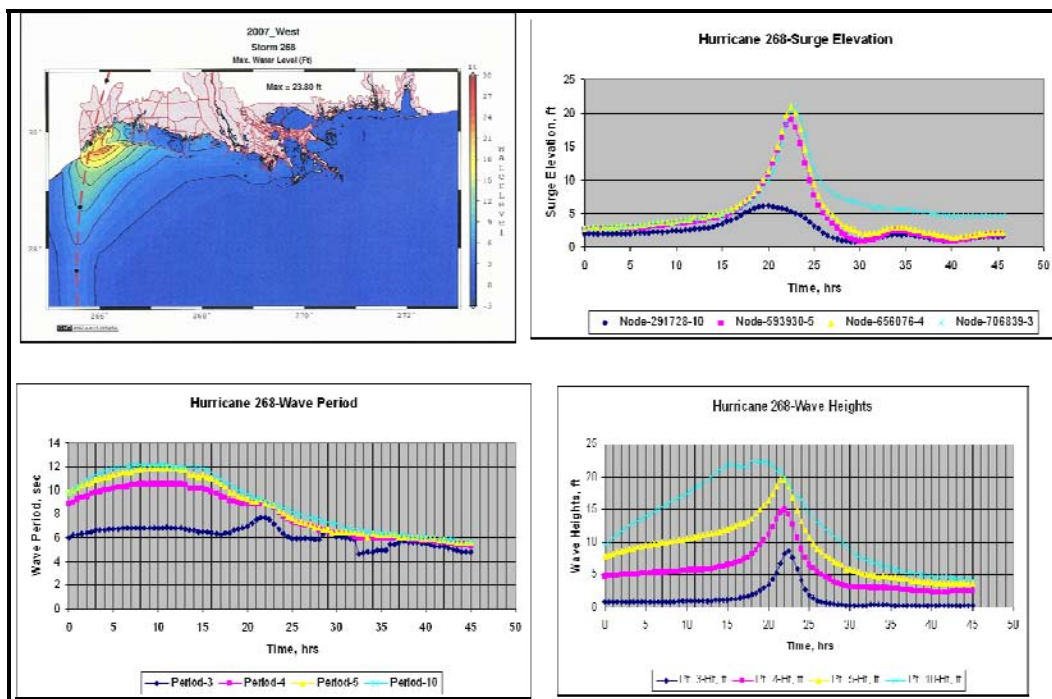
Figure 26. Sample output for Storm 268 from LACPR data set near Sabine Pass.

To use the data set of 152 hurricanes to perform a Monte Carlo analysis of jetty structure stability, the surge elevation was determined directly by the return period information at the node selected by LACPR (Figure 24). However, the wave information at this node was not relevant to waves at the structure, since the water depth was shallow. As a result, wave heights at Node 5 were correlated to the surge measurement at the LACPR Sabine Pass node where return period was determined. This resulted in a relationship for wave height as a function of return period. Wave period was then defined by (Bretschneider 1966):

$$T = 2.13\sqrt{H_s} \tag{4}$$

where T is wave period, in seconds, and H_s is the maximum significant wave height, in ft.

Some information is presented to characterize the information that was extracted from the LACPR with regard to Sabine Pass. Figure 27 shows maximum and minimum surge elevations at the jetty tips with respect to landfall location distance from Sabine Pass. Of particular interest were the negative water levels that can occur during a part of the hurricane approach. This was of interest with regard to the structure being attacked by wave action. It was found that wave conditions were reduced relative to the maximum height of a particular storm during instances of negative surge and wave approach angle relative to the structure was near zero degrees during a transition in wave direction. Figure 28 shows these conditions for Storm 227.
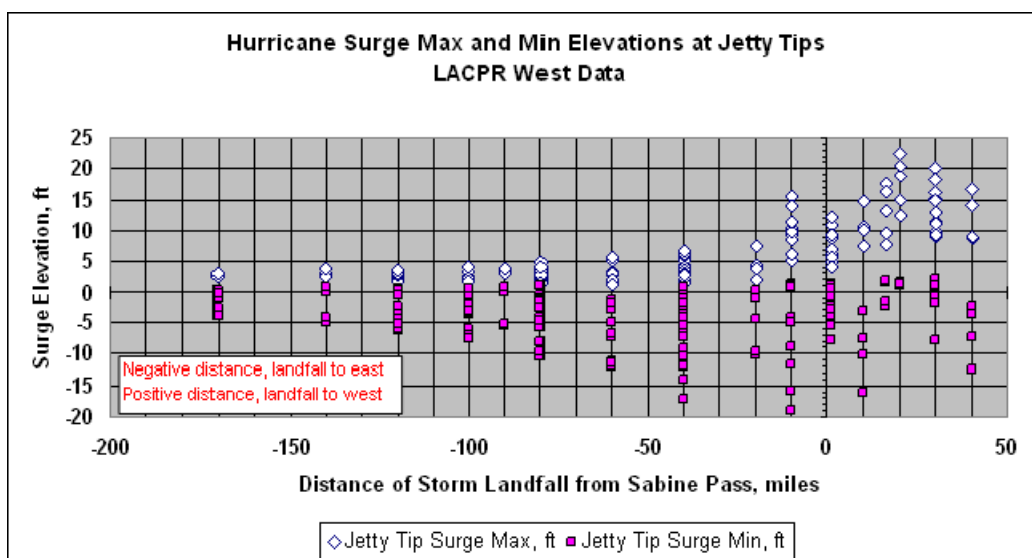
Figure 27. Surge max and min elevations at jetty tip (Point 5).
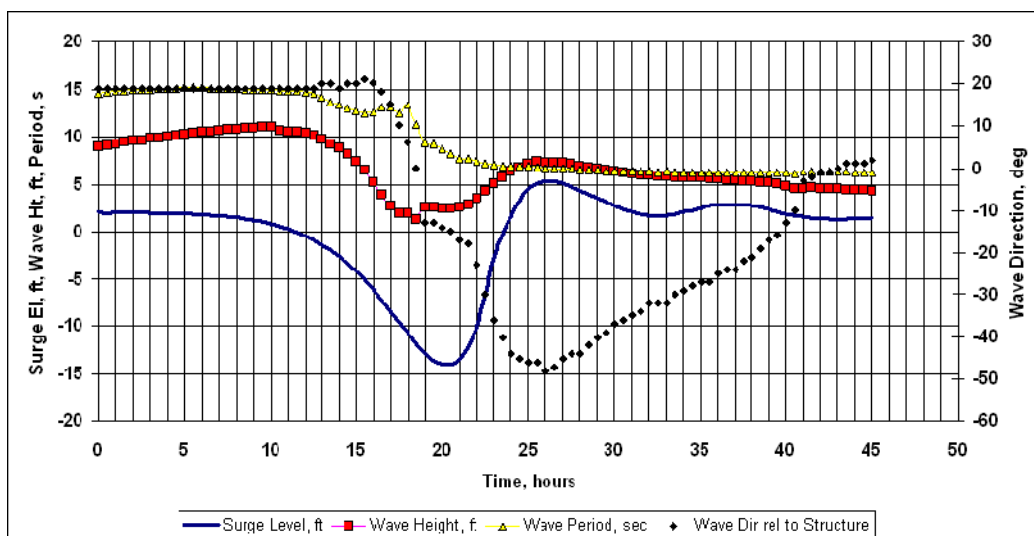
Figure 28. Storm 227, illustrating negative surge elevation at jetty tips.

Figure 29 shows a plot of the surge level at the jetty tip, Node location 5 (left y axis), and the return period (right y axis) for each storm are simulated. The x-axis is the storm number (LA West's 152 storms represented by identification numbers 201-362). The two data sets follow each other closely. This illustrates a direct correlation between the LACPR calculated return period at the shore gauge at Sabine Pass (Figure 29) and the Node 5 data. Figure 30 shows maximum surge level and maximum wave height from Node 5.
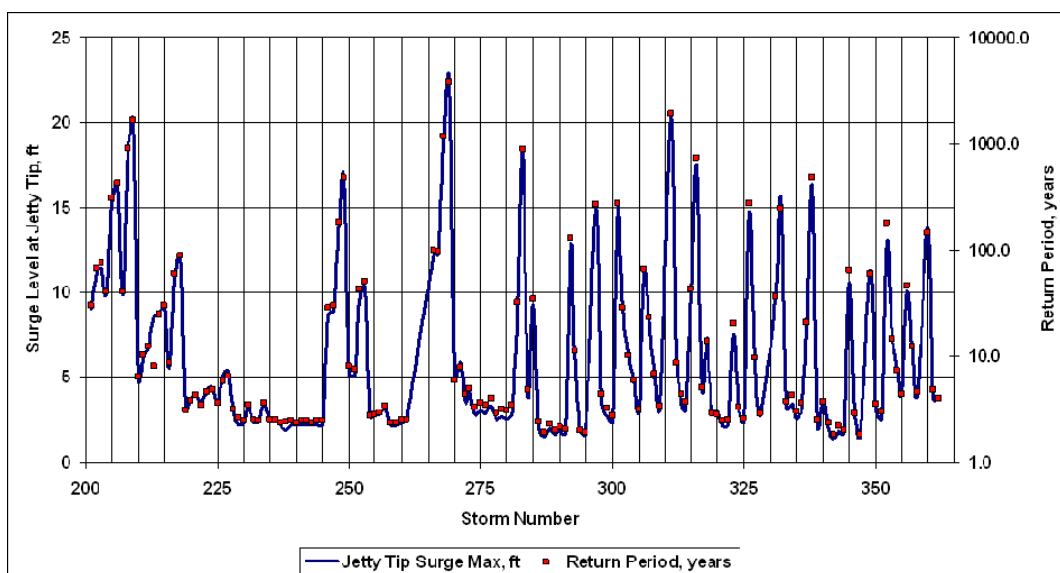
Figure 29. Maximum surge and return period at jetty tip for LACPR hurricanes.
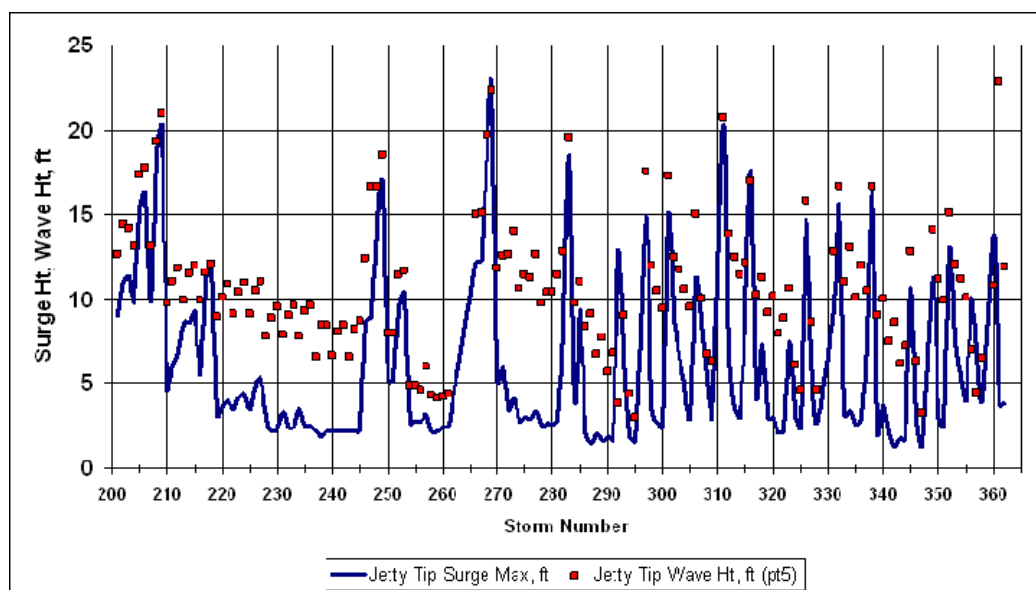
Figure 30. Maximum surge and wave height at jetty tip for LACPR hurricanes.

Figure 31 shows the variation in wave height with distance from hurricane landfall. Negative distance along the x-axis represents hurricanes land-falling to the east of Sabine Pass, and wave heights are typically less than those landfalling to west of Sabine Pass, except for one outlier that is for the strongest storm in the data set. Storms making landfall to the west produce the largest waves due to the counterclockwise circulation of the hurricane wind field.
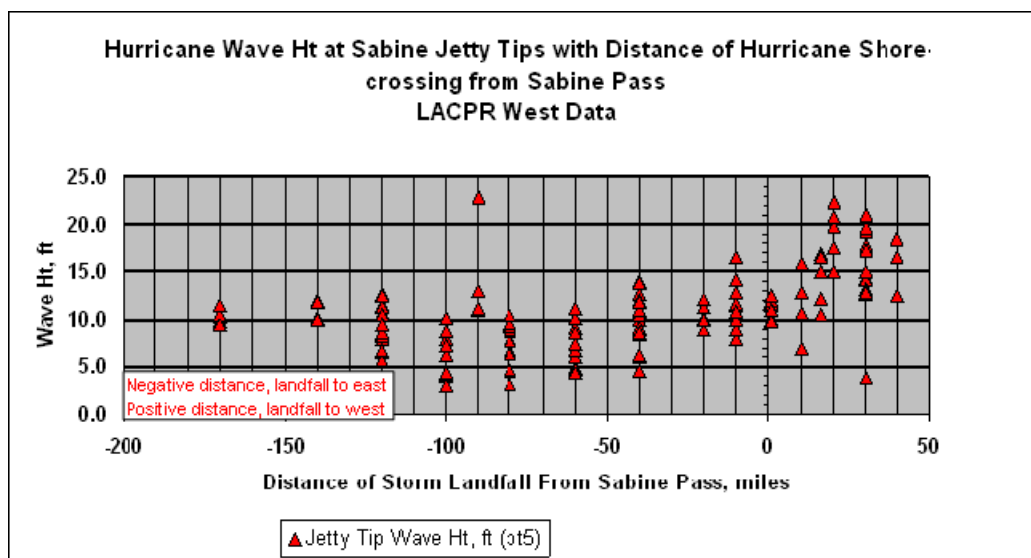
Figure 31. Maximum wave height variation at jetty tip with distance of hurricane landfall distance from Sabine Pass.

Relative sea level rise

Past and future rates of relative sea level rise affecting the jetties at Sabine Pass have contributions from regional subsidence, consolidation of the substrate beneath the jetties as a function of the weight of the structures, and eustatic changes in sea level. At the time of this study, the Corps recommended the National Research Council's (NRC 1987) method to estimate relative sea level change,

$$S(t) = \left(0.0012 + \frac{M}{1000}\right)t + bt^2 \tag{5}$$

in which S is the change in sea level over a given time, t; M is the local subsidence given in mm/year, which the NRC estimates as 12 mm/year (3.9 ft/century) for Sabine Pass based on tide records; and b represents the eustatic component, with one value given for each of three eustatic sea

level rise scenarios. Because the NRC's *M* value is within the range presented by Shinkle and Dokka (2004) (approximately the midpoint of their range), it was adopted and applied herein. At the time these calculations were made, Corps of Engineers guidance was to use the historic rate of relative sea level as a low estimate of future changes in sea level, and apply calculations from the NRC to bracket the upper range in future relative sea level rise (Table 5).

Table 5. Projected change in sea level at Sabine Pass over 50 years (from 2010 to 2060).

Extrapolate Historical Rate (Figure 32)	Scenario	NRC (1987)	USACE (2009a)
		S, ft (eustatic)	
0.93 + 0.2 ft	I	2.4[1] (0.4 eustatic)	1.3[4] (0.6 eustatic)
	II	2.7[2] (0.7 eustatic)	1.9[5] (1.3 eustatic)
	III	3.0[3] (1.1 eustatic)	2.5[6] (1.9 eustatic)

[1] M = 12 mm/year = 3.9 ft/century; b=9.186 x 10^{-5} ft/yr^2.

[2] M = 12 mm/year = 3.9 ft/century; b=2.165 x 10^{-4} ft/yr^2.

[3] M = 12 mm/year = 3.9 ft/century; b=3.445 x 10^{-4} ft/yr^2.

[4] M = 5.7 mm/year = 1.9 ft/century; b=7.774 x 10^{-5} ft/yr^2.

[5] M = 5.7 mm/year = 1.9 ft/century; b=2.034 x 10^{-4} ft/yr^2.

[6] M = 5.7 mm/year = 1.9 ft/century; b=3.297 x 10^{-4} ft/yr^2.

Since these sea level change calculations were made for the study, new guidance was released for the Corps of Engineers (USACE 2009a). This new guidance updated the NRC method with recent eustatic sea level change estimates and applies measured local sea level change at the project site, as shown in Figure 32, for Sabine Pass. For comparison, calculations based on the USACE (2009a) guidance are also included herein.

Table 5 shows calculations of sea level rise through extrapolation of the historical rate, application of the NRC (1987) method, and recent USACE (2009a) guidance. For this study, a relative sea level rise of 2.7 ft over the next 50 years was applied. This value approximates Scenario I of the NRC (1987) Method and Scenario III of the USACE (2009a), thereby falling within the range of both methods.
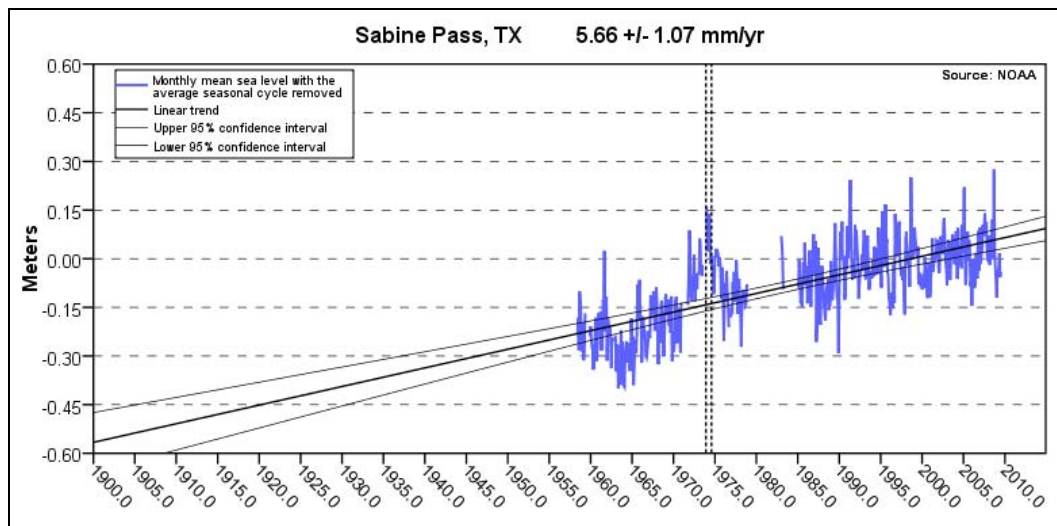
Figure 32. Change in mean sea level measured at Sabine Pass (5.66 ± 1.07 mm/year = 1.86 ± 0.4 ft/century) based on monthly means from 1958 to 2006 (NOAA 2008b).

4   Jetty Subsidence

Introduction

The purpose of this chapter is to document historical changes to the SNWW jetty system, including previous rehabilitation activities, to analyze what portion of elevation change has been due to each contributing factor, and to estimate potential future changes to jetty elevations with and without modifications to the jetty system. The time history of jetty elevation change can be described as being the original constructed elevation plus any rehabilitation activities, minus the sum of regional subsidence, stone dislodgement during storms, bed scour and settlement of structure, and consolidation of subsurface sediment. This chapter discusses the consolidation of the subsurface sediment as a function of the weight of jetty stone and duration of loading.

The magnitude of consolidation for sediment that is compressed by a weight is a function of the characteristics of the sediment, magnitude of the loading, and duration of the loading. The sediment substrate in the Sabine Pass region was formed as sea level flooded the Sabine valley to form an estuary, which filled in over the next 10,000 years with clay, silt, sand, and shell as well as peat deposits (Nelson and Bray 1970). One sediment core log available for the Sabine Pass navigation area (located near the East jetty) indicated approximately 50-60 ft of clay, silt, and mud (compressible sediment) overlaying a non-compressible sandy substrate (Nelson and Bray 1970). The former Sabine River channel, now filled with clay, silt, and mud, was estimated to be 120 ft below present sea level, or approximately 90 ft below the present-day sea bed (Kane 1959). Therefore, the thickness of compressible sediment in the vicinity of the Sabine Pass jetties is estimated to be between 50 and 90 ft.

Historical elevation changes

For the Sabine Pass jetty system, the initial jetty construction as well as subsequent rehabilitations of the structure and relative sea level rise increased the weight affecting the seabed. The degree to which the structure consolidated the substrate can be estimated from the difference in the as-constructed and 2003 jetty crest elevations for the parts of the jetties that were not likely to have been damaged due to storms. Based on the

stone stability analysis (Chapter 5), it was determined that the landward portions of the jetties were unlikely to have had severe storm damage. The average decrease in elevation for these areas was assumed to have been due to consolidation of the seabed as a function of loading by the jetties. For the East and West jetties, the average and standard deviation of the decrease in elevation were 1.9 ± 0.6 and 2.1 ± 0.9 ft, respectively (Figure 33). (Jetty crest elevations higher than the as-constructed elevation were omitted from the calculations.) These values give an estimate of the magnitude of consolidation that has occurred because of the jetty stone since construction.

Consolidation calculations

Terzaghi (1943) derived a relationship for primary consolidation, the process during which excess pore water pressure is dissipated from the particle matrix, based upon hydraulic principles. The assumptions for one-dimensional consolidation theory are: (1) a fully-saturated sediment system; (2) unidirectional flow of water; (3) one-dimensional compaction occurring in the opposite direction of flow; (4) a linear relationship between the change in sediment volume and the applied pressure (linear small-strain theory); and (5) validity of Darcy's Law, which states that the specific discharge (flow rate per area) through a porous medium is equal to the hydraulic gradient times the hydraulic conductivity (Yong and Warkentin 1966; Hornberger et al. 1998). For one-dimensional vertical flow, if the given loading, p, is less than the pre-consolidation loading, p_c, then the maximum consolidation, z_c, can be calculated as:

$$z_c = z_0 \left(\frac{C_{c0}}{1 + e_0} \log_{10} \frac{p}{p_0} \right) \quad if \ p < p_c \qquad (5a)$$

where:

   z_0 = initial thickness of compressible sediment
   C_{c0} = compression index, determined experimentally from a
        consolidation test for $p < p_c$
   e_0 = initial void ratio, equal to the volume of voids divided by the
        volume of solids and averaged over z_0
   p_0 = initial loading on the sediment.

a. East jetty

b. West jetty
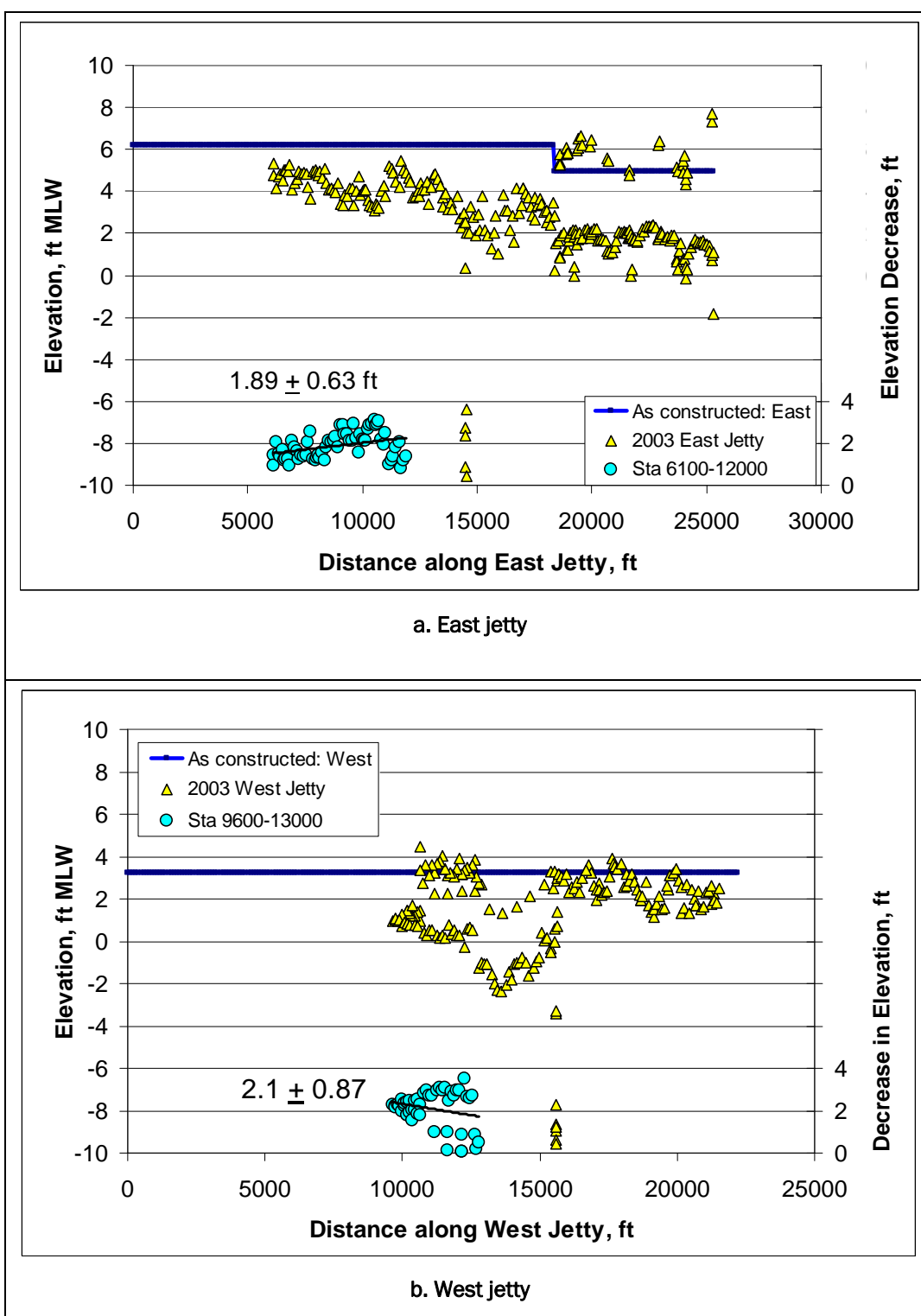
Figure 33. Jetty crest elevations and estimated decrease in structure elevation due to consolidation of the underlying substrate (average and standard deviation).

If the given loading, p, is greater than or equal to p_c, the maximum consolidation is calculated as:

$$z_c = z_0 \left(\frac{C_c}{1+e_0} \log_{10} \frac{p}{p_c} \right) \quad if \ p \geq p_c \qquad (5b)$$

where C_c is the compression index for $p > p_c$, determined experimentally from a consolidation test. The parameter z_0 can be estimated from sediment core data, regional depositional maps that represent the thickness of soft sediment, and high-resolution acoustic data at specific sites of interest with validation from sediment core data. For Sabine Pass, z_0 was set to the approximate thickness of compressible sediment beneath the jetty system equal to 55 ft for the East jetty, and 90 ft for the West jetty. Definitions for terms in Equations 5a and 5b are shown in Figure 34a.

The value of the pre-consolidation stress can be estimated from Casagrande's consolidation test, as illustrated in Figure 34b. To determine the pre-consolidation stress, the steps shown in Figure 34b are followed: (1) identify the point at the maximum radius of curvature, (2) draw a horizontal from that point, (3) draw a line tangent to that point, (4) draw a line bisecting (2) and (3); (5) draw a straight line from the over-consolidated portion of the curve, and finally determine the pre-consolidated loading by the intersection of (4) and (5). The magnitude of the pre-consolidation stress is decisive because it separates soils that are over-consolidated (i.e., these soils have experienced a greater load at some time in their past) from those that are under-consolidated (i.e., the present loading is the maximum that has occurred). Loading greater than the pre-consolidation stress will result in greater rates of consolidation than have previously occurred.

Figure 35 shows results of a consolidation test conducted for a sediment sample at 12.5-13.1 m depth from Chaland Headland, a barrier island restoration project in Louisiana that was completed in January 2007. Time-dependent consolidation was calculated for the jetty system assuming that sediment characteristics were similar to consolidation testing parameters available for Chaland Headland, Louisiana. Chaland Headland was the closest location with consolidation testing data available and values from this site were used as a guide in the calibration process.[1]

---

[1] A recommendation from this study is to take sediment cores in the area of the jetties and conduct consolidation tests to determine site-specific sediment parameters. This recommendation is discussed in the concluding section.
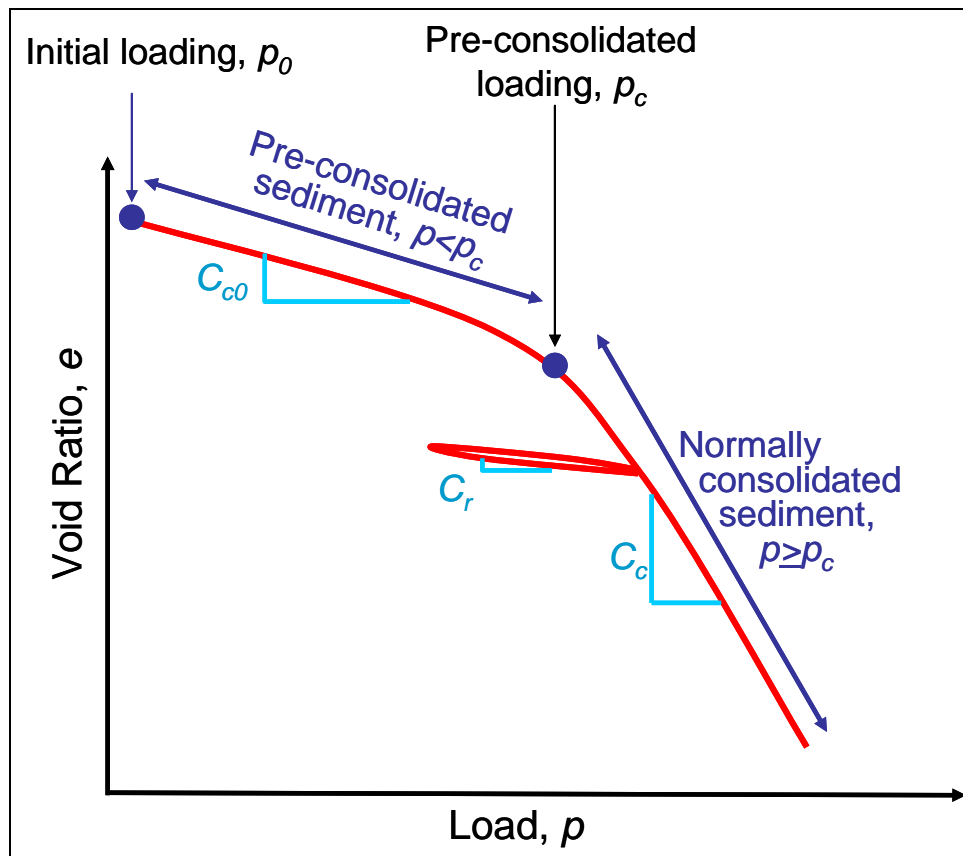
a. Definition of pre-consolidated and normally consolidated sediment.
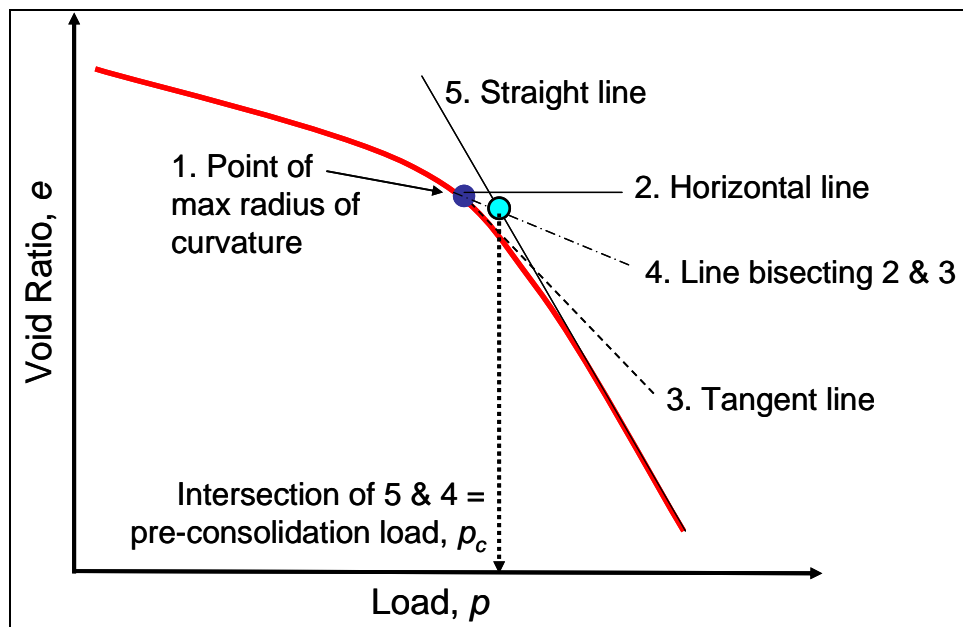
b. Determining pre-consolidation loading.

Figure 34. Parameters associated with consolidation testing.
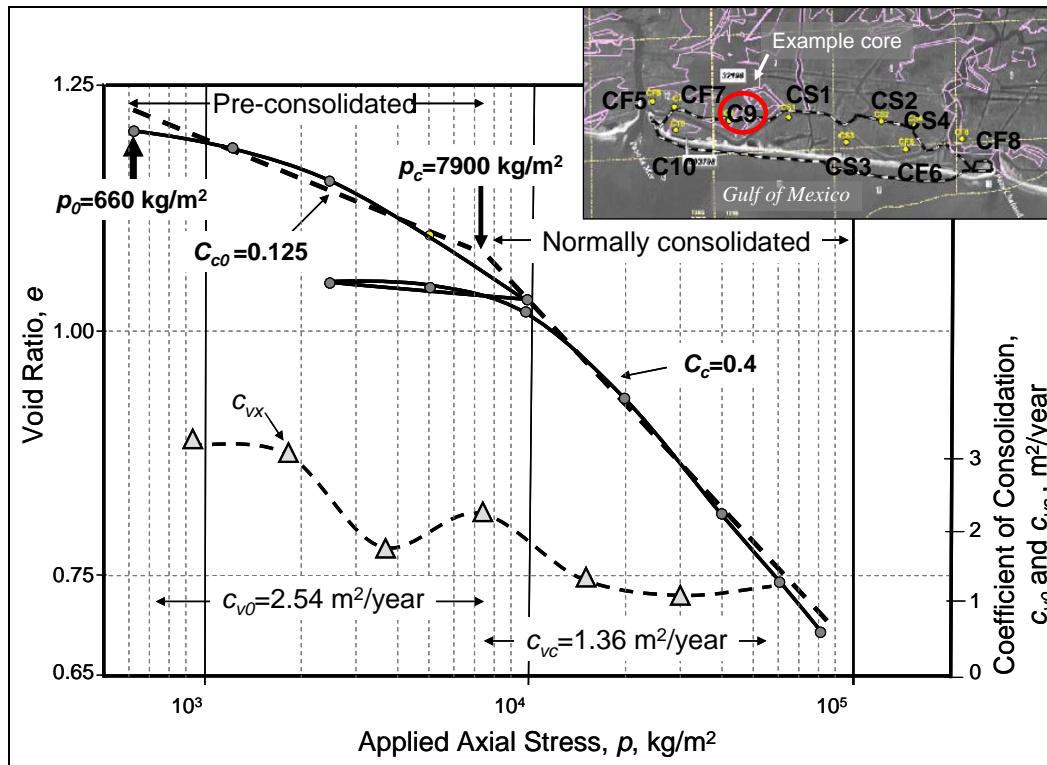
Figure 35. Example consolidation test from sediment sample taken at Chaland Headland, LA.

For the example shown in Figure 35, if the loading, *p,* is less than the pre-consolidation stress, then $p_0 = 660$ kg/m² and $C_{c0} = 0.125$ in Equation 4a. If *p* is greater than the pre-consolidation stress, then $p_c = 7,900$ kg/m² and $C_c = 0.4$ in Equation 4b.

Terzaghi's (1943) time-dependent relationship for consolidation is:

$$\frac{\partial u}{\partial t} = c_{v0} \frac{\partial^2 u}{\partial z^2} \quad \text{if } p < p_c \tag{6a}$$

$$\frac{\partial u}{\partial t} = c_{vc} \frac{\partial^2 u}{\partial z^2} \quad \text{if } p \geq p_c \tag{6b}$$

where:

    $u =$ pore water pressure in excess of hydrostatic pressure
    $t =$ elapsed time
    $z =$ vertical coordinate with the origin at the initial sediment surface
c_{v0} and $c_{vc} =$ a property of the compressible sediment called the coefficient of consolidation, which may vary depending on whether the loading is less than or greater than the pre-consolidation stress (Figure 36).
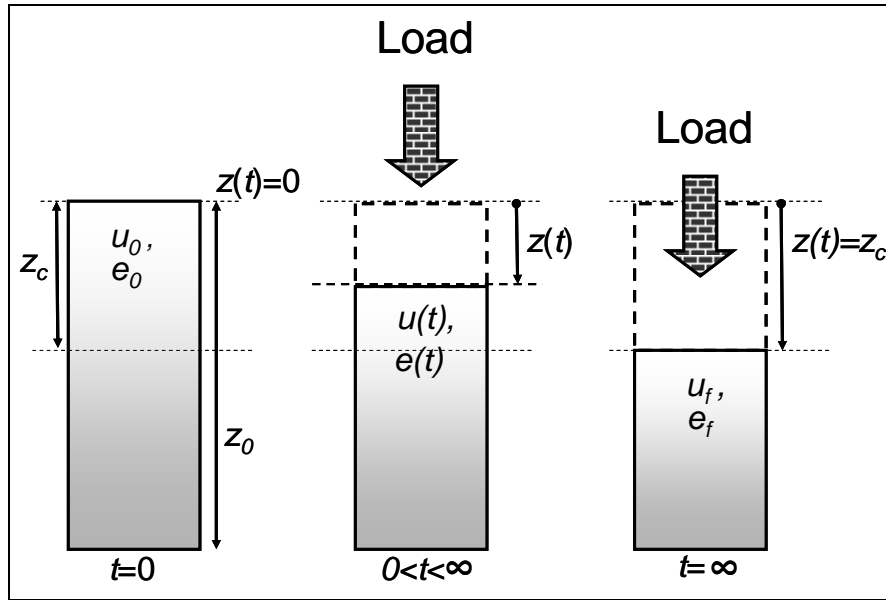
Figure 36. Definition sketch for consolidation relationship.

The proportion of the initial pore water pressure remaining at any time, $M(t)$, can be expressed as:

$$M(t) = \frac{1}{z_0} \int_0^{z_0} \frac{u}{u_0} dz = \frac{e(t) - e_f}{e_0 - e_f} \qquad (7)$$

in which:

u_0 = initial pore water pressure
$e(t)$ = average void ratio at any time
e_f = final average void ratio corresponding to the consolidation test results for the portion of the curve less than or greater than the pre-consolidation stress.

The variable $M(t)$ ranges from 1 to 0, at time $t = 0$ and infinity, respectively. The proportion of vertical consolidation that occurs at any time can also be expressed as:

$$z(t) = z_c(t) \left| \frac{e_0 - e(t)}{e_0 - e_f} \right| \qquad (8)$$

Combining Equations 7 and 8 gives

$$z(t) = z_c(t)\big(1 - M(t)\big) \tag{9}$$

where $M(t)$ can be expressed as (Dean 2002, p. 119),

$$M(t) = 8\sum_{n=1}^{\infty} \frac{e^{-[(2n-1)\pi]^2 c_{v0}t/4z_0^2}}{(2n-1)^2 \pi^2} \text{ for } p < p_c$$

$$M(t) = 8\sum_{n=1}^{\infty} \frac{e^{-[(2n-1)\pi]^2 c_{vc}t/4z_0^2}}{(2n-1)^2 \pi^2} \text{ for } p \geq p_c \tag{10 a,b}$$

and n is the index of the summation. In the numerical calculations, when the load changes from one time step to the next at a given location on the jetty (e.g., after a rehabilitation construction project), an effective time, t_e, is back-calculated corresponding to the new load and previous total consolidation at that location. The effective time is then incremented by the time step and used in Equations 9, 10a, and 10b to calculate consolidation at the next time step with the new load.

Results

The consolidation calculations were simulated beginning in 1833 so that the undisturbed substrate in the model was allowed to evolve to equilibrium with loading due to the weight of the water for 50 years prior to loading by the jetties. Then, each individual construction event was simulated separately, assuming that construction began at the shoreward portion of each jetty and extended offshore.

Consolidation parameters were calibrated within the range indicated by the Chaland Headland cores as well as typical values for estuarine sediment given by Holtz and Kovacs (1981, Table 9-3, p.404) by assuming that the East jetty had an average substrate thickness equal to 55 ft (average value of sediment core thickness determined by Nelson and Bray (1970)). Figures 37 and 38 show the calculations for the East and West jetties in which the consolidation averages between Stations 0 and 10,000 ft were used to calibrate the sediment consolidation parameters applied in the program. Using these same consolidation parameters, the West jetty was calibrated with a substrate thickness of 90 ft. Ninety feet is the maximum depth to the basal sand surface as discussed by Nelson and Bray (1970, their Figure 5, p. 56). West jetty Stations 12,700 to 15,500 ft were evaluated separately (see the following paragraph).
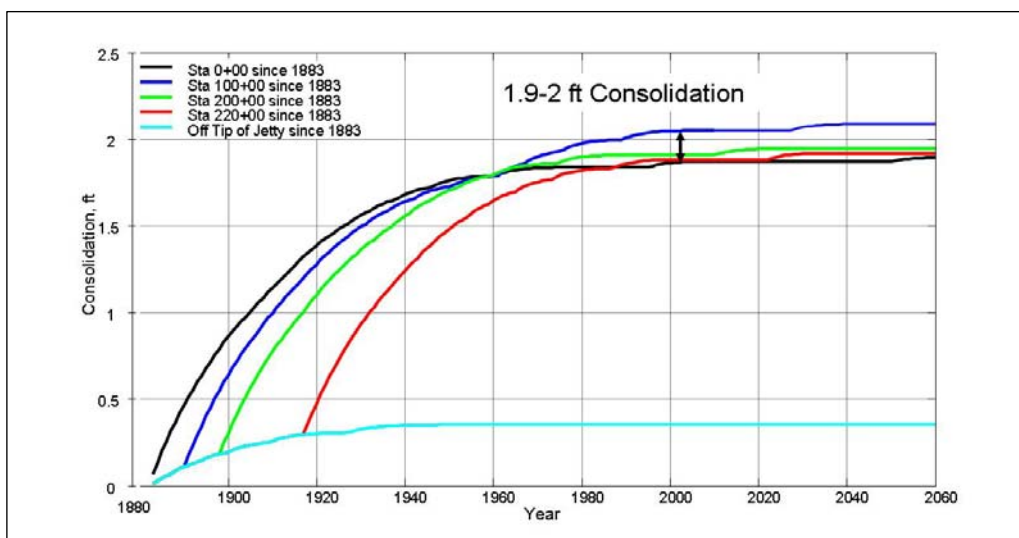
Figure 37. East jetty, with 55 ft substrate thickness.
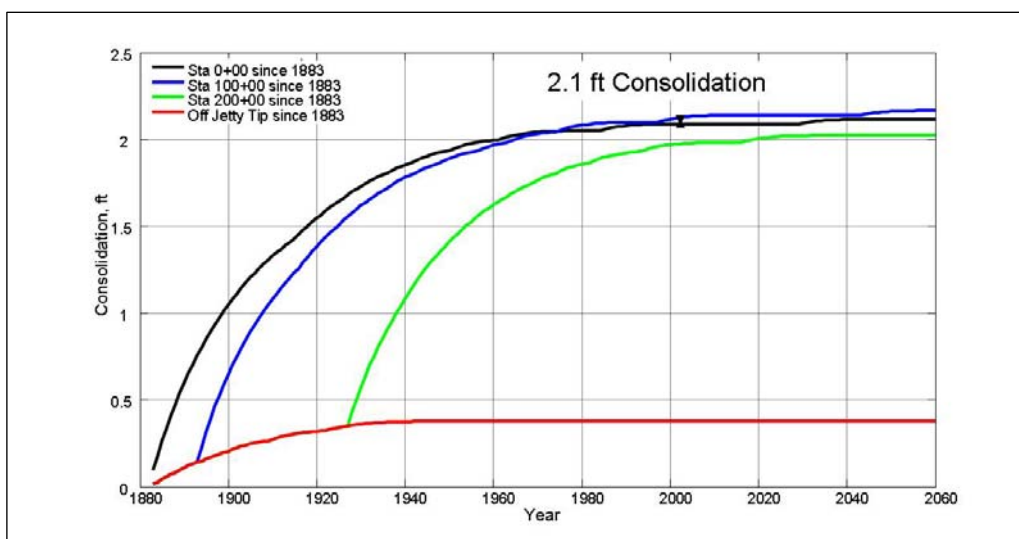
Figure 38. West jetty, with 90 ft substrate thickness.

West jetty elevations from approximately 12,700 to 15,500 ft experienced the greatest decrease in structure elevation initially due to high magnitudes of consolidation. Discussion in the rehabilitation history indicated that 2-4 ton stone was removed from the West jetty to reduce the loading on the substrate, and replaced with a concrete cap (during 1910-1911). However, it is not known how much stone was removed or how the removal of the stone and addition of the concrete cap changed the structure elevation. Without more information about the rehabilitation history, we cannot reliably calibrate the consolidation calculations for this region. The average decrease in elevation for this section was 3.7 ± 1.4 ft.

This analysis indicates that the majority of consolidation has occurred at the jetties with the existing design, and that any additional consolidation with the present weight will be minor from the present day condition through 2060.

5   Structural Stability for Existing Jetties

Introduction

The Sabine Pass jetties have a long historical evolution, as shown in Figures 5 and 6. Armor stone weight has increased at some locations over time to be more in line with modern jetty design. Figure 39 shows examples of jetty construction, and Figure 40 shows photos of the East and West jetty seaward ends.
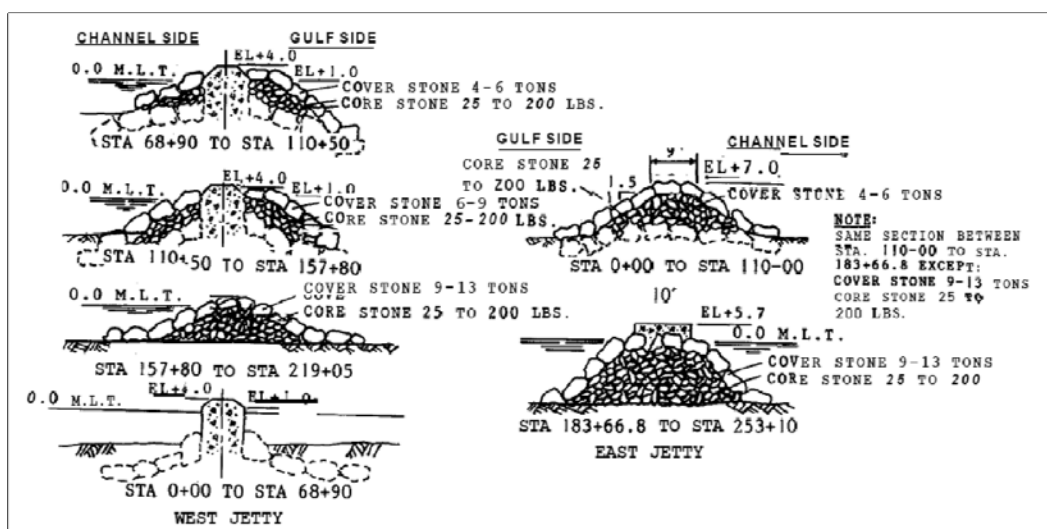
Figure 39. Jetty cross-sections at Sabine Pass.

Figure 40. Seaward end of the West (left) and East (right) jetties at high-water.

The critical elements in jetty structural design include the wave climate (e.g., wave height, period and direction) and the jetty composition (stone size/weight, number of armor layers, permeability and depth at the toe of the structure). To a certain extent, jetty composition controls wave height, if the wave becomes depth-limited and breaks (Melby 2005a). A damage

coefficient may be estimated that incorporates these structural and environmental elements and represents how much damage a structure might receive.

The damage coefficient, S (Melby 2005b), can be calculated for an individual storm at locations along the structure, to evaluate its structural stability. The value of S represents an eroded area of the jetty, typically at the waterline, normalized by a cross-sectional area of the stone in the jetty's armor layer. If the armor is of sufficient size for the local wave climate, damage values less than 2 are typically estimated for most if not all storms. Larger values of S indicate the likelihood of greater damage. Values of S greater than 10-20 indicate severe damage and possible breaching of the jetty. Greater S values indicate even more extensive damage.

In the analysis herein, values of S were accumulated at a given location along the structure if the calculated S value for each individual storm was greater than 1.5. This threshold value was chosen less than the typical value of 2.0 due to the single armor layer type of construction on most of the Sabine Pass jetties (see Figure 39). A value of 2.0 would be used if the structure had two armor stone layers. This means that as storms sequentially attack the jetties, if the wave conditions are more severe than the structure can withstand and damage values are greater than 1.5, the armor stone is displaced enough to create erosion on the jetty slope. The next storm producing a damage value greater than 1.5 will create additional erosion on the slope so that the eroded area has increased, or S values, proportional to this erosion, can be accumulated over the history of the structure.

To evaluate the jetties over a 50-year time period, a Monte-Carlo simulation based on local wave statistics from WIS (Wave Information Studies) and from the Louisiana Coastal Protection and Restoration (LACPR) hurricane database was developed, as discussed in Chapter 3. The LACPR data was extracted from computer runs of simulated hurricanes representative of this region. This database was applied at the request of the Galveston District.

Approach to long-term stability analysis

Structural stability relationships

In the development of the breakwater stability simulation, the relationship for maximum wave momentum flux by Hughes (2003a, 2003b, 2004, 2005) was used due to its applicability to steep water waves near breaking as is the case for waves in the vicinity of a breakwater,

$$\left[\frac{M_F}{\rho_w gh^2}\right]_{max} = A_0\left[\frac{h}{gT^2}\right]^{-A_{11}} \tag{11}$$

with:

$$A_0 = 0.639\left[\frac{H}{h}\right]^{2.026} \tag{12}$$

$$A_1 = 0.180\left[\frac{H}{h}\right]^{-0.391} \tag{13}$$

Fitting to laboratory data, generalized empirical stability equations were developed for the two most important breaker types, as shown next, where S is the eroded area due to waves during an event of duration t. The structure armor stability relationships were developed by Melby and Hughes (2004) and are shown below:

Plunging waves

$$S = \frac{N_m^5}{3125}\frac{N_z^{0.5}}{P^{0.9}(\cot\theta)^{2.5}}, \quad s_m \geq s_{mc} \tag{14}$$

Surging waves

$$S = \frac{N_m^5}{3125}\frac{N_z^{0.5}s_m^{5P/3}}{P^{0.9}}(\cot\theta)^{5P-2.5}, \quad s_m < s_{mc} \tag{15}$$

with the critical wave steepness, s_{mc}, separating plunging and surging wave breaking:

$$s_{mc} = -0.0035\cot\theta + 0.03316 \qquad (16)$$

and

$$N_m = \left(\frac{K_a[(M_F)_{max}/\gamma_w h^2]}{(S_r-1)}\right)^{1/2} \frac{h}{D_{n50}} \qquad (17)$$

with

$S = A_e/D^2_{n50}$ = normalized eroded area

A_e = eroded cross-sectional area

D_{n50} = nominal mean stone diameter

N_m = stability number

$N_z = t/T_m$ = number of waves at mean period during an event of duration t

T_m = mean wave period

P = structure permeability

Θ = seaward structure slope, from horizontal

$s_m = H_s/L_m$ = wave steepness

H_s = significant wave height

L_m = wavelength based on mean wave period

K_a = 1

γ_w = water specific weight.

The above relationships would provide the eroded stone area in a jetty cross-section for a storm of duration t. If the calculated value for S was less that 2.0, then conditions were not severe enough to produce damage to the structure. This value may be referenced in the Coastal Engineering Manual (Burcharth and Hughes 2003).As discussed earlier, a value of $S = 1.5$ was selected for this study due to the single layer of armor stone construction. Therefore, if for a given storm the damage, S, was greater than a value of 1.5, then this value was saved and as the storm scenarios were stepped through for 50 years, the value would be accumulated with other storms whose S value was greater than 1.5. The manner in which these accumulations of damage occur was presented by Melby (2005b) which references Melby and Kobayashi (1998). The temporal progression of mean eroded area as a function of time domain wave statistics is:

$$\overline{S}(t) = \overline{S}(t_n) + 0.025 \frac{(N_s)_n^5}{(T_m)_n^{0.25}} \left(t^{0.25} - t_n^{0.25} \right) \qquad for \quad t_n \le t \le t_{n+1} \qquad (18)$$

where $\overline{S}(t)$ and $\overline{S}(t_n)$ are predicted and known mean eroded areas at times t and t_n, respectively, with $t > t_n$. $N_s = H_s/(\Delta D_{n50})$ is a stability number based on the average of the highest one-third wave heights, $\Delta = Sr - 1$, where Sr is the armor stone specific gravity, and T_m is the mean period.

Monte Carlo simulation

The structure stability analysis was designed to use the wave information developed in Chapter 3 along with the structural relationships discussed in the previous section.

To provide the input wave conditions for calculation of progressive damage, an analysis of the Wave Information System data at Station 92 indicated that an average of nine storms per year would occur in the Gulf near the jetties. The directional approach of these storms was split about evenly with respect to whether the east jetty or the west jetty would be the most severely attacked. Application of this information will be discussed in the next section. Typical storm durations were examined and significant wave energy was present on average for 40 hours. For the 1980–1999 data set, a wave six feet or greater was present, on average, for forty hours. This was based on 32 storm events and excluded hurricanes.

Hurricane frequency is about once in every four to five years for the stretch of coast in the vicinity of Sabine Pass when examining historical data. Recent analytical modeling has subdivided the coastline into reaches and provided frequency of occurrence (Hallegatte 2007; Gray and Klotzbach 2009). These studies indicate Sabine Pass to be in a zone which receives hurricanes every four to five years. The results are somewhat dependent on the length of coastline that was used for the analysis. A five year return interval was chosen for this study. The duration of high energy waves for the LACPR data was in the range of 15–25 hours, and a relationship was developed for duration related to wave period.

A factor tempering the importance of duration of damaging waves comes from model testing that indicates most damage to a breakwater structure has occurred by the time 8,500 waves have attacked the structure. In the

realm of 6-sec to 12-sec waves, this means duration in the range of 14.2 to 28.3 hours of wave attack. This indicates that for the more normal seasonal storms, duration of 25 hours of wave attack is a reasonable number with respect to breakwater damage. In the case of hurricanes, the use of a duration relationship was applied based on information discussed previously.

The Monte Carlo simulation was programmed into an Excel spreadsheet using Visual Basic. As each time step progressed, a random number was generated that was then input into recurrence interval functions that determined the water level (tide stage and if a hurricane, surge level plus the tide level) and the wave height. Wave period was calculated from correlation analysis of the respective data sets of storm condition or hurricane. The gradual sea level rise was also included as time steps progressed in the calculation. At each time step, the damage S was calculated and accumulated if it exceeded the damage criteria value. As discussed earlier a typical value for damage to occur was for a value of S equal to 2. In the case of rock jetties, this value would be used for a double armor layer. As noted in Figure 39, the jetties at Sabine Pass for the most part, have a single armor layer. As a result, a conservative value of S equal to 1.5 was selected as the critical value to determine if damage would be accumulated.

Application to Sabine Pass

Jetty stations

Figure 41 shows the jetty stations to help locate areas of interest. A Monte Carlo simulation was run for each 1,000 ft station along the structure and a total damage value was calculated for that station. If the portion of the structure was considered protected from waves by being in the lee of the other jetty, e.g., waves from the southwest would attack the trunk of the West jetty and the East jetty, for the most part, would be protected from strong wave attack, the simulation was set up to split the number of yearly storms attacking that side of the structure. As mentioned earlier, the typical storms data indicated an even split in directional approach to the jetties. Therefore, instead of nine yearly storms, each jetty trunk received a conservative number of five storms attacking the East or West jetty trunk.
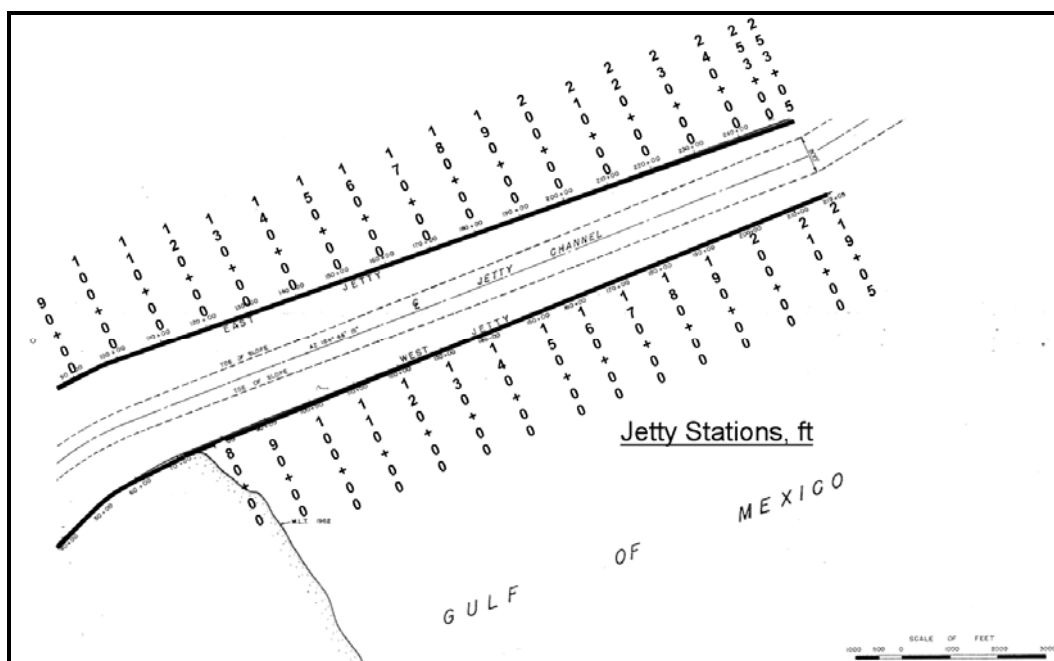
Figure 41. Jetty stations along East and West jetties.

However, the outer portions of the East and West jetties were permitted to receive exposure to the full seasonal number of nine storms. The stations receiving full storm exposure were Stations 220+00, seaward, on the East jetty, and Stations 190+00, seaward, on the West jetty. These separation stations were selected based in historical damage occurring on the channel side of the East and West structures.

Verification

The technique was verified for this location by simulating a 67-year interval from 1936 to 2003 for the East jetty tip, comparing the damaged profile of the structure, before its repair in 2003, to the cumulative damage, S. The calculated eroded area, represented by $S = 54$, was larger when compared with actual structure damage (measured as $S = 24$) over the time period. Figure 42 shows the damage progression with time and Figure 43 shows the region eroded between 1936 and 2003. There are some uncertainties associated with this verification, including the fact that determining the exact stone size in place at the initiation of the simulation is difficult. It is assumed there was at least 9 ton stone in place, since later repairs in the more landward stations were 9-13 tons. Also, there was a concrete cap placed on the 10-ft-wide crown in 1936. The larger calculated value indicates the conservative nature of the calculations, which come about by the following:
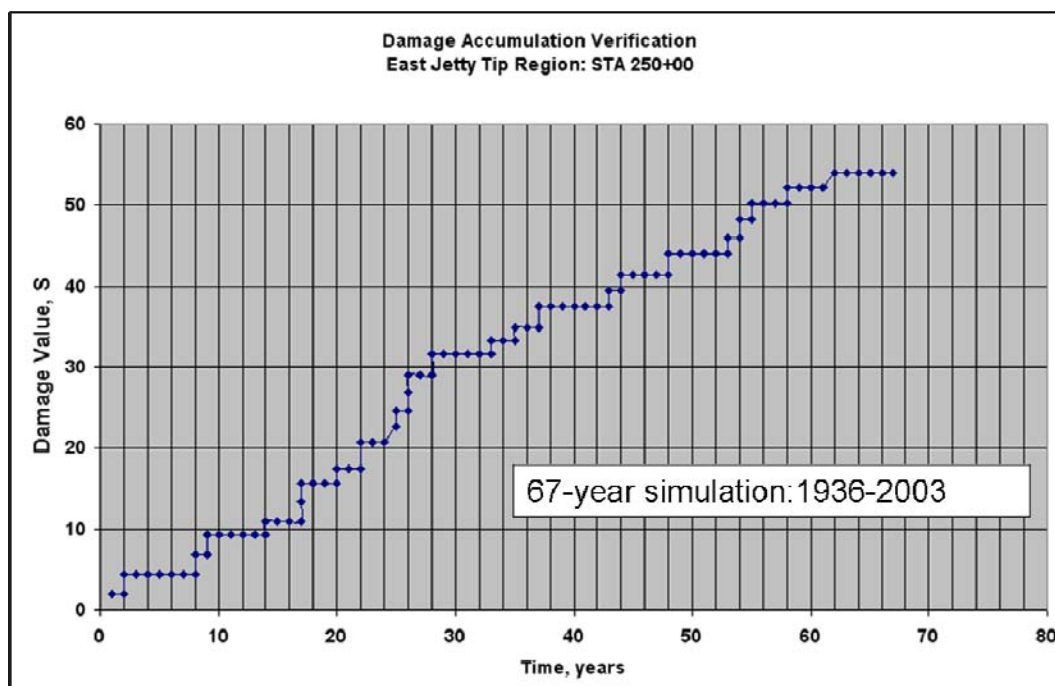
Figure 42. Verification of damage calculation.
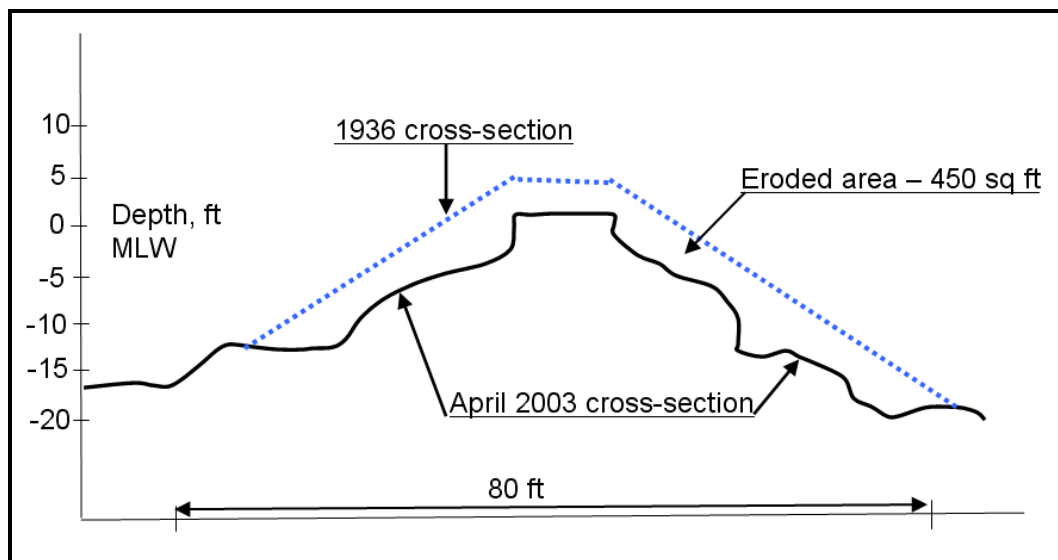
Figure 43. East jetty cross-section erosion, Station 250+00, 1936-2003.

- Stability equations are typically for a trunk section with head-on waves, a more severe condition than in a real-world situation. That is, there is no adjustment for wave obliquity, which would reduce damage relative to simulation results that assume waves approach perpendicular to the structure.

- There was no reduction in damage for a submerged structure, where damage would be expected to be less during high-water-level storms.

In a sensitivity analysis of this verification, it was noted that using a value of S equals 2.0 to determine if damage should be accumulated or not, the reduction in total accumulated damage was reduced over 50 percent for this particular scenario. However, as a factor of safety, a value of S of 1.5 was used in the study. Also, the depth in front of the structure was an important parameter controlling total damage received. Other damaged areas were examined and also compared favorably.

The simulation proceeded year-by-year, exposing the structures to typical storm frequencies with the wave parameters selected by a random number process using the developed return interval for storms relationships. The simulation included tide level variation, storm surge elevation and a progressive sea-level rise, as discussed in an earlier section of this report. The simulation was repeated one thousand times and averaged to produce a statistically representative value. Figure 44 shows a plot of the results of 1000 simulations for a section of the East jetty tip for the time frame of 2010 to 2060. This part of the jetty has been rehabbed with larger stone than some other parts of the structure. The average S value for the 1000 simulations was 10.0, with a standard deviation of 5.8, indicating some damage would occur over the 50-year period at this location.

Results for existing conditions

Following the verification, the East and West jetties were examined for the time period 2010-2060. Proceeding at 1,000-ft intervals, Figures 45 and 46 show expected damage along the breakwater in terms of the S damage value. This is plotted along with the 2003 jetty crest elevations. Accumulative values of S greater than 10 indicate significant damage and structure degradation (Burcharth and Hughes 2003). As seen in Figure 45, significant damage would be accumulated on the East jetty by year 2060 at stations seaward of Stations 200+00 (20,000 ft along the jetty), though the repaired, seaward areas (that are "spikes" of crest elevation) have substantially lower damage due to the increased armor stone size at these locations. The West jetty (see Figure 46) will have significant damage from Sta 190+00 (19,000 ft seaward along the jetty). Damage values tend to be lower on West jetty primarily because depths are less, resulting in lower wave energy, than those values along the East jetty.
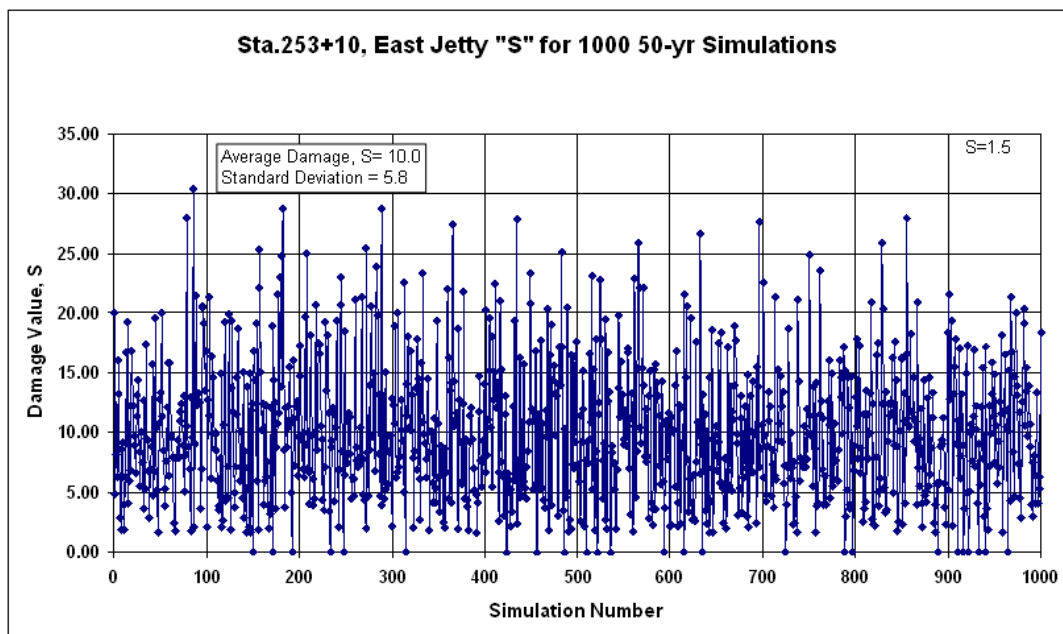
Figure 44. One-thousand 50-yr simulations of damage for East jetty.
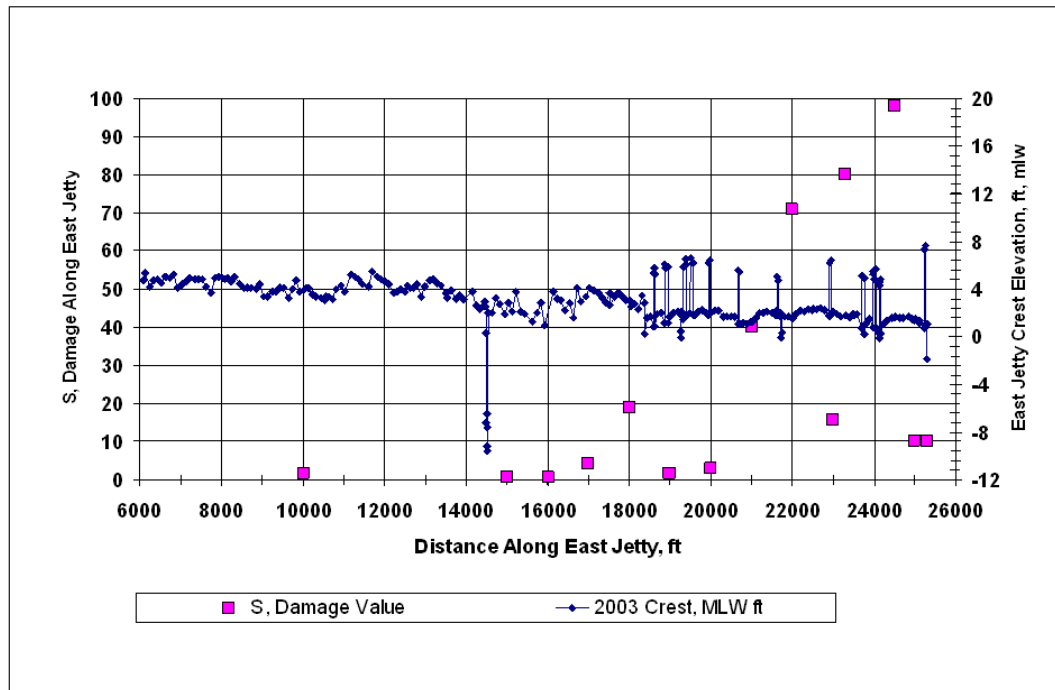
Figure 45. East jetty fifty-year damage values (2010-2060) along jetty for Sabine Pass wave climate and existing structure, plotted with 2003 jetty crest elevations.
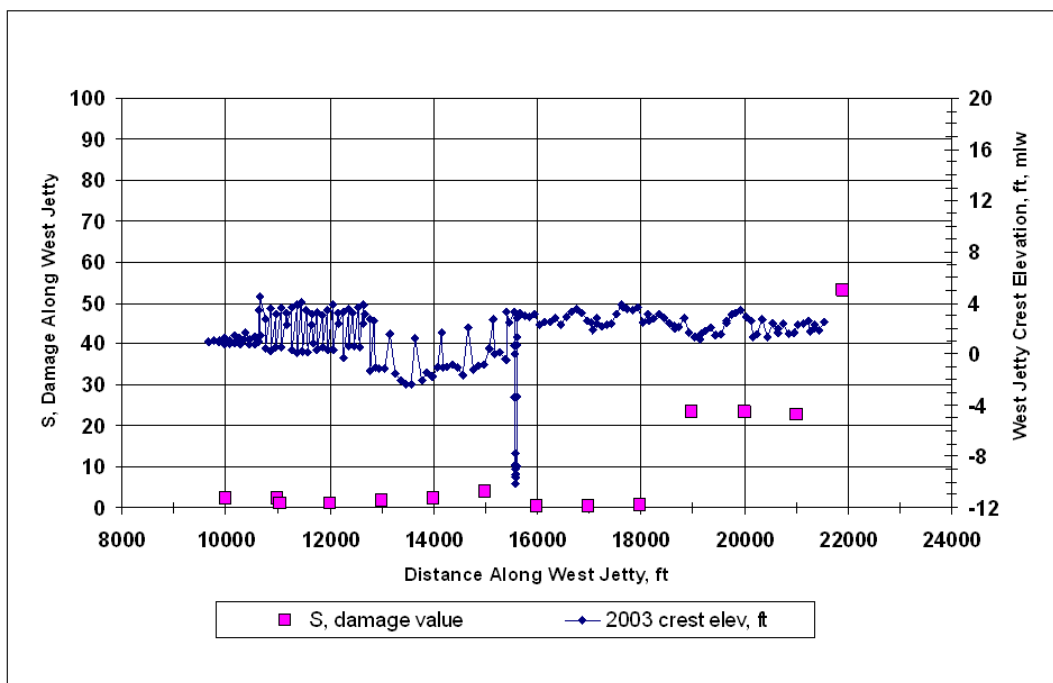
Figure 46. West jetty fifty-year damage values (2010-2060) along jetty for Sabine Pass wave climate and existing structure, plotted with 2003 jetty crest elevations.

The damage values were used to estimate structure crest elevations for hydrodynamic modeling of the 2060 condition. Figures 47 and 48 show the crest elevations of the non-rehabbed jetties determined for 2060 modeling effort, discussed in the next section.
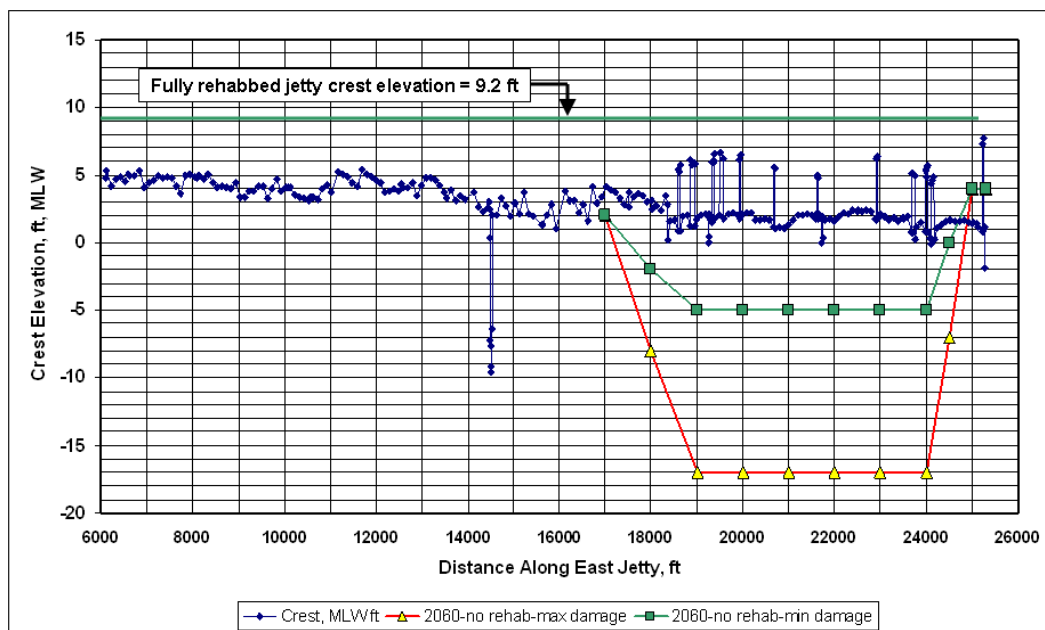
Figure 47. Year 2060 non-rehabbed East jetty crest elevations.
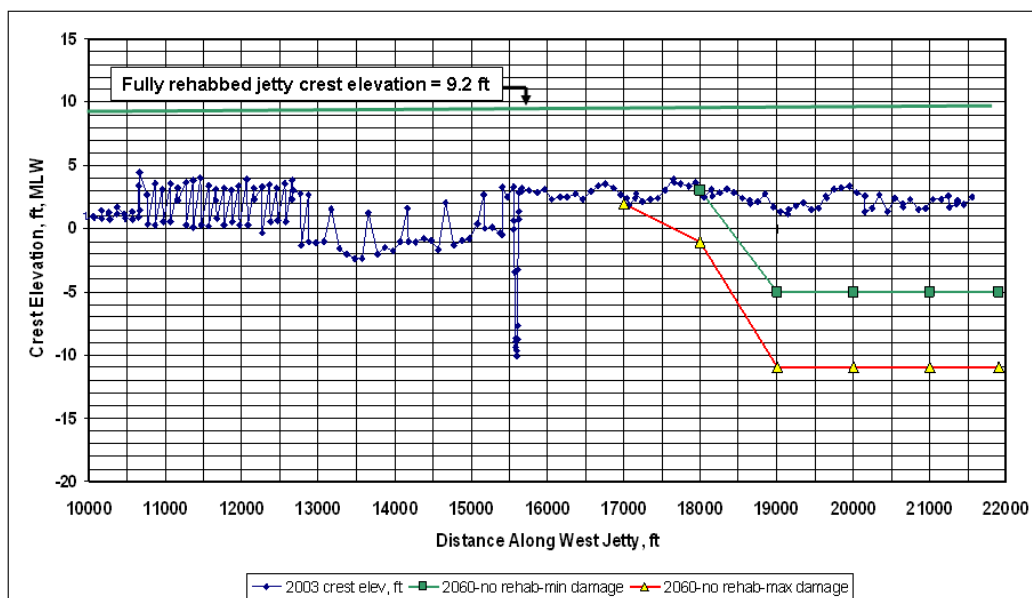
Figure 48. Year 2060 non-rehabbed West jetty crest elevations.

Two 2060 crest elevations are presented. These represent a potential range of jetty crests based on the structure stability simulations. A range is necessary since there has been no specific physical modeling done for conditions greater than $S = 20$. The S value can be converted to a damaged area of the jetty which, if applied, produces the greater destructive crest elevations of Figures 47 and 48. The less destructive crest elevations essentially reduce the structure elevation by one-half, which possibly could occur due to the displaced stone producing a buttressing effect to the remainder of the structure, which would then be less susceptible to further destruction. Laboratory studies would be required to more accurately quantify this damage.

For the rehabilitated 2060 condition, those regions with damage values greater than 20 can be redesigned with recommended stone size and raised to an elevation commensurate with sea level rise. After hydrodynamic and sediment pathway modeling of this condition, other reaches could be increased in elevation if it was thought that change was required to alleviate difficult flow conditions or possible increased sedimentation.

6   Development of Jetty Alternatives

Overview of alternatives

Alternatives for rehabilitation of the Sabine Pass jetties were developed to reduce the storm damage, as discussed in Chapter 5. Each rehabilitation alternative was assumed to be completed in 2010 and the simulations were evaluated after a 50-year period without any additional rehabilitation in the intervening years. Each plan was evaluated for the 2060 condition, including an increase in mean water level of 2.7 ft, as indicated by the sea level rise analysis. An "existing condition" alternative also was evaluated for 2060 so that each rehabilitation plan could be evaluated with a base condition for that time period. Table 6 presents an overview of each plan and simulation conducted.

Existing condition

This alternative was simulated with a 2003 jetty crest elevation and existing channel depth (42 ft MLW), as well as a 2060 elevation only considering the increase in relative sea level during the 50-year period (+2.7 ft). This implies that no additional structure damage would occur during this period.

Plan 1

Plan 1 consisted of dredging the channel to 48 ft MLW with no repairs or rehabilitation of the existing jetties. It was assumed that the 2003 jetty crest elevations were representative of the elevation in 2010 for Plan 1 simulations. Jetty elevations for simulations in year 2060 were obtained from the maximum damage curves shown in Figures 45 and 46.

Plan 2

Plan 2 simulations included deepening of the channel to 48 ft MLW and rehabilitating the entire length of the East and West jetties. Plan 2 assumed rehabilitation of the jetties to +9.2 ft MLW in 2010, which would result in the original as-constructed jetty elevation of +6.2 ft MLW in 2060. The MLW datum was adjusted for the increase in relative sea level of 2.7 ft plus an additional elevation loss of 0.3 ft due to consolidation from the additional weight of rehabilitation stone.

Table 6. Numerical model simulations.

Plan	Year	Storms	Water Level	Jetty Condition	Channel Depth, ft MLW
Existing	2003	Low- energy	Present	Present	42[1]
	2003	SE	Present	Present	42[1]
	2003	SW	Present	Present	42[1]
	2003	H266	Present	Present	42[1]
	2060	Low- energy	Elevated 2.7 ft[2]	Present	42[1]
	2060	SE	Elevated 2.7 ft[2]	Present	42[1]
	2060	SW	Elevated 2.7 ft[2]	Present	42[1]
	2060	H266	Elevated 2.7 ft[2]	Present	42[1]
Plan 1	2010	Low- energy	Present	Present	48
	2010	SE	Present	Present	48
	2010	SW	Present	Present	48
	2010	H266	Present	Present	48
	2060	Low- energy	Elevated 2.7 ft[2]	Maximum Deterioration	48
	2060	SE	Elevated 2.7 ft[2]	Maximum Deterioration	48
	2060	SW	Elevated 2.7 ft[2]	Maximum Deterioration	48
	2060	H266	Elevated 2.7 ft[2]	Maximum Deterioration	48
Plan 2	2010	Low- energy	Present	Full Rehab (+9.2 ft MLW in 2010)	48
	2010	SE	Present	Full Rehab (+9.2 ft MLW in 2010)	48
	2010	SW	Present	Full Rehab (+9.2 ft MLW in 2010)	48
	2010	H266	Present	Full Rehab (+9.2 ft MLW in 2010)	48
	2060	Low- energy	Elevated 2.7 ft[2]	Full Rehab (+6.2 ft MLW in 2060[3])	48
	2060	SE	Elevated 2.7 ft[2]	Full Rehab (+6.2 ft MLW in 2060[3])	48
	2060	SW	Elevated 2.7 ft[2]	Full Rehab (+6.2 ft MLW in 2060[3])	48
	2060	H266	Elevated 2.7 ft[2]	Full Rehab (+6.2 ft MLW in 2060[3])	48
Plan 3	2010	Low- energy	Present	Outer 4,000' Rehab (+9.2 ft MLW in 2010)	48
	2010	SE	Present	Outer 4,000' Rehab (+9.2 ft MLW in 2010)	48
	2010	SW	Present	Outer 4,000' Rehab (+9.2 ft MLW in 2010)	48
	2010	H266	Present	Outer 4,000' Rehab (+9.2 ft MLW in 2010)	48
	2060	Low- energy	Elevated 2.7 ft[2]	Outer 4,000' Rehab (+6.2 ft MLW in 2060[3])	48
	2060	SE	Elevated 2.7 ft[2]	Outer 4,000' Rehab (+6.2 ft MLW in 2060[3])	48
	2060	SW	Elevated 2.7 ft[2]	Outer 4,000' Rehab (+6.2 ft MLW in 2060[3])	48
	2060	H266	Elevated 2.7 ft[2]	Outer 4,000' Rehab (+6.2 ft MLW in 2060[3])	48

[1] Present channel depth without deepening.

[2] Change in water level caused by an increase in relative sea level from 2010 to 2060.

[3] Includes 0.3-ft reduction in jetty crest elevation because of additional subsurface consolidation caused by increased weight of rehabilitation stone. MLW in 2060 represents a new MLW datum calculated with the change in relative sea level.

Plan 3

Based on results of the storm damage calculations, Plan 3 was formulated to rehabilitate the outer 4,000 ft of the East and West jetties to +9.2 ft MLW in 2010, which would result in an elevation of +6.2 ft MLW (datum adjusted for increase in relative sea level and 0.3 ft of elevation loss due to consolidation) in 2060 for the outer 4,000 ft. This outer portion of the jetties experienced the majority of the storm damage in the stability analysis and this plan was formulated to minimize rehabilitation costs.

For each plan, three types of storms and one low energy wave condition were simulated. The "SE" condition represented a storm with waves from the southeast. This storm had a peak wave height of 5.2 m, with waves exceeding 3 m occurring for more than 24 hr. Wave period was typically 10 sec. The "SW" condition was a storm from the southwest. This storm wave was just over 2 m and remained at this level for about 12 hr, with a wave period of 8 sec. These two wave conditions were derived from NOAA NDBC buoy 42035. The hurricane storm "H266" was from the LACPR suite of hurricane events. This hurricane is a 100-yr event for the Sabine Pass area and approaches from the south, crossing the shoreline 20 miles west of Sabine Pass. The maximum surge elevation is 13.3 ft MLW at the shore. Maximum wave height at the jetties tips was 15 ft with 8.8 sec period and direction nearly perpendicular to the entrance and the shore-line. The low wave energy simulation has a maximum wave height of 0.6 ft with wave period of 3 sec.

7   Hydrodynamic Simulations

Overview

This chapter presents an overview of the Coastal Modeling System (CMS) and the application to the SNWW. The purpose of the CMS modeling was to characterize the hydrodynamic conditions at the site for existing conditions, with channel modifications, with channel and jetty modifications, and with two forecasted conditions, with and without modifications to the SNWW.

Coastal Modeling System

Overview

The Coastal Modeling System (CMS) consists of two coupled models; CMS-Wave and CMS-Flow. The following paragraphs describe each model.

CMS-Wave (Lin et al. 2008), previously called WABED (Wave-Action Balance Equation Diffraction), is a two-dimensional (2D) spectral wave model formulated from a parabolic approximation equation (Mase et al. 2005) with energy dissipation and diffraction terms. It simulates a steady-state spectral transformation of directional random waves co-existing with ambient currents in the coastal zone. The model operates on a coastal half-plane, implying that waves can propagate only from the seaward boundary toward shore. It includes features such as wave generation, wave reflection, and bottom frictional dissipation. In the present study, CMS-Wave was run with 3-hr time steps.

CMS-Flow (Buttolph et al. 2006), formerly called M2D, is a finite-volume numerical representation of the 2D depth-integrated continuity and momentum equations of water motion. In CMS, radiation stresses from surface waves force currents and change the water-surface elevation and, if required, the calculated current can be input to the wave model to transform waves propagating on it. Calculation cells are defined on a staggered, rectilinear grid and can have constant or variable side lengths. Momentum equations are solved in a time-stepping manner first, followed by solution of the continuity equation, in which the updated velocities calculated by the momentum equations are applied. CMS-Flow was run with 1-hr time

steps with wave-induced currents calculated from CMS-Wave applied every 3 hr.

The horizontal coordinate system was in Texas State Plane South Central and vertical datums were referenced to mean sea level (MSL). A requirement of CMS is that all horizontal and vertical datums are in SI units; therefore, all references are in meters.

Bathymetry and development of grid

Grids for CMS-Wave and CMS-Flow were developed from SNWW surveys and depths developed for a TABS-MDS grid to investigate potential salinity impacts (Brown et al. 2006). The CMS-Wave grid consisted of 100 m by 100 m grid cells, whereas the CMS-Flow grid was variable, ranging in cell size between 50 to 200 m in both alongshore and cross shore directions. The grids overlapped each other and both extended along the shoreline approximately 18.5 km (11.5 miles) west and 24.9 km (15.4 miles) east of Sabine Pass. The grids extended inland to include Sabine Lake and offshore to the 20-m water depth.

Calibration

Data available for model calibration were limited. As part of a potential salinity impact study, Brown et al. (2006) collected time-series observations of water level elevations, velocity, and salinity (Fagerburg 2001) from May 2001 to January 2002. The study focused on inland impacts of salinity; however, a tide gauge at Station 7 of the Brown et al study was located in the channel near the jetties (Figure 49). Unfortunately, the tide gauge was struck by a vessel on 1 June 2001 and failed. Water levels from this station from 19 May 2001 to 1 June 2001 were used for calibration.

Input data for the calibration was obtained from WAVCIS (Wave-Current-Surge Information System) Station CSI 03 of the Coastal Studies Institute (CSI) of Louisiana State University, which is located south of Vermillion Bay, LA, in approximately 5 m of water. Figure 50 compares hourly water levels from CMS (dashed line) to Station 7 (solid line). The model compares well to the tidal signal magnitude and phase.
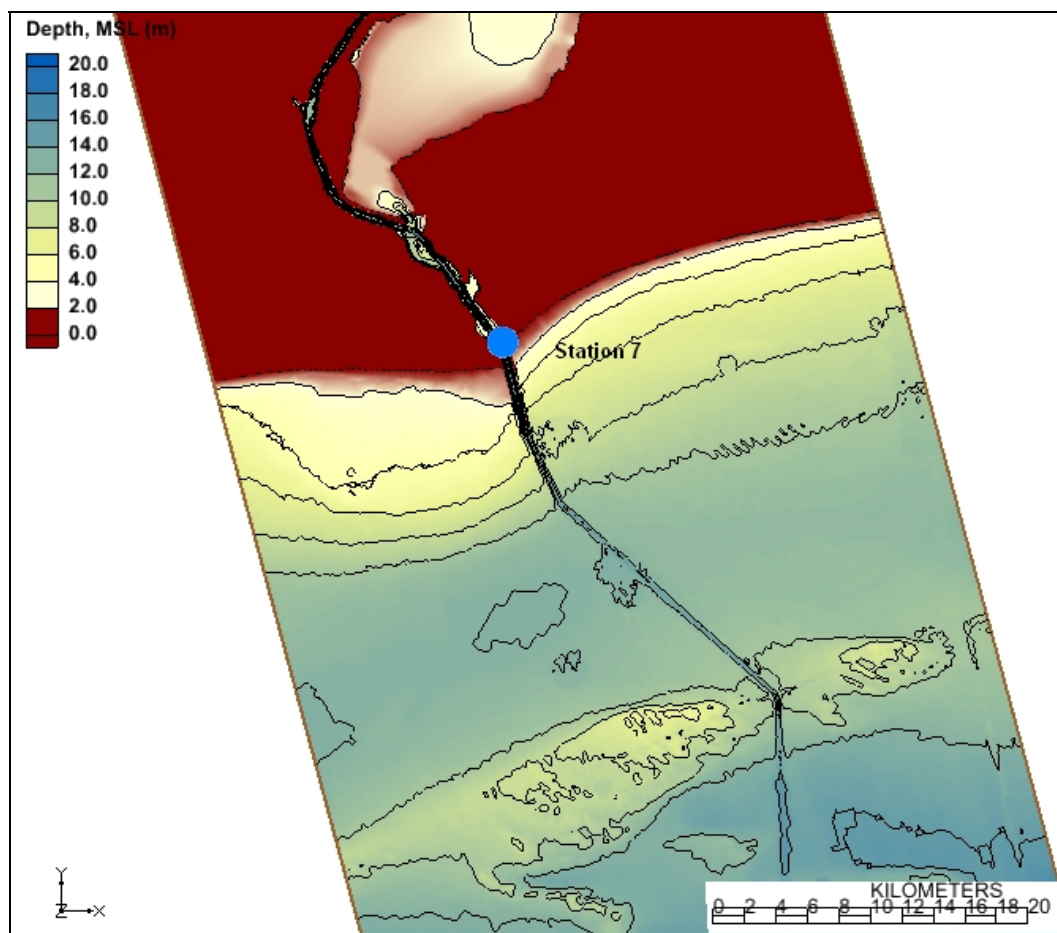
Figure 49. Location of tide gauge (blue circle) used in calibration of CMS.

Simulated events

Approach to selecting events for simulations

The potential for shoaling and scour were investigated for a range of hydrodynamic conditions experienced at the site. The simulations represented typical fair weather conditions and storms from the southeast and southwest over a duration of 5 days. A hurricane also was simulated, which included waves and surge of higher intensity than the storms, but over a shorter duration.

Each hydrodynamic condition was simulated for projected 2010 and 2060 water levels. As discussed previously, sea level rise in 2060 was 0.823 m (2.7 ft).
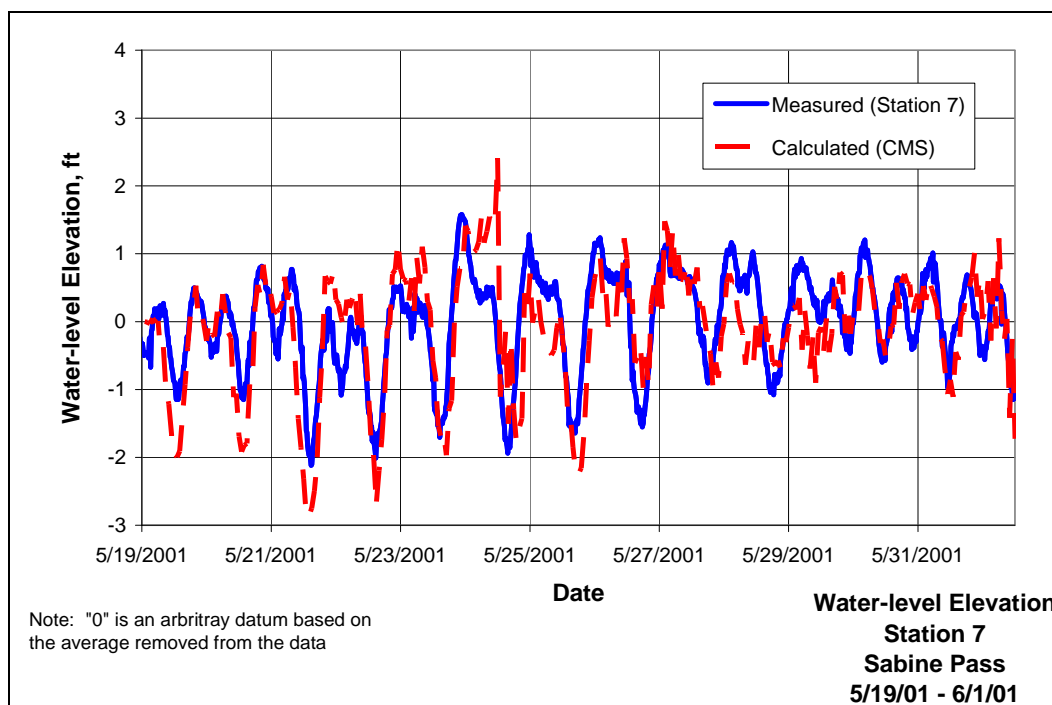
Figure 50. Comparison of calculated and measured water elevations.

Fair-weather conditions

The fair-weather condition was simulated over the period of 2 July through 6 July 2001. Input data to CMS-Flow was obtained from water levels observed from WAVCIS Station CSI 03. Although some wave information was available from CSI 03, mean wave direction was not recorded at the station. Therefore, wave information for CMS-Wave was obtained from Station 42035 of the NDBC. The buoy is located 22 nautical miles east of Galveston at a water depth of 13.7 m. Figure 51 shows input information for significant wave height (solid lines) on the left axis and 2010 and 2060 water levels (dashed and dotted lines, respectively) on the right axis. The discontinuity in wave height is due to wave direction moving offshore and away from Sabine Pass. These observations were omitted from the CMS-Wave input. Wave heights that approached Sabine Pass are low with a maximum of 0.182 m recorded.
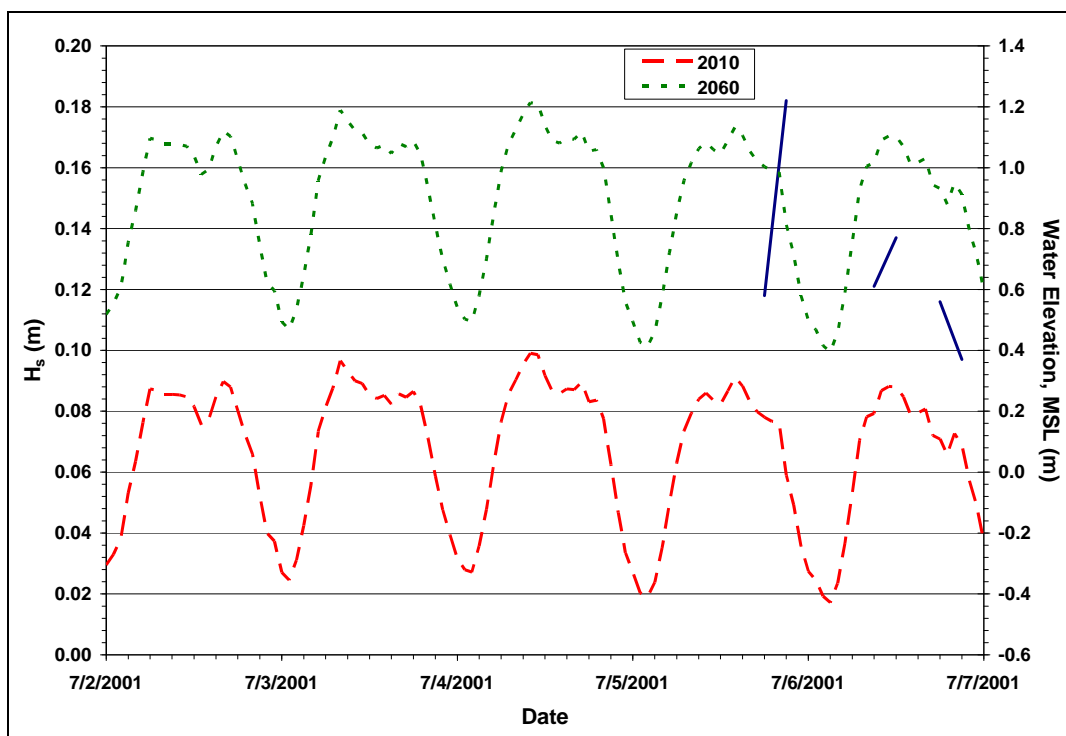
Figure 51. Input wave heights and water levels for fair-weather condition.

Storm conditions

Water levels for the storm conditions were obtained from WAVCIS Station CSI 03. Mean wave direction was not available at the station for the time periods simulated; therefore, wave information from NDBC Station 42035 was used for CMS-Wave input.

The Southeast storm simulated conditions from 13 July through 17 July 2003, and the input data, are shown in Figure 52. Maximum wave height during the period was 5.4 m and water levels reached 0.5 m and 1.3 m for years 2010 and 2060, respectively.

Input to the Southwest storm simulations are shown in Figure 53 for the period 17 January through 21 January 2006. A peak in wave height of 1.93 m occurred on 18 January, followed by a higher peak of 2.3 m on 19 January. Peak water levels were 0.5 m and 1.4 m for years 2010 and 2060, respectively.
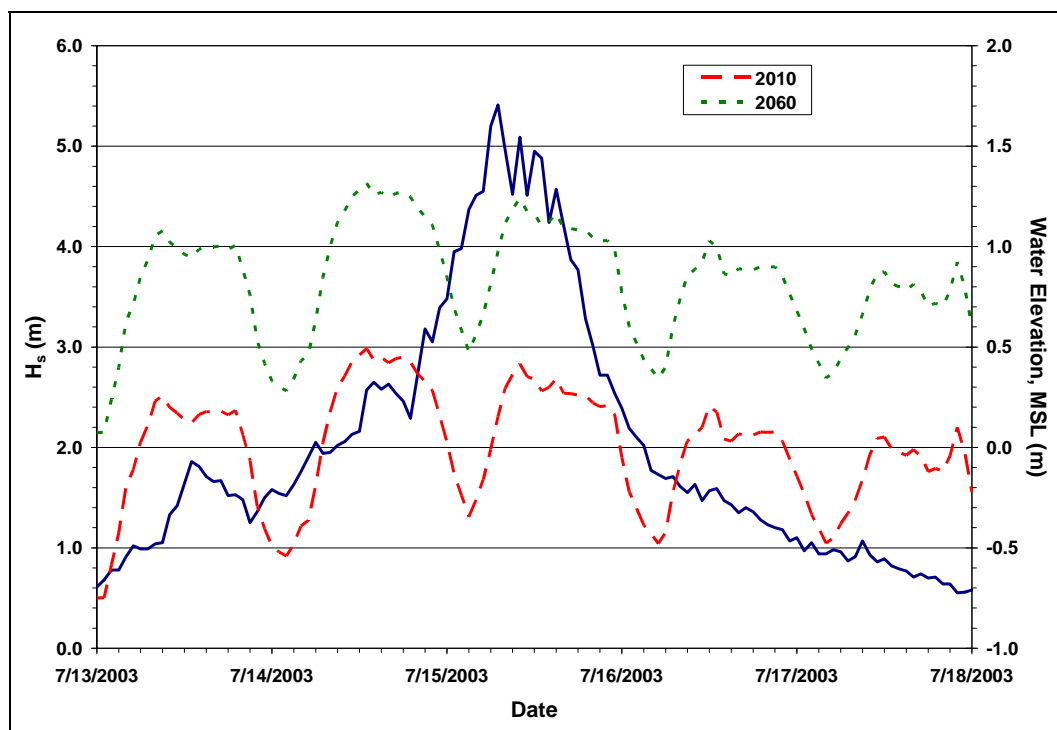
Figure 52. Input wave heights and water levels for Southeast storm.
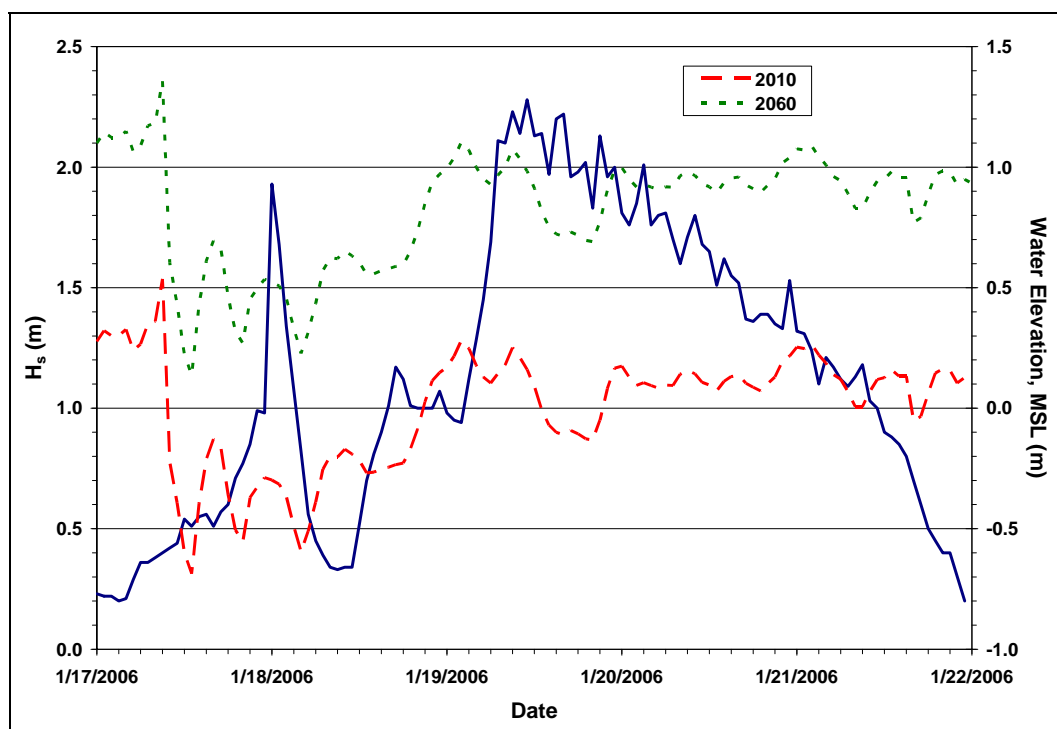
Figure 53. Input wave heights and water levels for Southwest storm.

Hurricane input was selected from the LACPR hurricane database. CMS input from Hurricane H266 is shown in Figure 54. Peak wave height was 6.1 m and peak water levels were 1.1 m and 1.9 m for years 2010 and 2060, respectively.
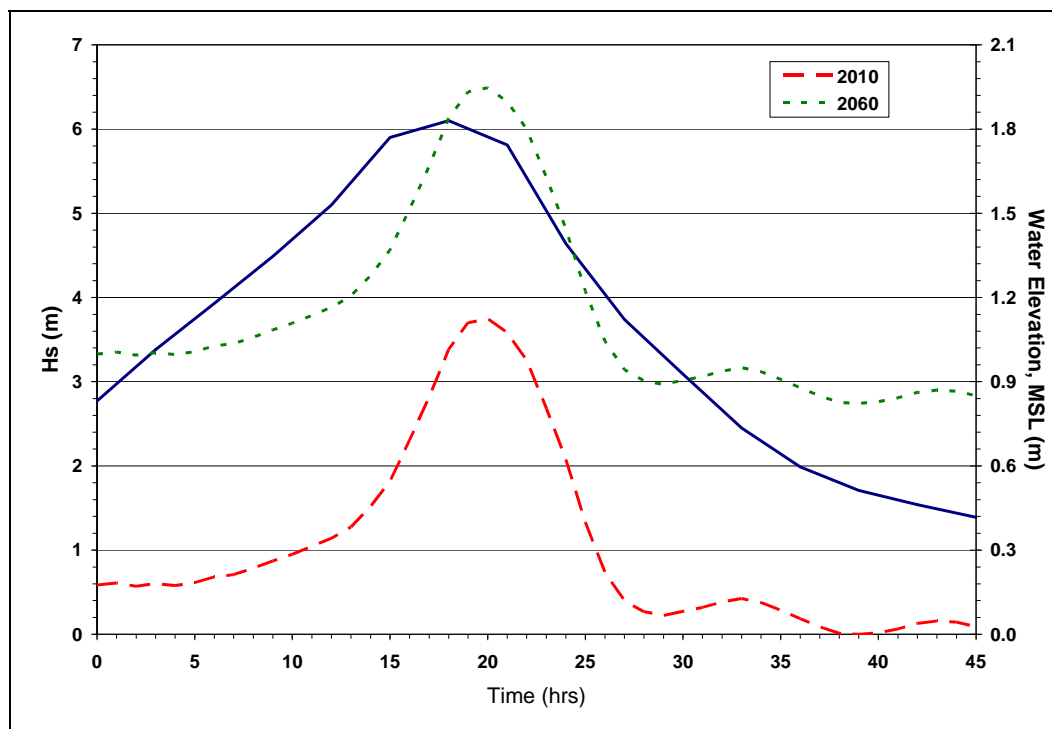
Figure 54. Input wave heights and water levels for H266.

Modeling of waves and flow

The CMS was applied to calculate nearshore waves and flow magnitude and direction. Model results were used to identify areas of potential channel shoaling and scouring of the jetties.

Potential channel shoaling

A parameter was computed based on sediment size and flow magnitude to determine locations of potential shoaling. Settling of suspended sediments can occur if the shear velocity, u_*, of the flow approaches the fall speed of the suspended sediment, w_s assuming the particles don't flocculate.

Therefore, if the ratio of u_* to w_s is less than unity, settling of suspended sediment should occur. The shear velocity is defined as:

$$u_* = \sqrt{\frac{\tau}{\rho}} \tag{19}$$

in which τ is shear stress of the flow and ρ is density of the fluid. Fall velocity was calculated by the optimization of Soulsby (1997):

$$w_s = \frac{\nu}{d_{50}} \sqrt{10.36^2 + 1.049 D_*^3} - 10.36 \tag{20}$$

where ν is kinematic viscosity, d_{50} is the sediment diameter, and D_* is the dimensionless particle size parameter.

Sediment samples collected by SWG between 1984 and 1996 showed d_{50} ranged between 0.002 and 0.06 mm in the jetty entrance channel and outer bar reaches. Fall speed was calculated with 0.03 mm grain size, which falls in the silt size range and is a size found in the outer bar reach in the vicinity of the jetty tips.

The suspension parameter, u_*/w_s, was calculated at all locations on the grid at each time step. Appendix A contains figures of all the storm simulations for each plan described in Table 6. Descriptions of selected results are given in the following section.

Low-energy wave condition

Figure 55 shows flow in the region of the existing jetty entrance channel and outer bar for the low energy simulation in year 2010. The vectors represent flow magnitude and direction. The magnitude of u_*/w_s is shown in the color bar. High values are indicated by red and values near unity are shown as dark blue. Values that fall below 1 indicate areas where flow is not strong enough to keep sediment in suspension. The parameter is high within the jetty entrance channel and decreases in the outer bar, where settling should occur.
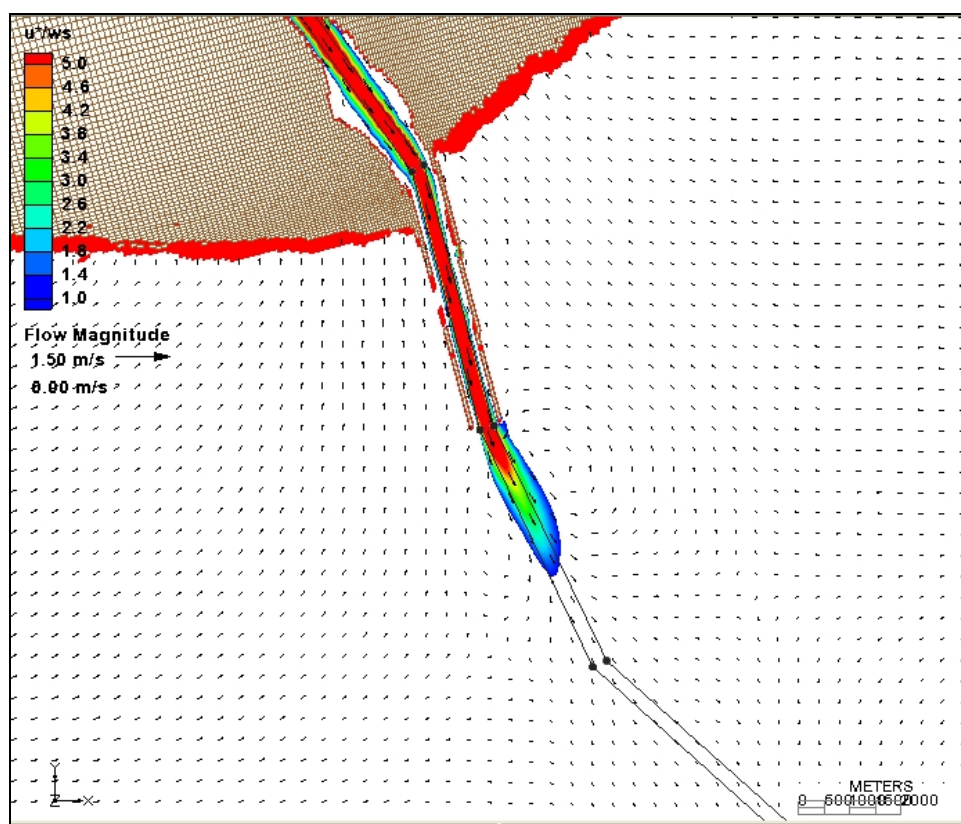
Figure 55. Flow patterns and suspension parameter for existing conditions and low energy simulation.

The existing condition also was simulated with low-energy waves and 2060 water levels (Figure 56). No deterioration of the jetties was assumed. The figure is similar to Figure 55 in that it shows settling to occur in approximately the same location in the outer bar channel, but also indicates a wider settling pattern outside the channel and settling occurring along portions of the West jetty closer to the shoreline.

Flow associated with the low energy simulation in 2010 with Plan 1 is shown in Figure 57. The suspension parameter contours are very similar to the existing condition. The patterns for Plan 2 and Plan 3 also are similar; however, the suspension parameter falls below 1.0 further into the Gulf with Plan 2. Plan 2 consists of rehabilitated jetties over their entire length. The constrained flow within the jetty channel has higher velocities than with the other plans, which keeps sediment in suspension further into the Gulf. The results of simulations with the low-energy waves indicate that dredging the channel to 48 ft MLW would have little effect on channel shoaling as compared to existing conditions.
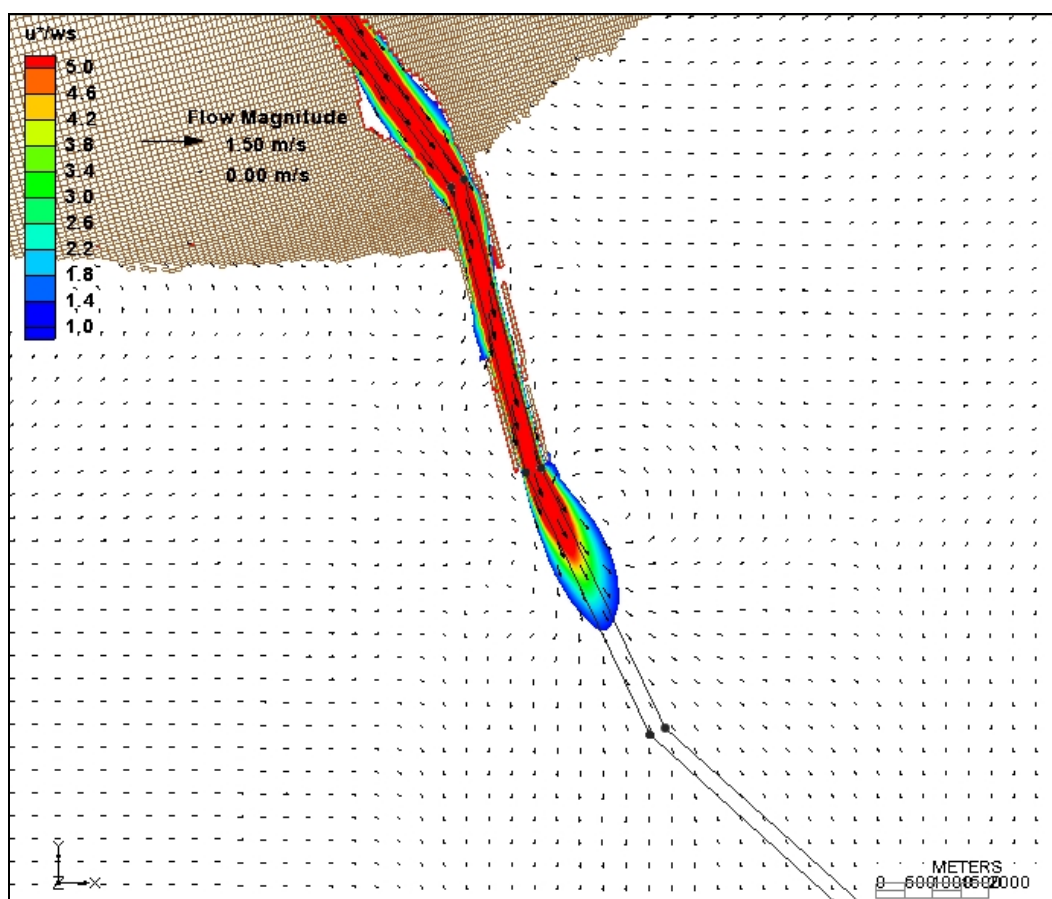
Figure 56. Flow patterns and suspension parameter for existing conditions
and low energy simulation in 2060.

Flow patterns and the suspension parameter for Plan 1 with the low-energy wave simulation in 2060 are shown in Figure 58. Settling occurs further into the outer bank reach and extends further outside east of the channel than Plan 1 in the 2010 condition. The same effect was observed with Plans 2 and 3.

Southwest storm

Flow associated with the SW storm is shown for existing conditions in Figure 59. The suspension parameter is high within the jetty channel and lower as the flow exits into the Gulf. The figure also shows flow vectors in the direction of the jetty gaps on the West jetty. The suspension parameter increases with flow direction, which indicates that suspended sediment is potentially transported into the channel from outside the jetties. Because the parameter is high within the jetties, sediment entering the jetty channel is probably transported to the outer bar reach and deposited.
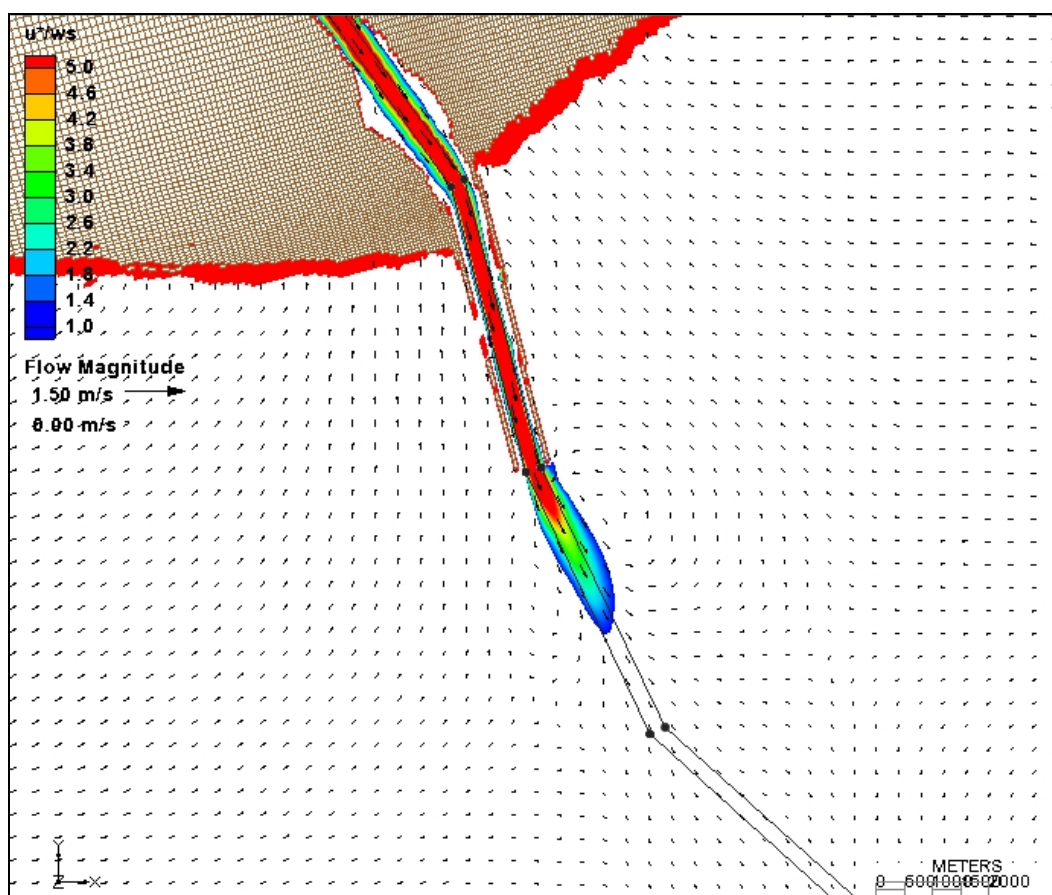
Figure 57. Flow patterns and suspension parameter for Plan 1 in 2010
and the low energy simulation.

The existing condition also was simulated with the SW storm and 2060
water levels (Figure 60). The suspension parameter contours are more
focused exiting the jetty than with the existing condition, but settling
occurs in the channel at approximately the same location. Additionally, the
figure indicates currents that flow over lower portions of the East jetty may
transport and deposit sediment outside of the jetty.

Figure 61 shows flow with Plan 2 in 2010. The suspension parameter is
high in the jetty channel but the intensity of the parameter decreases
immediately outside the jetty tips. However, the figure indicates settling
could occur in the same location in the channel as in the existing condi-
tion. Additionally, it appears settling could occur closer to the channel in
the outer bar reach. The simulations for Plans 1 and 3 showed similar
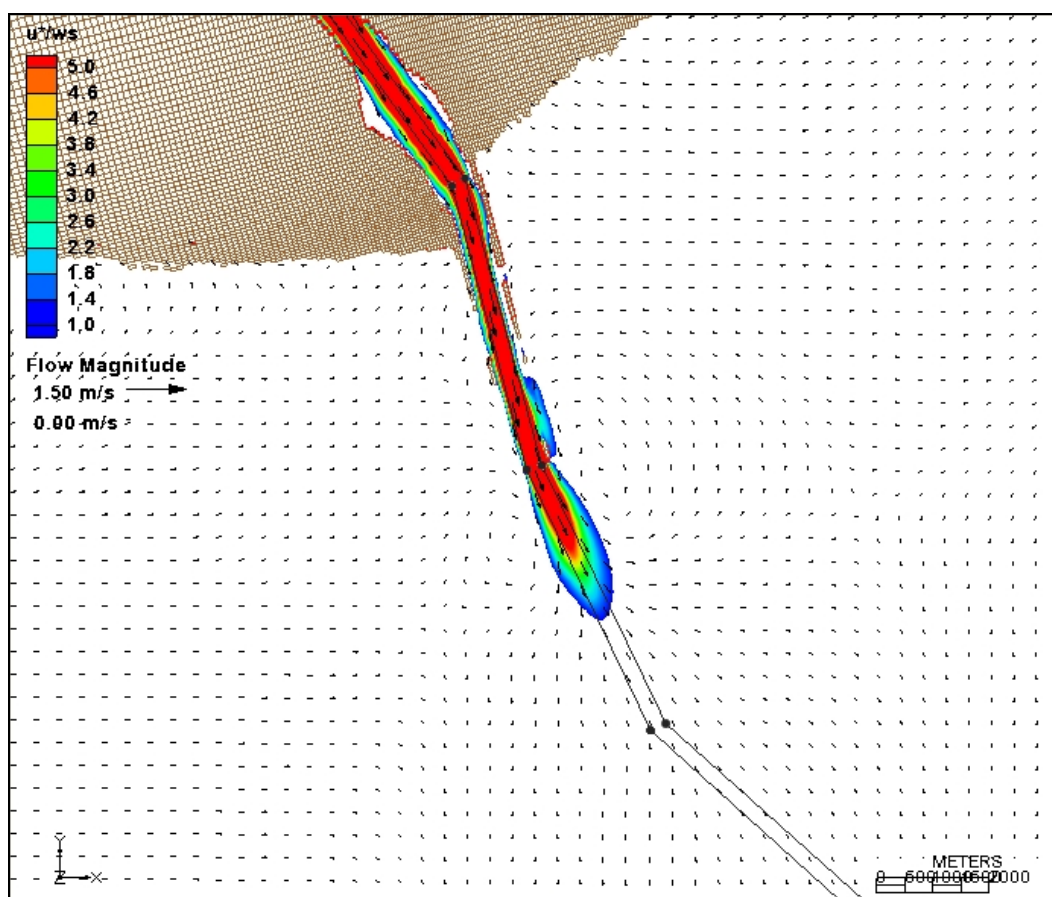results to the existing condition.

Figure 58. Flow patterns and suspension parameter for Plan 1 in 2060
and the low energy simulation.

The suspension parameter remains high in the jetty channel and extends further into the Gulf for Plan 2 with 2060 conditions (Figure 62). However, settling occurs in approximately the same location in the channel as in the existing condition. Plans 1 and 3 also show settling occurring in the same position.

Southeast storm

The existing condition with the SE storm shows a high suspension parameter extending outside of the jetty tips (Figure 63). The suspension parameter falls below 1.0 further into the outer bar reach than observed with the SW storm and the low-energy wave simulation. The figure also shows a northwest to southeast skewness to the suspension parameter contours, indicating settling may occur west of the channel near the jetties and east of the channel farther offshore.
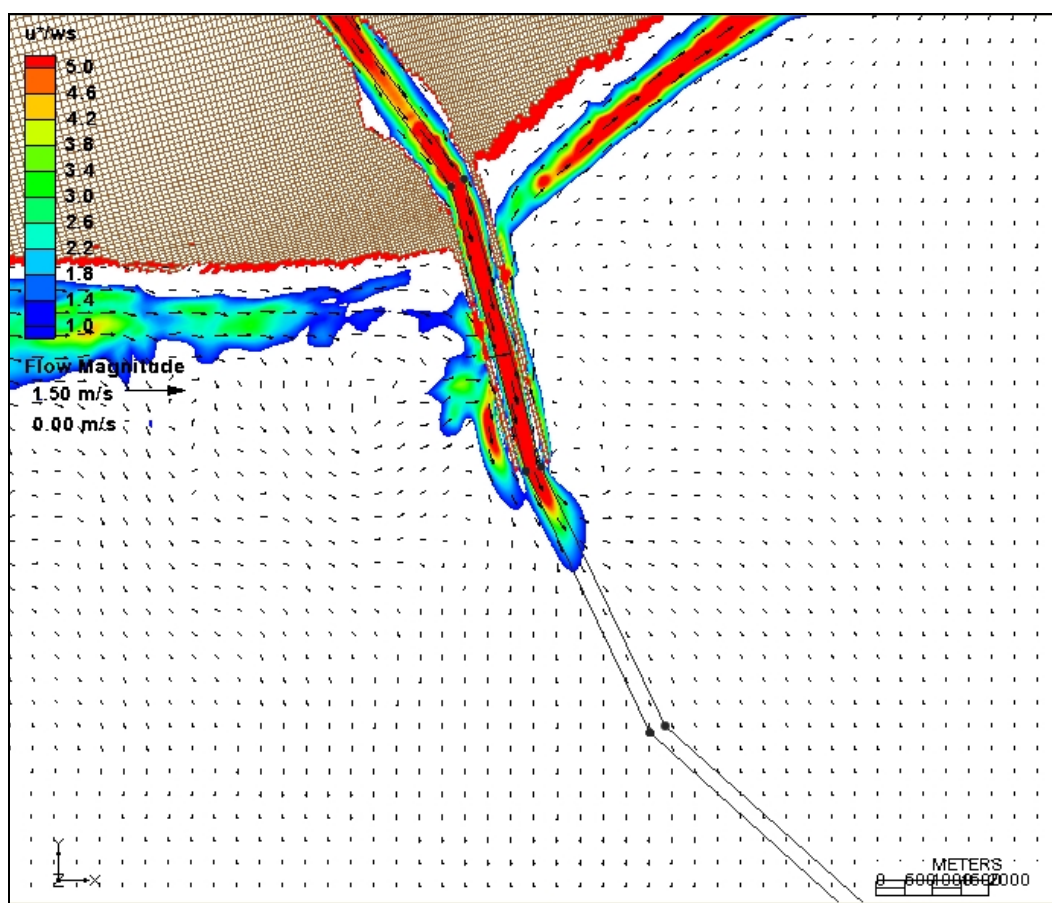
Figure 59. Flow patterns and suspension parameter for existing conditions and the SW storm.

Flow magnitude and the suspension parameter are higher in the jetty entrance channel for the SE storm at the 2060 water level (Figure 64). Settling is indicated in the channel at approximately the same location shown in Figure 63, but the suspension parameter contours are oriented to the west side of the channel.

Figure 65 shows flow patterns in 2010 with Plan 1. The suspension parameter contours are more aligned with the channel than observed with the existing condition, but also show a northwest to southeast orientation. Plans 2 and 3 also show skewness and all the plans show settling in approximately the same location as the existing condition.
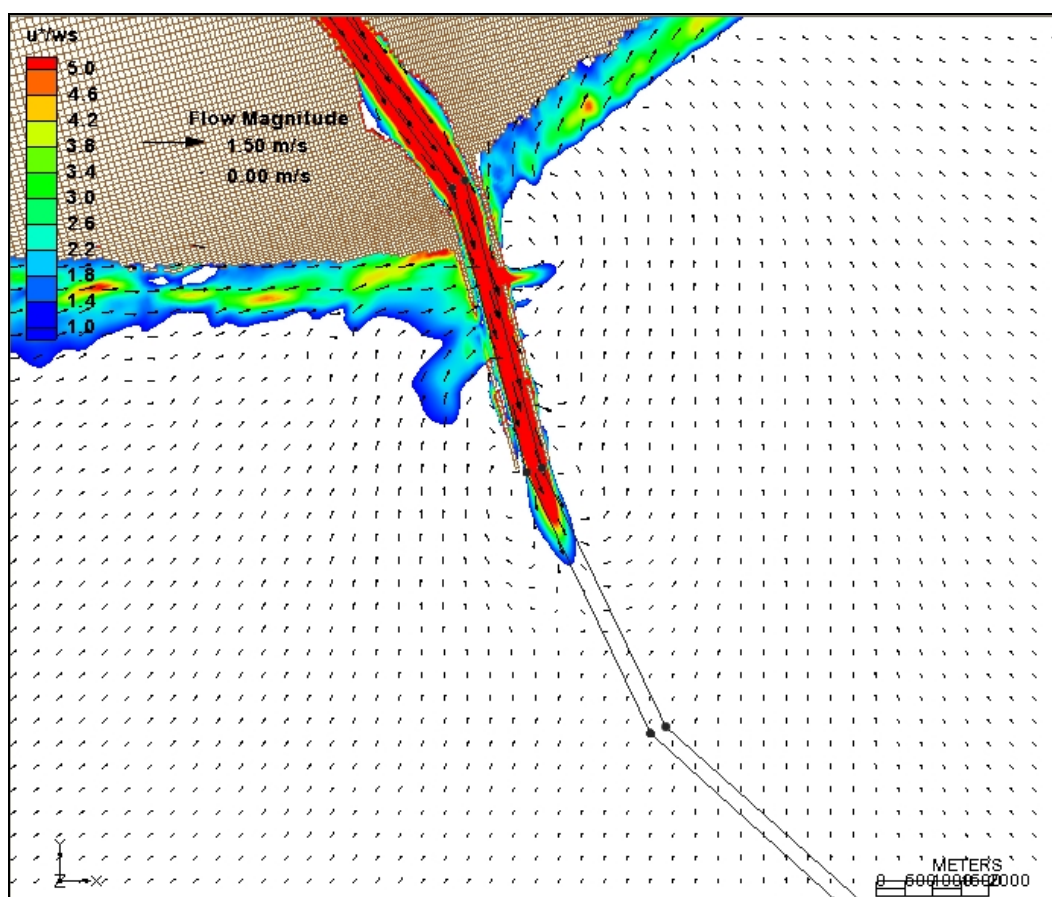
Figure 60. Flow patterns and suspension parameter for existing conditions
and the SW storm in 2060.

The flow patterns with Plan 1 for the SE storm in 2060 are shown in
Figure 66. Flow is directed out of the jetty entrance more southerly over
the deteriorated West jetty tips. The figure indicates settling would occur
on the west side of the outer bar channel, but also would occur within the
channel, but at a more shoreward location than existing conditions in
2060. Plans 2 and 3 also show a more southerly flow direction exiting the
jetty channel, but the direction change occurs at the West jetty tip.

Hurricane H266

Flow patterns for existing conditions with Hurricane H266 are shown in
Figure 67. Currents exiting the jetty channel are directed east, and the
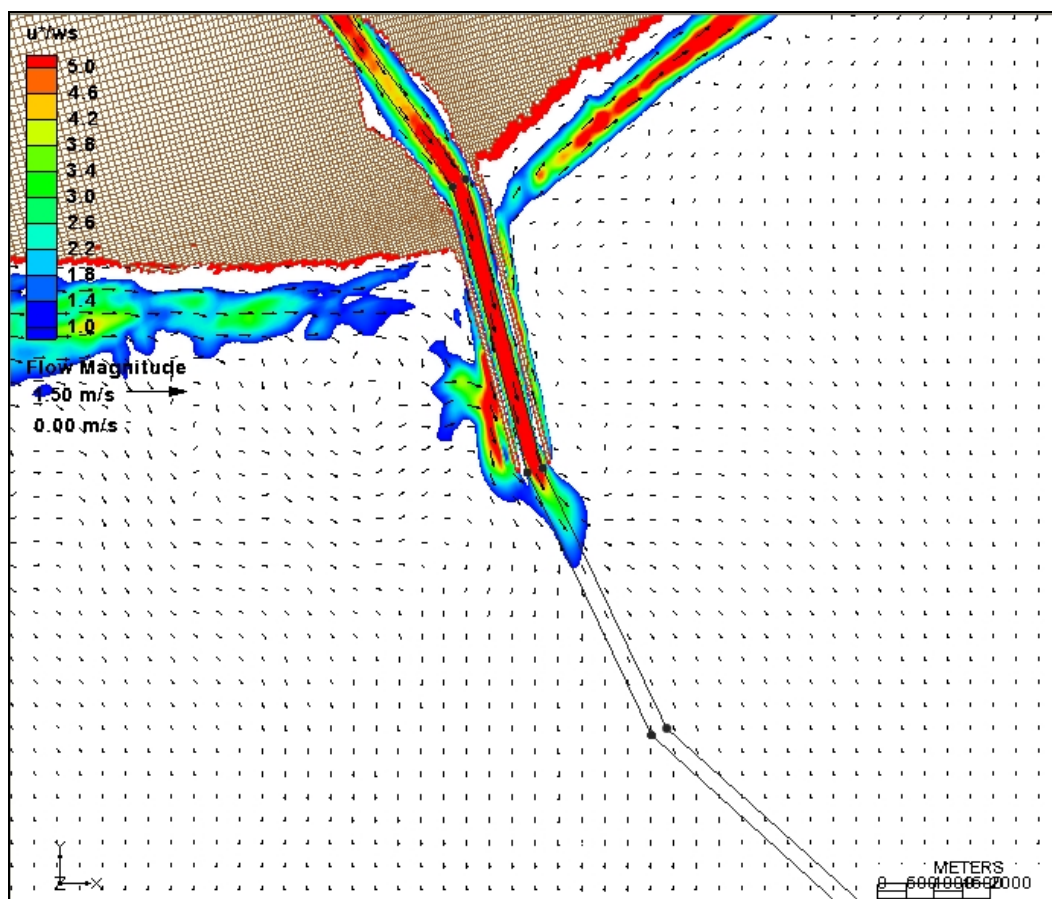figure indicates much of the settling would occur east of the channel.

Figure 61. Flow patterns and suspension parameter for Plan 2 and the SW storm in 2010.

Figure 68 shows the extent of suspension parameter contours is much less with the 2060 water level than with the existing condition. However, a higher intensity of the suspension parameter is observed along the East jetty where suspended sediment may transport out of the jetty channel.

A similar pattern to the existing condition is evident with Plan 3 for the H266 simulation in 2010 (Figure 69) with settling occurring mostly east of the channel. The result also was similar with Plans 1 and 2.

Flows also are directed to the east exiting the jetty channel for Plan 3 in 2060, but Figure 70 indicates the eastward extent in which settling would occur is much less. Flow capable of transporting sediment also exits the jetty channel along the gaps of the East jetty. Plan 1 flow exits the jetty channel along the entire length of the East jetty. Plan 2 flow exits through the jetty entrance and is diverted to the east. The suspension parameter contours have a sharper gradient with Plan 2 and settling occurs closer to the channel.
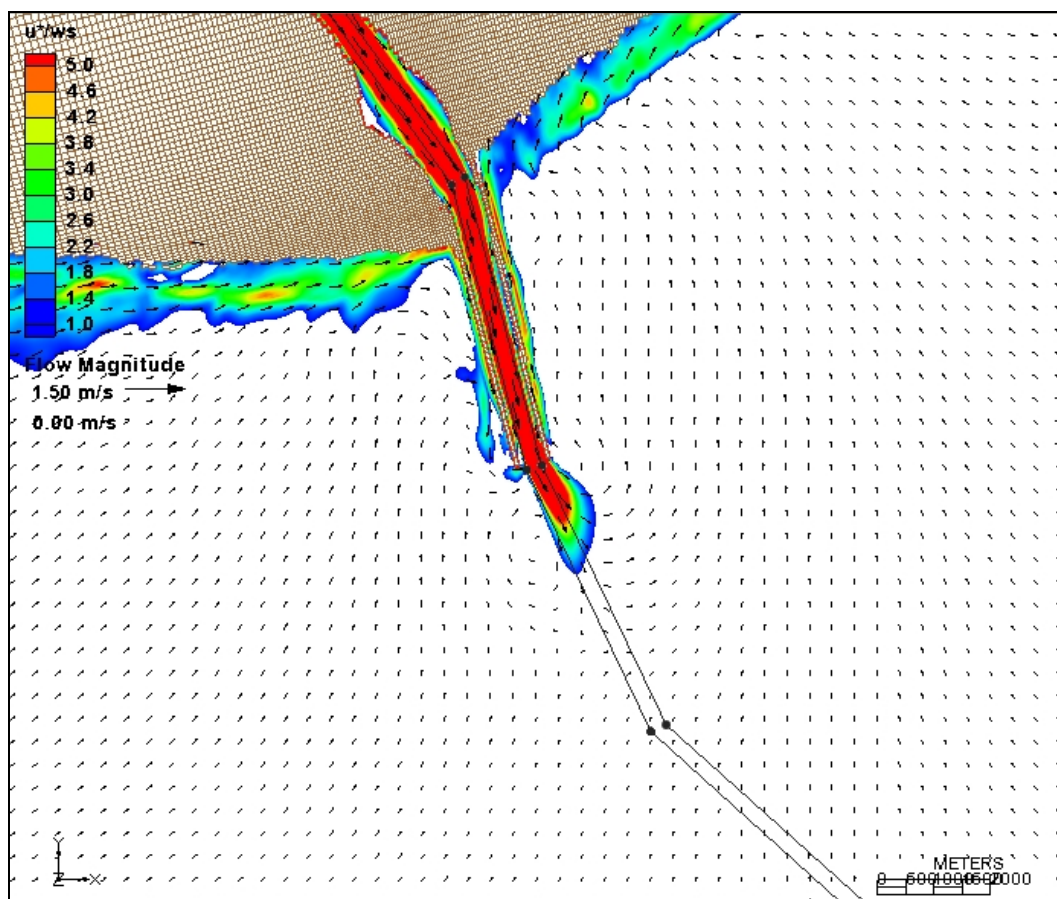
Figure 62. Flow patterns and suspension parameter for Plan 2 and the SW storm in 2060.

Potential scour

To determine areas of potential scour, the maximum flow at each grid cell during a storm of each plan was compared to the maximum flow for the existing condition. To evaluate the effect of sea level rise, the existing condition with the 2060 water level was compared to the existing condition in 2010 for each storm. Difference plots between all storms and plans and the existing conditions are shown in Appendix B.
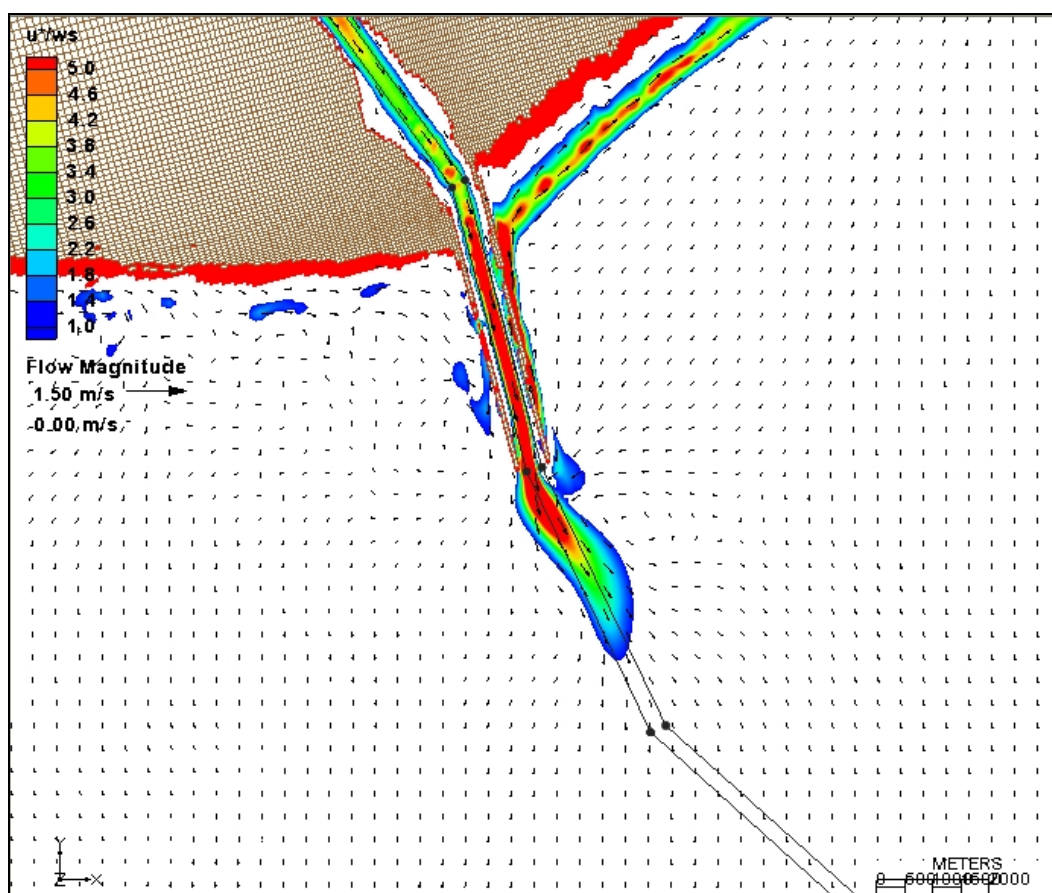
Figure 63. Flow patterns and suspension parameter for existing conditions and the SE storm.

Low-energy wave condition

Maximum flow differences between existing conditions in 2060 and existing conditions in 2010 for low-energy waves are shown in Figure 71. Positive values indicate that conditions in 2060 have a higher flow at a grid cell than the existing condition. Only differences exceeding ± 0.2 m/s were displayed. No differences were observed at the jetty tips and along the West jetty, except at the shoreline. However, flow increased more than 0.25 m/s along the outside of the East jetty and with an increase greater than 1.0 m/s near the shoreline. Additionally flow increased up to 0.6 m/s in the inner portion of the jetty entrance channel reach.

Figure 72 shows differences between Plan 1 and the existing condition for low-energy waves in 2010. All differences are within ± 0.2 m/s; essentially, Plan 1 has no effect on the present hydrodynamics with the low energy waves. Plans 2 and 3 gave similar results to Plan 1, only reduced flows were observed in areas in which the gaps of the jetties were rehabbed with the respective plan.
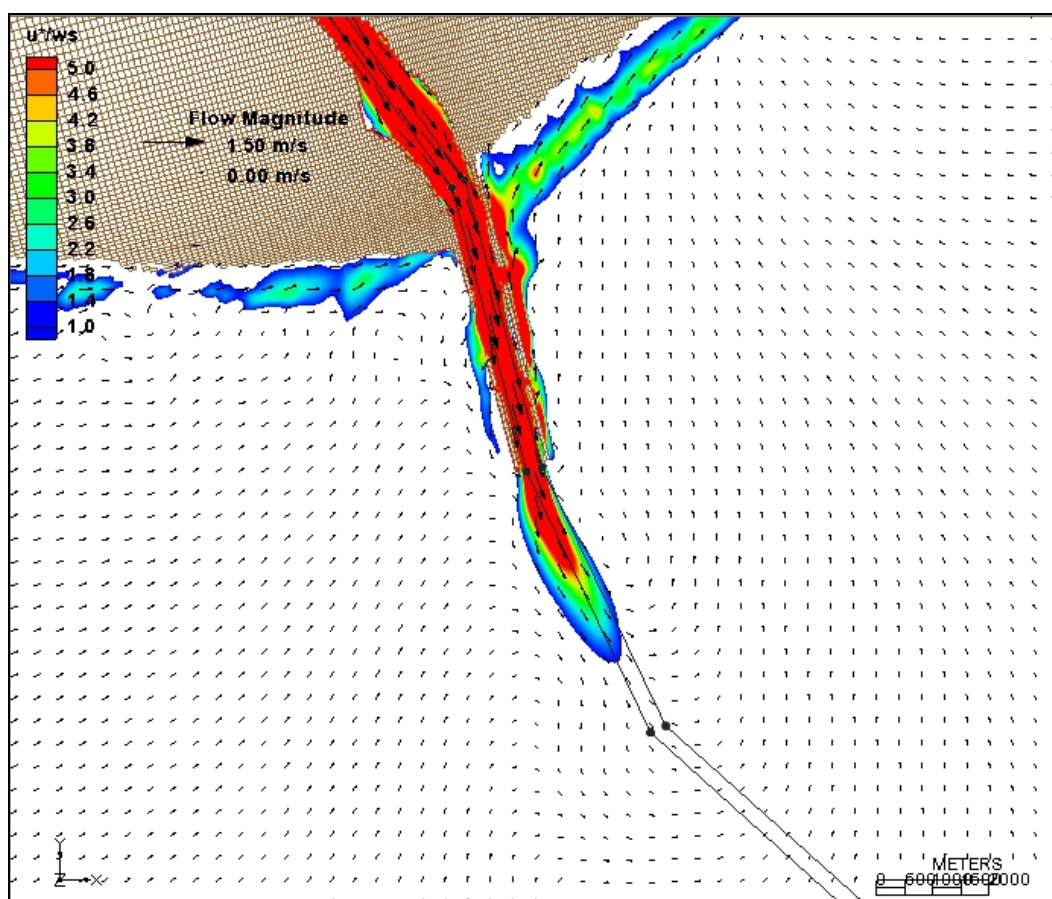
Figure 64. Flow patterns and suspension parameter for existing conditions and the SE storm in 2060.

Differences between Plan 1 and the existing condition for low-energy waves in 2060 are given in Figure 73. The figure shows similar results to the comparison at the 2010 water levels. Plan 3 also showed no changed compared to existing conditions. However with Plan 2, flow increased 0.5 m/s in the jetty channel and increased 0.4 m/s at the East jetty tip. Currents outside the jetties decreased. The total rehabilitation of the jetties confines the flow, which results in flow increases within the jetties and flow decreases along the outside of the jetties.

Southwest storm

Figure 74 shows maximum flow differences between existing conditions in 2060 and existing conditions in 2010 for the SW storm. Velocities in the channel decreased as much as 0.8 m/s with the 2060 water level. However, flow increased more than 1.0 m/s outside of the East jetty.
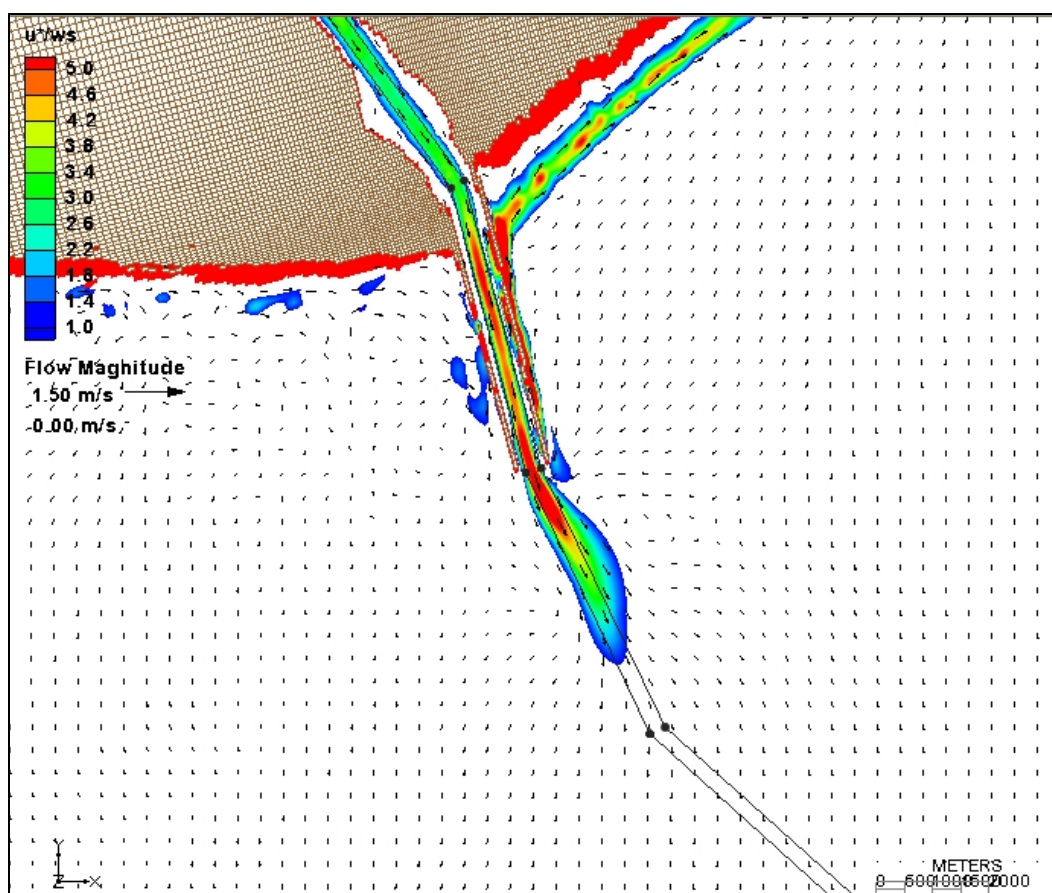
Figure 65. Flow patterns and suspension parameter for Plan 1 and the SE storm in 2010.

Differences between Plan 2 in 2010 and existing maximum flow conditions for the SW storm are shown in Figure 75. The only differences occur at grid cells where the jetties were rehabilitated. Plans 1 and 3 give similar results, indicating that no change in hydrodynamics occurs with the SW storm in 2010.

Difference in maximum flow between Plan 2 in 2060 compared to existing conditions is shown in Figure 76. Flow in the channel increases 0.4 to 0.5 m/s and increases to 0.6 m/s at the outer East jetty tip. Plan 1 currents decreased in 0.3 to 0.4 m/s in the outer portion of the jetty channel and increase up to 0.5 m/s along portions of the inside East jetty. Plan 3 showed no change in the channel, but flow increased up to 0.5 m/s along a portion of the East jetty.
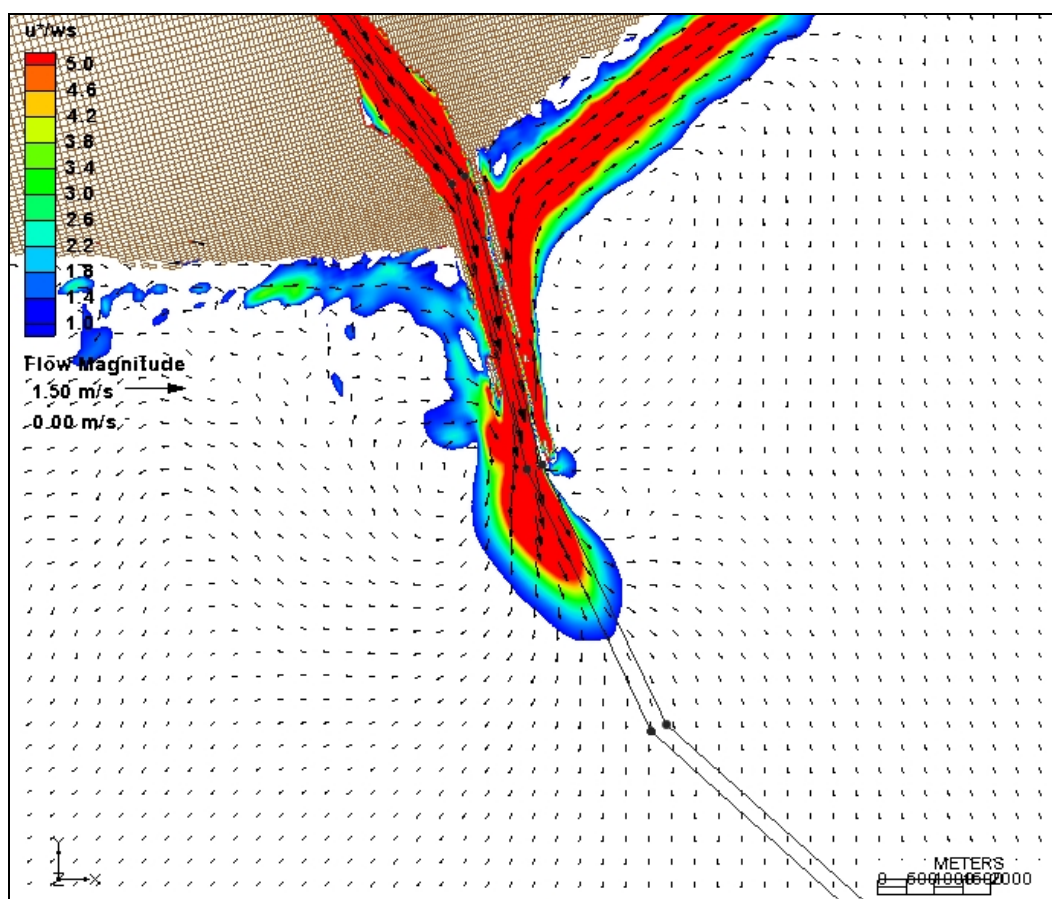
Figure 66. Flow patterns and suspension parameter for Plan 1 and the SE storm in 2060.

Southeast storm

Figure 77 shows maximum flow differences between existing conditions in 2060 and existing conditions in 2010 for the SE storm. Flow increases up to 1.0 m/s along the inside and outside of the East jetty, and increased 0.4 m/s at the shoreline of the West jetty. No difference in channel flow was observed, but flow decreased 0.4 m/s at both jetty tips. Additionally, currents decreased over the gap in the West jetty by 0.4 m/s.

The differences in maximum flow between Plan 1 in 2010 and existing conditions for the SE storm are shown in Figure 78. Flow decreased by 0.3 m/s and 0.4 m/s off the tips of the West and East jetties, respectively. Flow increased 0.4 m/s along the inner side of the outer East jetty. Plan 3 differences were similar with lesser decrease at the jetty tips. Plan 2 showed little change with exception to along both jetties where flow decrease 0.3 to 0.5 m/s.
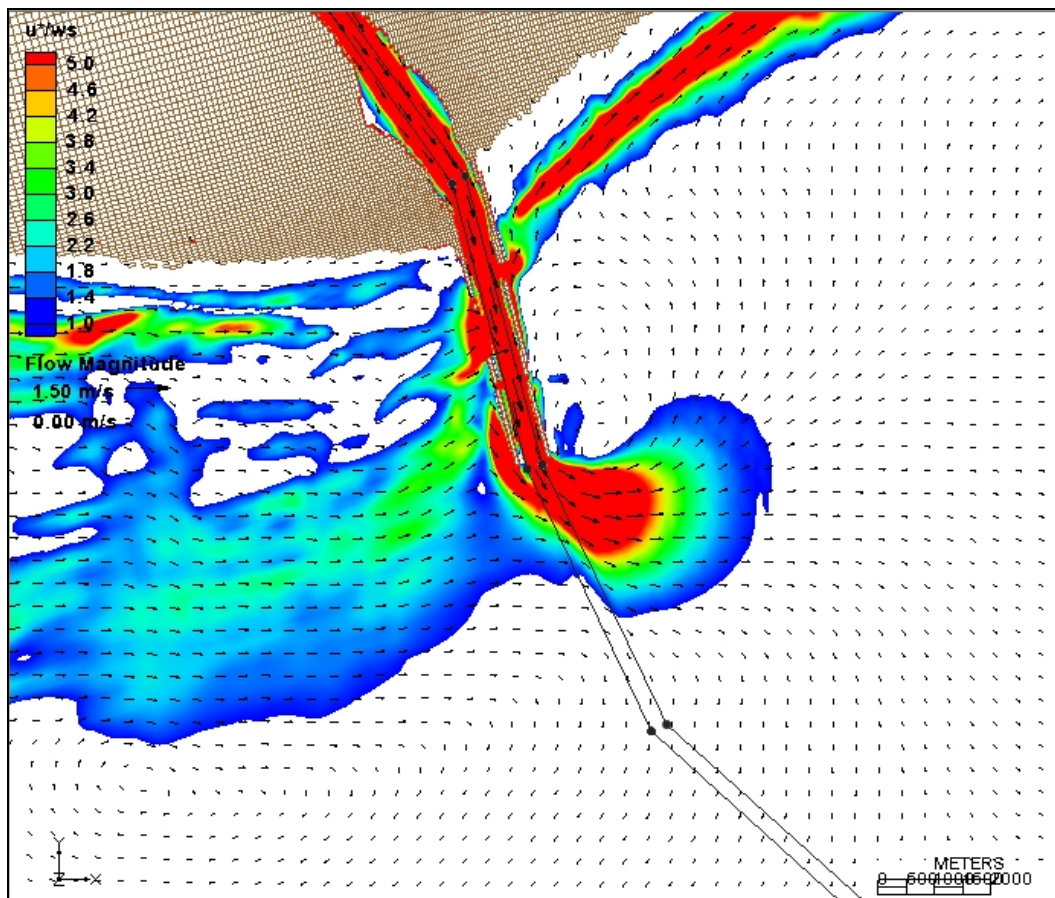
Figure 67. Flow patterns and suspension parameter for existing conditions and Hurricane H266.

Figure 79 shows maximum flow differences between Plan 1 in 2060 and existing conditions. Flow increases over 0.3 to 0.4 m/s along the outside of the East jetty where the jetty has deteriorated. Flow decreases over the deteriorated West jetty by 0.3 m/s. Plan 3 shows flow decreases of 0.3 to 0.6 m/s along the inside of the outer East jetty and decreases of 0.4 m/s along the inside of the outer West jetty. Currents at the jetty tips increased by 0.5 m/s with Plan 2, and flow decreased along most of East jetty 0.3 to 0.8 m/s.
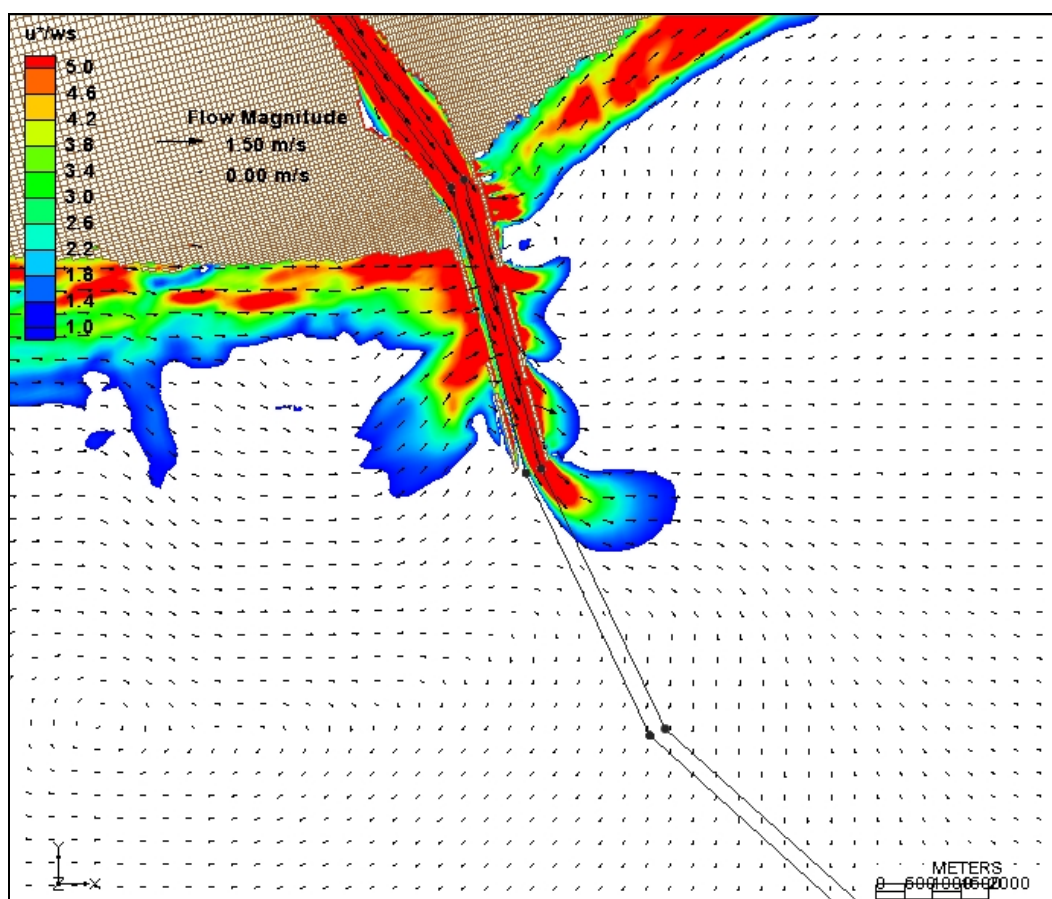
Figure 68. Flow patterns and suspension parameter for existing conditions
and Hurricane H266 in 2060.

Hurricane H266

Maximum flow differences between existing conditions in 2060 and exist-
ing conditions in 2010 for Hurricane H266 are shown in Figure 80. Flow
in the outer jetty entrance channel decreases 0.4 m/s, and flow decreases
at the West jetty tip. Additionally, flow outside of the East jetty tip
decreases 0.4 m/s. However, in the inner portion of the jetty channel, flow
increases 0.3 to 0.4 m/s. Currents at the shoreline near the West jetty
increase 0.4 m/s, and currents at the shoreline of the East jetty increase
0.6 m/s. Flow increases along both sides of the East jetty; 0.3 to 0.6 m/s
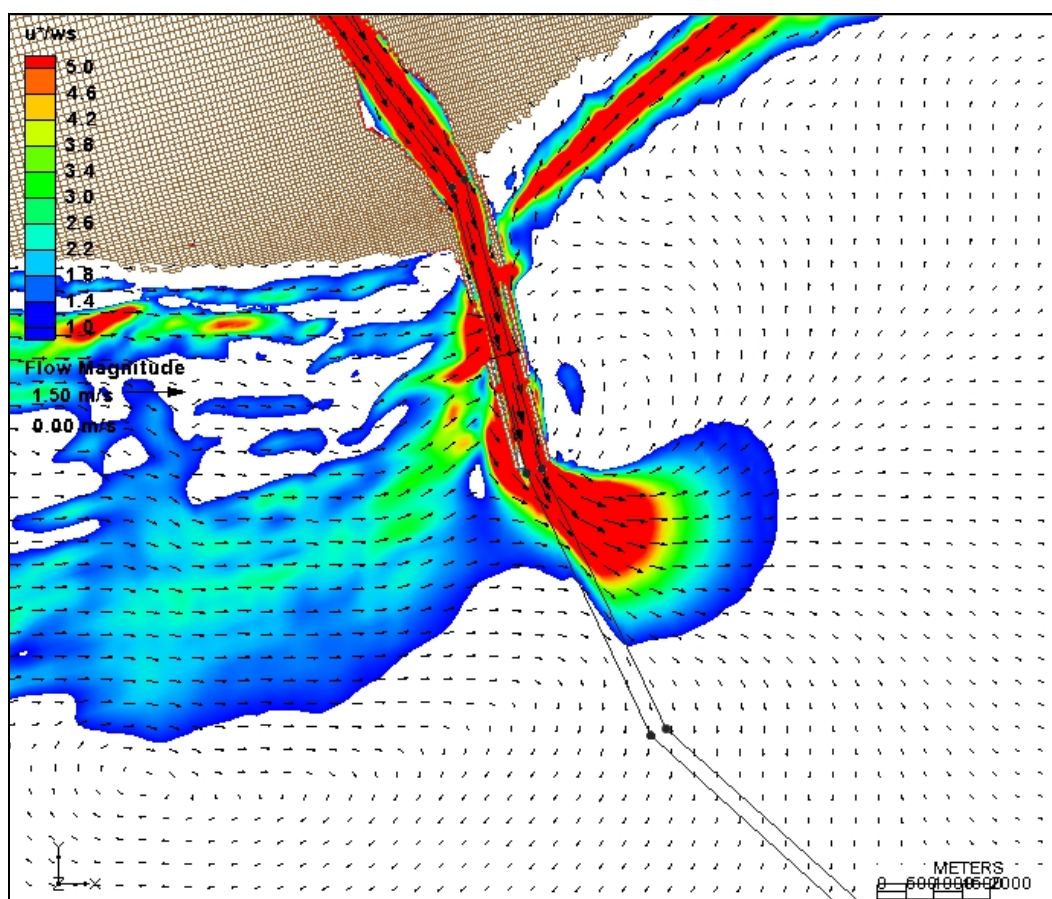on the inside and 0.5 to 0.6 m/s on the outside.

Figure 69. Flow patterns and suspension parameter for Plan 3 and Hurricane H266 in 2010.

Difference in maximum flow velocity between Plan 3 and existing conditions with Hurricane H266 in 2010 was limited to the outer portions of the jetties (Figure 81). Flow along the inside of the outer West jetty decreased 0.6 m/s and flow at the tip of the East jetty decreased 0.5 m/s. Plan 1 showed no difference with existing conditions. Plan 2 showed flow increase by 0.5 m/s on the inside of the outer East jetty and 0.3 m/s at the West jetty tip. Additionally, flow decreased 0.3 to 0.7 m/s along the West jetty and 0.3 to 1.1 m/s along portions of the East jetty.
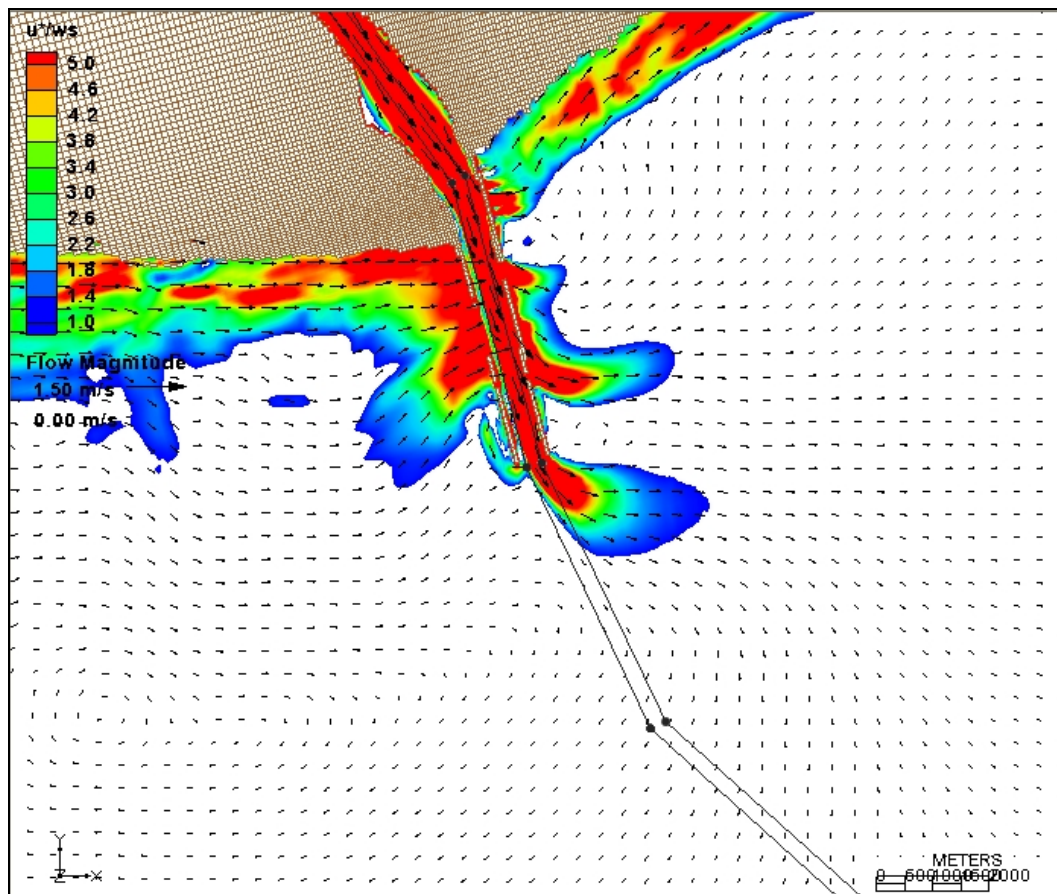
Figure 70. Flow patterns and suspension parameter for Plan 3 and Hurricane H266 in 2060.

Figure 82 shows maximum flow differences between Plan 3 in 2060 and existing conditions. Only minor differences are observed with the existing conditions. Flow decreased 0.3 m/s along the inside of the outer portion of the East jetty and 0.5 m/s along the inside of the outer portion of the East jetty. Plan 1 showed only 0.3 m/s increase in flow over the deteriorated portion of the outer West jetty. Plan 2 showed increased flow of 1.0 m/s at the West jetty tip and an increase of 0.3 to 0.6 m/s over most of the jetty channel. Flow decreases 0.6 m/s along the inside of the inside of the East jetty and over 1.0 m/s along the outside of the East jetty.
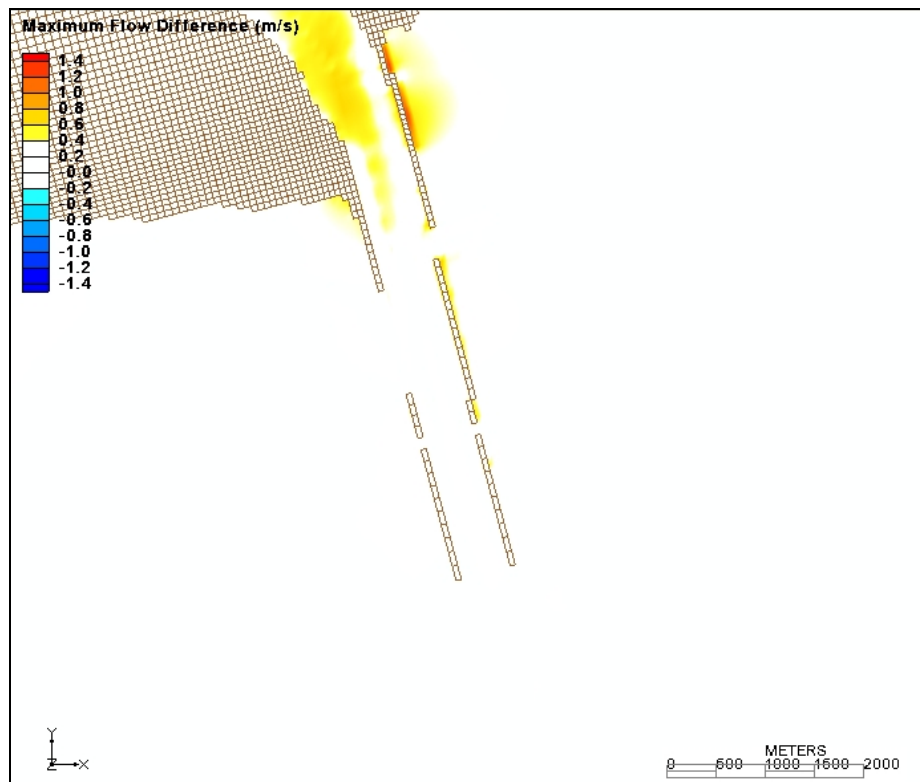
Figure 71. Difference in maximum flow magnitude between existing conditions in 2060 and existing conditions in 2010 for the low-energy wave simulation.

Figure 72. Difference in maximum flow magnitude between Plan 1 and existing conditions for the low-energy wave simulation in 2010.

Figure 73. Difference in maximum flow magnitude between Plan 1 and existing conditions for the low-energy wave simulation in 2060.
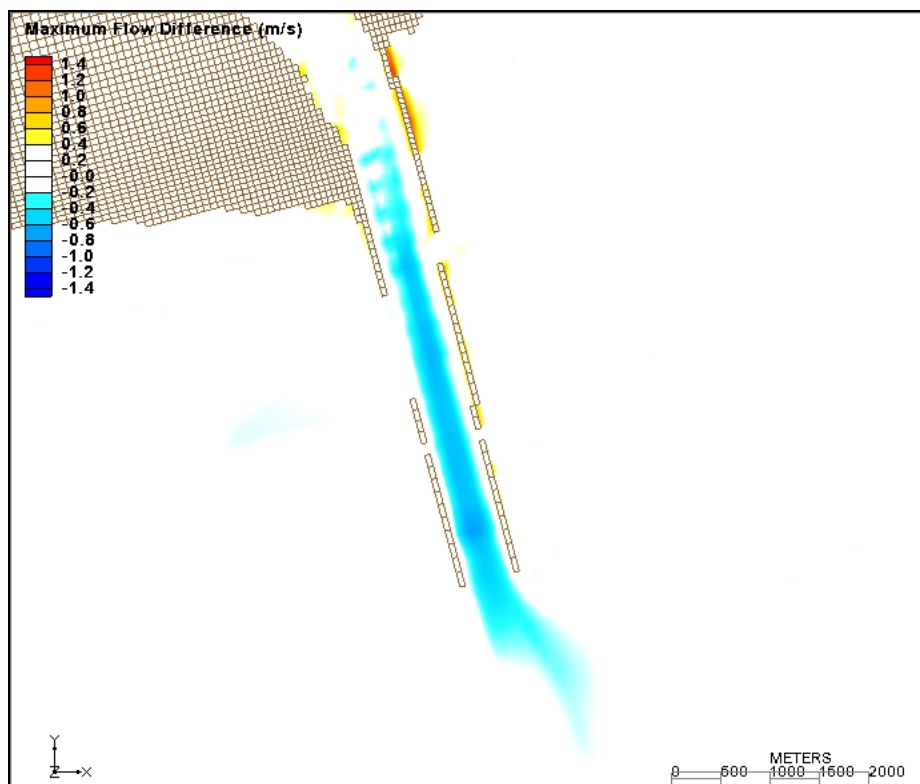

Figure 74. Difference in maximum flow magnitude between existing conditions in 2060 and existing conditions in 2010 for the SW Storm.
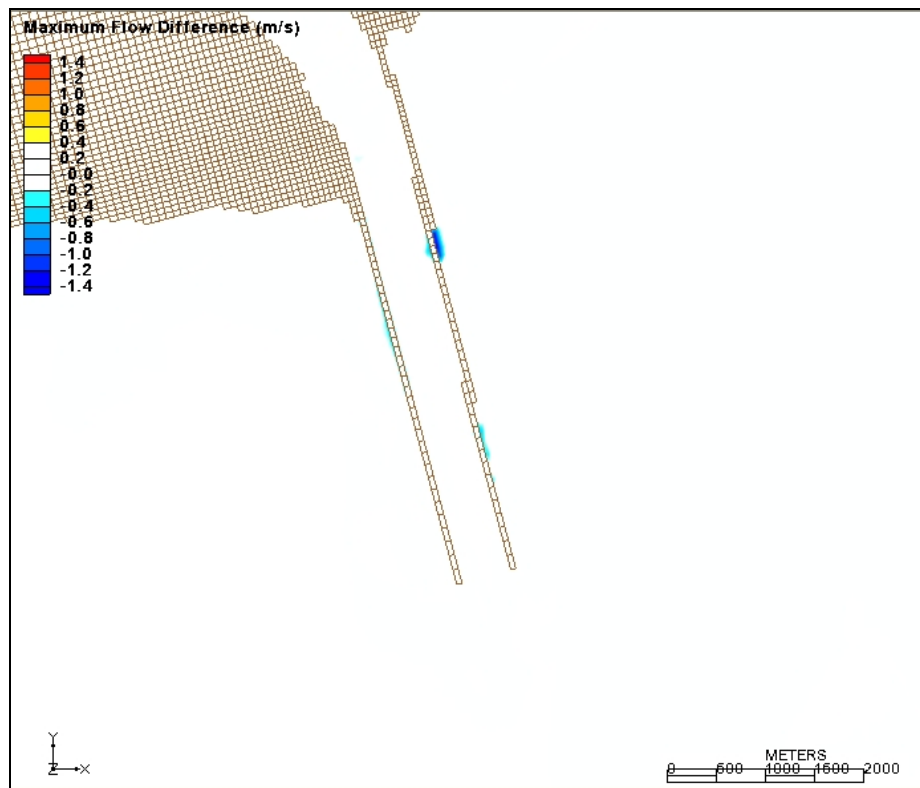
Figure 75. Difference in maximum flow magnitude between Plan 2 and existing conditions for the SW Storm in 2010.
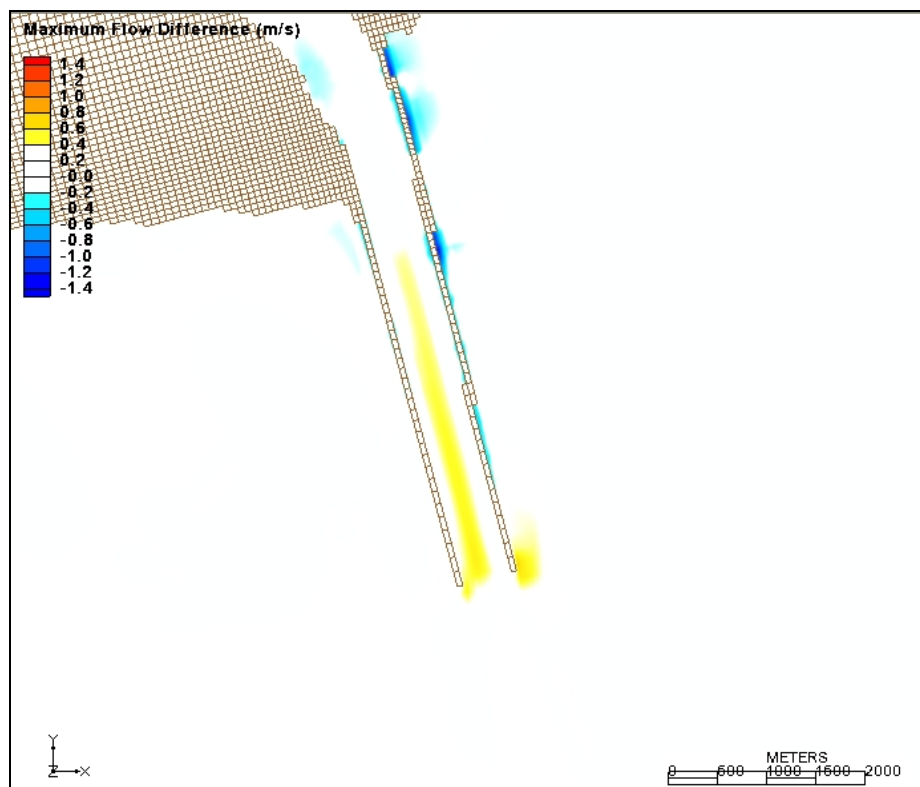

Figure 76. Difference in maximum flow magnitude between Plan 2 and existing conditions for the SW Storm in 2060.
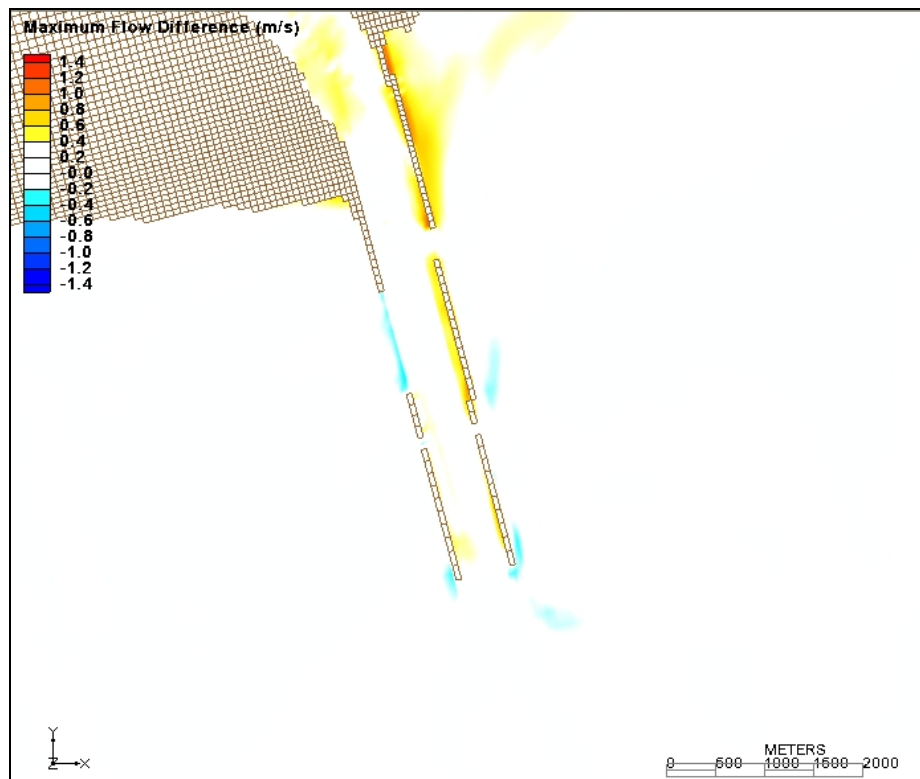
Figure 77. Difference in maximum flow magnitude between existing conditions in 2060 and existing conditions in 2010 for the SE Storm.

Figure 78. Difference in maximum flow magnitude between Plan 1 and existing conditions for the SE Storm in 2010.
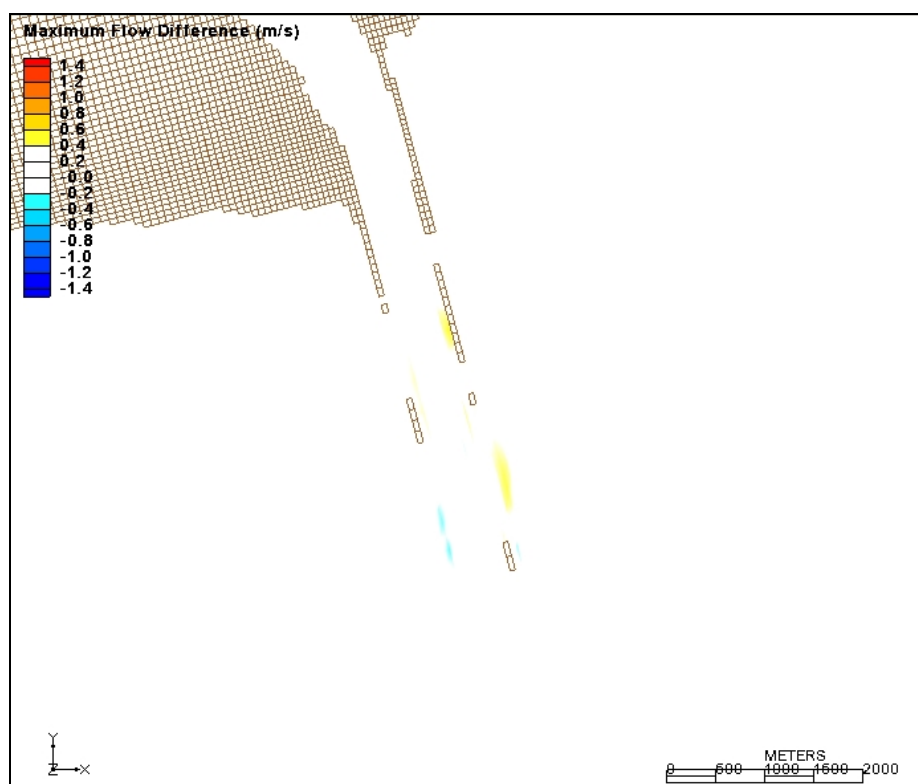
Figure 79. Difference in maximum flow magnitude between Plan 1 and existing conditions for the SE Storm in 2060.
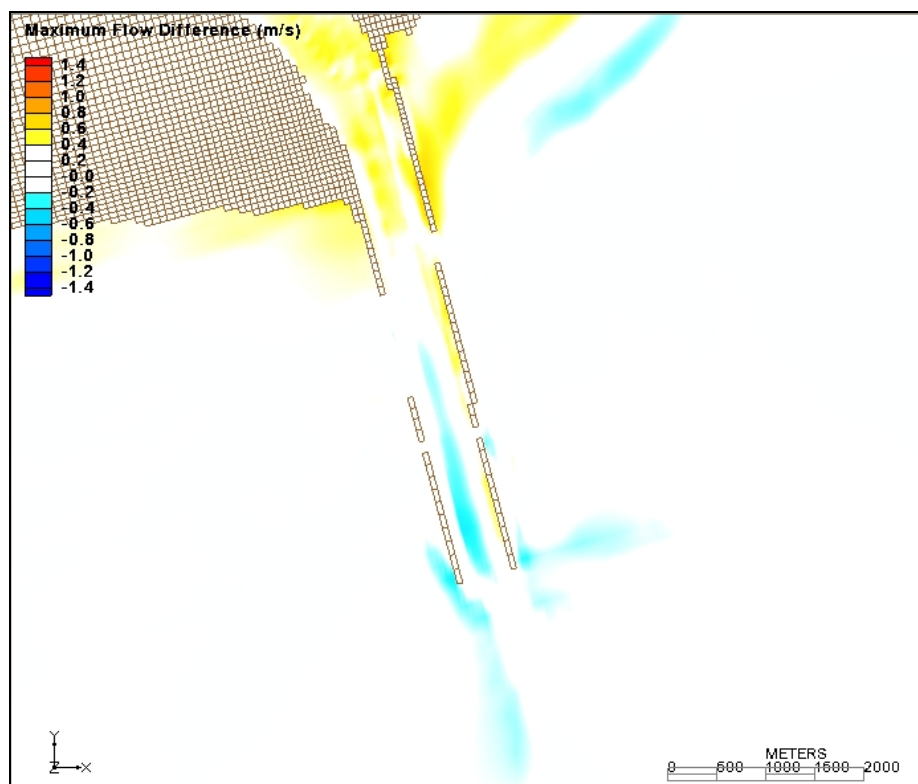

Figure 80. Difference in maximum flow magnitude between existing conditions in 2060 and existing conditions in 2010 for Hurricane H266.
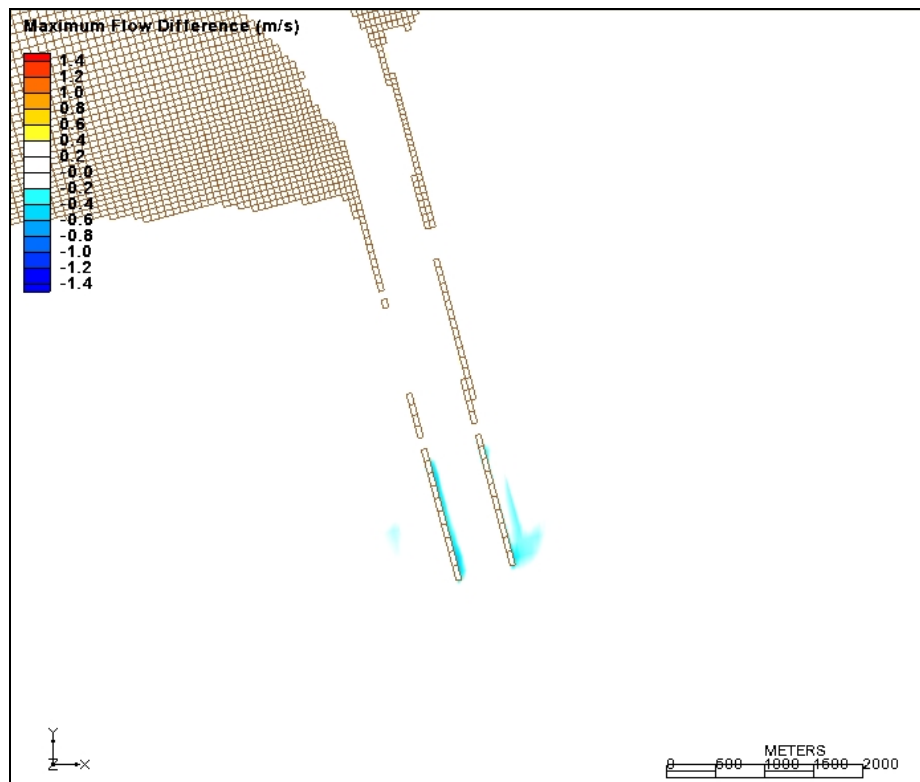
Figure 81. Difference in maximum flow magnitude between Plan 3 and existing conditions for Hurricane H266 in 2010.
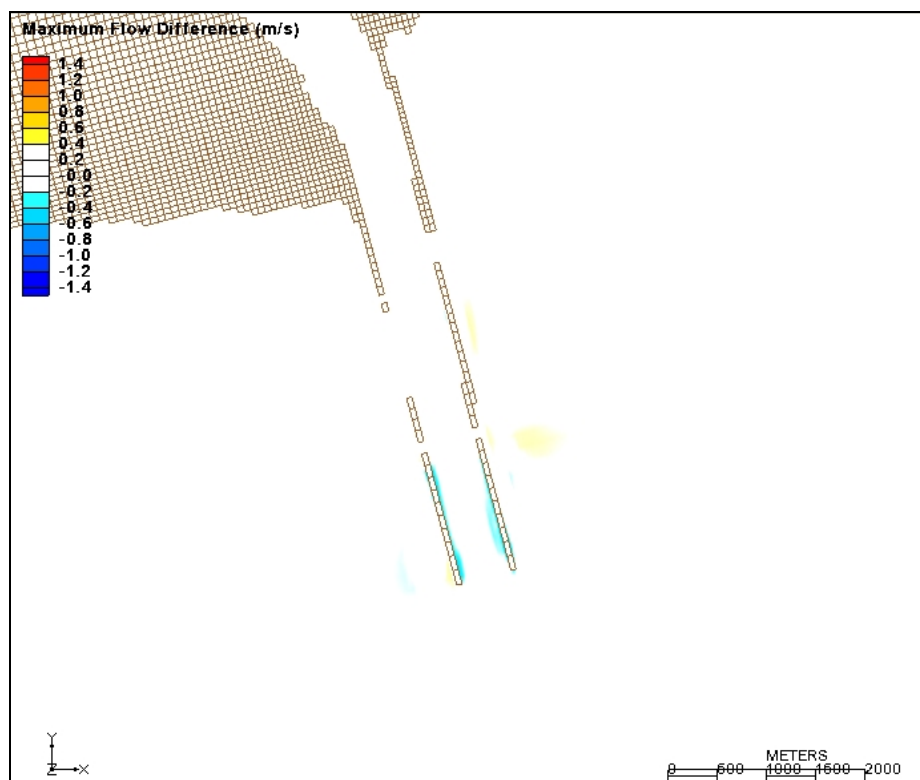

Figure 82. Difference in maximum flow magnitude between Plan 3 and existing conditions for Hurricane H266 in 2060.

8   Results

Numerical modeling

Results of the integrated wave, current, and sediment transport numerical model calculations were applied to infer the change in channel shoaling patterns and magnitudes for each of the plans considered, as well as to calculate the potential for scour at the base of the jetties. A suspension parameter was used to infer how cohesive sediment and fluid mud would be transported and deposited in the vicinity of the project area. Simulations were conducted for the existing condition jetties (2003), jetties in 2060 with no rehabilitation, and two options for rehabilitation as discussed previously. Each rehabilitation option was assumed to be completed in 2010, and these were reassessed with an increase in relative sea level in 2060. Four forcing conditions were used to simulate response: a low-energy wave condition, storms from the Southeast and Southwest, and a hurricane.

Comparison of the suspension parameter for each plan gave similar patterns and magnitudes of shoaling relative to the existing condition for the low-energy wave condition and each of the storms for 2010. None of the plans indicated that channel shoaling in the outer bar reach would be reduced. The plans differed from existing conditions for the storms in 2060, but the simulations showed that shoaling in the outer bar channel would continue at the same magnitude with possible differences in the location of deposition. To summarize, shoaling magnitudes appear to remain the same with all plans considered, but the location of channel shoaling may change in the outer bar region.

The highest flow differences indicated the potential for scour occurred between existing conditions in 2003 and existing conditions with the 2060 water level. Plans 1 and 3 showed increased flow over 1.0 m/s on the outside of the East jetty near the shoreline. The increase in flow at the shoreline is attributed to flow passing through the East jetty gaps and directed onshore along the outside of the jetty.

The differences in flows for all three plans compared to existing conditions were generally minor for 2010 conditions, with exception of Plan 2 with

Hurricane H266. Maximum flow differences between Plan 2 and existing conditions with Hurricane H266 in 2010, and with all the storms in 2060 showed that flow significantly increases in the jetty channel and at the jetty tips. In summary, the increase in flow for all plans indicates the potential for scour adjacent to the east jetty. Plan 2 indicates an additional potential for scour at the jetty tips. Calculations for Plans 1 and 3 indicated increased flow speeds along the eastern shoreline, which would increase the potential for flanking of the jetty.

Potential consolidation

Plan 1 is the option of no rehabilitation of the jetties. As shown in Figures 37 and 38, additional consolidation due to the jetty system is minor over the next 50 years (to 2060). The only change in jetty crest elevation relative to the mean water level is because of a rise in relative sea level. For this analysis, the Mean Low Water datum was recalculated each year with the projected increase in relative sea level as described previously (Scenario II with an increase of 2.7 ft in 50 years). The East and West jetty crest elevations as a function of distance along the structure are shown for Plan 1, with no rehabilitation (Figures 83 and 84). Without rehabilitation, the analysis indicated that the East jetty crest elevation would be approximately -1 to 2 ft MLW in 2060 and the West jetty would be at elevation -0.7 to -1.4 ft MLW by 2060 (red lines in Figures 83 and 84, respectively).
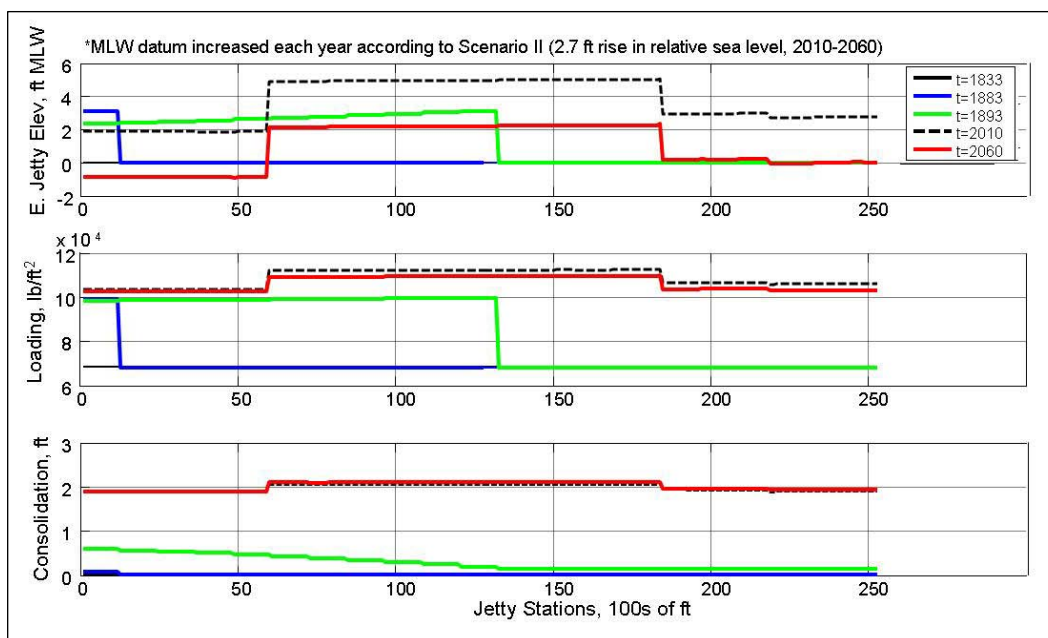

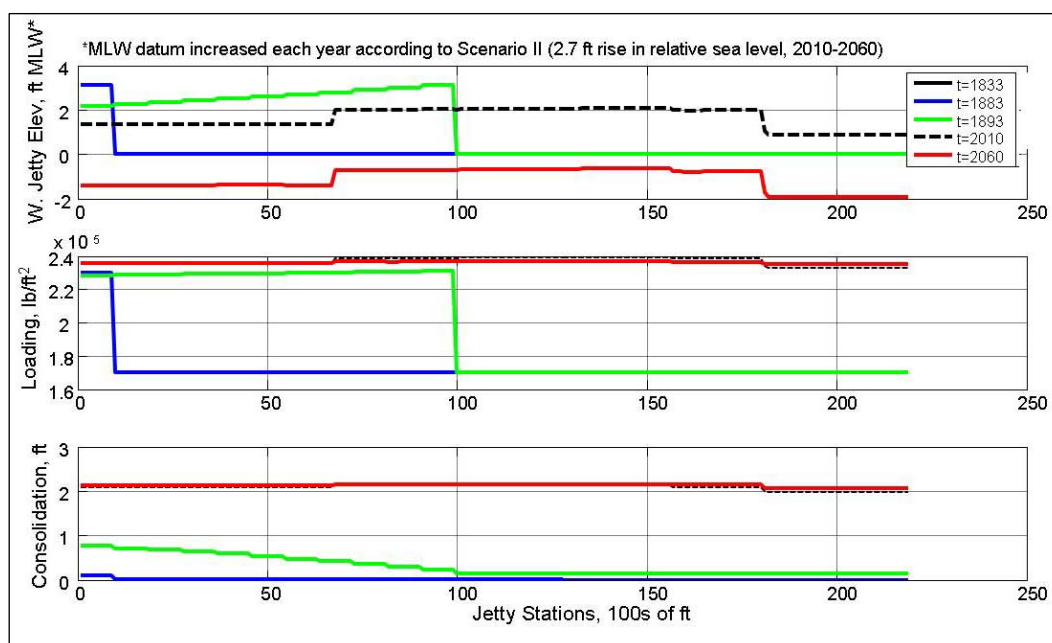Figure 83. East jetty crest elevation through time, Plan 1: no rehabilitation.

Figure 84. West jetty crest elevation through time, Plan 1: no rehabilitation.

Plan 2 is to rehabilitate both jetties such that the crest elevation in 2060 is approximately +6.2 ft MLW, the maximum elevation to which the East jetty was originally built in 1963-1964 (see Figure 4). For this analysis, the Mean Low Water datum was recalculated each year with the projected increase in relative sea level as described previously (Scenario II with 2.7 ft in 50 years). The analysis included the potential for consolidation due to the additional weight of the stone used to increase the elevation of the jetties. The analysis also estimated the required design crest elevation, if constructed in 2010, such that an elevation of +6.2 ft MLW would remain 50 years later, in 2060. All parameters in the consolidation program remained as determined previously.

For Plan 2, the jetties were rehabilitated such that their elevations in 2060 would equal +6.2 ft MLW. To obtain an elevation of +6.2 ft MLW in 2060, the East jetty would require an elevation of +9.2 ft MLW in 2010, and the West jetty would require construction to +9.3 ft MLW in 2010 (Figures 85 and 86). Note that 2.7 ft of this difference in elevation between 2010 and 2060 is due to relative sea level rise over the 50-year period, and the remaining 0.3 ft is due to the additional weight consolidating the under-lying substrate. Calculations for West jetty Stations 12,700 to 15,500 ft are very uncertain due to the large magnitudes of settlement in this area and the lack of known structure elevations to use for calibration of the con-solidation code.
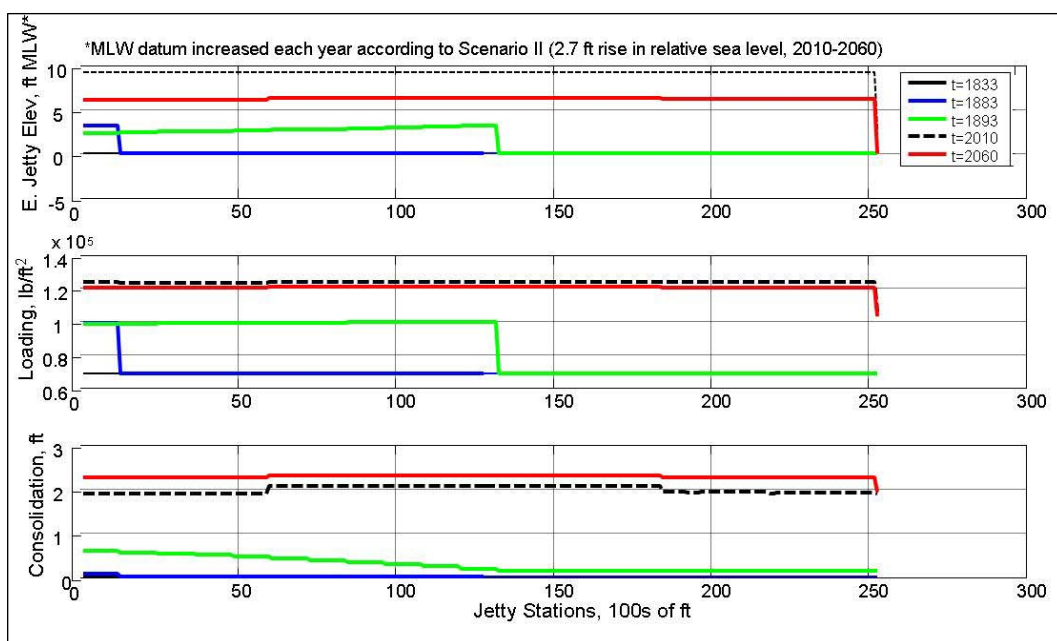
Figure 85. East jetty crest elevation through time, Plan 2: rehabilitation to +9.2 ft MLW.
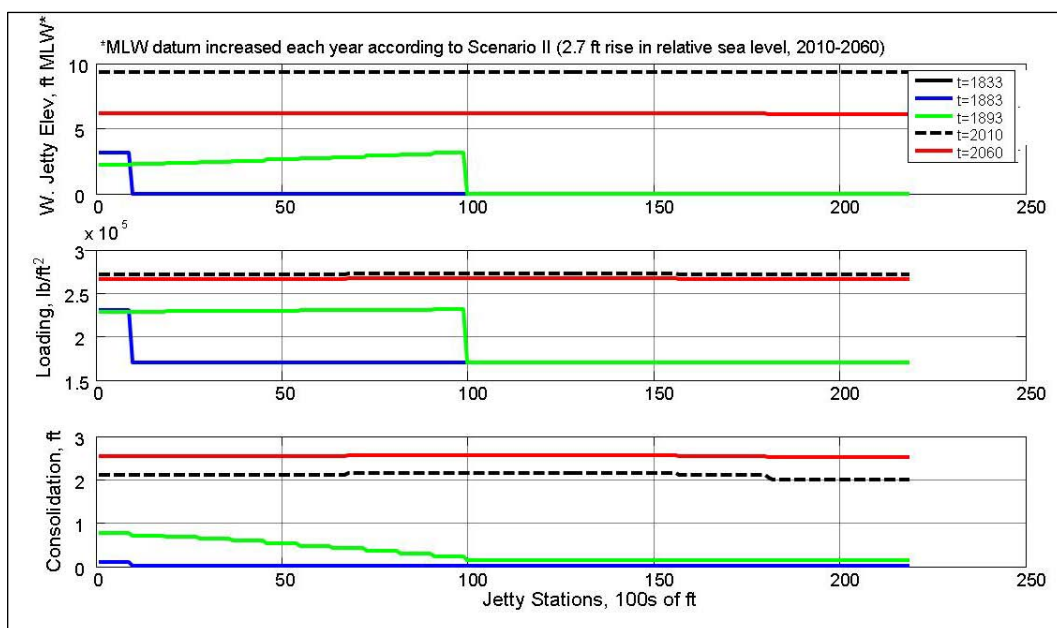

Figure 86. West jetty crest elevation through time, Plan 2: rehabilitation to +9.3 ft MLW.

Plan 3 increases the crest elevation of the outer 4,000 ft of both jetties to +9.2 ft MLW (East) and +9.3 ft (West) (Figures 87 and 88, respectively). With Plan 3, the East jetty crest elevation landward of Station 21,200 ft ranges between -1 and 2 ft MLW in 2060, whereas the seaward 4,000 ft is at +6.2 ft MLW (red line in top panel of Figure 87). For the West jetty,
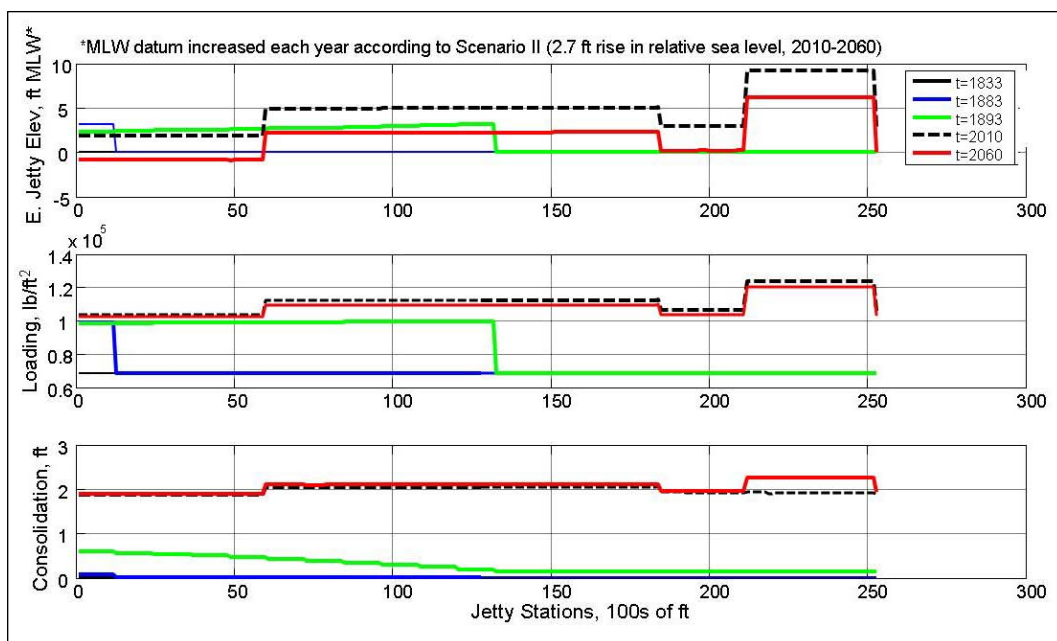
Figure 87. East jetty crest elevation through time, Plan 3: outer 4,000 ft to +9.2 ft MLW.
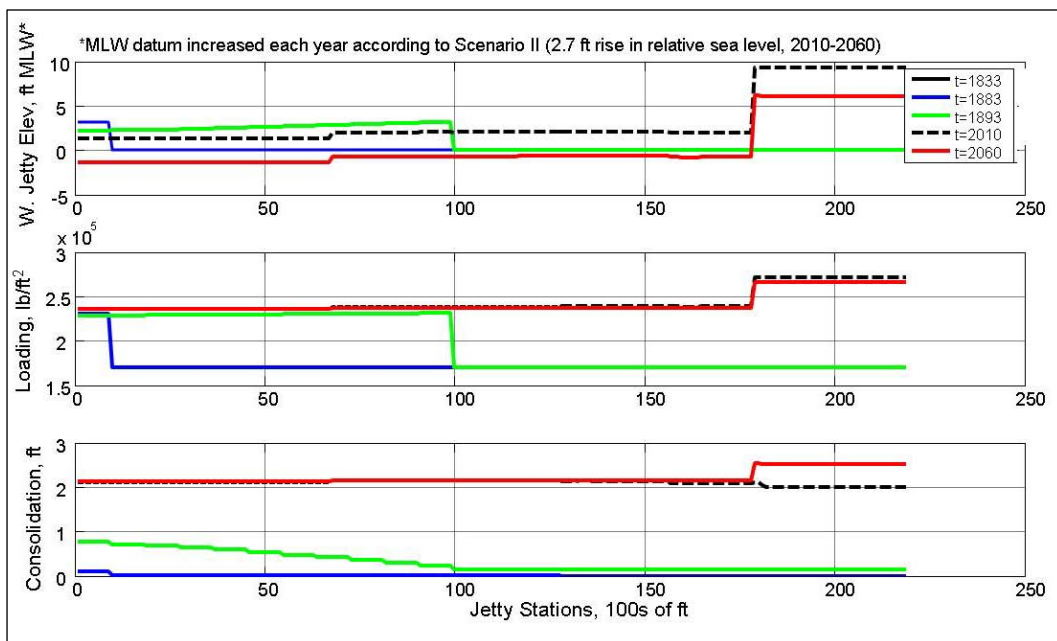

Figure 88. West jetty crest elevation through time, Plan 3: outer 4,000 ft to +9.3 ft MLW.

Plan 3 results in elevations landward of Station 17,900 ft ranging from -0.7 to -1.4 ft MLW in 2060 (Figure 88). The seaward 4,000 ft of the West jetty is +6.2 ft MLW in 2060.

Stability and storm damage

The Monte-Carlo simulations of jetty damage evolution found that significant damage would be accumulated on the East jetty by year 2060 at stations seaward of Stations 200+00 (20,000 ft along the jetty), though the previously repaired, seaward areas (that are "spikes" of crest elevation) have substantially lower damage due to the increased armor stone size at these locations. The West jetty will have significant damage from Station 190+00 seaward (19,000 ft seaward along the jetty). Damage values tend to be lower on the West jetty primarily because depths are less, resulting in lower wave energy, than along the East jetty.

For the rehabilitated 2060 condition, those regions with damage values greater than 20 can be redesigned with recommended stone size and raised to an elevation commensurate with sea level rise. After hydrodynamic and sediment pathway modeling of this condition, other reaches could be increased in elevation if it was thought that change was required to alleviate difficult flow conditions or possible increased sedimentation.

If the structures are to be rehabilitated, the Monte Carlo method developed for the Sabine-Neches site may be applied for stone sizing. Figure 89 shows a design curve developed from the site specific wave conditions based on LACPR hurricane data and WIS wave data. For a given depth along the jetty, a stone size would be selected so that its S value would be at most 20, and possibly a lesser value to minimize damage. The horizontal red curve defines the upper limit that would be desired. Note that each stone size shown has two curves. The "flank" stone curves are recommended for the more shoreward jetty locations and the "seaward end" represents portions of jetty that could receive wave attack from the side open to the sea and waves entering the channel that could impinge on the jetties and cause damage. To make final jetty design cross-sections, a physical model study is recommended to minimize cost.
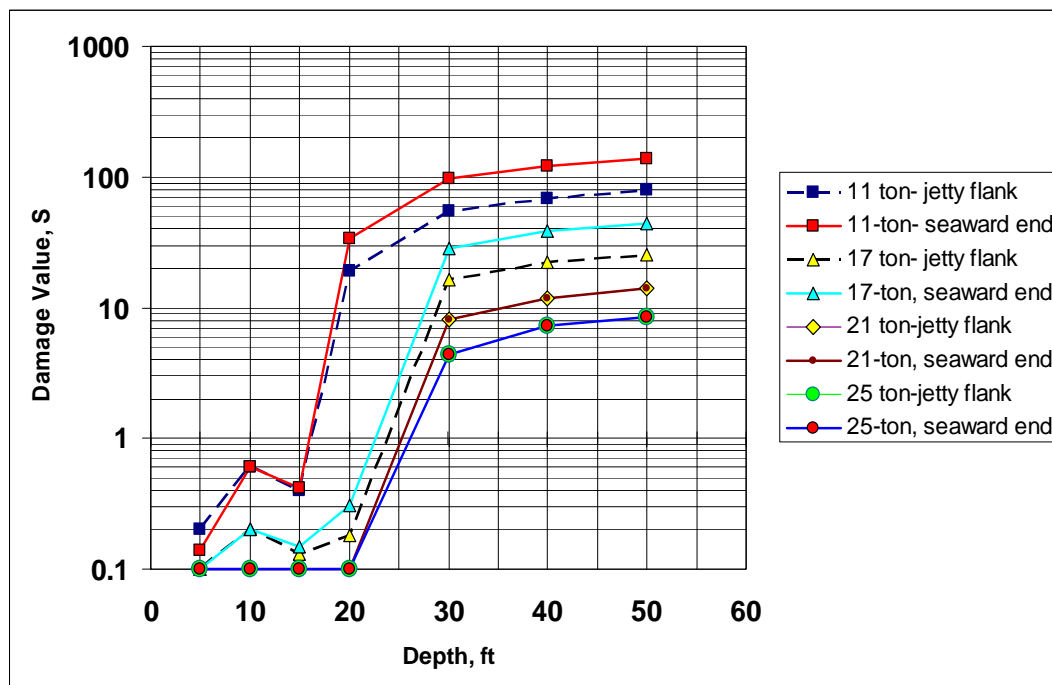
Figure 89. Jetty damage value, S, for jetty flank and seaward end armor stone over a 50-year period.

9 Conclusions and Recommendations

Overview

This study assessed the present and future condition of the Sabine Pass jetty system through three tasks. These tasks evaluated the stability of the jetty to storm waves; the decrease in relative jetty elevation through time due to consolidation of the underlying substrate and relative sea level rise; and waves, currents, and potential sediment transport pathways in the vicinity of the jetties and navigation channel. Each task assessed the existing condition, a hypothetical jetty condition in 50 years without rehabilitation, and various repair scenarios that were assumed to occur in 2010 and were assessed after 50 years.

Recommendations from these analyses are that the Sabine jetties should be rehabilitated to best maintain navigability of the channel throughout a 50-year project life. The recommended alternatives are either Plan 2 or Plan 3, although Plan 3 would most likely cost less and therefore is the recommended alternative. This recommendation is based on comparing the relative benefits of each plan to existing conditions for several key elements. In Table 7, the relative benefit ("+" symbol), detriment ("-" symbol), or no change ("=" symbol) of each plan as compared to the present-day jetty system with 2060 water level is illustrated.

Table 7. Ranking of rehabilitation alternatives relative to present-day jetties and water level in 2060.

Rehabilitation Alternative Evaluated in 2060[1]	Reduction in...				Increased Safety	Total Relative Ranking
	Shoaling	Channel Cross-Current	Cross-Current at Jetty Tips	Scour at Structure Base		
Plan 1 (No rehabilitation)	=	=	=	=	-	-
Plan 2 (Rehabilitation of jetties to +6.2 ft MLW)	=	=	=[2]	-	+	=/+
Plan 3 (Rehabilitation of seaward 4,000-ft of both jetties to +6.2 ft MLW)	=	=	=	=	+	=/+

KEY:
= means no change from present-day jetty system with 2060 water level
+ means greater benefit as compared to present-day jetty system with 2060 water level
- means less benefit as compared to present-day jetty system with 2060 water level

[1] All Alternatives included channel deepening to 48 ft MLW.

[2] Slightly greater current deemed insignificant to navigation.

Discussion

The attributes and detriments of each plan can be assessed through an understanding of how the jetties have evolved through time along with calculations presented herein. Plan 1 consists of no rehabilitation of the jetties. In 2060, Plan 1 would have deteriorated jetty tips due to storm damage and an increase in relative sea level which may increase shoaling in the outer portions of the jetty channel. However, the shear stress analysis indicated high magnitudes of shear stress for all plans, implying that there would be no change in channel shoaling in the jetty channel. Seaward of the jetties, calculations indicated differences in the seaward excursion of shear stress that would be of sufficient magnitude to transport sediment. These differences would not result in changes to the total shoaling volumes, only to the location of sedimentation. As a result, there was no change for any of the Plans for relative shoaling magnitudes as compared to the with-out project simulation in 2060.

Channel cross-current during flood flow could be of significance for navigation in regions of the landward portion of the West jetty that would exist with Plans 1 and 3. Velocity calculations indicated slight increases in cross-current speeds; however, the momentum of the channelized flow between the jetties minimizes this effect and realigns these cross-channel currents with the main channel flow, so navigation would not be impacted.

Cross-currents at the entrance would be more concentrated for Plan 2, because the entrance would be the only entry for flood flow into the channel. Plans 1 and 3 would have portions of the jetty at lower elevation which would permit flood flow into the channel through additional regions. The numerical modeling calculations indicated only a slight increase in cross-currents at the jetty channel, which is deemed insignificant to navigation.

The potential for jetty scour is inferred from the magnitude of currents adjacent to the structures. Calculations for Plan 2 indicated an increase in current magnitude along the outer portion of the jetties. The modeling system applied herein calculates the depth-averaged current speed, and therefore the change in current speed at the base of the structure is not directly known. However, the increase in the depth-averaged current magnitude implies an increase in the potential for scour at the base of the structure. The total magnitude of potential scour was not evaluated, but Plan 2 was rated lower than the other Plans in this category.

Qualitatively, the overall safety was assumed to be higher for Plans 2 and 3 as compared to Plan 1. The deteriorated jetty tips of Plan 1 would create a navigation hazard as vessels attempted to locate the entrance and navigate over submerged jetty stone. The increase in jetty elevation for the full length of both jetties in Plan 2 would also eliminate small craft from accidentally exiting the jetty system over the lower parts of the structure and potentially impacting the submerged jetty as has occurred historically. Plan 3, which consists of raising the seaward 4,000-ft of both jetties, would facilitate location of the Sabine Pass entrance and eliminate navigation hazards around the jetty tips. However, Plan 3 would still have the potential for damage of vessels on landward portions of the jetties. With sufficient navigation marking for the submerged portion of the jetties, this hazard would be minimized for Plan 3.

Optimizing rehabilitation design

As part of future structure rehabilitation, several data collection efforts are recommended to optimize design:

1. To better understand the relationship between storm waves and water level, it is recommended that a post-Hurricane Ike survey of the Sabine Pass jetties be analyzed. Hurricane Ike made landfall in the Galveston, TX area on September 12-13, 2008, and storm water level measurements at Sabine Pass were approximately 12.5 ft, which is approximately a 100-year storm. Associated wave height for such an event in the LACPR data is about 15 ft; however, wave heights in the vicinity of Sabine Pass were nearly 20 ft for Hurricane Ike at NOAA Buoy 42035, so this event was a severe test for the jetties. This survey would provide information about how the present jetties responded to an approximate 100-year storm. At a minimum, the survey should include measurements of crest elevations and a low water inspection of the structures.

2. For a more comprehensive evaluation of potential consolidation of the SNWW jetties, it is recommended that sediment cores be taken every 2,000 ft along the length of each jetty. For the portion of the West jetty that has experienced severe settlement (Stations 12,700 to 15,500 ft), it is recommended that sediment cores be taken every 500 ft (5 cores in this region). In addition, two cores off the seaward tip of each jetty are recommended at 2000-ft spacing. Ideally, all cores would be taken to 50-70 ft depth (or depth of maximum penetration). The number of cores with this recommendation would be approximately 14 along the East jetty, plus 2 off the seaward tip, and 18 along the West jetty, plus 2 off the seaward

tip, totaling 36 cores. For all cores, consolidation tests should be performed to determine site-specific sediment parameters.

Based on these measurements, additional studies are recommended to refine and optimize design.

1. This study presented preliminary guidance for sizing the armor stone based on choosing an acceptable damage level. This analysis was likely conservative in that it assumed waves would break perpendicular to the structure, whereas oblique wave approach would occur more often. A physical model study is recommended to optimize the required stone size.

2. To best quantify the shoaling rate in the channel, a combination of field, laboratory, and numerical studies are recommended. In situ sediment would be taken from the Sabine Pass seabed and subjected to waves and currents in a laboratory setting. ERDC has a SedFlume laboratory designed to determine the erosion and sedimentation rates for cohesive sediments. Parameters determined in the SedFlume would be applied within a numerical model of cohesive sediment transport for the various design alternatives.

3. The numerical model showed increases in current magnitude over 1.0 m/s along the outside of the East jetty, especially near the shoreline for the 2060 water level as compared to the existing water level. The increase in currents will occur gradually as sea level increases. However, the higher currents can potentially cause scour and consideration should be given to protecting the outside of the East jetty and shoreline. It is recommended that the potential for erosion of the shoreline, flanking of the East jetty, and scour at the seabed be investigated within a three-dimensional cohesive sediment transport model. If these processes are deemed to be of concern over the 50-year project lifetime, it is recommended that the rehabilitation design consider options to reduce the likelihood of structural damage or failure.

4. Regardless of which Plan is selected, it is recommended that long-term beach change on the adjacent shorelines be evaluated within the context of relative sea level rise, potential increase in storm frequency and severity, and increased water levels over the project lifetime.

References

Bretschneider, C. L. 1966. Wave generation by wind, deep and shallow water, Chapter. 3. In *Estuary and Coastline Dynamics*, ed. A. T. Ippen. McGraw-Hill, Inc.

Brown, G. L., M. S. Sarruff, R. Vemulakonda, G. H. Nail, J. Stokes, and B. Mann. 2009. Numerical model study of potential salinity impacts due to proposed navigation improvements to the Sabine-Neches Waterway, TX. Draft report in review.

Buttolph, A. M., C. W. Reed, N. C. Kraus, N. Ono, M. Larson, B. Camenen, H. Hanson, T. Wamsley, and A. K. Zundel. 2006. *Two-dimensional depth-averaged circulation model CMS-M2D: Version 3.0, Report 2: Sediment transport and morphology change*. ERDC/CHL TR-06-09. Vicksburg, MS: U.S. Army Engineer Research and Development Center.

Burcharth, H. F., and S. A. Hughes. 2003. Rubble-mound structure loading and response. In: *Coastal Engineering Manual, Part VI , Fundamentals of Design,* Chapter VI-5, ed. B. Mullen. Engineer Manual 1110-2-1100. Washington, DC: U.S. Army Corps of Engineers.

Dean, R. G. 2002. *Beach nourishment theory and practice, advanced series on ocean engineering*, Vol. 18. River Edge, NJ: World Scientific Press.

Dokka, R. K. 2006. Modern-day tectonic subsidence in coastal Louisiana. *Geology* 34(4): 281-284.

Fagerburg, T. 2001. *Field Data Collection Summary Report for the Sabine-Neches Waterway Study*. Memorandum For Record, submitted to SWG.

Gray, W., and P. Klotzbach. 2009. United States Landfall Probability Webpage. http://tropical.atmos.colostate.edu/, last updated 9 August 2009, accessed 21 September 2009.

Hallegatte, S. 2007. The use of synthetic hurricane tracks in risk analysis and climate change damage assessment. *Journal of Applied Meteorology and Hydrology* 46(11):1956-1966.

Holtz, R. D., and W. D. Kovacs. 1981. An introduction to Geotechnical Engineering. Prentice-Hall Civil Engineering and Engineering Mechanics Series, N. M. Hewmark and W. J. Hall, Editors, 733 p.

Hornberger, G. M., J. P. Raffensperger, P. L. Wiberg, and K. N. Eshleman. 1998. Elements of physical hydrology. Baltimore, MD: Johns Hopkins University Press, 302 p.

Hughes, S. A. 2003a. *Wave momentum flux parameter for coastal structure design.* Coastal and Hydraulics Engineering Technical Note. ERDC/CHL CHETN-III-67. Vicksburg, MS: U.S. Army Engineer Research and Development Center.

Hughes, S. A. 2003b. *Estimating irregular wave runup on smooth, impermeable slopes.* Coastal and Hydraulics Engineering Technical Note. ERDC/CHL CHETN-III-68. Vicksburg, MS: U.S. Army Engineer Research and Development Center.

Hughes, S. A. 2004. Wave momentum flux parameter: A descriptor for nearshore waves. *Coastal Engineering Journal, Elsevier* 51(11):1067-1084.

Hughes, S. A. 2005. *Estimating irregular wave runup on rough, impermeable slopes*, Coastal and Hydraulics Engineering Technical Note, ERDC/CHL CHETN-III-70. Vicksburg, MS: U.S. Army Engineer Research and Development Center.

Kane, H. E. 1959. Late quaternary geology of Sabine Lake and vicinity, Texas and Louisiana. *Transactions, Gulf Coast Association Geologic Society* (9):225-235.

King, D. B. 2007. *Wave and beach process modeling for Sabine Pass to Galveston Bay, Texas, shoreline erosion feasibility study.* ERDC/CHL TR-07-06. Vicksburg, MS: U.S. Army Engineer Research and Development Center.

Komen, G., L. Cavaleri, M. A. Donelan, K. Hasselmann, S. Hasselmann, and P.A.M.E. Janssen. 1994. Dynamics and modelling of ocean waves, Cambridge University Press, 522 pp.

Leuttich, R. A., Jr., J. J. Westerink, and N. W. Scheffner, 1992. *ADCIRC: An advanced three-dimensional circulation model for shelves, coasts, and estuaries. Report 1 Theory and methodology of ADCIRC-2DD1 and ADCIRC-3DL*, Technical Report DRP-92-6 prepared for Department of the Army, U.S. Army Corps of Engineers, Washington, DC, November 1992. 141pp.

Lin, L., Z. Demirbilek, H. Mase, and J. Zheng. 2008. *CMS-Wave: A nearshore spectral wave processes model for coastal inlets and navigation projects.* ERDC/CHL TR-08-13. Vicksburg, MS: U.S. Army Engineer Research and Development Center.

Mase, H., H. Amamori, and T. Takayama. 2005. Wave prediction model in wave-current coexisting field. *Proceedings 12th Canadian Coastal Conference* (CD-ROM).

Mason, C. 1981. *Hydraulics and stability of five Texas inlets.* Miscellaneous Paper CERC-81-1, Fort Belvoir, VA: U.S. Army Engineer Coastal Engineering Research Center.

Maynord, S. T. 2003. *Ship effects before and after deepening of Sabine-Neches Waterway, Port Arthur, Texas.* ERDC/CHL TR-03-15. Vicksburg, MS: U.S. Army Engineer Research and Development Center.

McBride, R. A., and M. R. Byrnes. 1997. Regional variations in shore response along barrier island systems of the Mississippi River delta plain: historical change and future prediction. *Journal of Coastal Research* 13(3):628–655.

McBride, R. A., M. J. Taylor, and M. R. Byrnes. 2007. Coastal morphodynamics and Chenier-Plain evolution in southwestern Louisiana, USA: A geomorphic model. *Geomorphology* 88:367-422.

Melby, J. A. 2005a. *Breakwater and revetment armor stability.* Coastal and Hydraulics Engineering Technical Note, ERDC/CHL CHETN-III-71. Vicksburg, MS: U.S. Army Engineer Research and Development Center.

Melby, J. A. 2005b. *Damage development on stone-armored breakwaters and revetments.* Coastal and Hydraulics Engineering Technical Note, ERDC/CHL CHETN-III-64 (revised). Vicksburg, MS: U.S. Army Engineer Research and Development Center.

Melby, J. A., and N. Kobayashi, N. 1998a. Progression and variability of damage on rubble mound breakwaters. *J. Wtrwy., Port, Coast., and Oc., Engrg.* 124(6):286-294, ASCE, Reston, VA.

Melby, J. A., and S. A. Hughes. 2004. Armor stability based on wave momentum flux. *Proc. of Coastal Structures 2003*, ASCE, Reston, VA

Morang, A. 2006. *North Texas sediment budget.* ERDC/CHL TR-04-02. Vicksburg, MS: U.S. Army Engineer Research and Development Center.

National Oceanographic and Atmospheric Administration (NOAA). 2005. Tides and currents, tidal station locations and ranges, Sabine Pass jetties. http://tidesandcurrents.noaa.gov/station_info.shtml?stn=8770570+Sabine+Pass+North+,+TX, last updated 16 March 2005, accessed 17 September 2009.

National Oceanographic and Atmospheric Administration (NOAA). 2008a. *Tides and currents, tidal station locations and ranges, Sabine Pass jetties.* http://tidesandcurrents.noaa.gov/tides09/tab2ec4.html#110, last updated 3 November 2008, accessed 17 September 2009.

National Oceanographic and Atmospheric Administration (NOAA). 2008b. *Tides and currents, mean sea level trends, 8770570 Sabine Pass, TX.* http://tidesandcurrents.noaa.gov/sltrends/sltrends_station.shtml?stnid=8770570, last updated 9 December 2008, accessed 17 September 2009.

National Oceanographic and Atmospheric Administration (NOAA) Coastal Services Center. 2009. *Historical Hurricane Tracks* http://csc-s-maps-q.csc.noaa.gov/hurricanes/.

National Research Council (NRC). 1987. *Responding to changes in sea level: engineering implications.* Commission of Engineering and Technical Systems, National Research Council, National Academy Press, Washington, D.C.

Nelson, H. F., and E. E. Bray. 1970. Stratigraphy and history of the Holocene sediments in the Sabine-High Island area, Gulf of Mexico. In *Deltaic Sedimentation Modern and Ancient: SEPM Special Publication 15*, ed. J. P. Morgan, 48-77.

Parchure, T. M., S. Maynord, and S. Sarruff. 2005. *Desktop study for sediment-related problems at the Sabine-Neches Project.* Vicksburg, MS: U.S. Army Engineer Research and Development Center.

Sargent, F. E., and R. R. Bottin. 1989. *Case histories of Corps breakwater and jetty structures.* Technical Report REMR-CO-3, Report 9: Southwestern Division. Vicksburg, MS: U.S. Army Engineer Waterways Experiment Station.

Shinkle, K., and R. K. Dokka, 2004. *Rates of vertical displacement at benchmarks in the lower Mississippi Valley and the northern Gulf Coast.* National Oceanic and Atmospheric Administration Technical Report 50, 135 p.

Smith, J. M., A. R. Sherlock, and D. T. Resio. 2001. *STWAVE: Steady-State Spectral Wave Model User's manual for STWAVE, Version 3.0.* ERDC/CHL SR-01-1. Vicksburg, MS: U.S. Army Engineer Research and Development Center.

Smith, J. M. 2007. *Modeling nearshore waves for Hurricane Katrina.* ERDC TN-SWWRP-07-6. Vicksburg, MS: U.S. Army Engineer Research and Development Center, https://swwrp.usace.army.mil.

Soulsby, R. L., 1997. *Dynamics of marine sands.* London, UK: Thomas Telford Publications.

Terzaghi, K. 1943. *Theoretical soil mechanics.* New York, NY: John Wiley and Sons.

U.S. Army Corps of Engineers. 1992. CEDAS (Coastal Engineering Data Analysis System)-Wave Prediction, Extremal Significant Wave Height Analysis. ACES Technical Reference by D. A. Leenknecht, A. Szuwalski, and A. R. Sherlock. Version 1.07.

U.S. Army Corps of Engineers (USACE). 2009a. *Incorporating sea-level change considerations in civil works programs.* Engineering Circular 1165-2-211. Washington, DC: Headquarters, U.S. Army Corps of Engineers.

U.S. Army Corps of Engineers (USACE). 2009b. *Navigation Data Center.* http://www.iwr.usace.army.mil/ndc/index.htm, last updated 24 June 2009, accessed 14 September 2009.

U.S. Army Corps of Engineers (USACE). 2009c. Wave Information Studies, Database. http://frf.usace.army.mil/cgi-bin/wis/atl/atl_main.html

U.S. Army Corps of Engineers New Orleans District. 2009. Louisiana Coastal Protection. New Orleans District, 7400 Leake Avenue, New Orleans, Louisiana 70118. www.lacpr.usace.army.mil

U.S. Army Engineer District (USAED), Galveston. 1983. *Galveston County shore erosion study, Feasibility report on beach erosion control, Volume 2, Gulf shoreline study site report.* Galveston, TX: U.S. Army Engineer District, Galveston.

U.S. Army Engineer District (USAED), Galveston. 1999. *Fiscal Year Annual Report of the Secretary of the Army on Civil Works Activities.* Galveston, TX: U.S. Army Engineer District, Galveston.

U.S. Army Engineer District (USAED), Galveston. 2007. *Sabine-Neches Waterway Channel Improvement Project, Draft Feasibility Report and Draft Environmental Impact Statement.* Galveston, TX: U.S. Army Engineer District, Galveston.

Yong, R. N., and B. P. Warkentin. 1966. *Introduction to Soil Behavior.* Chapter 8. New York, NY: Macmillan Company, 176-234.

Appendix A: Plots of Calculated Flow and Suspension Parameters
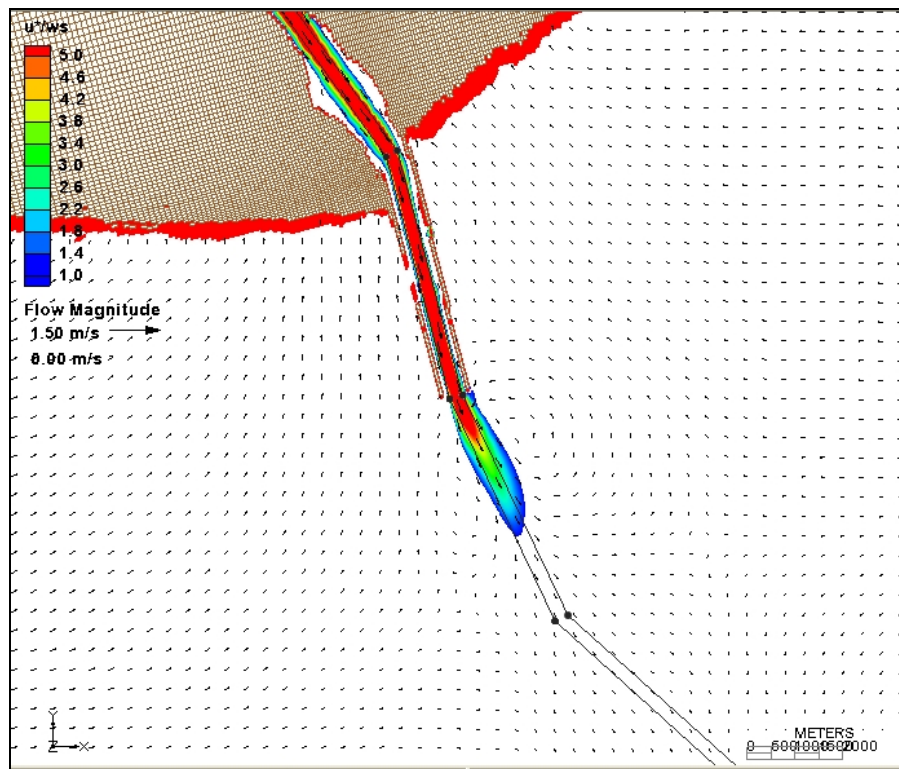
Figure A1. Flow patterns and suspension parameter for existing conditions
and low-energy simulation.
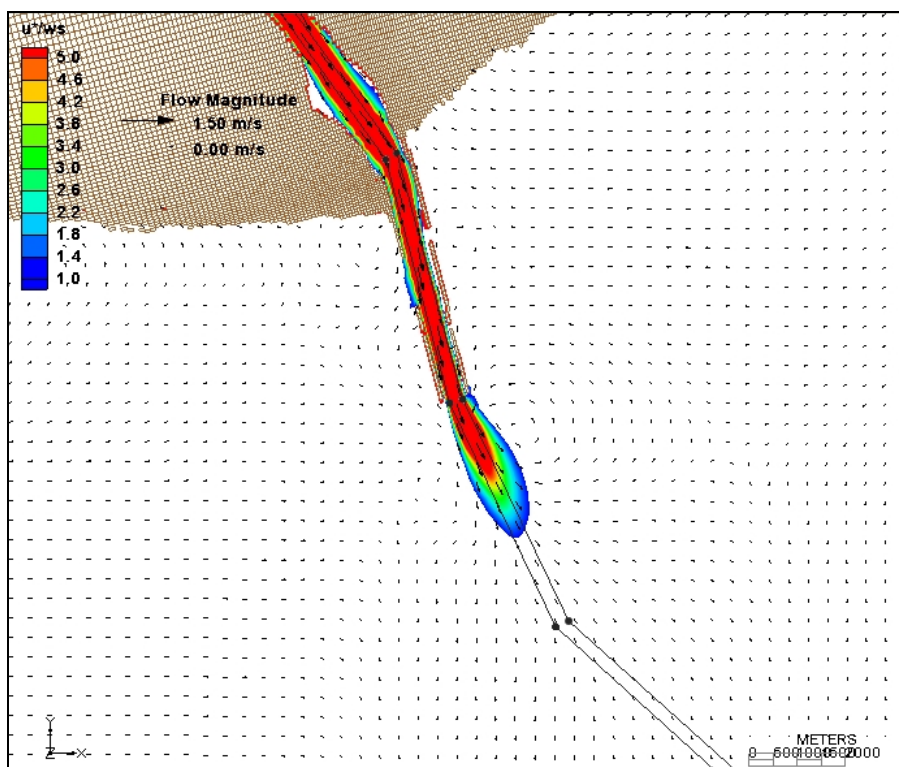
Figure A2. Flow patterns and suspension parameter for existing conditions
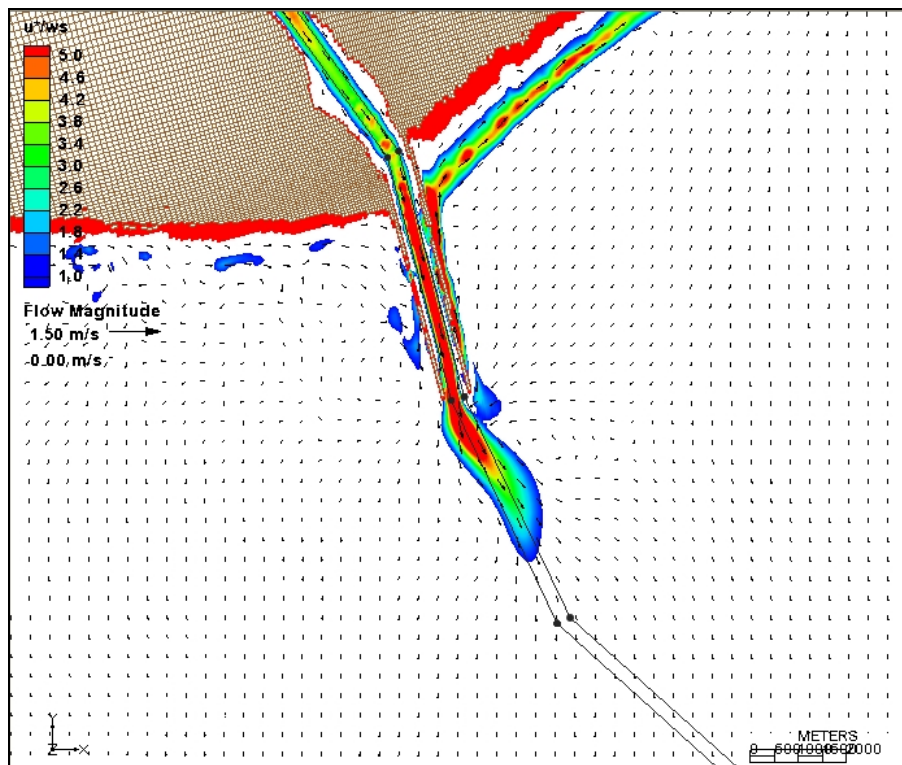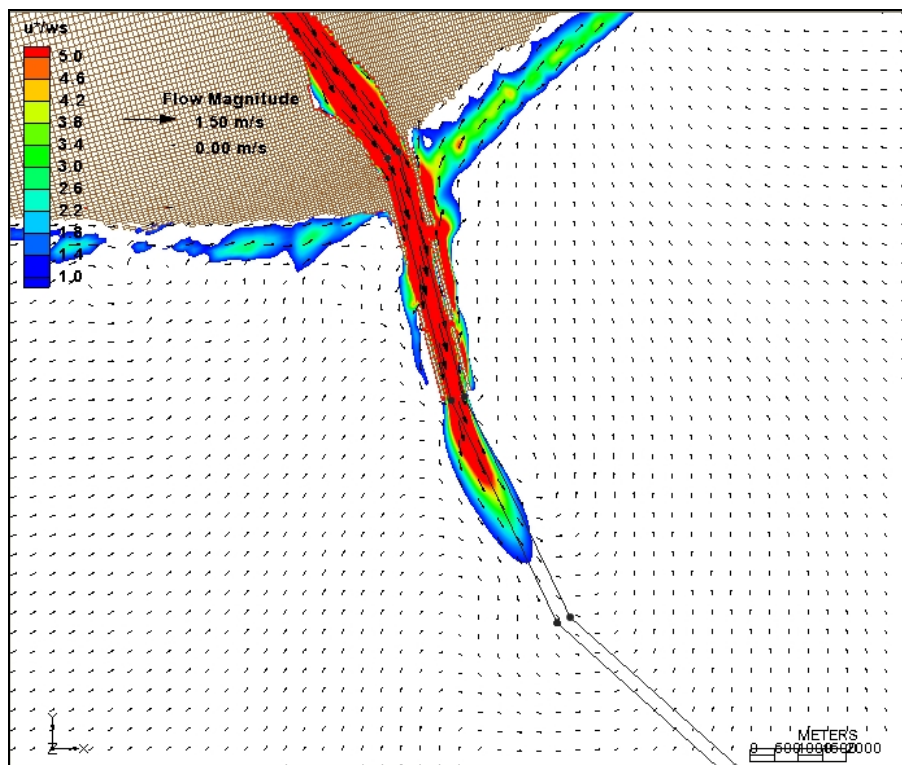and low-energy simulation in 2060.
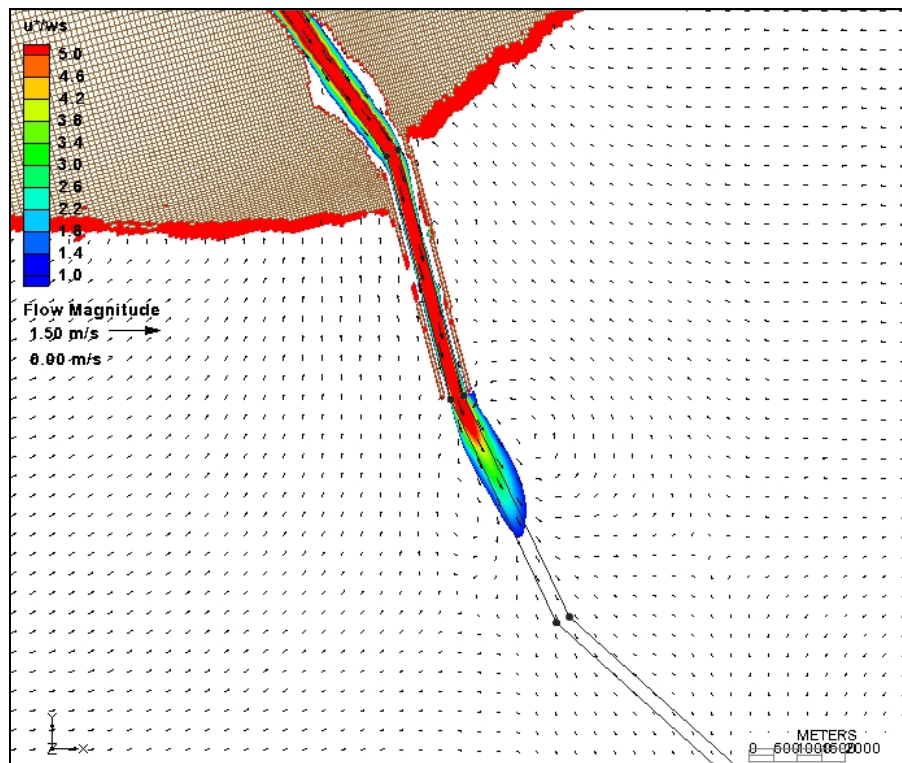
Figure A3. Flow patterns and suspension parameter for Plan 1 in 2010
and the low-energy simulation.
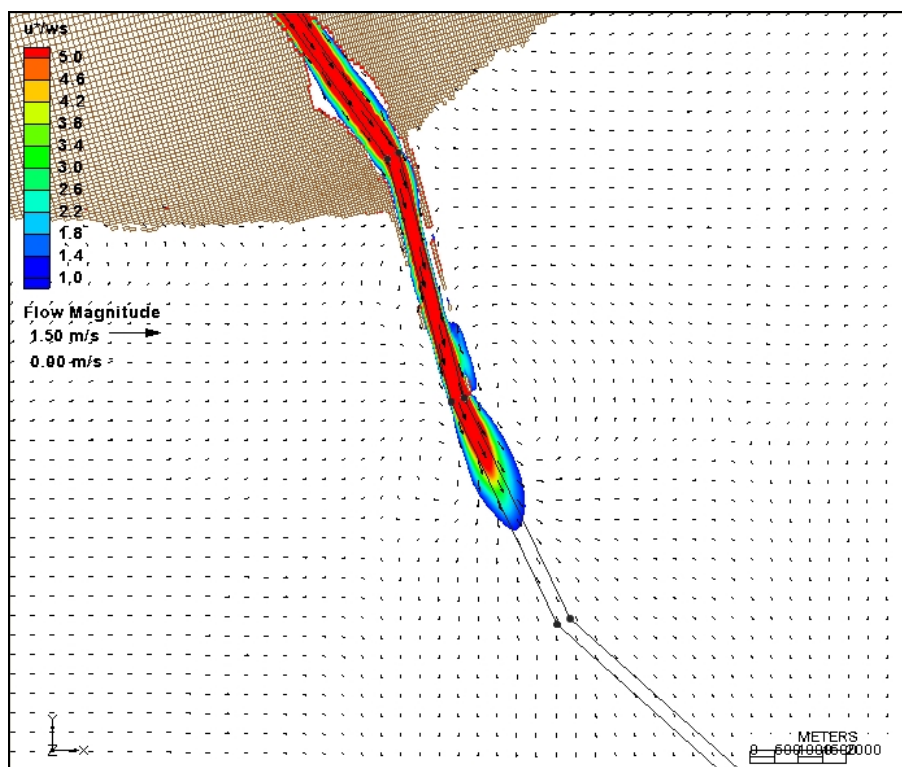
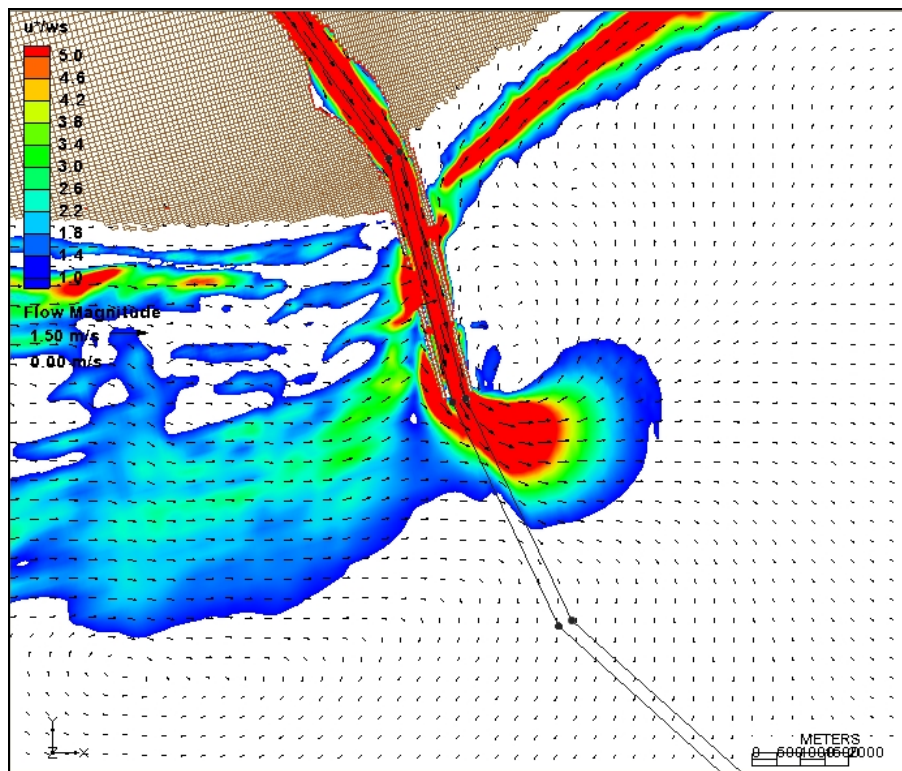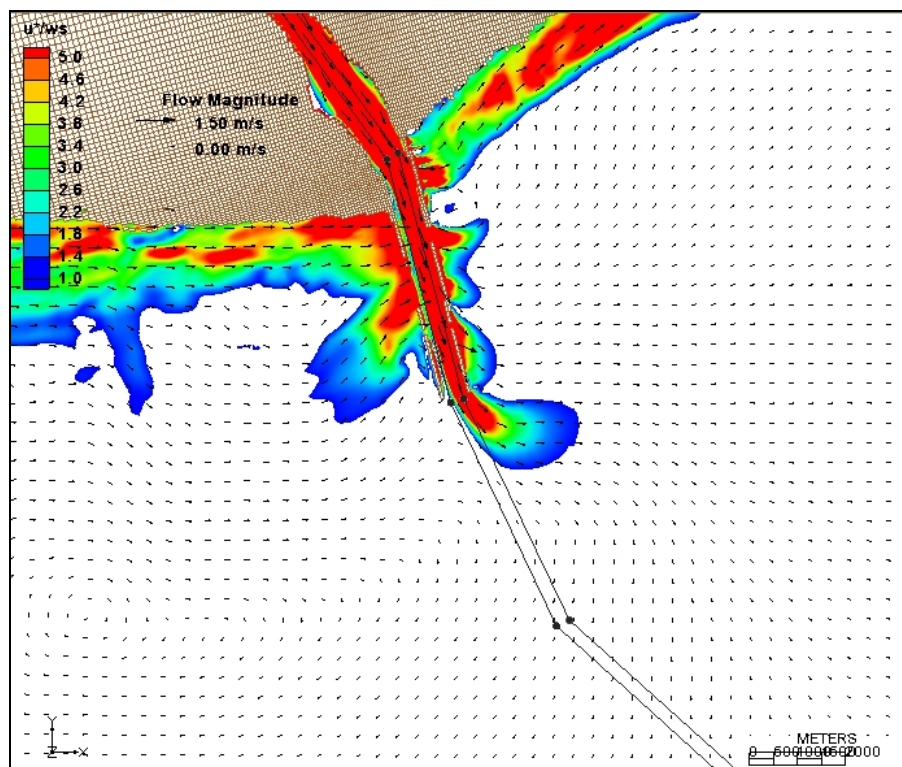Figure A4. Flow patterns and suspension parameter for Plan 1 in 2006
and the low-energy simulation.
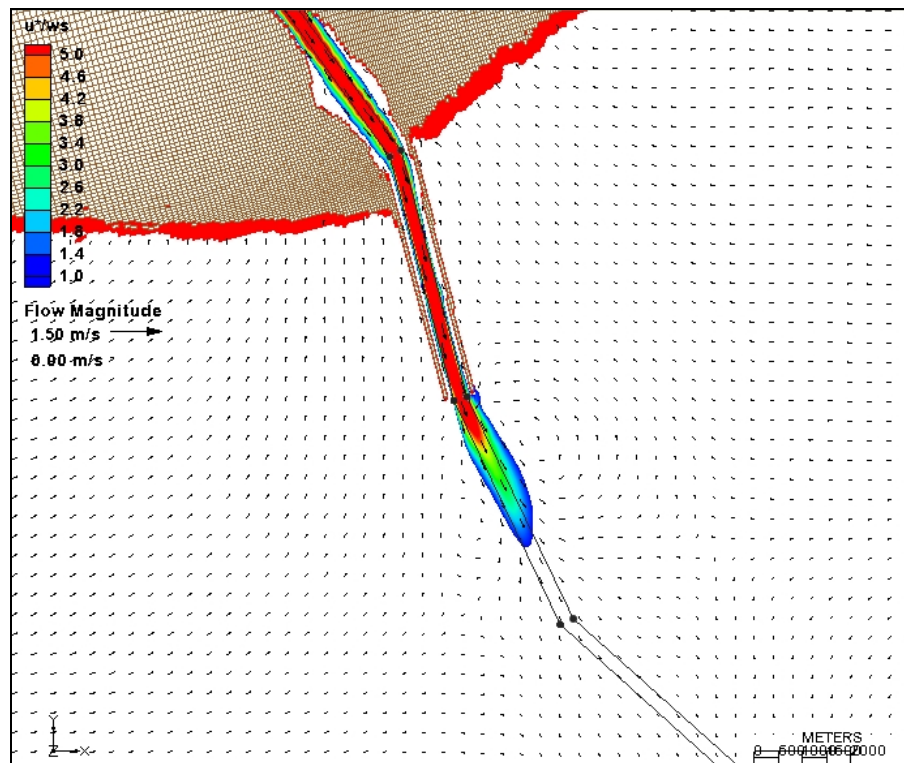
Figure A5. Flow patterns and suspension parameter for Plan 2 in 2010 and the low-energy simulation.
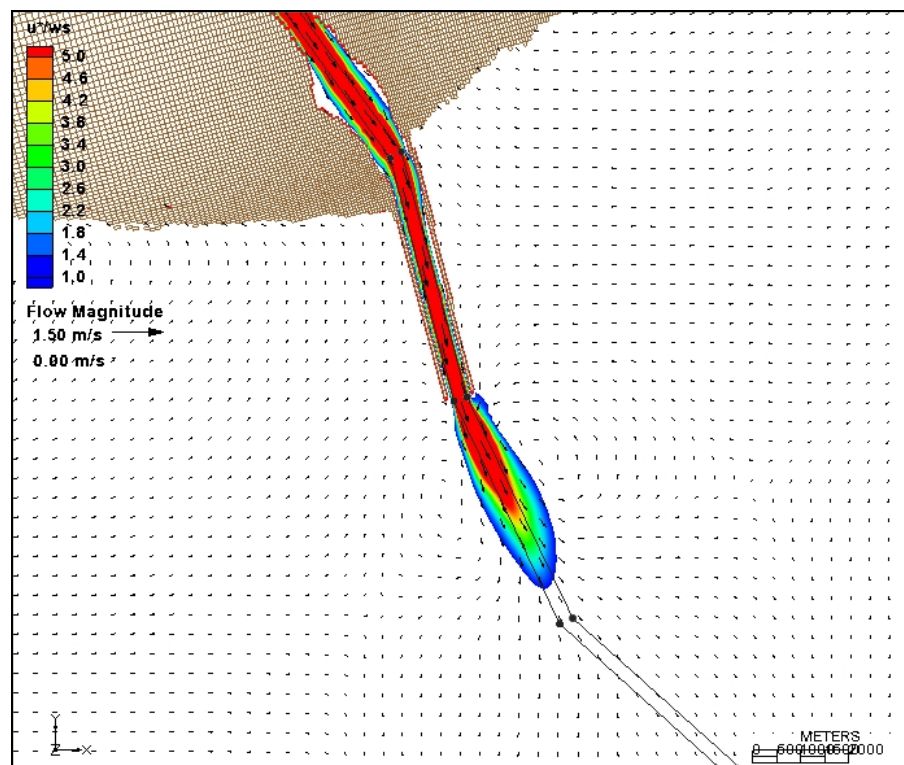
Figure A6. Flow patterns and suspension parameter for Plan 2 in 2060 and the low-energy simulation.
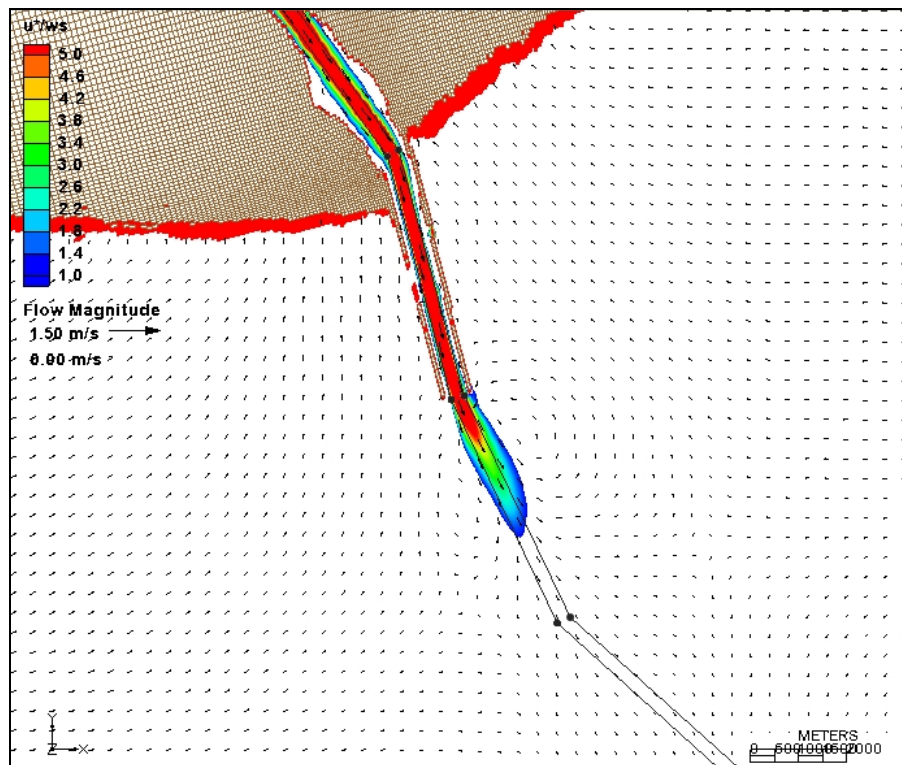
Figure A7. Flow patterns and suspension parameter for Plan 3 in 2010
and the low-energy simulation.
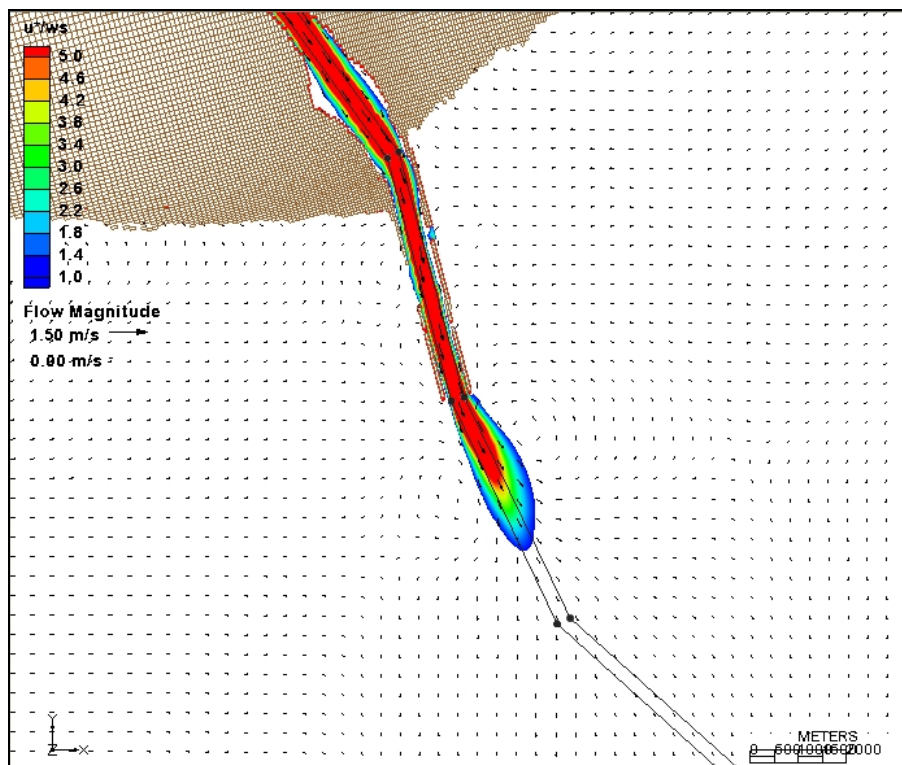
Figure A8. Flow patterns and suspension parameter for Plan 3 in 2060
and the low-energy simulation.
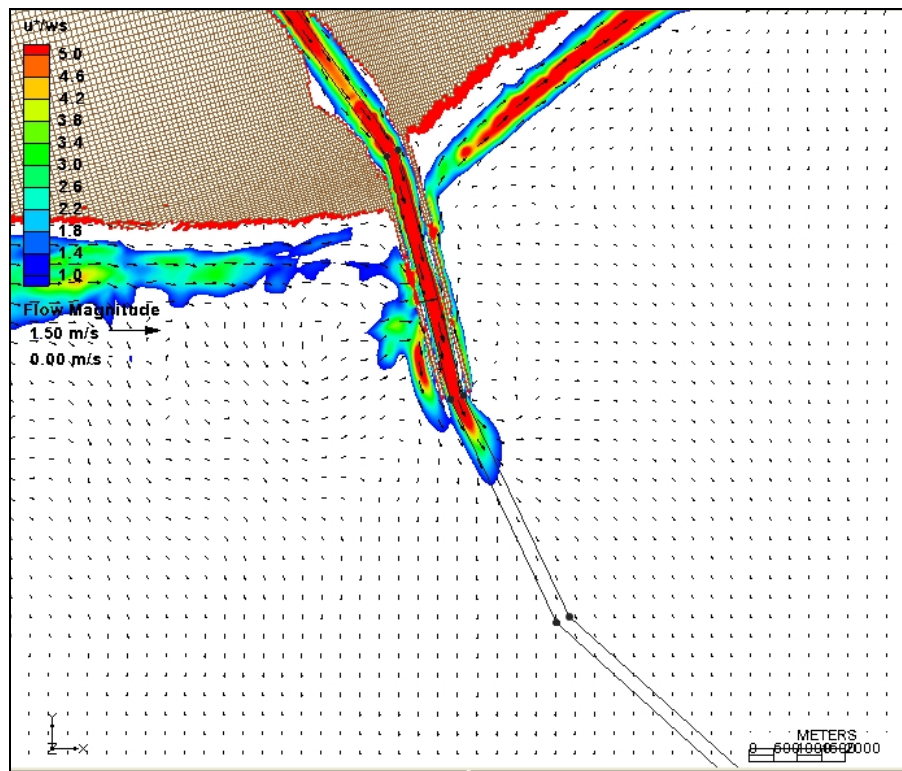
Figure A9. Flow patterns and suspension parameter for existing conditions and the SW storm.
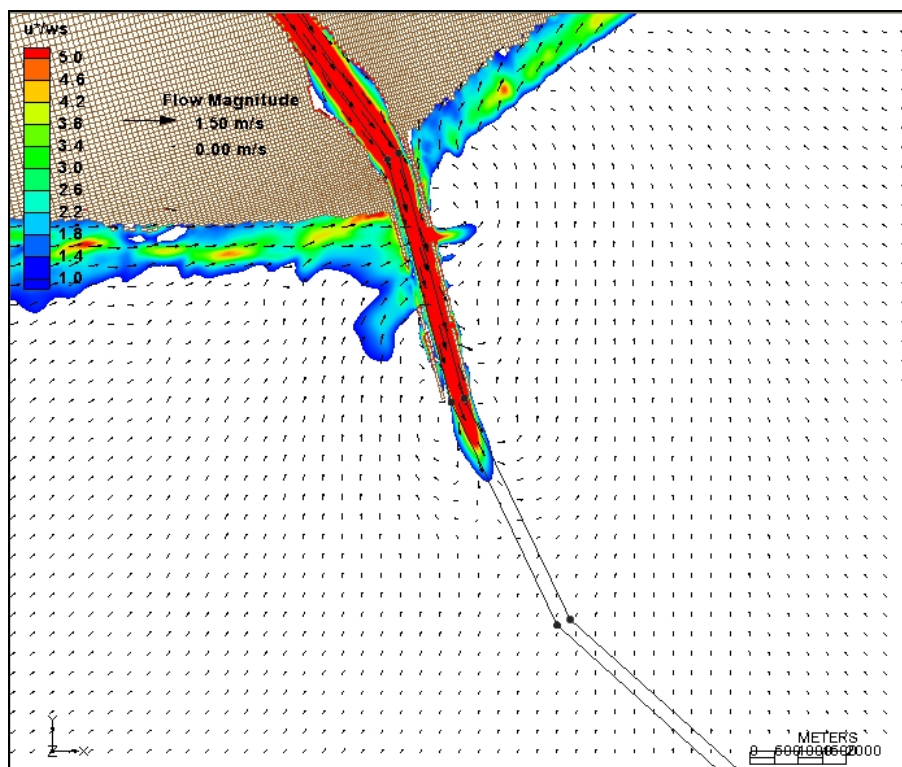
Figure A10. Flow patterns and suspension parameter for existing conditions and the SW storm in 2060.
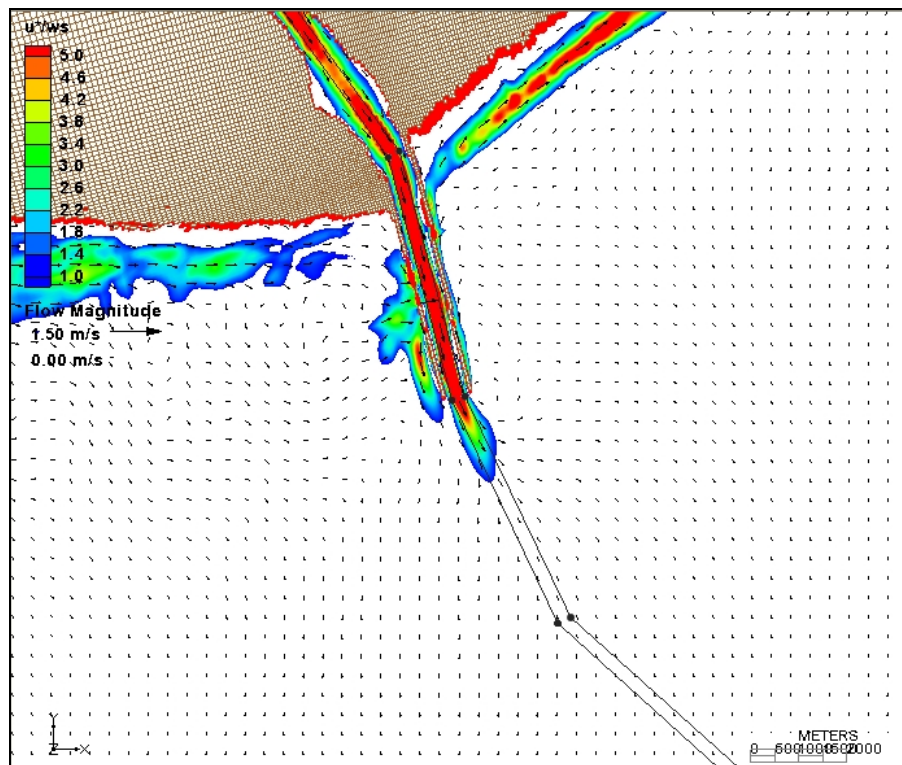
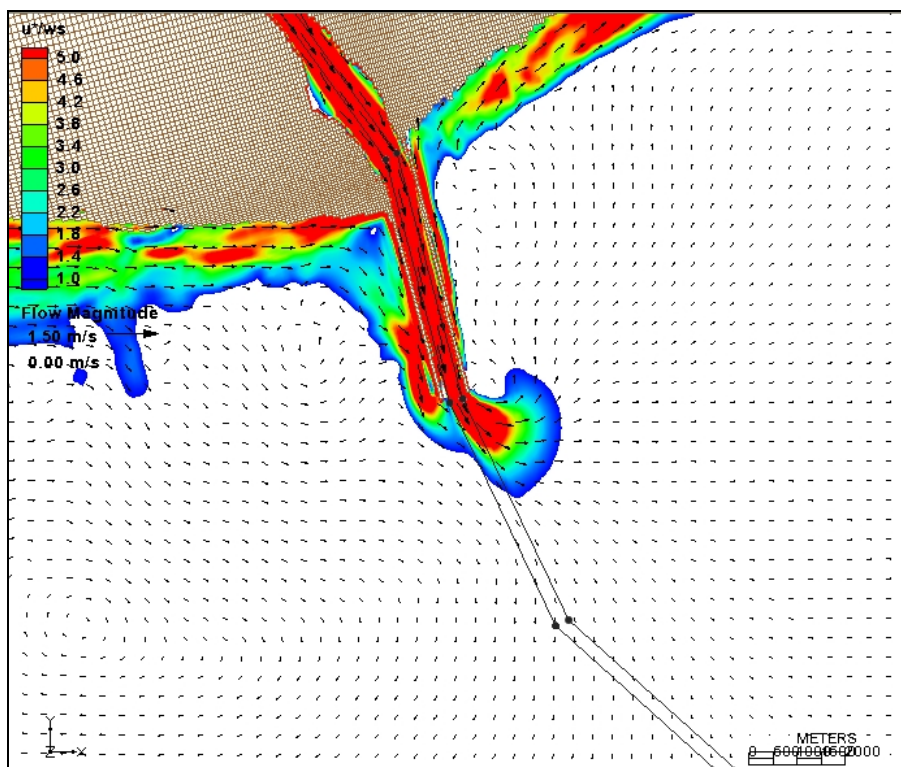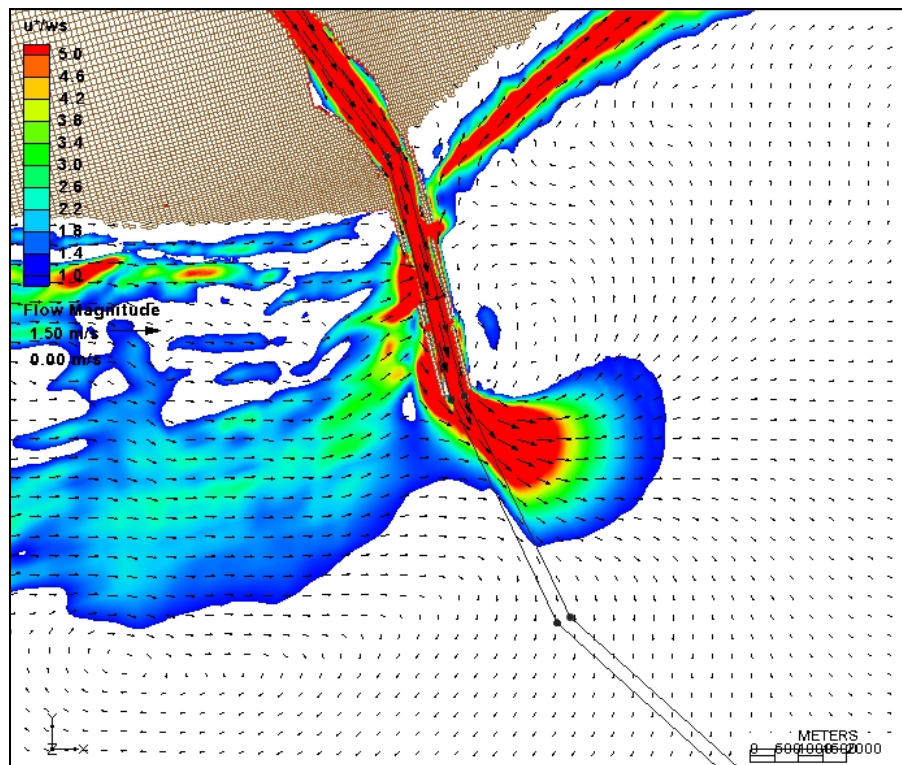Figure A11. Flow patterns and suspension parameter for Plan 1
and the SW storm in 2010.
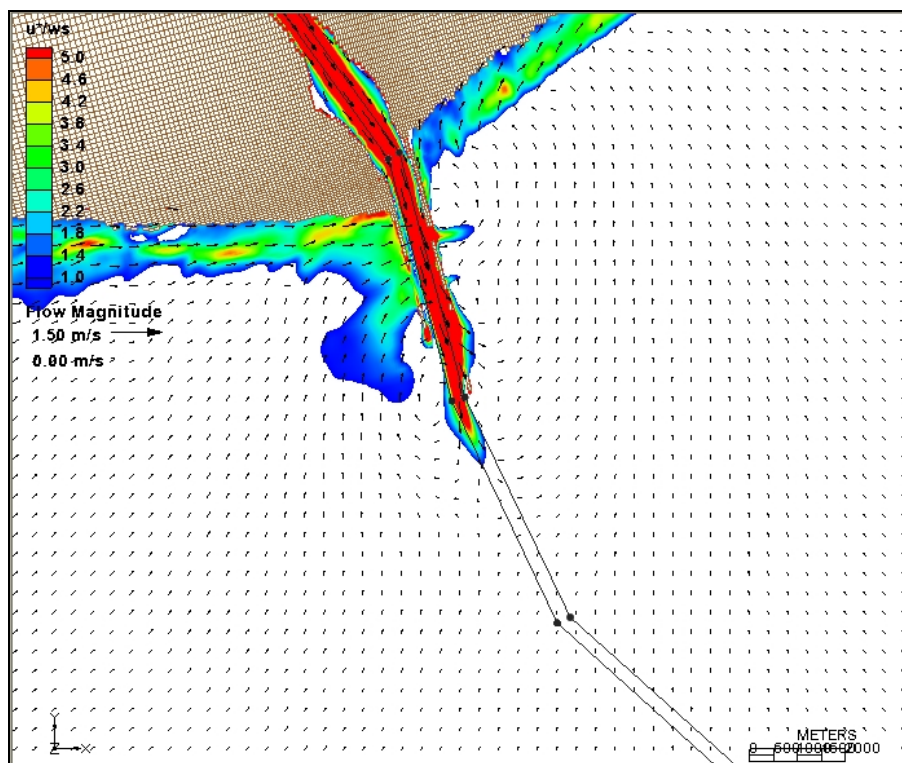
Figure A12. Flow patterns and suspension parameter for Plan 1
and the SW storm in 2060.
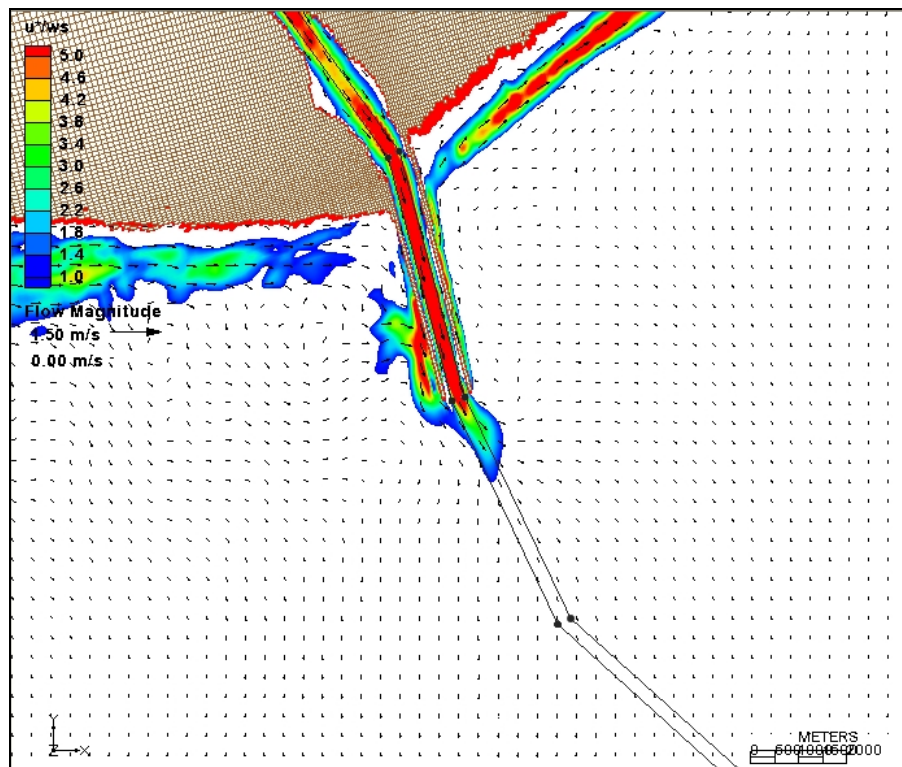
Figure A13. Flow patterns and suspension parameter for Plan 2
and the SW storm in 2010.
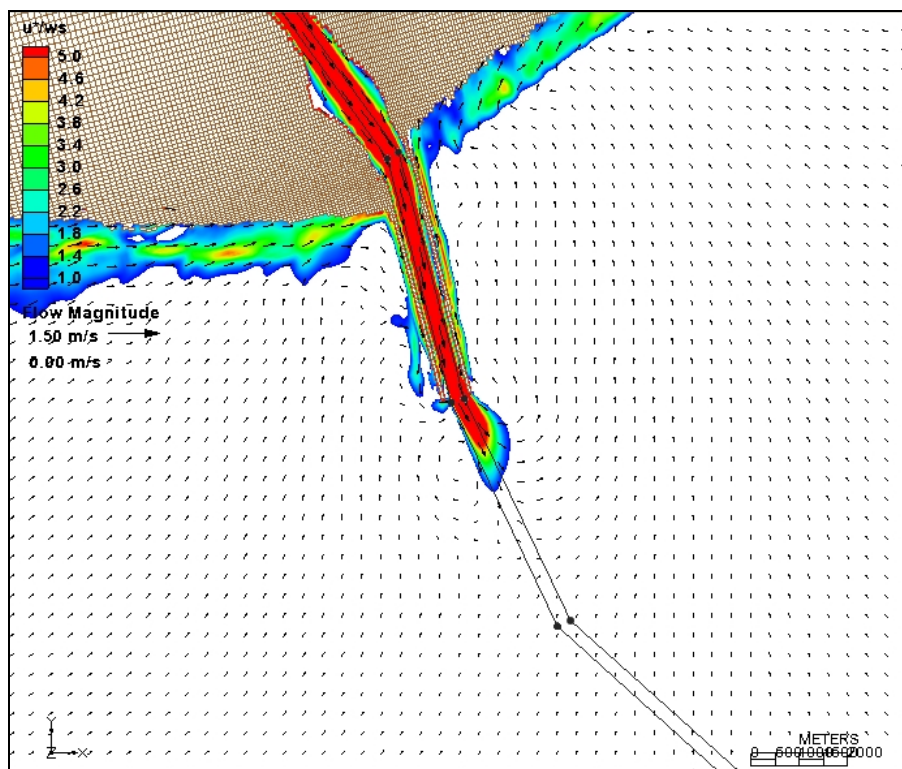
Figure A14. Flow patterns and suspension parameter for Plan 2
and the SW storm in 2060.
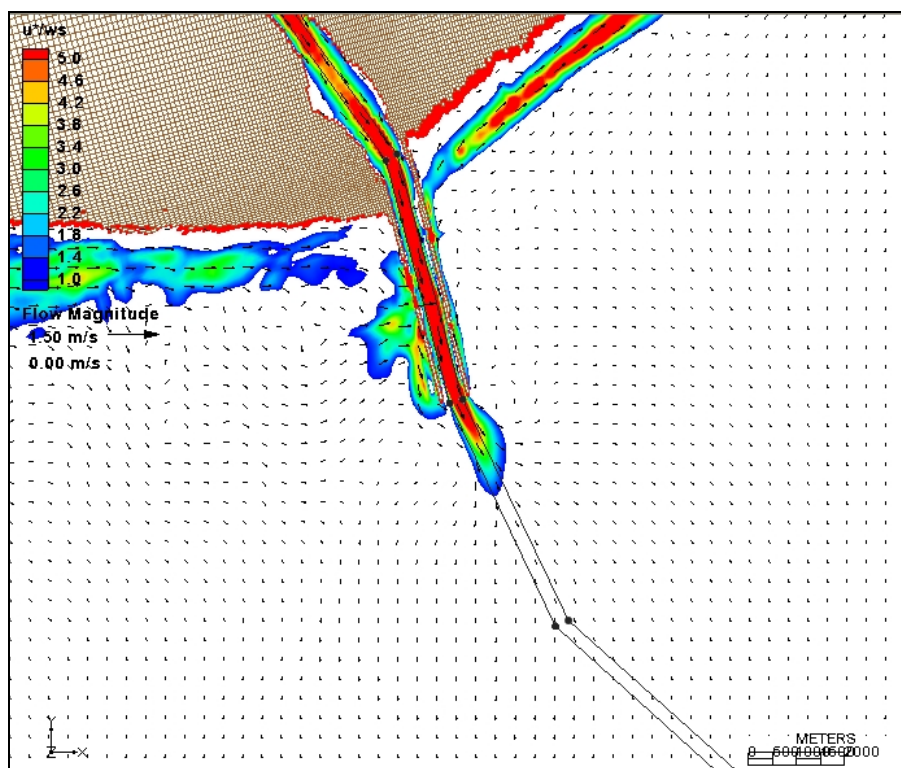
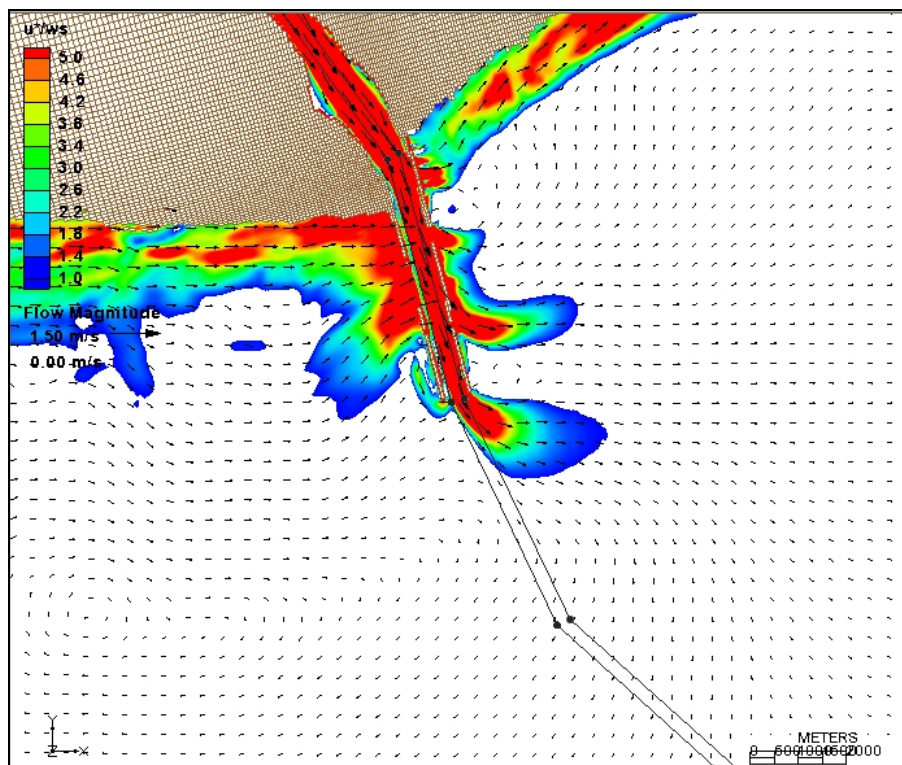Figure A15. Flow patterns and suspension parameter for Plan 3
and the SW storm in 2010.
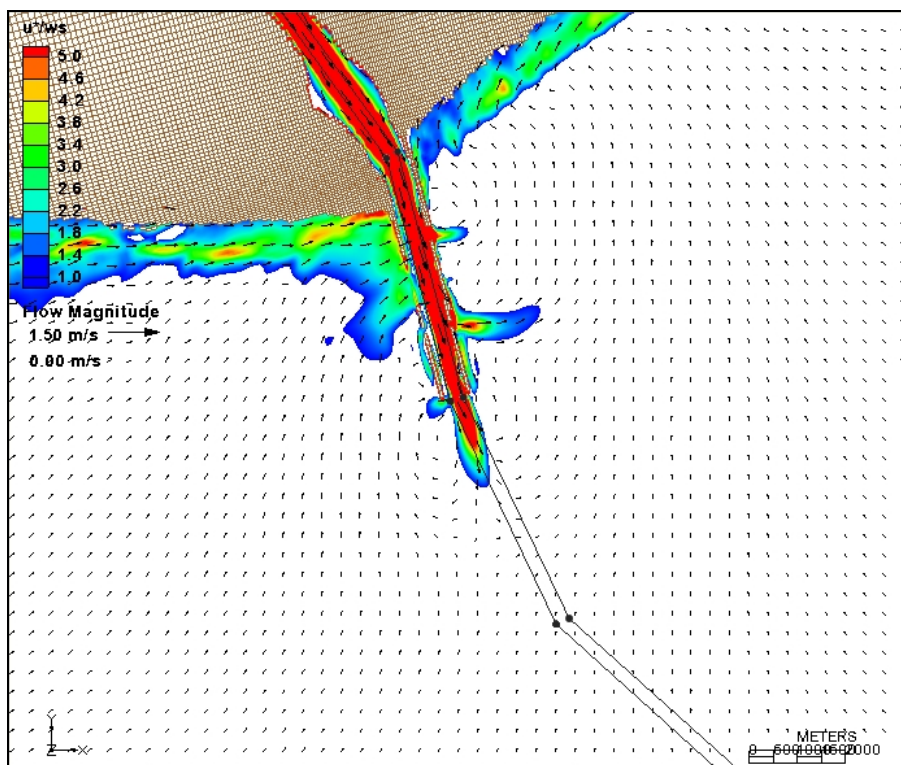
Figure A16. Flow patterns and suspension parameter for Plan 3
and the SW storm in 2060.

Figure A17. Flow patterns and suspension parameter for existing conditions and the SE storm.

Figure A18. Flow patterns and suspension parameter for existing conditions and the SE storm in 2060.
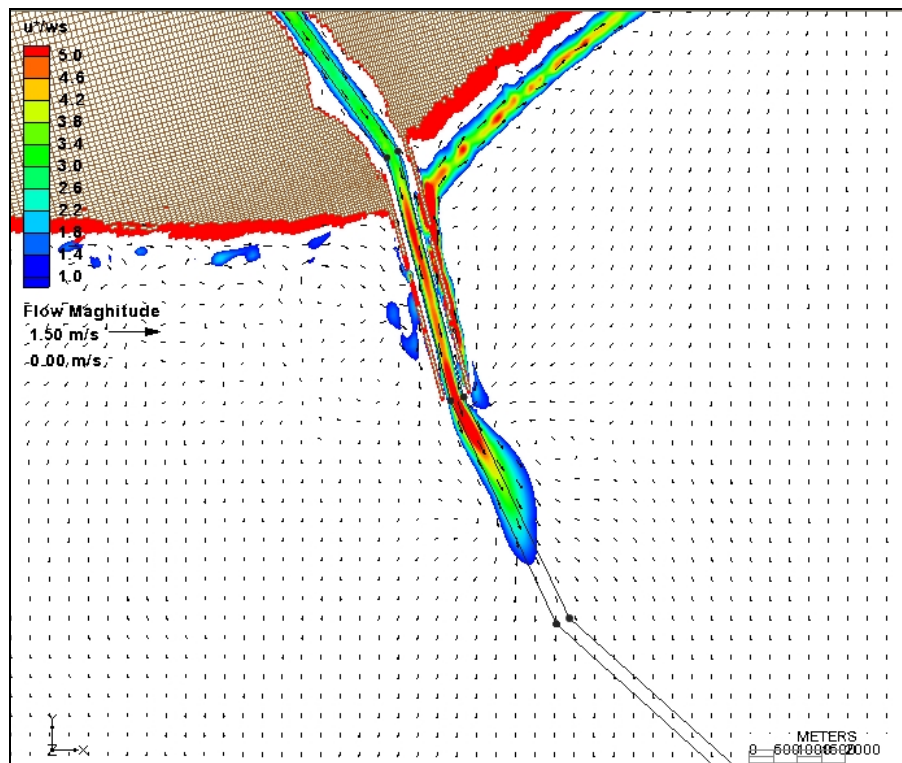
Figure A19. Flow patterns and suspension parameter for Plan 1
and the SE storm in 2010.
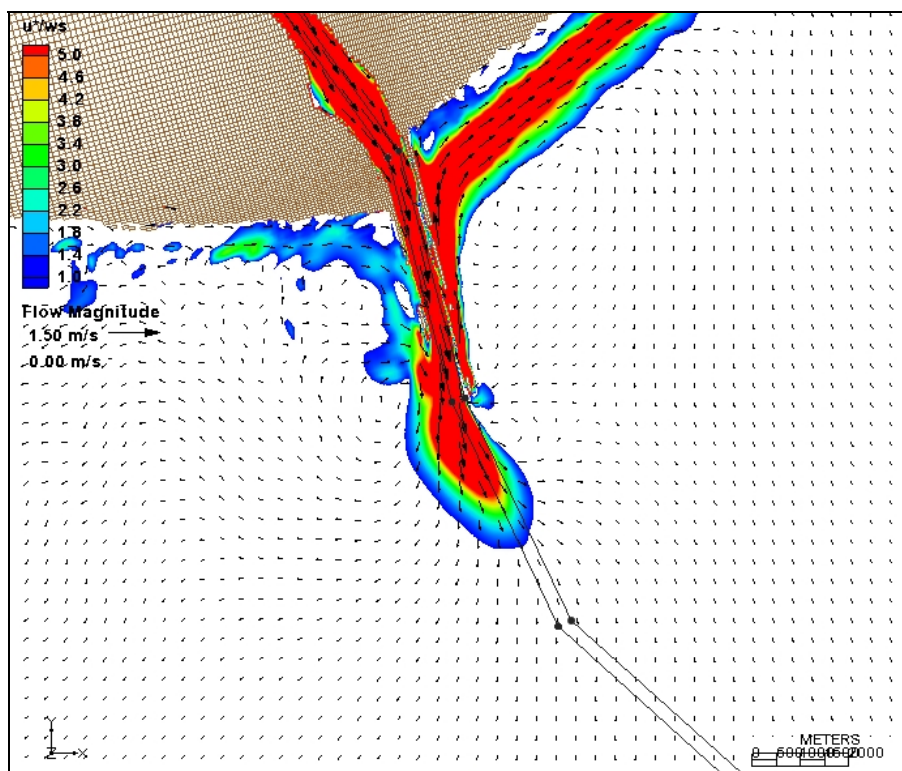
Figure A20. Flow patterns and suspension parameter for Plan 1
and the SE storm in 2060.
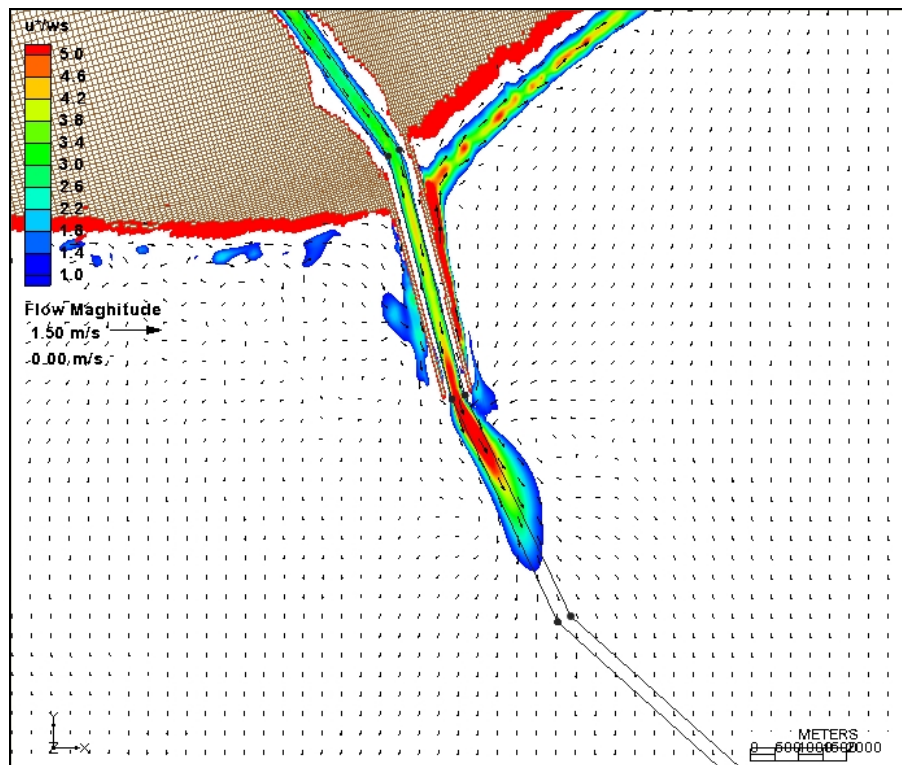
Figure A21. Flow patterns and suspension parameter for Plan 2
and the SE storm in 2010,
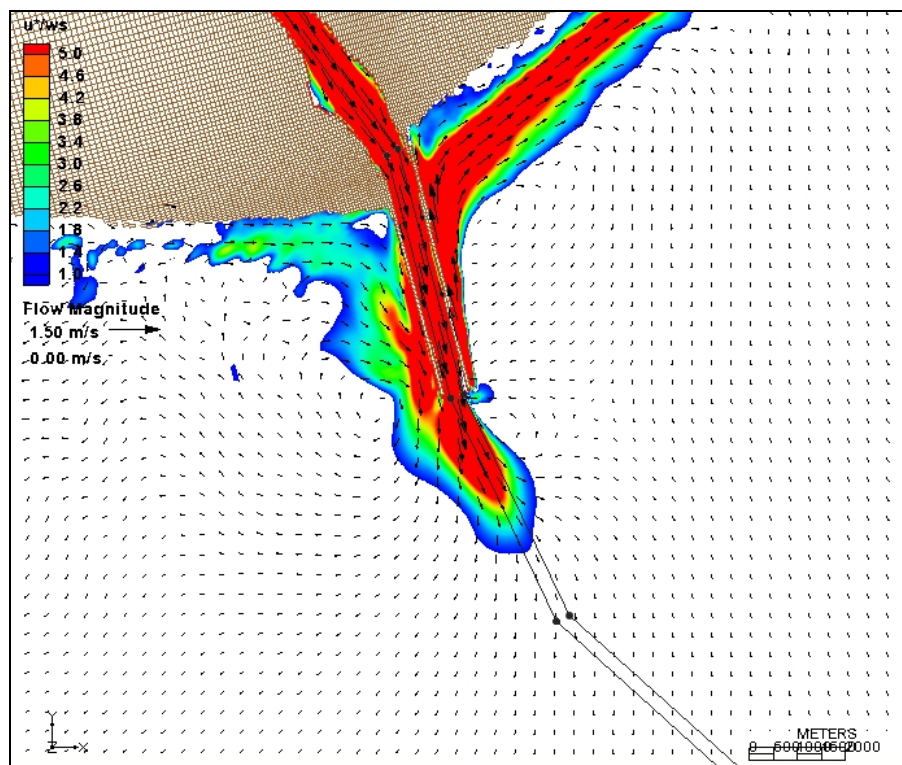
Figure A22. Flow patterns and suspension parameter for Plan 2
and the SE storm in 2060.
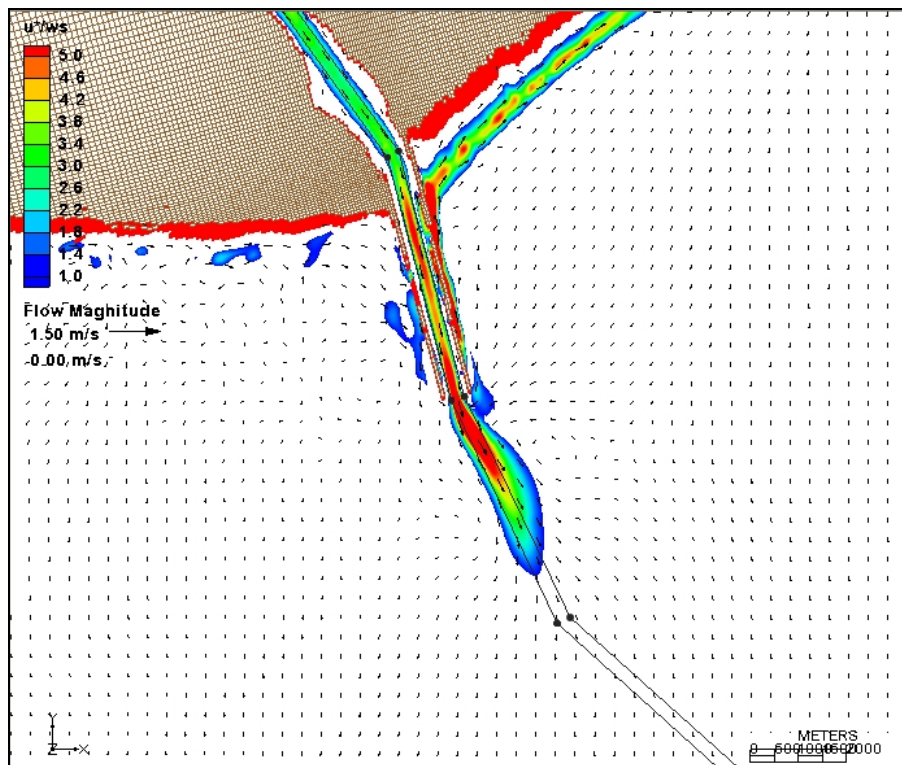
Figure A23. Flow patterns and suspension parameter for Plan 3
and the SE storm in 2010.
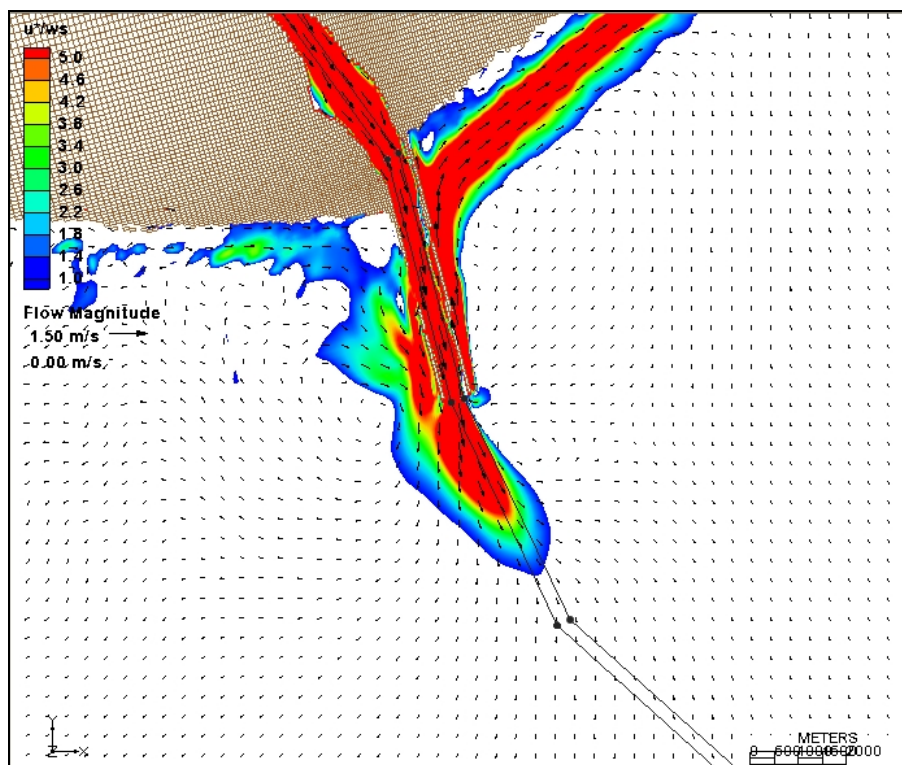
Figure A24. Flow patterns and suspension parameter for Plan 3
and the SE storm in 2060.

Figure A25. Flow patterns and suspension parameter for existing conditions and Hurricane H266.

Figure A26. Flow patterns and suspension parameter for existing conditions and Hurricane H266 in 2060.
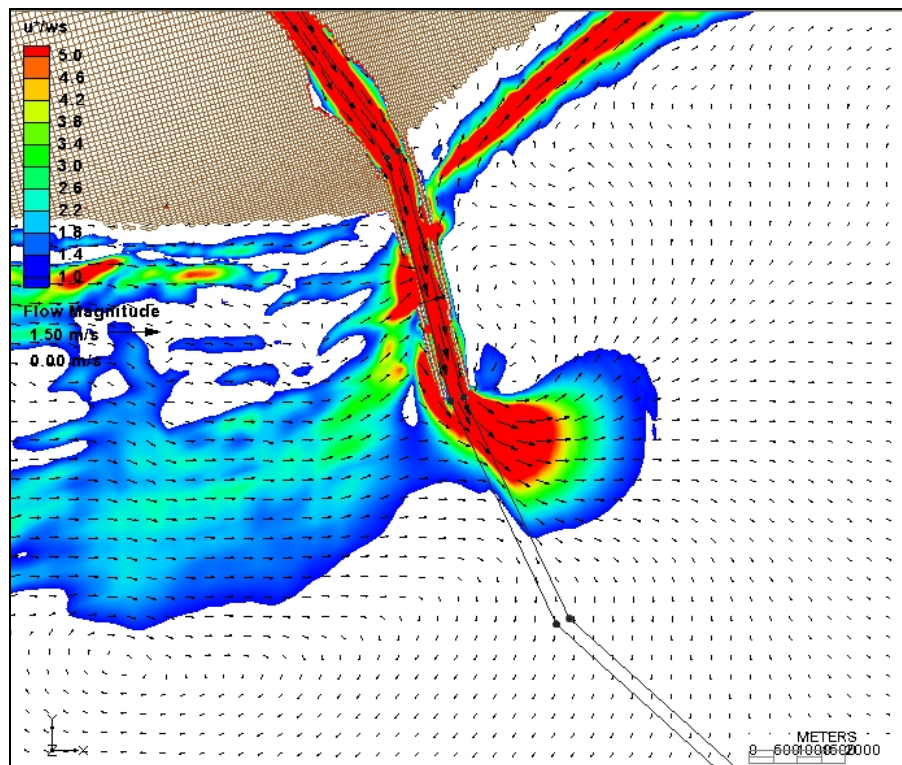
Figure A27. Flow patterns and suspension parameter for Plan 1
and Hurricane H266 in 2010.
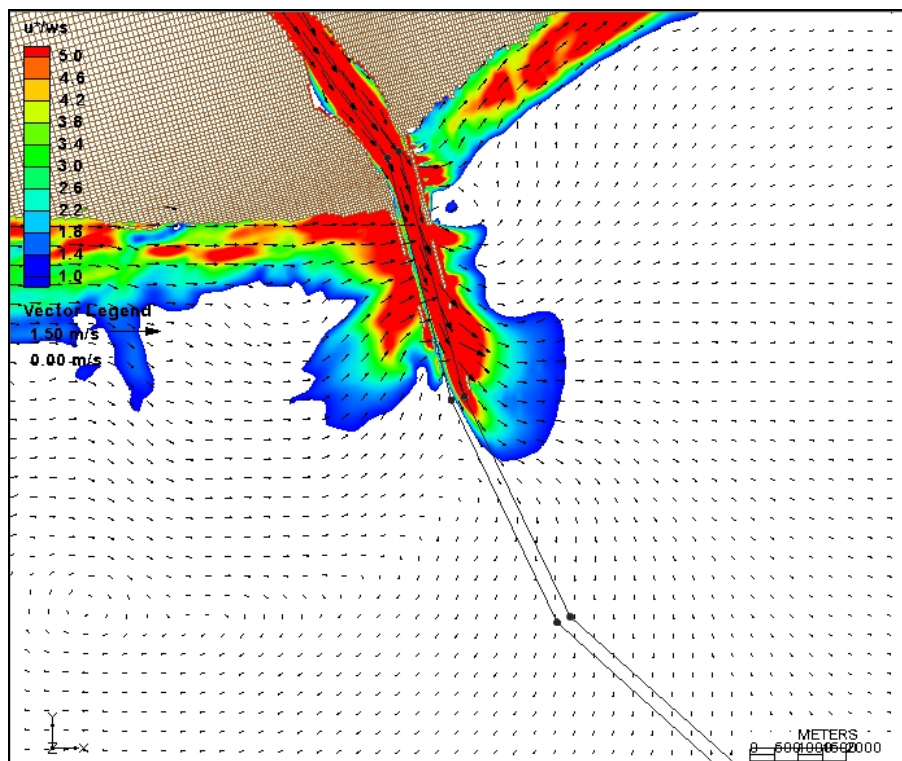
Figure A28. Flow patterns and suspension parameter for Plan 1
and Hurricane H266 in 2060.
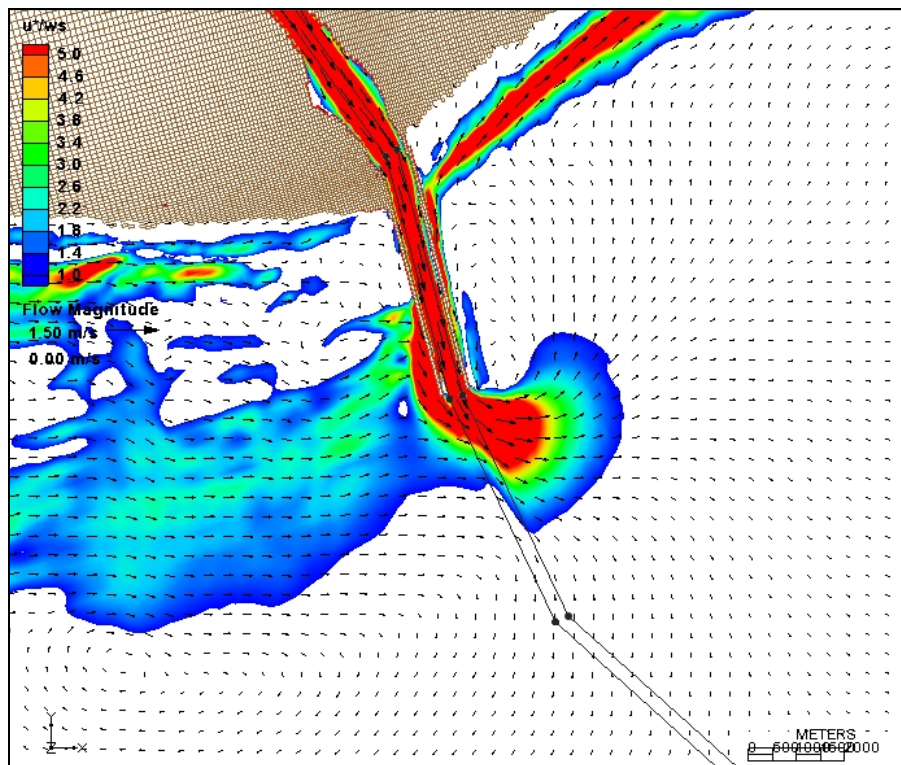
Figure A29. Flow patterns and suspension parameter for Plan 2
and Hurricane H266 in 2010.

Figure A30. Flow patterns and suspension parameter for Plan 2
and Hurricane H266 in 2060.

Figure A31. Flow patterns and suspension parameter for Plan 3
and Hurricane H266 in 2010.

Figure A32. Flow patterns and suspension parameter for Plan 3
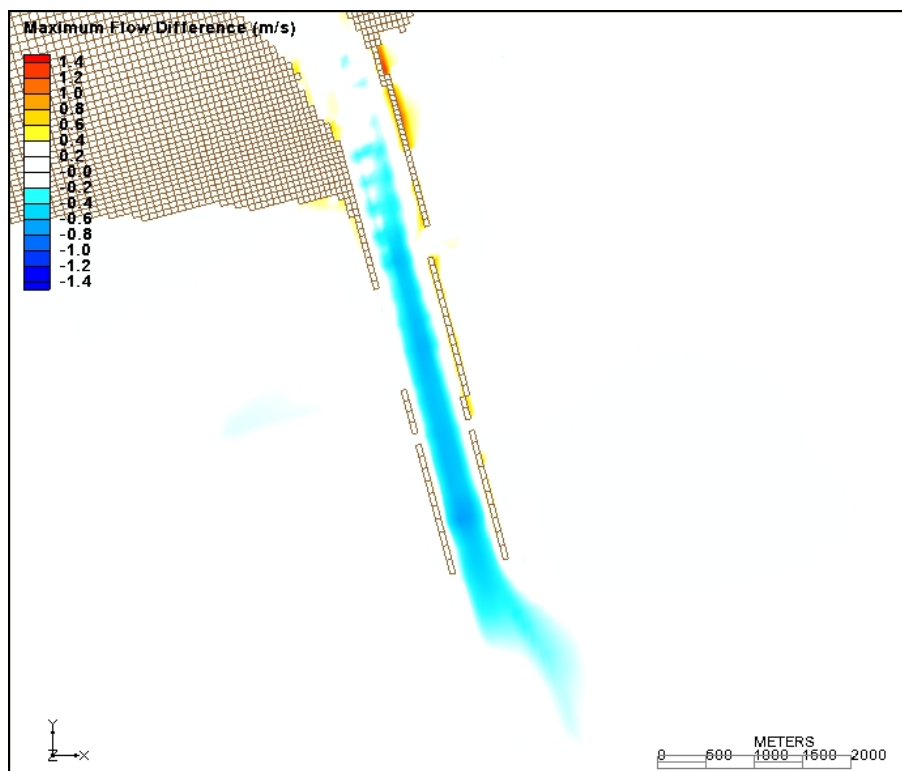and Hurricane H266 in 2060.

Appendix B: Comparison of Calculated Maximum Flow for each Plan
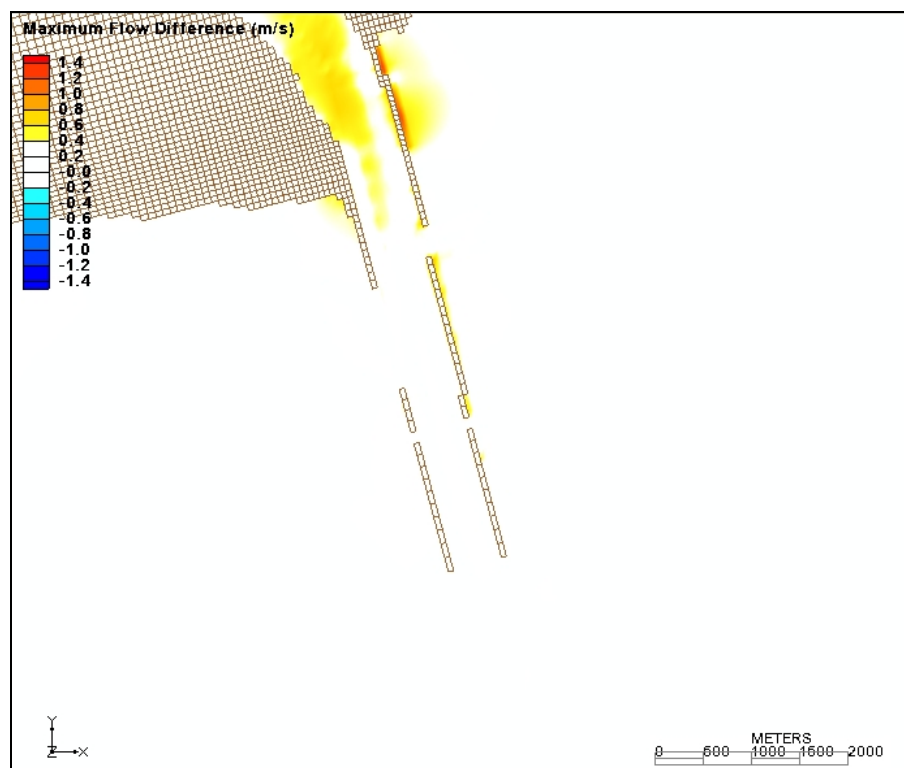
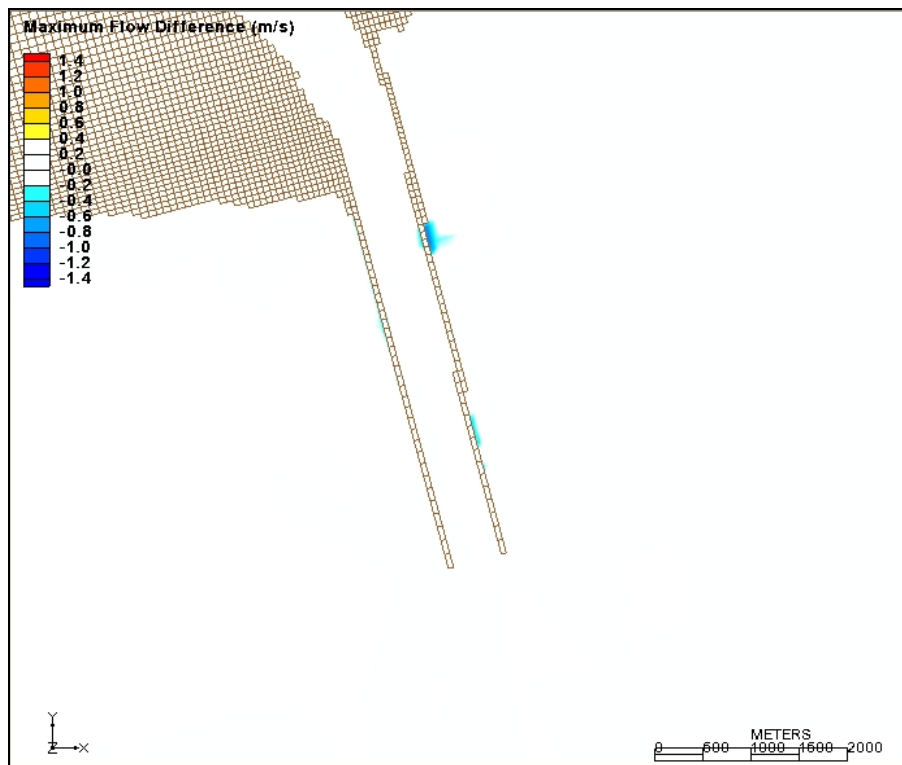Figure B1. Difference in maximum flow magnitude between existing conditions in 2060 and existing conditions in 2010 for the low-energy wave simulation.

Figure B2. Difference in maximum flow magnitude between Plan 1 and existing conditions for the low-energy wave simulation in 2010.
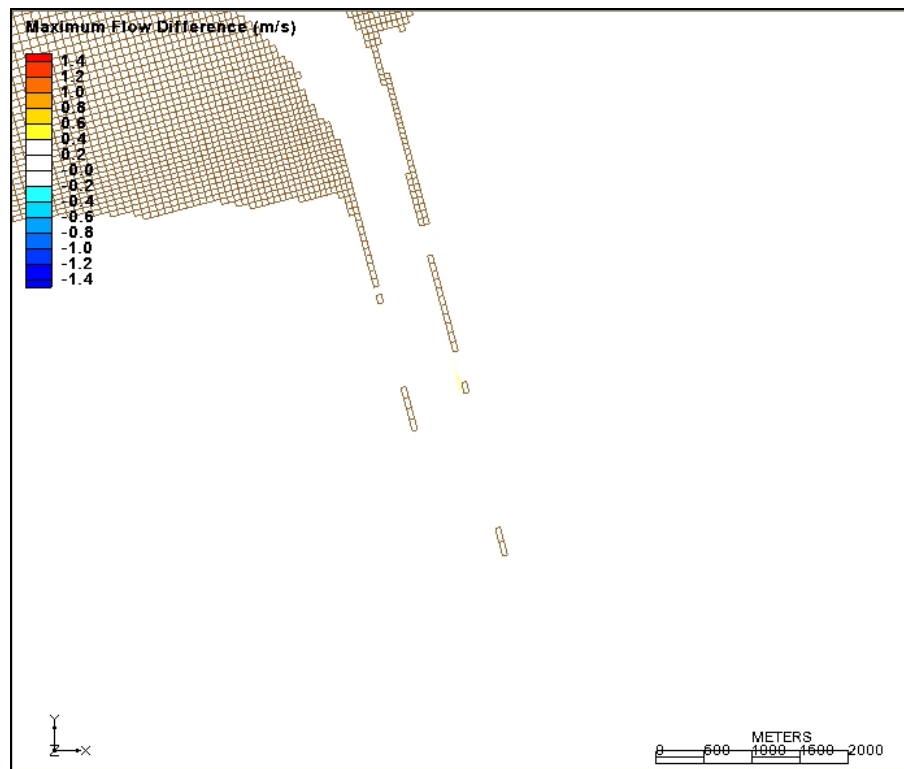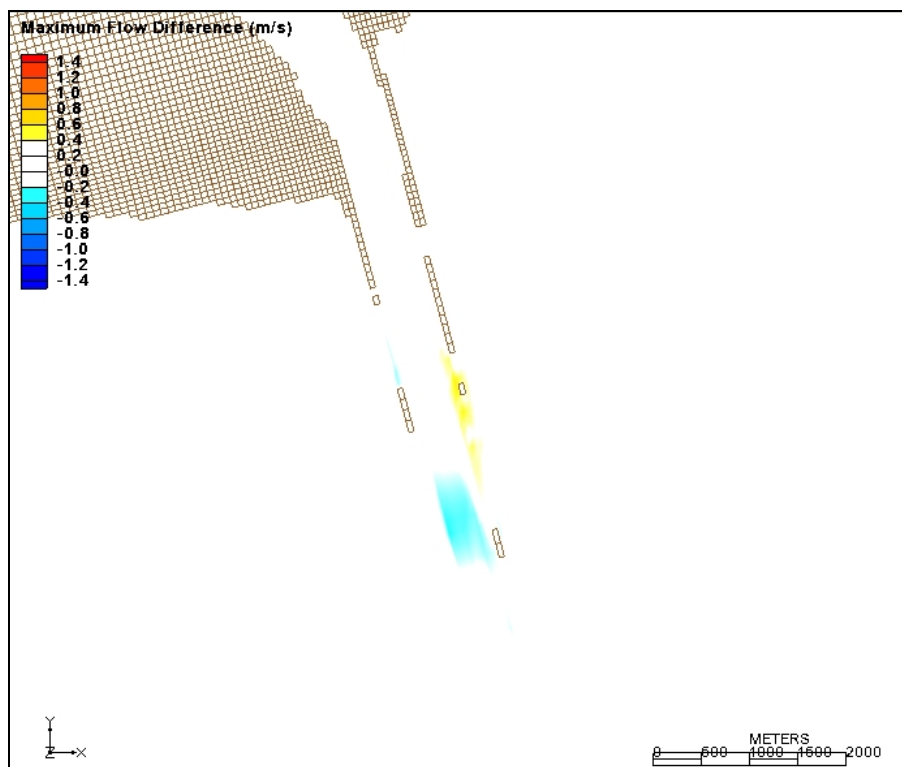
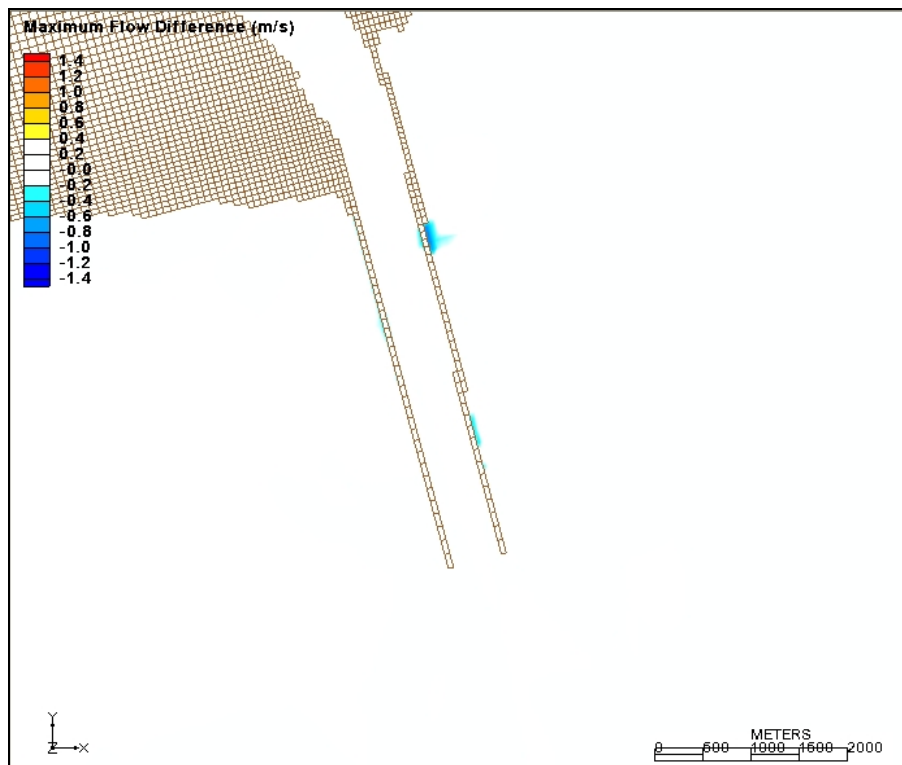Figure B3. Difference in maximum flow magnitude between Plan 1 and existing conditions for the low-energy wave simulation in 2060.
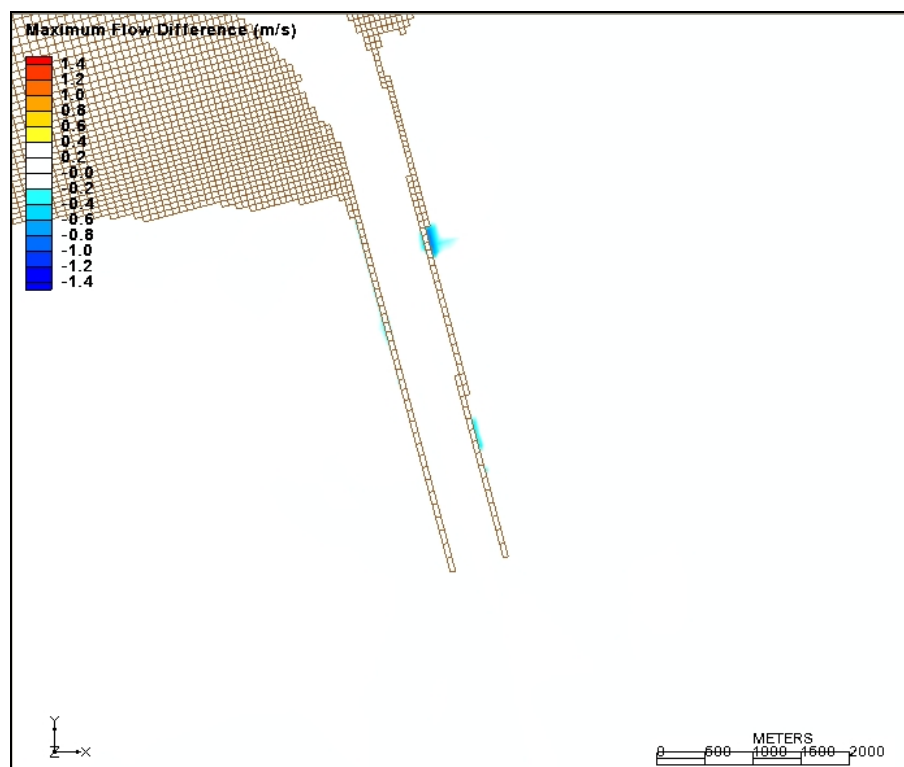
Figure B4. Difference in maximum flow magnitude between Plan 2 and existing conditions for the low-energy wave simulation in 2010.
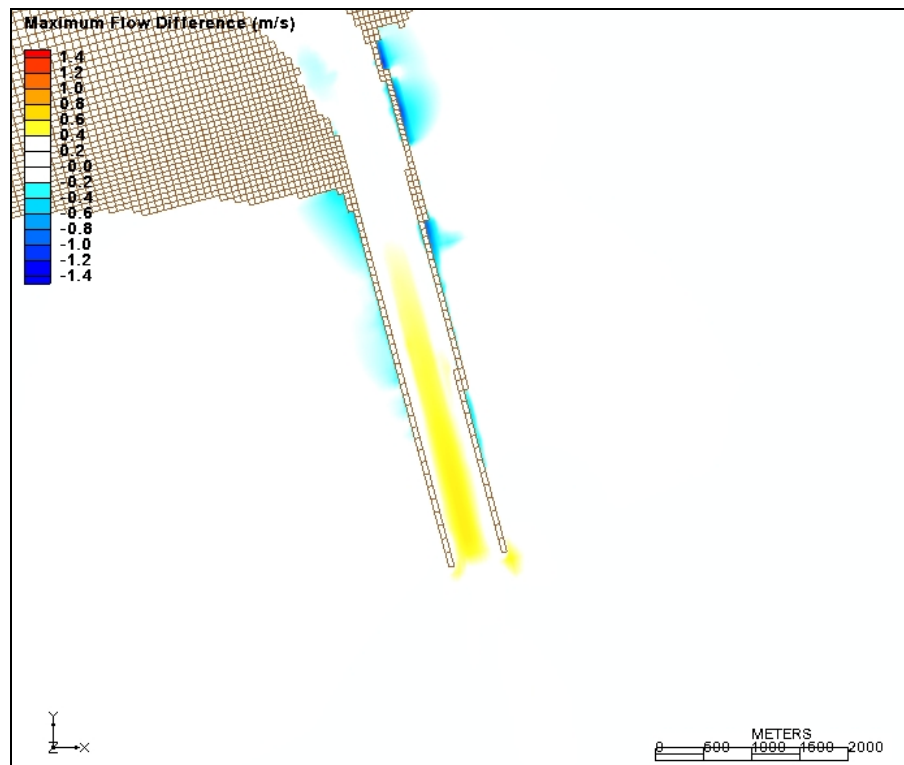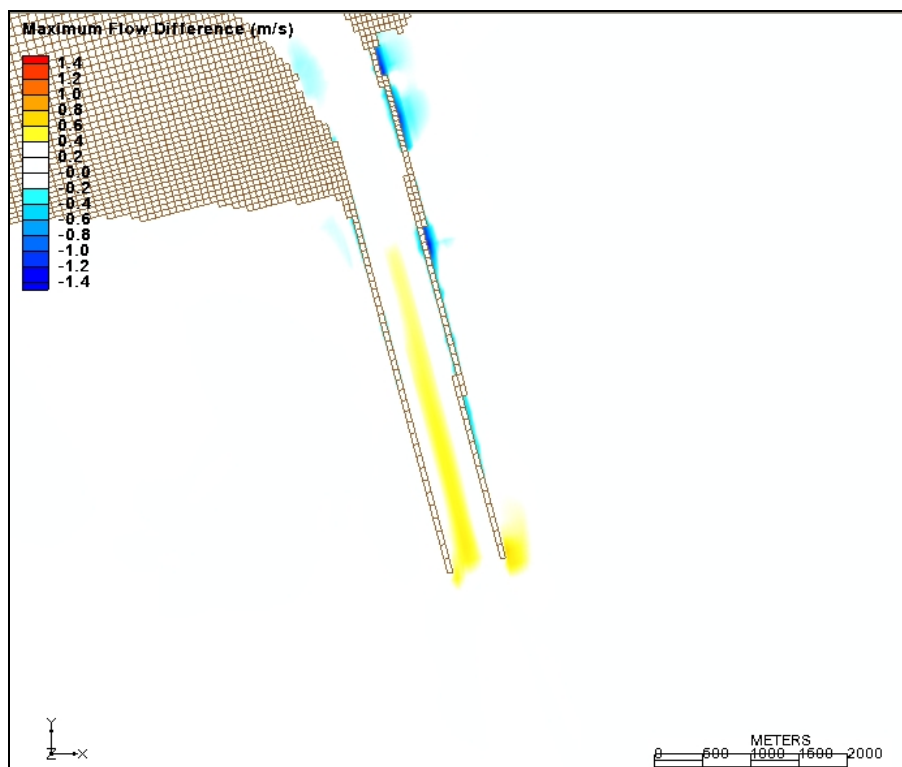
Figure B5. Difference in maximum flow magnitude between Plan 2 and existing conditions for the low-energy wave simulation in 2060.

Figure B6. Difference in maximum flow magnitude between Plan 3 and existing conditions for the low-energy wave simulation in 2010.
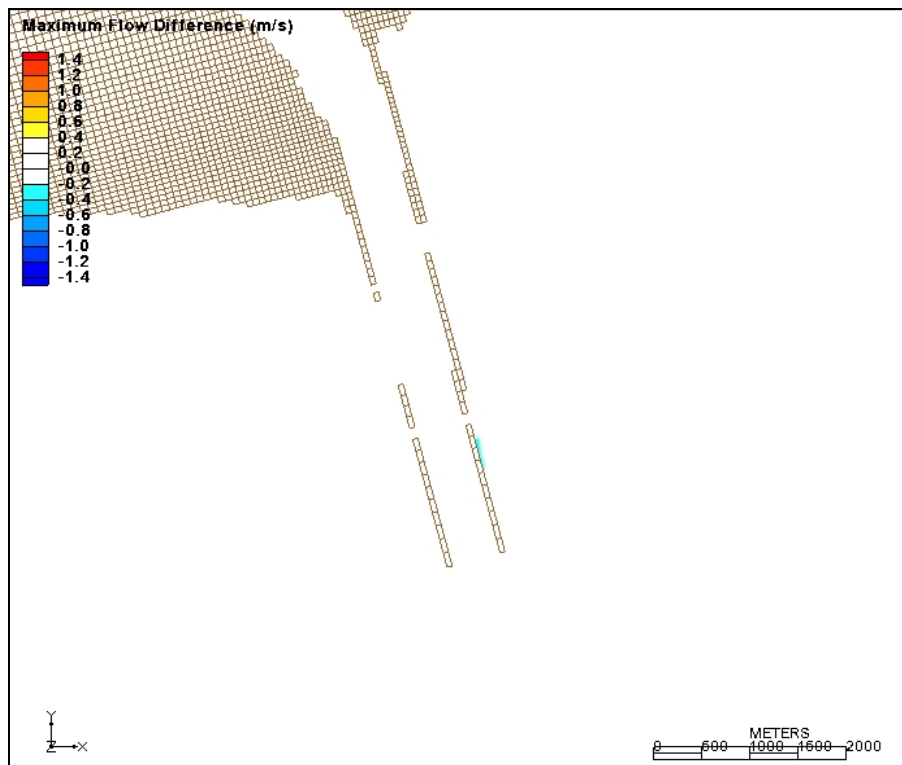
Figure B7. Difference in maximum flow magnitude between Plan 3 and existing conditions for the low-energy wave simulation in 2060.

Figure B8. Difference in maximum flow magnitude between existing conditions in 2060 and existing conditions in 2010 for the SW Storm.
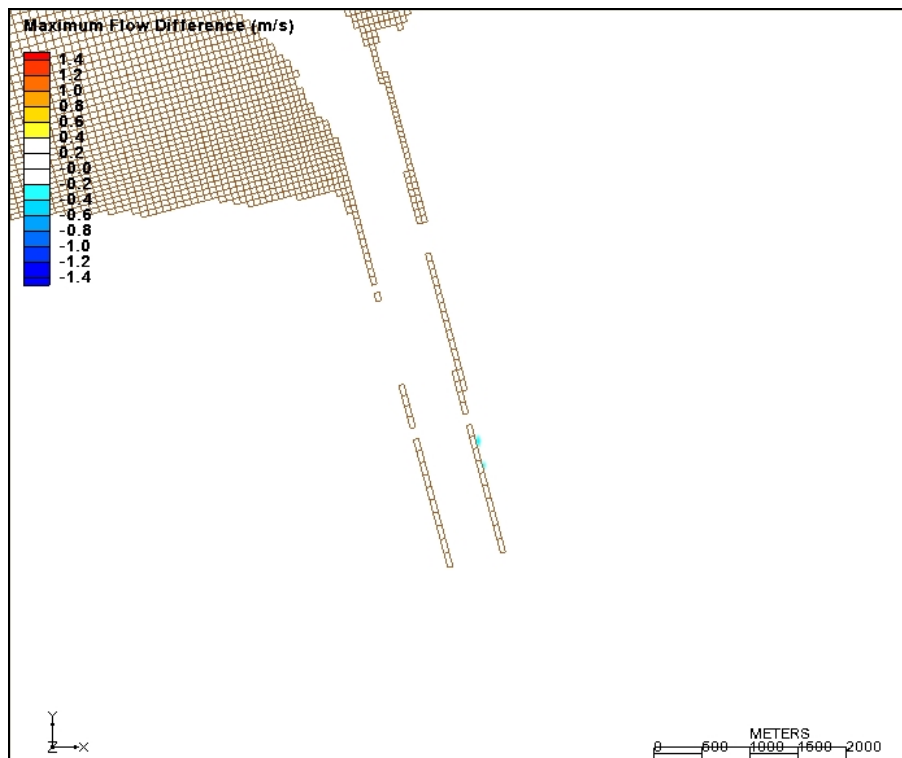
Figure B9. Difference in maximum flow magnitude between Plan 1 and existing conditions for the SW Storm in 2010.

Figure B10. Difference in maximum flow magnitude between Plan 1 and existing conditions for the SW Storm in 2060.

Figure B11. Difference in maximum flow magnitude between Plan 2
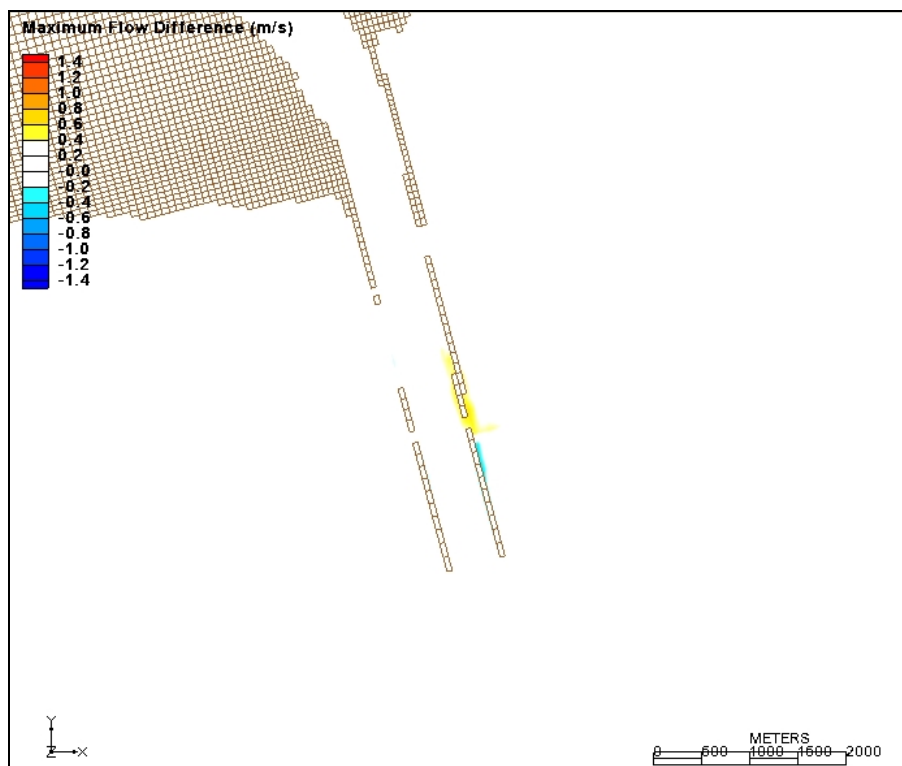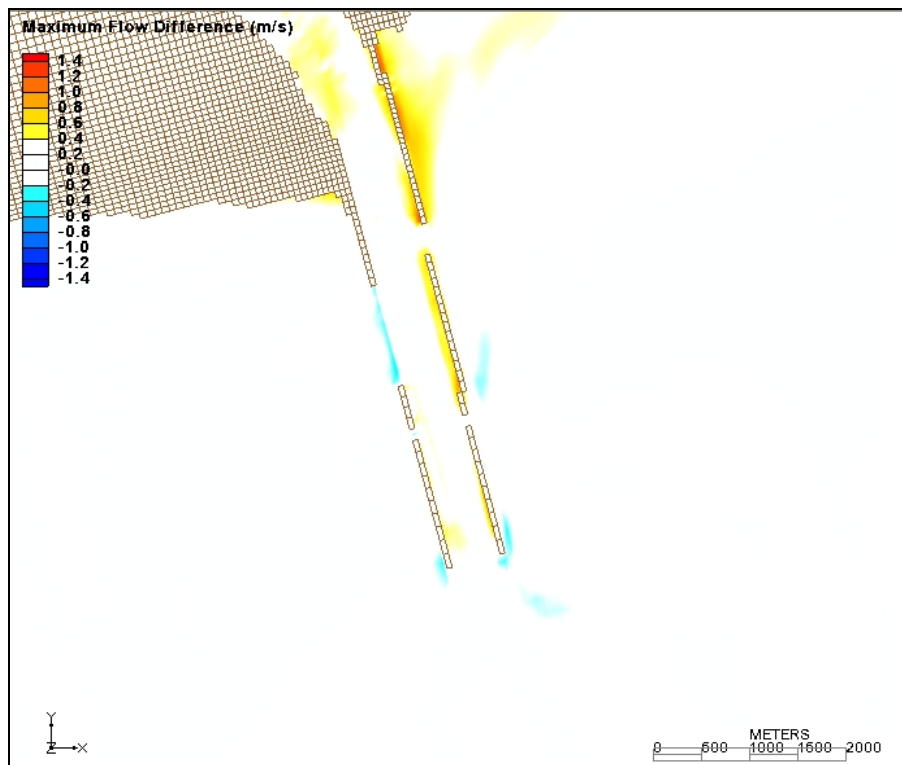and existing conditions for the SW Storm in 2010.

Figure B12. Difference in maximum flow magnitude between Plan 2
and existing conditions for the SW Storm in 2060.

Figure B13. Difference in maximum flow magnitude between Plan 3
and existing conditions for the SW Storm in 2010.

Figure B14. Difference in maximum flow magnitude between Plan 3
and existing conditions for the SW Storm in 2060.

Figure B15. Difference in maximum flow magnitude between existing conditions in 2060 and existing conditions in 2010 for the SE Storm.
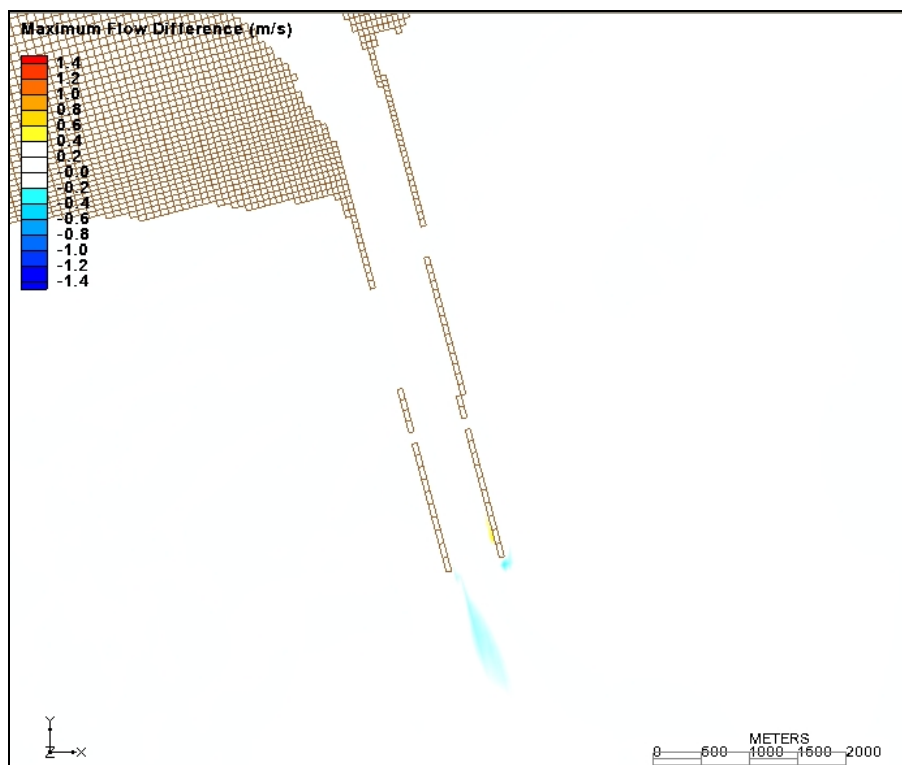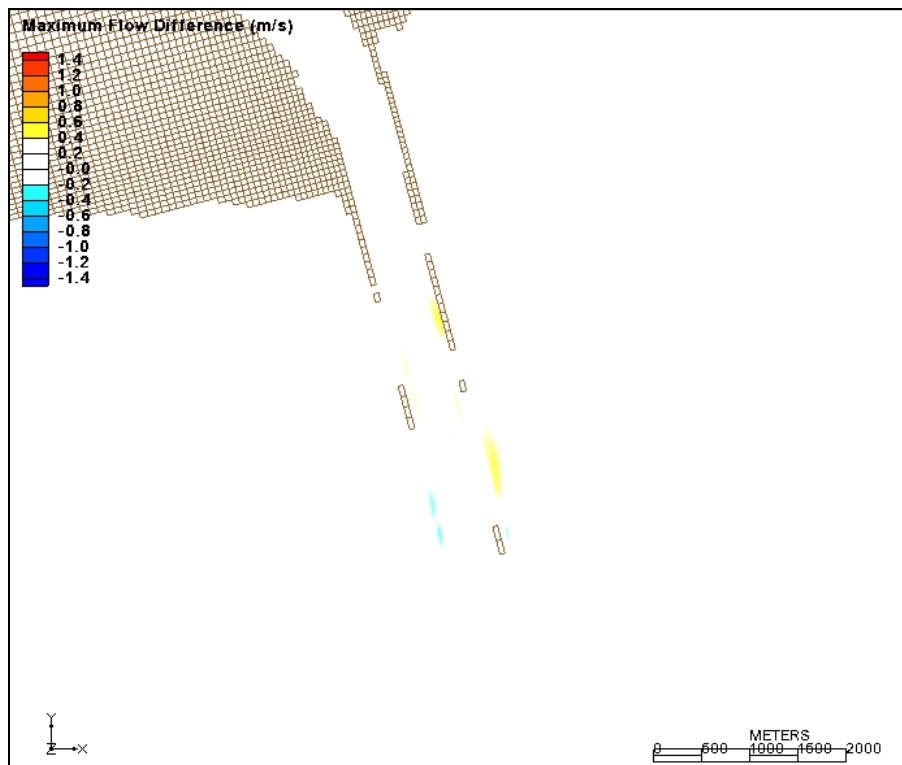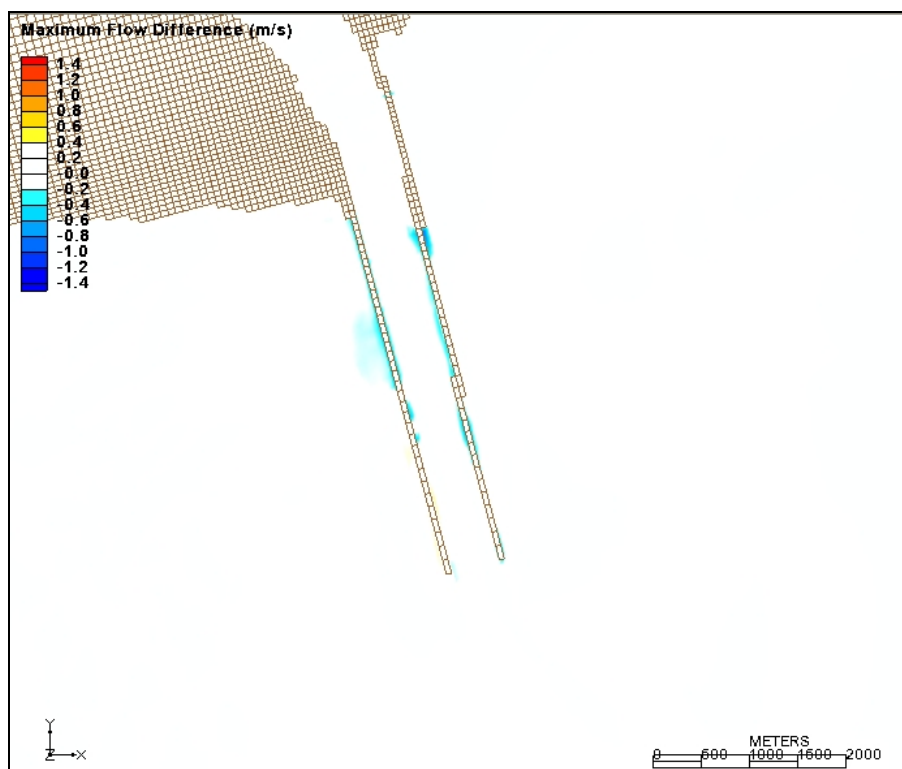

Figure B16. Difference in maximum flow magnitude between Plan 1 and existing conditions for the SE Storm in 2010.

Figure B17. Difference in maximum flow magnitude between Plan 1
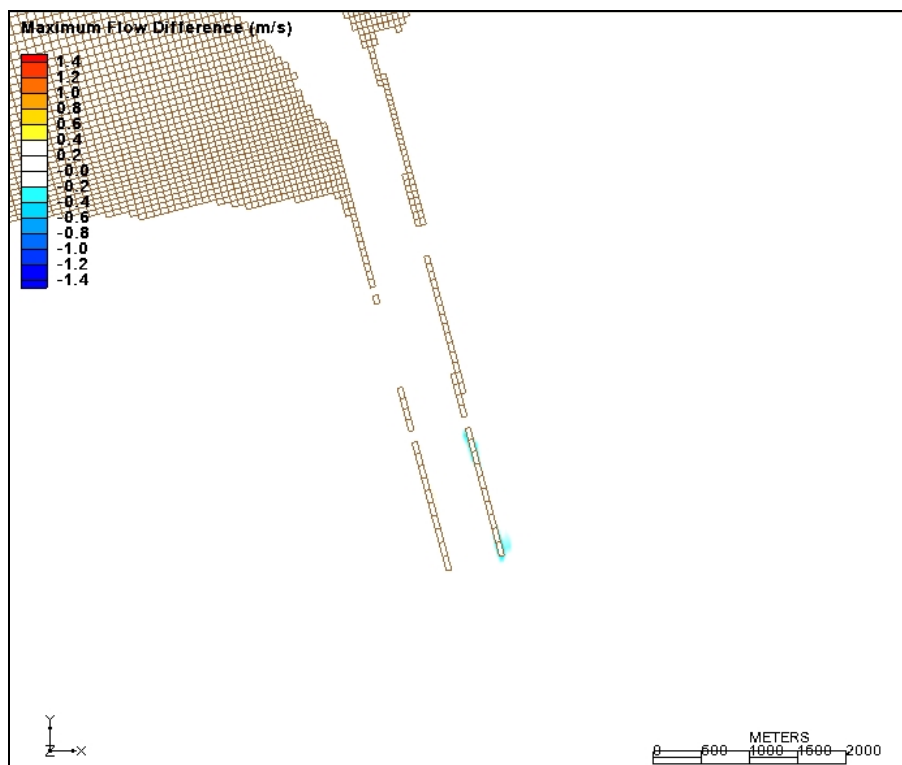and existing conditions for the SE Storm in 2060.

Figure B18. Difference in maximum flow magnitude between Plan 2
and existing conditions for the SE Storm in 2010.

Figure B19. Difference in maximum flow magnitude between Plan 2 and existing conditions for the SE Storm in 2060.

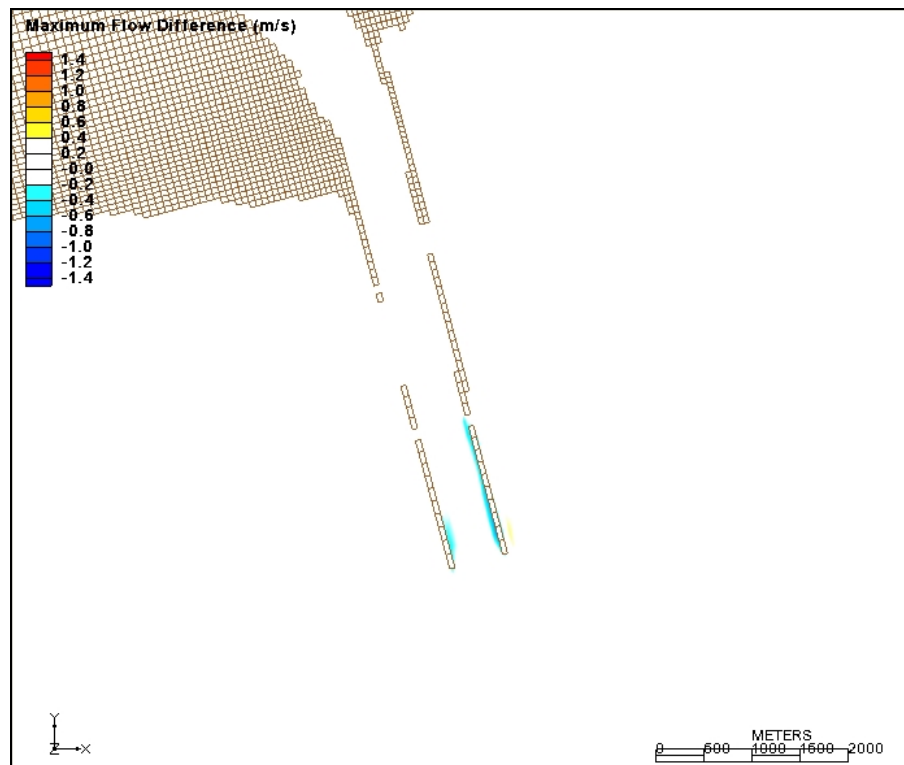Figure B20. Difference in maximum flow magnitude between Plan 3 and existing conditions for the SE Storm in 2010.

Figure B21. Difference in maximum flow magnitude between Plan 3
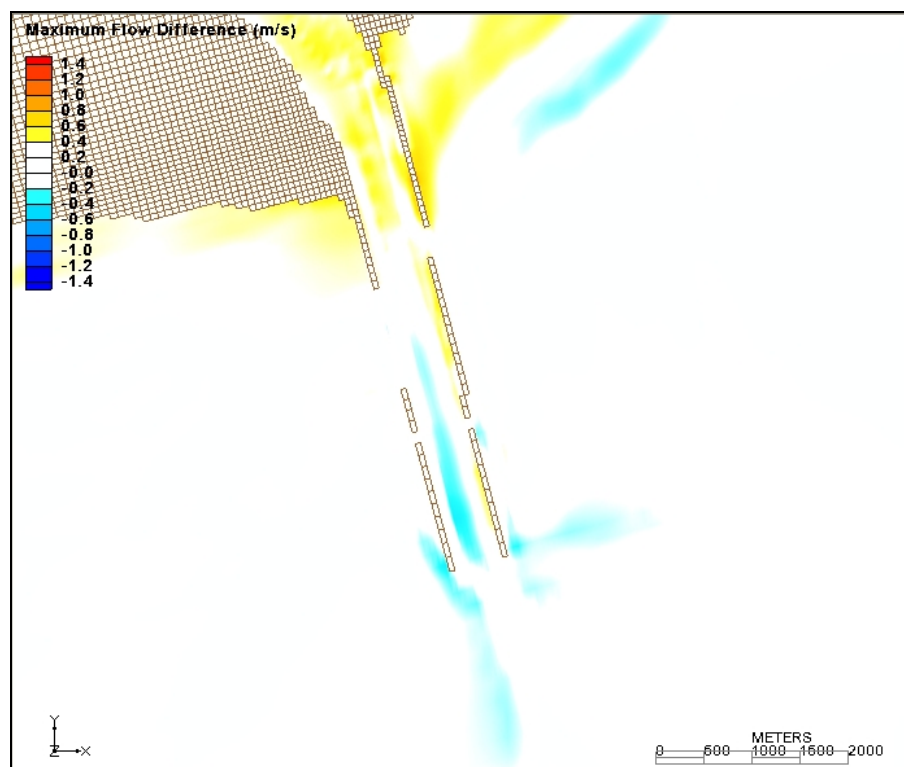and existing conditions for the SE Storm in 2060.

Figure B22. Difference in maximum flow magnitude between existing conditions
in 2060 and existing conditions in 2010 for Hurricane H266.

Figure B23. Difference in maximum flow magnitude between Plan 1
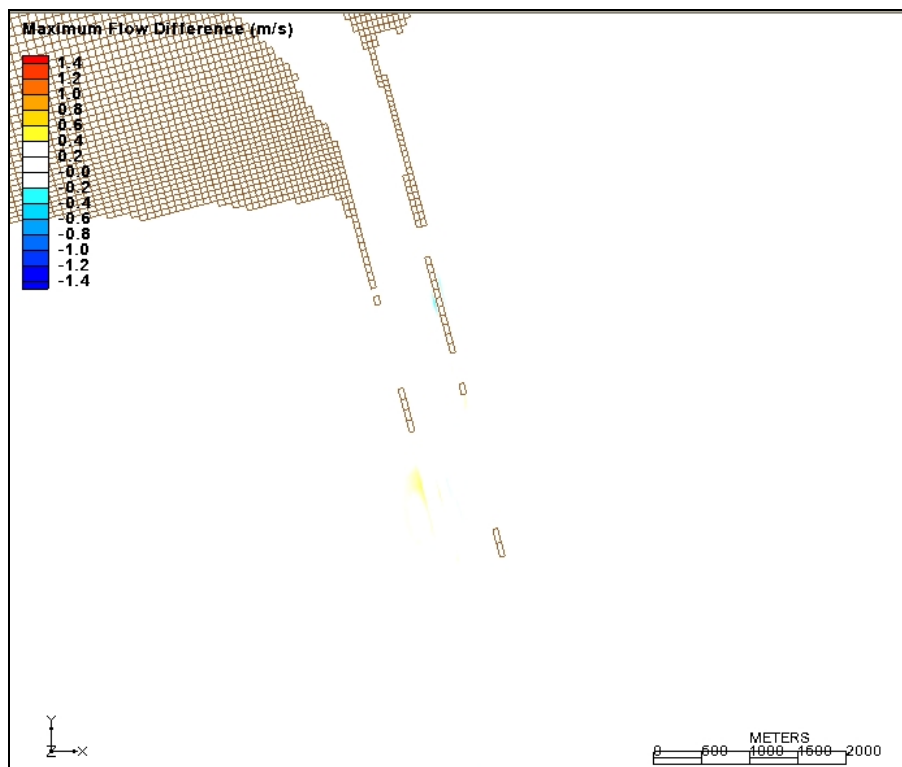and existing conditions for Hurricane H266 in 2010.

Figure B24. Difference in maximum flow magnitude between Plan 1
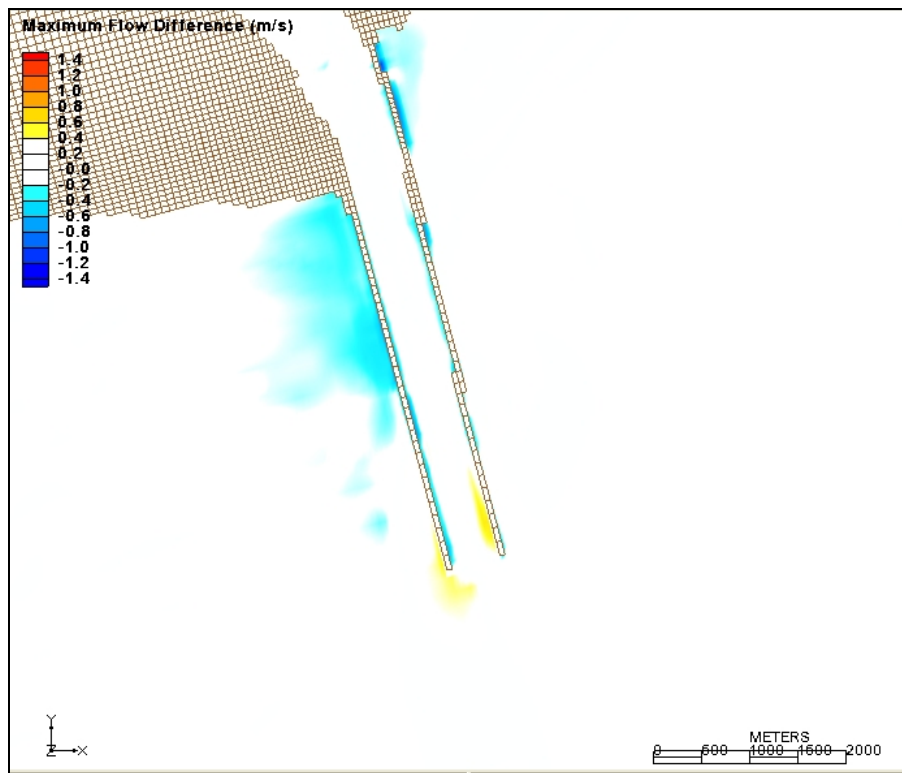and existing conditions for Hurricane H266 in 2060.

Figure B25. Difference in maximum flow magnitude between Plan 2 and existing conditions for Hurricane H266 in 2010.
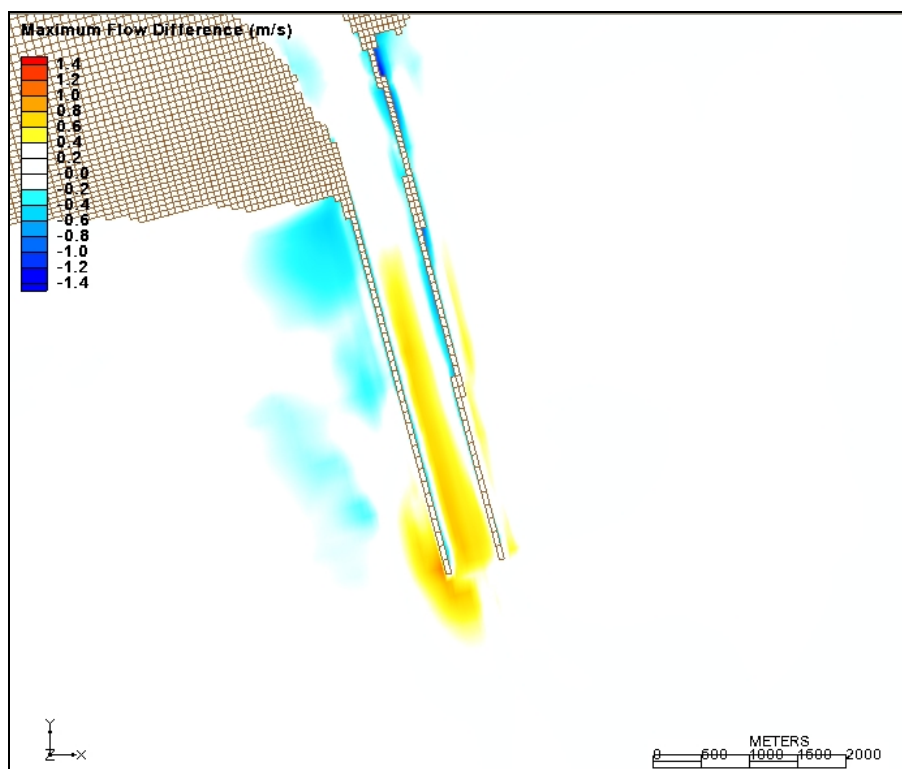

Figure B26. Difference in maximum flow magnitude between Plan 2 and existing conditions for Hurricane H266 in 2060.
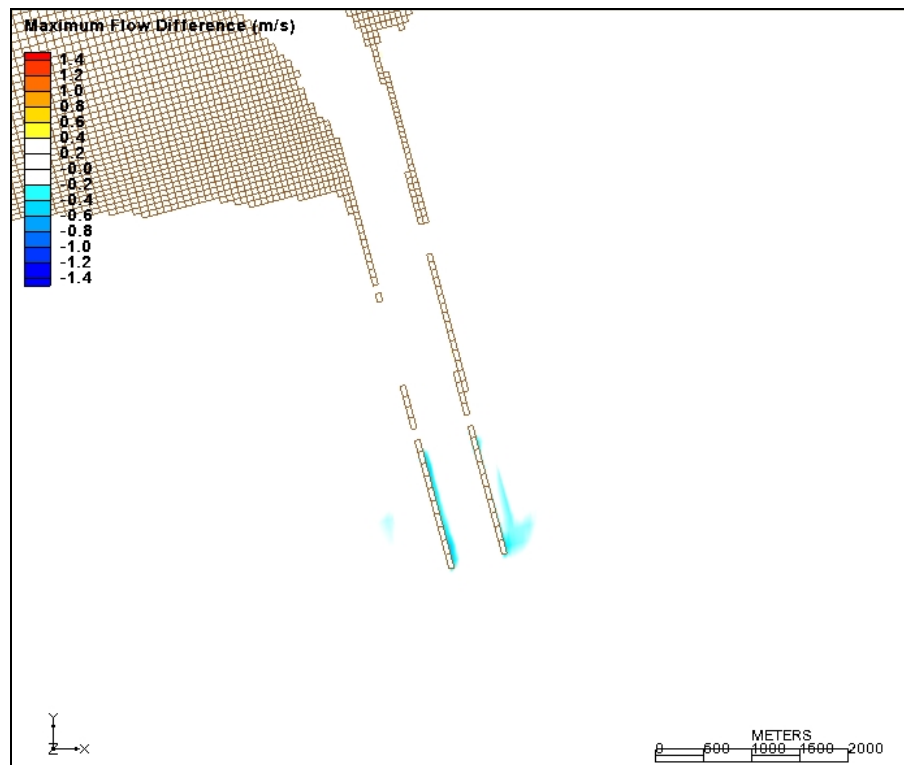
Figure B27. Difference in maximum flow magnitude between Plan 3
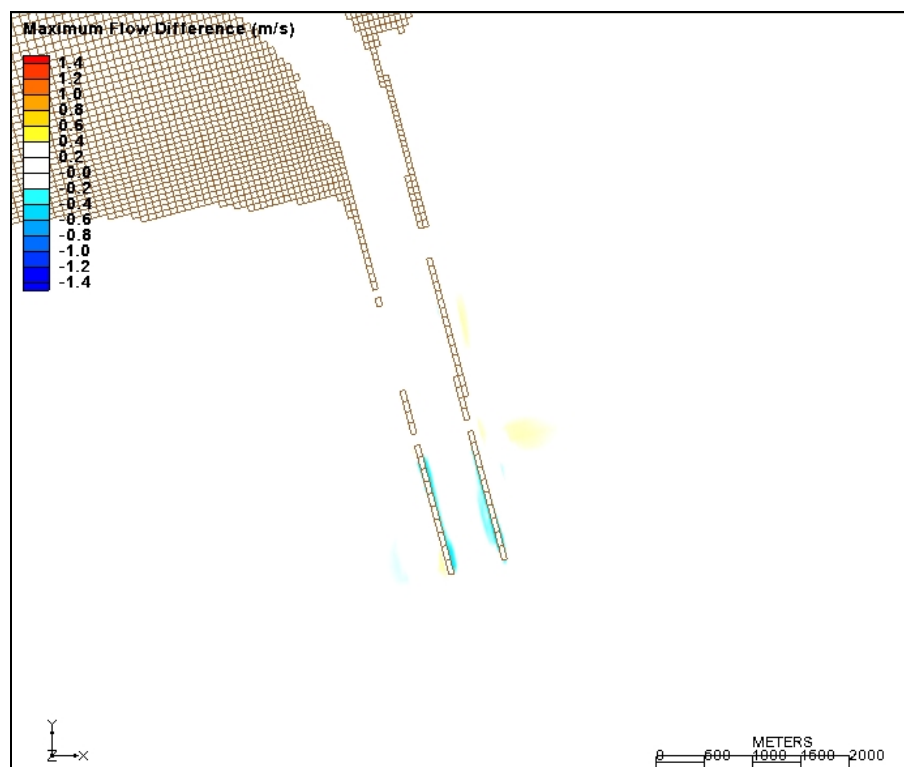and existing conditions for Hurricane H266 in 2010.

Figure B28. Difference in maximum flow magnitude between Plan 3
and existing conditions for Hurricane H266 in 2060.

REPORT DOCUMENTATION PAGE

1. REPORT DATE *(DD-MM-YYYY)* April 2010	2. REPORT TYPE Final report	3. DATES COVERED *(From - To)*

4. TITLE AND SUBTITLE

Sabine-Neches Waterway, Sabine Pass Jetty System: Past and Future Performance

5a. CONTRACT NUMBER

5b. GRANT NUMBER

5c. PROGRAM ELEMENT NUMBER

6. AUTHOR(S)

William C. Seabergh, Earnest R. Smith, and Julie D. Rosati

5d. PROJECT NUMBER

5e. TASK NUMBER

5f. WORK UNIT NUMBER

7. PERFORMING ORGANIZATION NAME(S) AND ADDRESS(ES)

U.S. Army Engineer Research and Development Center
Coastal and Hydraulics Laboratory
3909 Halls Ferry Road
Vicksburg, MS 39180-6199

8. PERFORMING ORGANIZATION REPORT NUMBER

ERDC/CHL TR-10-2

9. SPONSORING / MONITORING AGENCY NAME(S) AND ADDRESS(ES)

U.S. Army Engineer District, Galveston
Jadwin Building
2000 Fort Point Road
Galveston, TX 77550

10. SPONSOR/MONITOR'S ACRONYM(S)

11. SPONSOR/MONITOR'S REPORT NUMBER(S)

12. DISTRIBUTION / AVAILABILITY STATEMENT

Approved for public release; distribution is unlimited.

13. SUPPLEMENTARY NOTES

14. ABSTRACT

This study evaluated the present and future functionality of the Sabine Pass jetties considering planned deepening of the Sabine-Neches Waterway Navigation Channel from 42 to 48 ft mean low water (MLW) and possible rehabilitation of the jetty system. The Sabine Pass jetties were constructed to their full length (East jetty, 25,270 ft; West jetty, 21,860 ft) between 1880 and 1930 and, during the 130 years since construction began, have incurred loss of elevation and damage because of regional subsidence, scour at the base of the structures, storms, disintegration of the original fascine (willow) mats used as foundation for the structures, and consolidation of the underlying substrate. This study evaluated the 2003 condition of the jetties and anticipated functionality in 50 years given change in relative sea level at the site, future consolidation of the underlying substrate, and possible storm damage. Three integrated tasks evaluated 1) the stability of the jetties to storm waves, 2) the decrease in structure elevation through time relative to the mean water level caused by consolidation of the underlying substrate and relative sea level rise, and 3) waves, currents, and potential sediment transport pathways in the vicinity of the jetties and navigation channel. Each task assessed the 2003 "existing" condition, a hypothetical jetty condition in 50 years without rehabilitation, and two repair scenarios that were assumed to occur in 2010 and were assessed after 50 years.

(Continued)

15. SUBJECT TERMS

Consolidation	Jetty stability	Sabine-Neches Waterway
Jetty rehabilitation	Navigation	Shoaling
	Numerical modeling	Texas and Louisiana

16. SECURITY CLASSIFICATION OF:

a. REPORT	b. ABSTRACT	c. THIS PAGE	17. LIMITATION OF ABSTRACT	18. NUMBER OF PAGES	19a. NAME OF RESPONSIBLE PERSON
UNCLASSIFIED	UNCLASSIFIED	UNCLASSIFIED		150	19b. TELEPHONE NUMBER *(include area code)*

14. Abstract (Concluded)

The repair scenarios were rehabilitation of the entire length of both jetties vs. rehabilitation of the seaward 4,000 ft. Both alternatives would be constructed to elevations of +9.2 ft MLW (East) and +9.3 ft MLW (West). Shear stresses from numerical calculations of waves, currents, and water levels were applied to indicate the potential for cohesive sediment transport and channel shoaling magnitudes.

Recommendations from these analyses were that the jetties should be rehabilitated to +9.2 ft/+9.3 ft MLW to ensure safe navigation and reduce channel shoaling, and that stone size should be increased to approximately 17-18 tons for stability during storms and higher water levels. Repair of the seaward 4,000 ft of both jetties provided similar navigation benefits (reduction in waves and currents, no change in total shoaling) as restoration of the full length of both jetties. Physical model studies are recommended to optimize stone size for rehabilitation. Numerical modeling is recommended to assess the potential for scour of the seabed in the vicinity of the jetties, and to determine magnitudes of channel shoaling for cohesive sediment. Numerical shoreline modeling with anticipated water levels over the project lifetime is recommended to assess the likelihood for structure flanking and minimize adjacent beach erosion.